

MECHANISMS OF ALPHA-GLYCOSIDASES

by

SHIN NUMAO

B.Sc., McGill University, 1997

A THESIS SUBMITTED IN PARTIAL FULFILMENT OF  
THE REQUIREMENTS FOR THE DEGREE OF

DOCTOR OF PHILOSOPHY

in

THE FACULTY OF GRADUATE STUDIES

(Department of Chemistry)

We accept this thesis as conforming  
to the required standard

THE UNIVERSITY OF BRITISH COLUMBIA

April 2003

© Shin Numao, 2003

## Abstract

$\alpha$ -Retaining glycosidases are a class of hydrolytic enzymes that cleave  $\alpha$ -glycosidic linkages with net retention of configuration at the anomeric center. The finer details of the mechanisms of two such enzymes, Golgi  $\alpha$ -mannosidase II and human pancreatic  $\alpha$ -amylase, were investigated in order to gain better understanding of this class of enzymes.

$\alpha$ -Retaining mannosidases, like all other retaining glycosidases, employ a double displacement mechanism in which a transient glycosyl-enzyme intermediate is formed. In order to isolate or "trap" this key intermediate, two active site probes were synthesized for family 38  $\alpha$ -mannosidases. Both 5-fluoro- $\beta$ -L-gulosyl fluoride and 2-deoxy-2-fluoro- $\alpha$ -D-mannosyl-fluoride were shown to be poor substrates for Golgi  $\alpha$ -mannosidase II at room temperature. In both cases, by lowering the temperature, the lifetime of the intermediate increased so that the species was experimentally observable. Structural studies using X-ray crystallography showed that in both cases, the intermediate sugars adopted a  ${}^1S_5$  skew boat conformation, suggesting that the intermediate formed during the hydrolysis of the natural substrate also adopts this conformation. This suggests that intermediate distortion is an important part of the catalytic mechanism in  $\alpha$ -glycosidases.

$\alpha$ -Amylases are a family of  $\alpha$ -retaining glycosidases involved in glucose polymer digestion. Several members of this family are activated in the presence of chloride ion. To investigate the mechanism of this phenomenon, a series of mutations were made to the residues constituting the chloride ion-binding site in human pancreatic  $\alpha$ -amylase (HPA). Kinetic analysis of the resultant mutants showed that one of these residues,

Arg337, in the absence of chloride, effectively inhibits the enzyme by modulating the  $pK_a$  of the acid/base catalyst. The chloride ion activates HPA by relieving this inhibition through charge shielding. Upon mutation of this residue, the mutant HPA became a chloride-independent enzyme with full catalytic activity.

Using a novel substrate, 2,4-dinitrophenyl  $\alpha$ -maltotrioxide, a new rapid screen was developed to identify potential HPA inhibitors. Using this screen, D-gluconohydroximino-1,5-lactam (GHIL) was determined to be a potential HPA inhibitor. Kinetic analysis of this compound showed that GHIL is a poor inhibitor of HPA with a  $K_i$  value of 11 mM. However, in the presence of substrate, HPA will take this compound and modify it to create a more potent inhibitor *in situ*. This modification is most likely the result of a transglycosylation of the substrate to the inhibitor.

# Table of contents

|  |      |
|--|------|
| Abstract.....  | i    |
| Table of contents.....   | iii  |
| List of figures.....   | vii  |
| List of tables.....  | ix   |
| List of schemes.....   | ix   |
| List of abbreviations.....   | x    |
| List of abbreviations.....   | x    |
| Acknowledgments.....   | xiii |
| Chapter 1 Introduction.....  | 1    |
| 1.1 Glycosidases.....  | 3    |
| 1.2 Catalytic mechanism of glycosidases.....   | 6    |
| 1.3 Mechanism of inverting glycosidases.....   | 6    |
| 1.4 Mechanism of retaining glycosidases.....   | 7    |
| 1.5 Detailed mechanistic studies of $\beta$ -glycosidases.....                             | 8    |
| 1.5.1 The catalytic nucleophile.....   | 10   |
| 1.5.2 The oxocarbenium ion-like transition state.....                                      | 11   |
| 1.5.3 The general acid/base catalyst.....  | 13   |
| 1.5.4 The covalent intermediate.....   | 18   |
| 1.5.5 Trapping of the covalent intermediate.....   | 20   |
| 1.5.6 Non-covalent interactions.....   | 22   |
| 1.5.7 Sugar conformations.....   | 24   |
| 1.6 $\alpha$ -Retaining versus $\beta$ -retaining glycosidases.....                        | 25   |
| 1.7 Aim of the thesis.....   | 29   |
| Chapter 2 Family 38 $\alpha$ -mannosidases.....  | 31   |
| 2.1 General introduction.....  | 32   |
| 2.1.1 Asparagine-linked glycosylation.....   | 32   |
| 2.1.2 Family 38 $\alpha$ -mannosidases.....  | 35   |
| 2.1.3 Lysosomal $\alpha$ -mannosidase.....   | 38   |
| 2.1.4 Golgi $\alpha$ -mannosidase II.....  | 39   |
| 2.1.5 Structural aspects of Golgi $\alpha$ -mannosidase II.....                            | 40   |
| 2.2 Specific aims of this study.....   | 42   |
| 2.3 Results and discussion – the catalytic nucleophile of bovine kidney LAMAN.....         | 43   |
| 2.3.1 Rationale for the selection of the inactivator.....                                  | 43   |
| 2.3.2 Synthesis of 5-fluoro- $\beta$ -L-gulosyl fluoride.....                              | 43   |
| 2.3.3 Kinetics studies of 5FGulF with bovine kidney LAMAN.....                             | 45   |
| 2.3.4 Labelling experiments.....   | 47   |
| 2.3.5 Conclusions.....   | 51   |
| 2.4 Results and discussion – structural characterization of the covalent intermediate..... | 52   |
| 2.4.1 Rationale for the experiments.....   | 52   |
| 2.4.2 Kinetic analysis of the inactivation of the Asp341Asn mutant GMII by 5FGulF.....     | 53   |
| 2.4.3 Mass spectrometric analysis of the intermediate formed with 5FGulF.....              | 55   |
| 2.4.4 Structural analysis of the covalent intermediate.....                                | 56   |

|  |     |
|--|-----|
| 2.4.5 Kinetic analysis of the inactivation of the wild-type GMII by 5FGulF.....                                | 60  |
| 2.4.6 Structural analysis of the intermediate formed during 5FGulF hydrolysis by wild-type GMII.....           | 62  |
| 2.4.7 Synthesis of an alternative inactivator.....   | 62  |
| 2.4.8 Kinetic analysis of the interaction of 2FManF with GMII.....   | 64  |
| 2.4.9 Mass spectrometric analysis of the intermediate formed during 2FManF hydrolysis by Asp341Asn mutant..... | 65  |
| 2.4.10 Structural analysis of the intermediate formed during 2FManF hydrolysis by Asp341Asn mutant GMII.....   | 66  |
| 2.4.11 Implications of the skew boat conformation.....   | 70  |
| 2.4.12 Conclusions and future studies.....   | 75  |
| Chapter 3 The chloride ion-binding site in $\alpha$ -amylases.....   | 77  |
| 3.1 General introduction.....  | 78  |
| 3.1.1 Family of $\alpha$ -amylases.....  | 78  |
| 3.1.2 Chloride-dependent and independent $\alpha$ -amylases.....   | 80  |
| 3.1.3 Structure of the chloride ion-binding site.....  | 82  |
| 3.2 Specific aim of this study.....  | 83  |
| 3.3 Results and discussion.....  | 85  |
| 3.3.1 Rationale for the mutations to HPA.....  | 85  |
| 3.3.2 Structural analysis of the mutant enzymes.....   | 86  |
| 3.3.3 Kinetic analysis of HPA - Dependence on chloride of wild-type and mutant enzyme activity.....            | 90  |
| 3.3.4 Kinetic analysis of wild-type HPA.....   | 93  |
| 3.3.5 Kinetic analysis of Arg195 mutant HPA.....   | 94  |
| 3.3.6 Kinetic analysis of Arg337 mutant HPA.....   | 96  |
| 3.3.7 Kinetic analysis of Asn298 mutant HPA.....   | 99  |
| 3.3.8 Attempts at chemical rescue of inhibition.....   | 100 |
| 3.3.9 Evolutionary implications.....   | 102 |
| 3.3.10 Possible future directions.....   | 103 |
| Chapter 4 Substrates and inhibitors of $\alpha$ -amylase.....  | 106 |
| 4.1 General introduction.....  | 107 |
| 4.1.1 Human pancreatic $\alpha$ -amylase.....  | 107 |
| 4.1.2 Transglycosylation.....  | 108 |
| 4.1.3 Inhibitors of $\alpha$ -amylase.....   | 110 |
| 4.1.3.1 Proteinaceous inhibitors of $\alpha$ -amylase.....   | 111 |
| 4.1.3.2 Carbohydrate-based inhibitors of $\alpha$ -amylase.....  | 113 |
| 4.1.4 Substrates and assays for $\alpha$ -amylases.....  | 118 |
| 4.2 Specific aims of this study.....   | 123 |
| 4.3 Results and discussion-part I: Development of a convenient assay.....                                      | 125 |
| 4.3.1 Rationale for the design of the novel substrates.....  | 125 |
| 4.3.2 Synthesis of $\alpha$ DNP-G2.....  | 125 |
| 4.3.3 Synthesis of $\alpha$ DNP-G3.....  | 127 |
| 4.3.4 Kinetic analysis of $\alpha$ DNP-G2 as a substrate for HPA.....  | 129 |
| 4.3.5 Analysis of the products of HPA catalysed cleavage of $\alpha$ DNP-G2.....                               | 129 |
| 4.3.6 Kinetic analysis of $\alpha$ DNP-G3 as a substrate for HPA.....  | 131 |

|  |     |
|--|-----|
| 4.3.7 Analysis of the products of HPA catalysed cleavage of $\alpha$ DNP-G3 .....      | 132 |
| 4.3.8 Kinetic analysis of DNP-Glc as a substrate for HPA .....                         | 134 |
| 4.3.9 Conclusions and future directions.....   | 136 |
| 4.4 Results and discussion: Rapid screening of monosaccharide inhibitors.....          | 137 |
| 4.4.1 Rationale for searching for monosaccharide inhibitors .....                      | 137 |
| 4.4.2 Rapid screen for identifying potential HPA inhibitors .....                      | 137 |
| 4.4.3 Positive control for the new screen.....   | 138 |
| 4.4.4 Design of a rapid screen for identifying potential elongated HPA inhibitors      | 142 |
| 4.4.5 Results of the rapid $\alpha$ -amylase screen for potential inhibitors .....     | 143 |
| 4.4.6 Analysis of GHIL as an inhibitor of HPA .....                                    | 145 |
| 4.4.7 Conclusions and future directions.....   | 151 |
| Chapter 5 Experimental .....   | 153 |
| 5.1 Synthesis .....  | 154 |
| 5.1.1 Synthesis of 5-fluoro- $\beta$ -L-gulosyl fluoride .....                         | 154 |
| 5.1.2 Synthesis of 2-deoxy-2-fluoro- $\alpha$ -D-mannosyl fluoride .....               | 156 |
| 5.1.3 Synthesis of 2,4-dinitrophenyl $\alpha$ -D-mannoside .....                       | 157 |
| 5.1.4 Synthesis of 2,4-dinitrophenyl $\alpha$ -maltoside.....                          | 159 |
| 5.1.5 Synthesis of 2,4-dinitrophenyl $\alpha$ -maltotrioside .....                     | 161 |
| 5.2 Protein Chemistry .....  | 165 |
| 5.2.1 Site directed mutagenesis.....   | 165 |
| 5.2.2 Growth and expression of recombinant HPA from Pichia Pastoris.....               | 167 |
| 5.2.3 Purification of recombinant deglycosylated HPA .....                             | 167 |
| 5.2.4 Circular dichroism spectroscopy.....   | 168 |
| 5.3 Enzymology .....   | 169 |
| 5.3.1 General methods for kinetic analysis.....  | 169 |
| 5.3.1.1 UV-spectroscopy.....   | 169 |
| 5.3.1.2 Fluoride electrode .....   | 169 |
| 5.3.1.3 DNS-assay.....   | 169 |
| 5.3.2 Kinetic analysis of bovine kidney LAMAN .....                                    | 170 |
| 5.3.2.1 Steady state kinetics.....   | 170 |
| 5.3.3 Kinetic analysis of Drosophila melanogaster Golgi $\alpha$ -mannosidase II ..... | 170 |
| 5.3.3.1 Steady state kinetics.....   | 170 |
| 5.3.3.2 Inactivation studies .....   | 171 |
| 5.3.4 Kinetic analysis of the chloride binding site mutant HPA.....                    | 172 |
| 5.3.5 Kinetic analysis of HPA using the novel substrates .....                         | 173 |
| 5.3.6 Kinetic analysis of inhibitors of HPA.....                                       | 173 |
| 5.3.6.1 Rapid assay for determining inhibition potential.....                          | 173 |
| 5.3.6.2 Kinetic analysis of the GHIL as an inhibitor of HPA .....                      | 174 |
| 5.3.7 HPLC product analysis .....  | 175 |
| 5.3.8 Mass spectrometric analysis .....  | 175 |
| 5.3.8.1 Analysis of the covalent intermediate formed on LAMAN.....                     | 175 |
| 5.3.8.2 Analysis of the covalent intermediate formed on GMII .....                     | 176 |
| 5.3.8.3 Product analysis of HPA reactions .....  | 177 |
| References:.....   | 178 |
| Appendix I .....   | 185 |
| Fundamental Equations for Enzyme Kinetics.....   | 186 |

|  |     |
|--|-----|
| Enzyme kinetics in the presence of a mechanism-based inactivator ..... | 190 |
| Enzyme kinetics in the presence of a reversible inhibitor .....        | 192 |
| Appendix 2.....  | 197 |

# List of figures

|             |   |    |
|-------------|---|----|
| Figure 1.1  | The hydrolysis reaction catalyzed by glycosidases.....  | 3  |
| Figure 1.2  | Stereochemical outcome of a glycosidase reaction.....   | 4  |
| Figure 1.3  | Subsites nomenclature in endo-glycosidases.....   | 5  |
| Figure 1.4  | Proposed mechanism for an inverting $\alpha$ -glycosidase.....  | 7  |
| Figure 1.5  | Proposed mechanism for a retaining $\alpha$ -glycosidase.....   | 9  |
| Figure 1.6  | Chemical rescue of a nucleophile mutant glycosidase.....  | 11 |
| Figure 1.7  | Structure of the oxocarbenium ion-like transition state.....  | 11 |
| Figure 1.8  | Representative structures of transition state analogues for glycosidases.....                                   | 13 |
| Figure 1.9  | Structures of bicyclic inhibitors.....  | 15 |
| Figure 1.10 | The lateral protonation mechanism.....  | 17 |
| Figure 1.11 | Chemical rescue by azide of an acid/base mutant glycosidase.....  | 18 |
| Figure 1.12 | Fluoro-inactivators and their mechanism of action.....  | 21 |
| Figure 1.13 | Trapping of an intermediate using mutant enzyme.....  | 22 |
| Figure 1.14 | Conformations adopted during glycosidase hydrolysis.....  | 24 |
| Figure 1.15 | Structures of imino-sugars.....   | 27 |
| Figure 2.1  | Biosynthetic pathway for N-linked glycosylation.....  | 33 |
| Figure 2.2  | Lysosomal degradation pathway for N-linked glycoproteins.....   | 35 |
| Figure 2.3  | Sequence alignment for family 38 $\alpha$ -mannosidases.....  | 37 |
| Figure 2.4  | Structure of <i>Drosophila</i> GMII.....  | 41 |
| Figure 2.5  | Inhibition of bovine lysosomal $\alpha$ -mannosidase by 5FGulF.....   | 46 |
| Figure 2.6  | ESI-MS experiments on peptic digests of bovine kidney LAMAN.....  | 49 |
| Figure 2.7  | ESI-MS-MS spectrum of the 5-fluoro-gulosyl peptide.....   | 50 |
| Figure 2.8  | Inactivation of Asp341Asn mutant GMII by 5FGulF.....  | 54 |
| Figure 2.9  | Reactivation of the 5-fluoro-gulosyl GMII.....  | 55 |
| Figure 2.10 | Mass spectra of Asp341Asn mutant GMII labelled with 5FGulF.....   | 56 |
| Figure 2.11 | Structure of the covalent intermediate formed during the hydrolysis of 5FGulF by the Asp341Asn mutant GMII..... | 58 |
| Figure 2.12 | Inactivation of wild-type GMII by 5FGulF.....   | 61 |
| Figure 2.13 | Mass spectra of wild-type GMII labelled with 5FGulF.....  | 61 |
| Figure 2.14 | Structure of the covalent intermediate formed during the hydrolysis of 5FGulF by wild-type GMII.....            | 63 |
| Figure 2.15 | Mass spectra of Asp341Asn mutant GMII labelled with 2FManF.....   | 66 |
| Figure 2.16 | Structure of the covalent intermediate formed during the hydrolysis of 2FManF by Asp341Asn mutant GMII.....     | 67 |
| Figure 2.17 | Comparison of intermediates from 2FManF and 5FGulF hydrolysis.....  | 69 |
| Figure 2.18 | Benefits of adopting the skew boat conformation.....  | 71 |
| Figure 2.19 | Comparison of intermediates in $\alpha$ - and $\beta$ -retaining glycosidases.....                              | 72 |
| Figure 2.20 | Comparison $\alpha$ - and $\beta$ -retaining glycosidases.....  | 74 |
| Figure 3.1  | Sequence alignment of representative members of family 13 $\alpha$ -amylases.....                               | 79 |
| Figure 3.2  | Structure of human pancreatic $\alpha$ -amylase.....  | 81 |
| Figure 3.3  | The chloride ion-binding site residues.....   | 83 |
| Figure 3.4  | Structures of the mutant enzymes.....   | 87 |
| Figure 3.5  | The dependence of mutants on chloride concentration.....  | 92 |

|             |  |     |
|-------------|--|-----|
| Figure 3.6  | The pH profiles for the wild-type HPA .....                                      | 94  |
| Figure 3.7  | The pH profiles for the activities of the R195 mutants HPA .....                 | 96  |
| Figure 3.8  | The pH profiles for the activities of the R337 mutants HPA .....                 | 97  |
| Figure 3.9  | The catalytic acid/base residues and Arg337 .....                                | 98  |
| Figure 3.10 | Reduction of rates by overlapping pK <sub>a</sub> values .....                   | 99  |
| Figure 3.11 | The pH profiles for the activity of the N298S mutant HPA.....                    | 100 |
| Figure 3.12 | Guanidine inhibition of Arg337Ala mutant .....                                   | 101 |
| Figure 4.1  | Subsite for HPA.....   | 108 |
| Figure 4.2  | Mechanism for the transglycosylation.....  | 109 |
| Figure 4.3  | Hypothetical Michaelis-Menten type plot for a transglycosylating enzyme          | 110 |
| Figure 4.4  | Tendamistat complexed to porcine pancreatic $\alpha$ -amylase .....              | 112 |
| Figure 4.5  | Structure of acarbose .....  | 114 |
| Figure 4.6  | Structure of the modified “acarbose” .....                                       | 115 |
| Figure 4.7  | Structure of the extended inhibitors .....                                       | 117 |
| Figure 4.8  | Structure of salacinol .....   | 118 |
| Figure 4.9  | Structures of two blocked substrates .....                                       | 120 |
| Figure 4.10 | Structure of a fluorescence quenched substrate.....                              | 122 |
| Figure 4.11 | Products analysis of the HPA catalyzed reaction of $\alpha$ DNP-G2 .....         | 130 |
| Figure 4.12 | Structure of $\alpha$ CNP-G3.....  | 132 |
| Figure 4.13 | Product analysis of the HPA catalyzed reaction of $\alpha$ DNP-G3 after 20 ..... | 134 |
| Figure 4.14 | The Michaelis-Menten plot $\alpha$ DNP-Glc hydrolysis .....                      | 135 |
| Figure 4.15 | Product analysis of the HPA catalyzed reaction of $\alpha$ DNP-Glc.....          | 135 |
| Figure 4.16 | Hydrolysis of $\alpha$ DNP-G3 in the presence acarbose. ....                     | 139 |
| Figure 4.17 | Pre-incubation experiment.....   | 141 |
| Figure 4.18 | Binding mode of GHIL in HPA .....  | 146 |
| Figure 4.19 | Product analysis of extension reaction with GHIL.....                            | 150 |

## List of tables

|   |     |
|---|-----|
| Table 1.1 $K_i$ values for various bicyclic glucose analogues ..... | 16  |
| Table 1.2 $K_i$ values for imino-sugars .....                       | 28  |
| Table 4.1 $IC_{50}$ values for extended inhibitors .....            | 117 |
| Table 4.2 Kinetic parameters for substrates of HPA .....            | 123 |
| Table 5.1 Oligonucleotides used in thesis.....                      | 166 |

## List of schemes

|  |     |
|--|-----|
| Scheme 2.1 The synthesis of 5FGulF and the proposed synthesis of 5FManF .....      | 44  |
| Scheme 2.2 A kinetic model of the reaction of fluorosugars with glycosidases ..... | 45  |
| Scheme 2.3 An outline of the synthesis of 2FManF .....                             | 64  |
| Scheme 4.1 Kinetic model for transglycosylation and hydrolysis.....                | 110 |
| Scheme 4.2 Sample scheme for a coupled assay .....                                 | 120 |
| Scheme 4.3 Outline for the synthesis of $\alpha$ DNP-G2.....                       | 126 |
| Scheme 4.4 Outline for the synthesis of $\alpha$ DNP-G3.....                       | 128 |

## List of abbreviations

|                   |   |
|-------------------|---|
| Abg               | <i>Agrobacterium</i> sp. $\beta$ -retaining glucosidase |
| $\alpha$ DKIE     | $\alpha$ -deuterium kinetic isotope effect              |
| $\alpha$ DNP-G2   | 2,4-dinitrophenyl $\alpha$ -maltoside                   |
| $\alpha$ DNP-G3   | 2,4-dinitrophenyl $\alpha$ -maltotrioside               |
| $\alpha$ DNP-G4   | 2,4-dinitrophenyl $\alpha$ -maltotetraoside             |
| $\alpha$ DNP-G5   | 2,4-dinitrophenyl $\alpha$ -maltopentaoside             |
| $\alpha$ DNP-G6   | 2,4-dinitrophenyl $\alpha$ -maltohexaoside              |
| $\alpha$ DNP-Glc  | 2,4-dinitrophenyl $\alpha$ -D-glucoside                 |
| 2FManF            | 2-deoxy-2-fluoro- $\alpha$ -D-mannosyl fluoride         |
| 5FGulF            | 5-fluoro- $\beta$ -L-gulosyl fluoride                   |
| 5FManF            | 5-fluoro- $\alpha$ -D-mannosyl fluoride                 |
| Ac <sub>2</sub> O | acetic anhydride  |
| AcCl              | acetyl chloride   |
| AcOH              | acetic acid   |
| AHA               | <i>Alteromonas halioplanctis</i> $\alpha$ -amylase      |
| Bcx               | <i>Bacillus circulans</i> $\beta$ -retaining xylanase   |
| BMGY              | buffered glycerol-complex medium                        |
| BMMY              | buffered methanol-complex medium                        |
| BSA               | bovine serum albumin                                    |
| CD                | circular dichroism                                      |
| Cex               | <i>Cellulomonas fimi</i> $\beta$ -retaining xylanase    |
| CGTase            | cyclodextrin glucanotransferase                         |
| DABCO             | diazobicyclo[2.2.2]octane                               |
| DMF               | <i>N,N</i> -dimethyl formamide                          |
| DNFB              | 2,4-dinitrofluorobenzene                                |
| DNP               | 2,4-dinitrophenol                                       |
| DNP-Man           | 2,4-dinitrophenyl $\alpha$ -D-mannoside                 |
| DNS               | 3,5-dinitrosalicylic acid                               |
| ELSD              | evaporative light scattering detector                   |
| ER                | endoplasmic reticulum                                   |
| ESI               | electrospray ionization                                 |
| Et <sub>2</sub> O | diethyl ether   |
| EtOAc             | Ethyl acetate   |
| EtOH              | ethanol   |
| FRET              | fluorescence resonance energy transfer                  |
| Fuc               | fucose  |
| G1                | glucose   |
| G2                | maltose   |
| G2F               | $\alpha$ -maltosyl fluoride                             |
| G3                | maltotriose   |
| G3F               | $\alpha$ -maltotriosyl fluoride                         |
| G4                | maltotetraose   |
| G5                | maltopentaose   |

|                  |  |
|------------------|--|
| G6               | maltohexaose   |
| Gal              | galactose  |
| GHIL             | D-gluconohydroximino-1,5-lactam                              |
| Glc              | glucose  |
| GlcNAc           | <i>N</i> -acetylglucosamine                                  |
| GMII             | Golgi $\alpha$ -mannosidase II                               |
| h                | hours  |
| HPA              | human pancreatic $\alpha$ -amylase                           |
| HPLC             | high pressure liquid chromatography                          |
| IC <sub>50</sub> | inhibitory concentration                                     |
| LAMAN            | lysosomal $\alpha$ -mannosidase                              |
| LB               | Lauria Bertani medium  |
| LC               | liquid chromatography  |
| MALDI-TOF        | matrix assisted laser desorption ionization - time of flight |
| Man              | mannose  |
| MeOH             | methanol   |
| MS               | mass spectrometry  |
| MS-MS            | tandem mass spectrometry                                     |
| NBS              | <i>N</i> -bromosuccinimide                                   |
| NeuAc            | sialic acid  |
| NMR              | nuclear magnetic resonance                                   |
| PCR              | polymerase chain reaction                                    |
| PetEt            | petroleum ether 35-60  |
| PNP              | <i>p</i> -nitrophenol  |
| PNP-G2           | <i>p</i> -nitrophenyl $\alpha$ -maltoside                    |
| PNP-G3           | <i>p</i> -nitrophenyl $\alpha$ -maltotrioside                |
| PNP-G4           | <i>p</i> -nitrophenyl $\alpha$ -maltotetraoside              |
| PNP-G5           | <i>p</i> -nitrophenyl $\alpha$ -maltopentaoside              |
| PNP-G6           | <i>p</i> -nitrophenyl $\alpha$ -maltohexaoside               |
| PPA              | porcine pancreatic $\alpha$ -amylase                         |
| sat.             | saturated  |
| SDS-PAGE         | sodium dodecasulfate-polyacrylamide gel electrophoresis      |
| TFA              | trifluoroacetic acid   |
| TLC              | thin layer chromatography                                    |
| UV               | ultraviolet  |
| YPD              | yeast extract peptone digest                                 |

## Amino acid Abbreviations

|               |   |     |
|---------------|---|-----|
| Alanine       | A | Ala |
| Arginine      | R | Arg |
| Asparagine    | N | Asn |
| Aspartate     | D | Asp |
| Cysteine      | C | Cys |
| Glutamate     | E | Glu |
| Glutamine     | Q | Gln |
| Glycine       | G | Gly |
| Histidine     | H | His |
| Isoleucine    | I | Iso |
| Leucine       | L | Leu |
| Lysine        | K | Lys |
| Methionine    | M | Met |
| Phenylalanine | F | Phe |
| Proline       | P | Pro |
| Serine        | S | Ser |
| Threonine     | T | Thr |
| Tryptophan    | W | Trp |
| Tyrosine      | Y | Tyr |
| Valine        | V | Val |

## Kinetic constants

|                    |  |
|--------------------|--|
| $k_{\text{cat}}$   | Catalytic rate constant                            |
| $K_{\text{d}}$     | Dissociation constant                              |
| $K_{\text{i}}$     | Dissociation constant for enzyme-inhibitor complex |
| $k_{\text{i}}$     | First order rate constant of inactivation          |
| $k_{\text{react}}$ | First order rate constant of reactivation          |
| $V_{\text{max}}$   | Maximal rate of an enzyme catalyzed reaction       |
| $K_{\text{m}}$     | Michaelis-Menten constant                          |

# Acknowledgments

I would like to thank a number of people whose help and collaboration were invaluable during the course of my research at UBC. First of all, I would like to thank my supervisor, Professor Stephen G. Withers for taking me into his lab and letting me stay for the past 6 years. I am indebted for your advices, encouragement and above all, for your patience. I would also like to thank Professor Christopher M. Overall for access to his lab and for all of his advice, especially in the early part of my PhD. I would especially like to thank Dr. Edwin Rydberg, Mrs. Yili Wang, and Mrs. Karen Rupitz for getting me started in the lab.

Much of this PhD would not have been possible without the collaboration of a number of groups. I would like to thank Professor Gary Brayer, Dr. Robert Maurus, Dr. Gary Sidhu, and Dr. Chunmin Li for their efforts in solving numerous structures of human pancreatic  $\alpha$ -amylase. I would also like to thank Professor David R. Rose and Dr. Douglas A. Kuntz for their supply of wild-type and mutant Golgi  $\alpha$ -mannosidase II, as well as for their efforts in solving structure of the covalent intermediates of these enzymes. Many thanks go to Professor Ole K. Tollersrud and Mr. Gry Evjen for their supply of bovine kidney  $\alpha$ -mannosidase. I would also like to thank Professor Mario Pinto for the library of potential  $\alpha$ -amylase inhibitors. I would also like to thank Dr. Tanja Wrodnigg, Dr. Hongming Chen, and Mr. Seung Li for synthesizing several key compounds. Many thanks also to Mr. Shouming He for helping me obtain my MS data.

I would like to thank Dr. Iben Damager and Professor Gregory Dake for the critical reading of this thesis. Of course, I would like to thank members of the Withers

group and Overall group, both past and present, for providing such a great working environment.

I'd like to thank several people for their support of my mental well-being. Many thank Jeanie Dougan and Tam Corbett for their constant prayers. I'd also like to thank my brother for his advice and perspectives on life. Finally, I am indebted to my parents for their constant support throughout this degree.

# Preface

Part of the material in Chapter 2 and Chapter 3 was previously reported in the following publications:

Numao S, He S, Evjen G, Howard S, Tollersrud OK, Withers SG: **Identification of Asp197 as the catalytic nucleophile in the family 38  $\alpha$ -mannosidase from bovine kidney lysosomes.** *FEBS Lett* (2000) 484: 175-178.

Numao S, Maurus R, Sidhu G, Wang Y, Overall CM, Brayer GD, and Withers SG: **Probing the role of the chloride ion in the mechanism of human pancreatic  $\alpha$ -amylase.** *Biochemistry* (2002) 41: 215-225.

The first of these papers involved the chemical labelling and identification of a catalytic residue in bovine kidney lysosomal  $\alpha$ -mannosidase. I was involved in the kinetic characterization of the inhibition of the inhibitor with this enzyme. I also labelled the enzyme and was involved in the analysis of mass spectrometric data. Finally I wrote the paper with minor modifications from my supervisor.

The second paper involved the mutational, structural and kinetic analysis of human pancreatic  $\alpha$ -amylase (HPA). I was involved in the mutation, expression and purification of HPA I also did the kinetic characterization of these mutant HPAs. Finally, I wrote this paper with modifications from my supervisor.

Signature of corresponding author:

# **Chapter 1 Introduction**

Carbohydrates are a class of biomolecules found ubiquitously in nature. Traditionally, these molecules have been seen as important in maintaining the structural integrity of organisms or as means of storage of energy. The classic examples of carbohydrates playing these two roles are the two major of polymers of glucose, namely, cellulose and starch.

In reality, however, the biological role of carbohydrates is much more diverse than would be suggested by these 'stereotypical' functions. Recent studies have shown that, among other things, sugars are involved in cell-cell adhesion (1), protein folding (2), protein trafficking (3) and signal transduction (4). In other words, these biomolecules add another level of control to the already complex dynamic of biological systems.

In order for carbohydrates to be involved in these varying roles, a number of enzymes that make and break specific bonds with sugars are required. There are two major classes of enzymes associated with such sugar metabolism – the glycosidases and the glycosyltransferases. The glycosidases are mainly involved in the cleavage of linkages between sugars while the glycosyltransferases are involved in the formation of these linkages. Considering the diversity in both the structure and function of carbohydrates, it is no surprise that there are huge numbers of these processing enzymes, each usually involved in the formation or cleavage of a specific sugar linkage.

This diversity of enzymes and the numerous biological pathways with which they are involved makes these classes of enzymes potential targets for drug design (5). In order to do this rationally, the detailed mechanisms of these enzymes must be understood. This thesis focuses on the mechanism of one class of glycosidases, the  $\alpha$ -retaining glycosidases.

## 1.1 Glycosidases

Glycosidases, or glycosyl hydrolases, are a group of enzymes that catalyse the hydrolysis of glycosidic linkages. The reaction is formally a nucleophilic substitution at the anomeric carbon of the donor sugar (glycone) and involves the displacement of a leaving group (aglycone) by an acceptor molecule (Figure 1.1). In the case of hydrolysis, this acceptor is a water molecule.

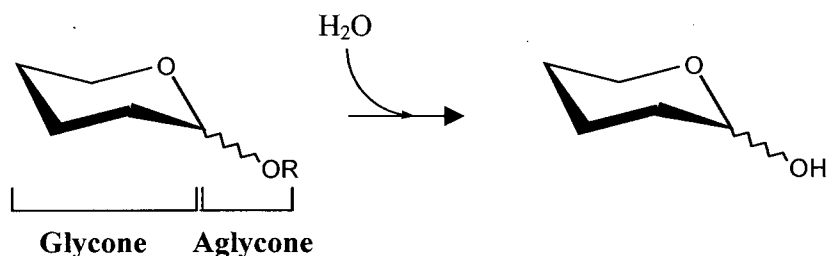


Figure 1.1 The hydrolysis reaction catalyzed by glycosidases.

In nature, the aglycone is often another sugar. However, this aglycone specificity is fairly flexible and synthetic glycosides containing aryl or halide leaving groups have been shown to act as substrates for many glycosidases. In contrast, the specificity towards the glycone portion is quite stringent and often only one type of sugar will be hydrolysed well by a particular enzyme. Therefore, the glycone specificity is often used in classifying or naming these glycosidases. In addition, these enzymes can be further subdivided based on the stereochemistry at the anomeric centre of the substrate and product. A glycosidase is classified as either an “ $\alpha$ ” or “ $\beta$ ” glycosidase based on the anomeric configuration of the substrate. Usually, an  $\alpha$ -glycosidase will only hydrolyse an  $\alpha$ -glycoside while a  $\beta$ -glycosidase will only hydrolyse a  $\beta$ -glycoside. The glycosidase

can further be grouped as either retaining or inverting (Figure 1.2) based on the anomeric stereochemistry of the product with respect to the substrate.

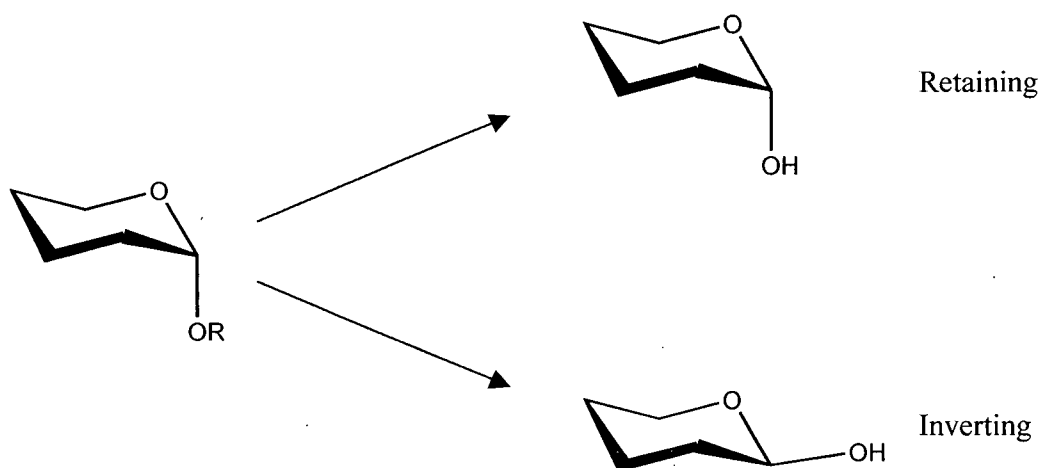


Figure 1.2 Stereochemical outcome of a glycosidase reaction, illustrated with an  $\alpha$ -glycosidase.

Therefore, the overall name of a glycosidase comes from the combination of these three classifications. For example, an enzyme that catalyzes the hydrolysis of an  $\alpha$ -glucoside with net retention of configuration at the anomeric centre is named an  $\alpha$ -retaining glucosidase.

In many cases, the substrate for a glycosidase will be a polymer in which case, the glycosidase may be classified as endo- or exo-glycosidase depending on the cleavage pattern of the substrate. Endo-glycosidases will cleave in the middle of a polymer while an exo-glycosidase cleaves from either ends of the polymer. In the case of endo-glycosidases, there are thought to be a number of “subsites” to accommodate the binding of polymer substrates. Each of these subsites would bind to a monomer subunit. To designate these subsites, Davies *et al.* proposed that the subsites flanking the bond to be cleaved be designated +1 (towards the reducing end of the polymer) and -1 (towards the

non-reducing end of the polymer) (6). The subsites further down would then be +2, +3, +4, etc or -2, -3, -4, etc. (Figure 1.3).

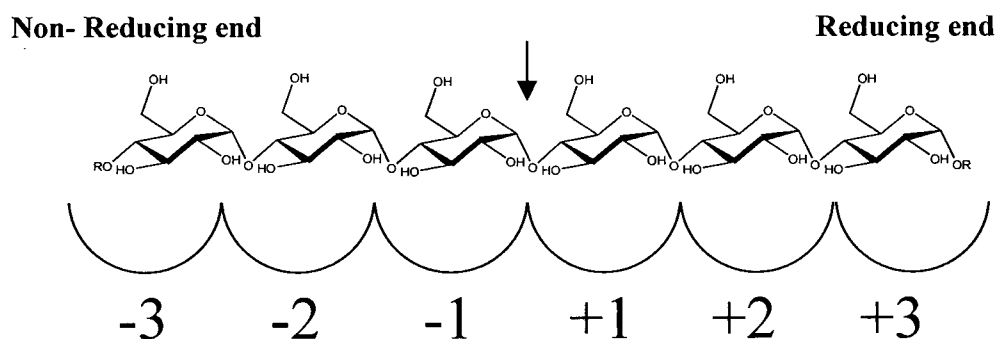


Figure 1.3 Nomenclature for subsites in endo-glycosidases, here shown for the case of an endo-glucosidase. The arrow refers to the bond being cleaved.

In addition to these traditional ways of classifying glycosidases, a more recent classification method through amino acid sequence homology has been developed (7-9). According to primary structure analysis, over 6000 glycosidases have been grouped into 89 families, with these numbers growing rapidly. This information is now available on the Internet (URL: <http://afmb.cnrs-mrs.fr/CAZY/>).

Although this classification is based on sequence similarities alone, members of a particular family often share other properties. For example, a particular family of glycosidase will exclusively contain either retaining or inverting glycosidases (10). Furthermore, in most cases, a family will be specific for either  $\alpha$ - or  $\beta$ -glycosides. Recently, the three-dimensional structures of many glycosidases have been solved. In all cases, the three-dimensional fold of the catalytic domain was conserved within families (11), further validating the hypothesis that members of a particular family are homologous. This is also consistent with the fact that families share common features such as stereochemical outcome.

## 1.2 Catalytic mechanism of glycosidases

The full catalytic efficiency of glycosidases has only recently been recognized when the half-life for solvolysis of an unactivated glycosidic linkage ( $\beta$ -methyl glucoside) under physiological conditions was determined to be 5 million years (12). Since glycosidases can hydrolyse glycosidic linkages under similar conditions with rates of up to  $1000 \text{ s}^{-1}$ , this means that they effect approximately a  $10^{17}$  fold increase in rate. In order to efficiently catalyze hydrolysis of these unreactive molecules, glycosidases primarily use one of two mechanisms, depending on whether the enzyme is inverting or retaining. The original versions of these mechanisms were first proposed by Koshland in 1953 (13), and were based on the stereochemical outcome of the reactions, as well as on known chemical mechanisms of similar uncatalyzed reactions. While the general features of the proposed mechanisms have stood the test of time, the finer details of how the enzyme achieves this significant rate enhancement have been added and refined over the years (14-18).

## 1.3 Mechanism of inverting glycosidases

An inverting glycosidase catalyzes a single step nucleophilic substitution at the anomeric centre whereby a water molecule displaces the aglycone (Figure 1.4) (13). This reaction goes through an oxocarbenium ion-like transition state, similar to the intermediate formed during the acid-catalyzed hydrolysis of glycosides (19). Two key active site carboxylic acid residues are known to be important in assisting this nucleophilic substitution. One of these residues acts as a catalytic base and is responsible for deprotonating the incoming water molecule. The other residue acts as a general acid catalyst and protonates the glycosidic oxygen, assisting it in departure. Consistent with

this hypothesis, all three-dimensional structures of inverting glycosidases solved to date have two carboxylic acid residues in their active site. From these structures, the average distance between these two residues was initially found to be 9.5 Å (20) though since this time, other structures of inverting glycosidases have revealed a broader range of separation (172). Regardless of the exact distance, this space allows for the attack of the water molecule in the presence of the aglycone.

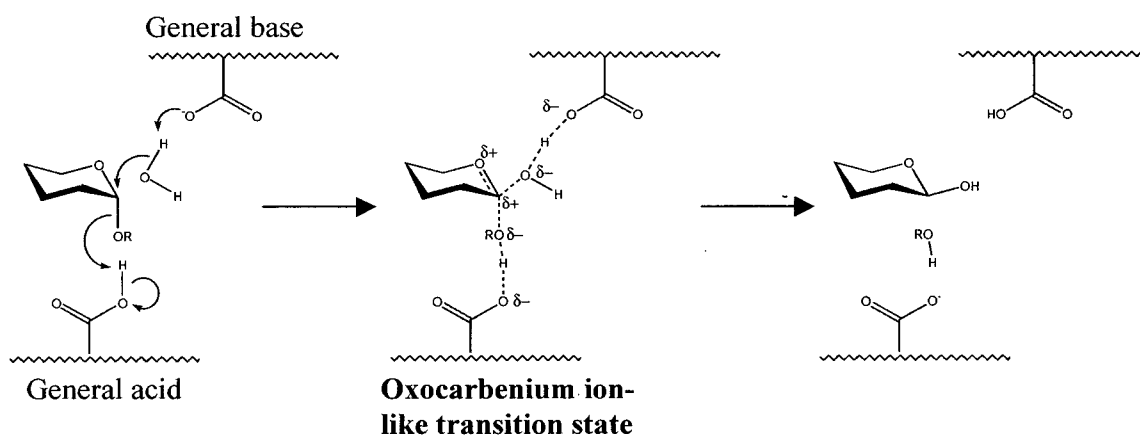


Figure 1.4 Proposed single displacement mechanism for an inverting  $\alpha$ -glycosidase.

For the purpose of this thesis, this group of enzymes will not be discussed in further detail.

## 1.4 Mechanism of retaining glycosidases

The original catalytic mechanism proposed by Koshland for retaining glycosidases was a two-step process (Figure 1.5) involving two displacement reactions at the anomeric centre (13) and therefore, referred to as the double displacement mechanism. In the first step of this mechanism, referred to as the glycosylation step, a catalytic nucleophile (a residue in the enzyme active site) makes a backside attack at the anomeric carbon of the glycone. This nucleophilic substitution results in the formation of

a covalent glycosyl-enzyme intermediate with inversion of stereochemistry at the anomeric centre. Departure of the aglycone is assisted by general acid catalysis, provided by another residue in the active site. In the second step of this reaction, referred to as the deglycosylation step, nucleophilic attack by a water molecule results in the hydrolysis of this intermediate. In this step, the conjugate base of the catalytic acid residue is thought to deprotonate the incoming water, assisting it with the attack. The overall reaction is therefore the hydrolysis of the glycosidic bond with net retention of configuration at the anomeric carbon. If the incoming nucleophile is not a water molecule but rather an alcohol, such as the hydroxyl group on a sugar, the reaction results in the formation of another glycosidic linkage. This phenomenon, referred to as transglycosylation, is seen in glycosidases under high substrate concentrations.

### **1.5 Detailed mechanistic studies of $\beta$ -glycosidases**

Since this initial proposal of the double displacement mechanism, numerous studies to verify this mechanism, as well as additional studies to further elucidate the details have been carried out. According to the particular attributes being characterized, these studies can be grouped into the following categories:

- 1) the catalytic nucleophile
- 2) the oxocarbenium ion-like transition state
- 3) the acid/base catalyst
- 4) the covalent intermediate
- 5) non-covalent interactions
- 6) sugar conformations.

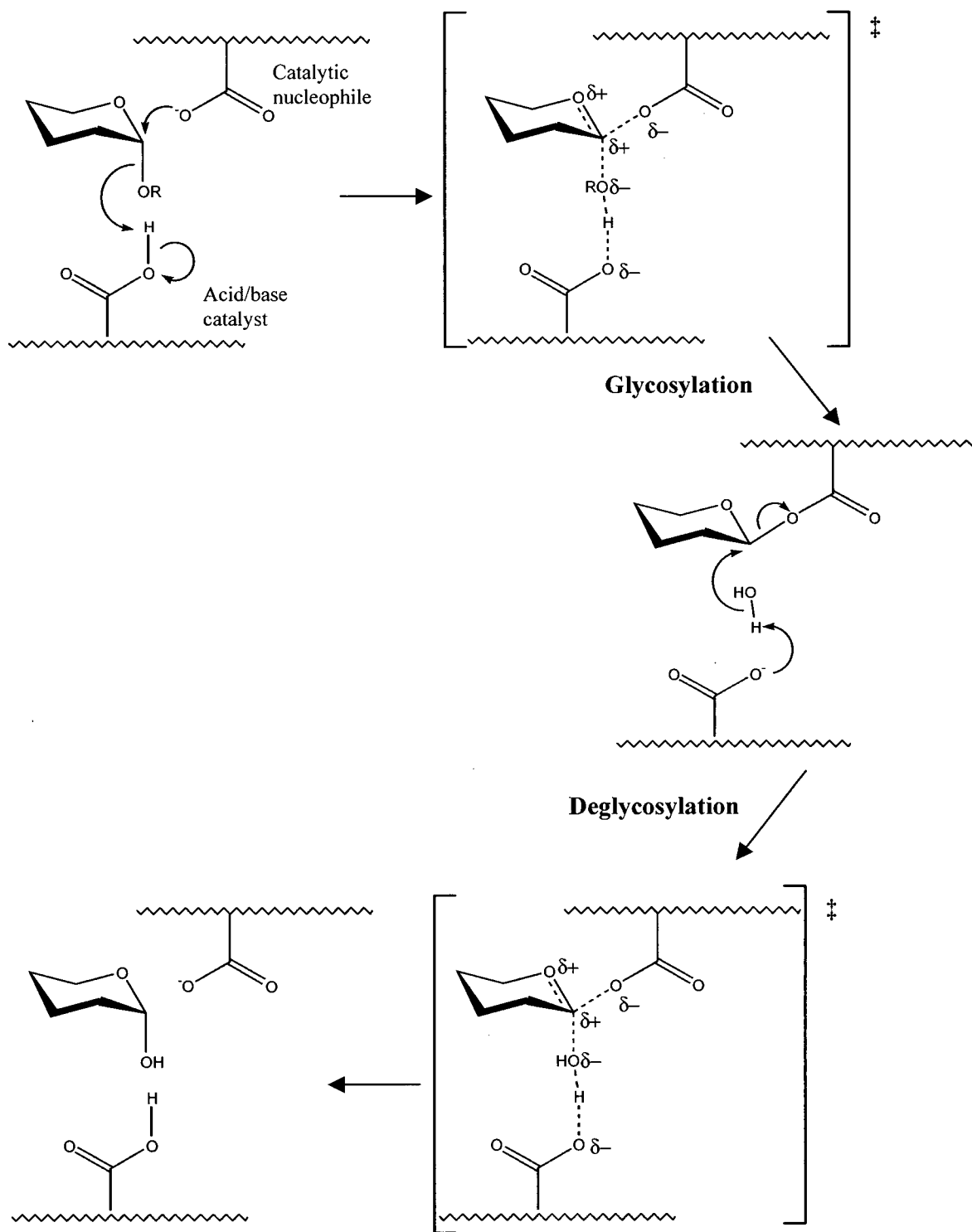


Figure 1.5 Proposed double displacement mechanism for a retaining  $\alpha$ -glycosidase.

Many of the detailed mechanistic studies on retaining glycosidases have been carried out on  $\beta$ -retaining glycosidases. This was in large part due to the availability of cloned enzymes that could be used as models, and the relative ease of synthesis of the substrates required for these glycosidases compared with their  $\alpha$ - counterparts.

### **1.5.1 The catalytic nucleophile**

Three-dimensional structures of glycosidases with a ligand bound in the active site reveal a carboxylic acid residue (aspartate or glutamate) positioned to potentially act as a nucleophile (21). From primary structure analysis, these carboxylic acids are conserved between all glycosidases of the same family (11), suggesting that they play a very important role. This role has been further elucidated through mutational studies and trapping experiments (the latter will be described in 1.5.5).

Mutation of these putative catalytic nucleophiles from a carboxylic acid to an alanine in the  $\beta$ -retaining glucosidase from *Agrobacterium* sp. (Abg) resulted in essentially an inactive enzyme ( $10^7$  fold decrease in  $k_{\text{cat}}$ ) (22). Such a rate decrease is expected considering the importance of the catalytic nucleophile in the double displacement mechanism. Interestingly, in the presence of a small external nucleophile such as azide ion, this mutant enzyme exhibits significant cleavage (up to one-tenth the original  $k_{\text{cat}}$ ) when using activated glycosidic substrates (20). The stereochemical outcome of the reaction in this case is net-inversion of configuration at the anomeric centre. This result suggests that the azide, which does not require general base catalysis for nucleophilic attack, is replacing the carboxylate as the nucleophile in the first step (Figure 1.6). In other words, the mutation has converted the mechanism of a retaining glycosidase to that of an inverting enzyme. This chemical “rescue” is a general

phenomenon with  $\beta$ -retaining glycosidases and it has been a method for verifying the identity of the catalytic nucleophile through mutagenesis (18).

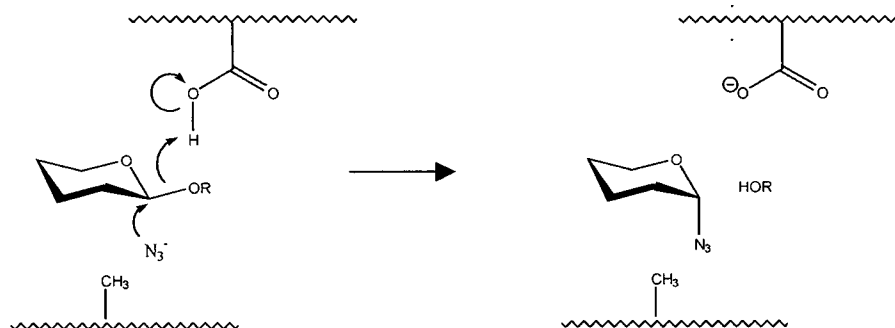


Figure 1.6 Mechanism for the chemical rescue by azide of the activity of a nucleophile mutant glycosidase.

### 1.5.2 The oxocarbenium ion-like transition state

The transition states for both the glycosylation and deglycosylation steps are thought to closely resemble oxocarbenium ions. In this structure, the positive charge developed on the sugar is distributed between the anomeric carbon and the ring oxygen. Because of this charge distribution, resulting from partial double bond formation between the ring oxygen and anomeric carbon, there is a requirement that C-5, O-5, C-1 and C-2 be on the same plane. Therefore, the transition state for cleavage of a glucoside, for example, would most likely adopt a half-chair conformation (Figure 1.7).

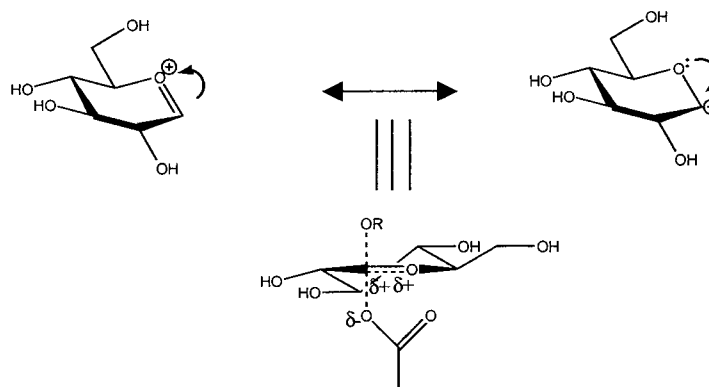


Figure 1.7 Proposed structure of the oxocarbenium ion-like transition state for hydrolysis of a glucoside.

Support for this kind of transition state has come in several different ways. One of the key pieces of evidence comes from  $\alpha$ -deuterium kinetic isotope effects ( $\alpha$ DKIE) measured with several  $\beta$ -retaining glycosidases (23-27). For example, in the case of Abg, in both the glycosylation step and deglycosylation steps, the ratio of the rates for hydrolysis of the normal substrate compared with that of a substrate deuterated at the anomeric carbon ( $k_H/k_D$ ) was found to be greater than unity (26). Exchanging the  $\alpha$ -deuterium affects the C-H bend vibrational mode (seen in  $sp^3$  hybridized structures) more than the C-H out-of-plane bend vibrational mode (seen in  $sp^2$  hybridized structures). Therefore, a positive  $\alpha$ DKIE is indicative of the transition state having more  $sp^2$  character than the ground state, indicating that the anomeric carbon is  $sp^2$  hybridized at both transition states. This is also consistent with Brønsted plot analysis for Abg, which suggests that there is significant cleavage of the bond to the leaving group at the transition state (dissociative) of the glycosylation step (26).

Circumstantial evidence for the charge distribution comes from the use of fluorine-substituted sugars as substrates. Placing an electron-withdrawing group such as fluorine at the 2- or 5- position of the sugar inductively destabilizes positive charge development at the anomeric carbon and ring oxygen respectively. As would be expected for a reaction with an oxocarbenium ion-like transition state, this modification reduces the rate of hydrolysis significantly in  $\beta$ -retaining glycosidases (28, 29). Replacement of hydroxyl groups with fluorine will also modify potential non-covalent interactions of the substrate with the enzyme. Therefore, this decrease in activity may also in part be due to loss of transition state stabilization by the enzyme arising from such interactions (30).

Enzymes are generally believed to catalyze reactions by binding better to the transition state than to the ground state, leading to the suggestion that transition state analogues should act as very good inhibitors of enzymes. With the glycosidases, it has been estimated from the rate enhancement observed, that the affinity of the enzyme towards the transition state should correspond to a 'dissociation constant' on the order of  $10^{-22}$  M (12). Therefore, compounds that closely resemble an oxocarbenium ion should be extremely tight binding inhibitors of glycosidases. Indeed, a number of compounds either mimicking the shape or charge distribution of the transition state have been found to be good inhibitors of  $\beta$ -retaining glycosidases with  $K_i$  values in the nanomolar range (Figure 1.8).

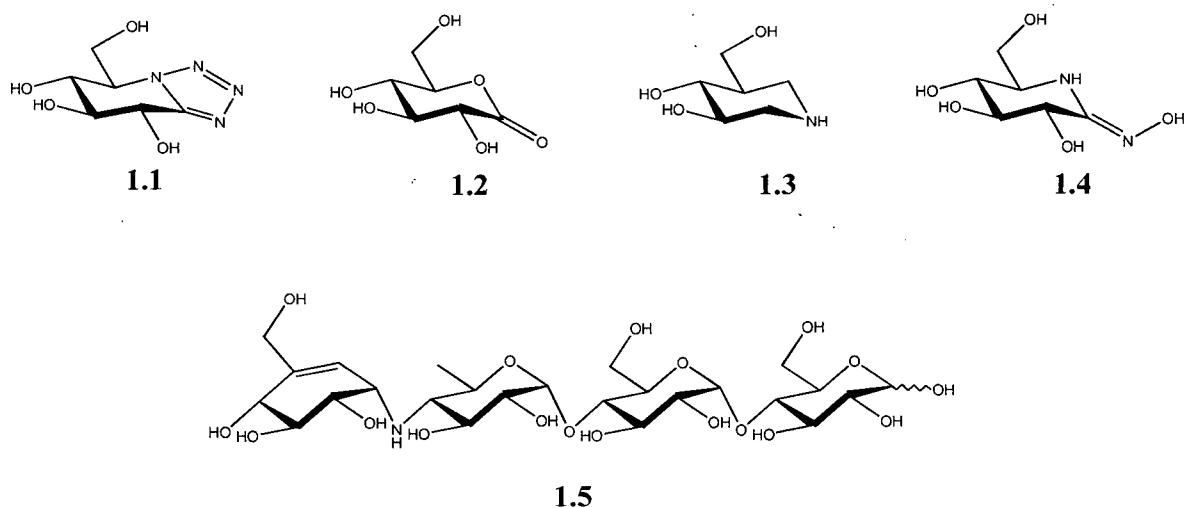


Figure 1.8 Some representative structures of proposed transition state analogues for glycosidases: gluco-tetrazole (1.1), gluconolactone (1.2), isofagamine (1.3),  $\beta$ -hydroxygluconolactam (1.4), and acarbose (1.5).

### 1.5.3 The general acid/base catalyst

As with the catalytic nucleophile, the acid/base catalyst plays an important part in the hydrolysis of glycosidic bonds. This can be seen from the drastic lowering of rates seen in mutational studies where the acid/base catalyst is altered to a residue unable to

perform this task (15, 31, 32). This is consistent with model studies on small molecules done by Kirby *et al.*, where it was suggested that general acid/base catalysis might account for as much as 8-9 kcal mol<sup>-1</sup> in transition state stabilization (33).

From structural studies, this acid/base catalyst was also found to be a carboxylic acid residue situated around 5.5 Å away from the catalytic nucleophile (20). The shorter distance compared with the inverting glycosidases reflects the fact that the active site does not require simultaneous accommodation of both the aglycone and a water molecule.

Interestingly, when the distance between the two active site carboxylic acids was increased by mutating the catalytic glutamate (acid/base catalyst) to an aspartate in the β-retaining xylanase from *Bacillus circulans* (Bcx), the second-order rate constant ( $k_{cat}/K_m$ ) was found to be 400 fold lower than the rate for the wild-type enzyme (34). Decreasing the distance between the residues by modifying the same glutamate to a carboxymethylated cysteine resulted in a 25 fold lowering of the rate. Although this decrease is significant, it was not as large as that associated with the complete removal of a carboxylic acid (by mutation to glutamine), which results in no measurable activity on xylan, a substrate requiring acid catalysis. This suggests that the precise positioning of this residue is important, but not essential for catalysis. In contrast, decreasing the length of the residue acting as the catalytic nucleophile in the same enzyme by making a Glu78Asp mutation resulted in very large lowering of the rate (1600-5000 fold) (35).

Despite this apparent leniency in positioning, some interesting observations concerning the location of the acid/base catalyst have been made from studies with bicyclic sugar analogue inhibitors. It was observed that the tetrazole (1.1) and imidazole

(1.6) analogues of glucose (Figure 1.9) were good inhibitors of  $\beta$ -retaining glucosidase such as sweet almond  $\beta$ -glucosidase (36, 37). In contrast, the 1,2,3-triazole (1.7) analogue had significantly higher  $K_i$  values (38) (see Table 1.1), even though structural analysis had shown that the sugar ring adopts similar half chair conformations in all four cases. When analogues of other sugars were synthesized, the results were generally the same with their respective glycosidase. This difference in inhibition was attributed to the presence and orientation of a lone pair at the glycosidic nitrogen of compounds 1.1 and 1.6, which is thought to be positioned exactly to interact with the acid/base catalyst. This lone pair is not present in the poor inhibitor 1.7.

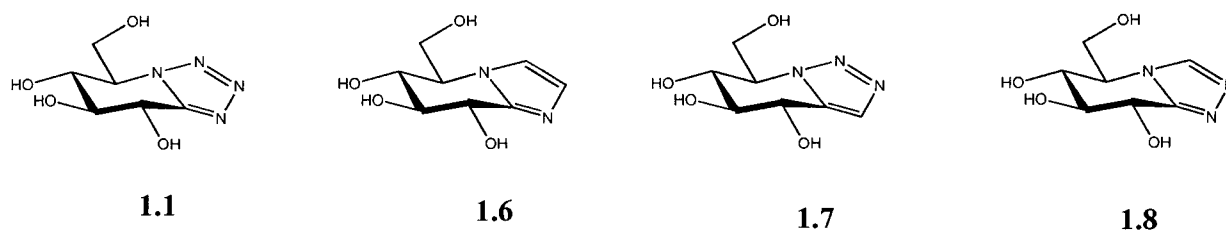


Figure 1.9 Structures of bicyclic inhibitors of  $\beta$ -glycosidases: gluco-tetrazole (1.1), gluco-imidazole (1.6), 1,2,3-gluco-triazole (1.7), and 1,2,4-gluco-triazole (1.8).

This led to the proposal that the acid/base catalyst was not positioned above or below the plane of the sugar, as schematically drawn in Figure 1.5, but rather in-plane in a “lateral” position (Figure 1.10) (39). To confirm this hypothesis, the 1,2,4-triazole analogue 1.8 (Figure 1.9) was synthesized (40). Since this compound contains a “glycosidic” nitrogen, it is expected to be a good inhibitor of  $\beta$ -retaining glucosidases. Indeed, this glucose analogue was found to be an inhibitor of a  $\beta$ -retaining glucosidase from almond with a  $K_i$  value in the low micromolar range (Table 1.1). Again, the manno- and galacto- analogues showed similar inhibitory activities towards their respective  $\beta$ -retaining glycosidases.

|                               | 1.1         | 1.6         | 1.7            | 1.8        |
|-------------------------------|-------------|-------------|----------------|------------|
| $\beta$ -glucosidase (almond) | 150 $\mu$ M | 0.1 $\mu$ M | > 8000 $\mu$ M | 19 $\mu$ M |

Table 1.1 Comparison of the  $K_i$  values for various bicyclic glucose analogues with sweet almond  $\beta$ -glucosidase (39).

One corollary of this lateral protonation hypothesis is that there are two possible directions from which protonation can take place – either from the *anti* or *syn* side of the ring oxygen (Figure 1.10). In fact, from three-dimensional structural alignment studies, it has been found that all the acid/base catalysts of all  $\beta$ -retaining glycosidases are located in either of these positions. Further evidence for this *anti* or *syn* classification came from inhibition studies using the imidazole sugar with a “*syn* protonator” and an “*anti* protonator”. Because these imidazole sugars have lone pairs *anti* to the ring oxygen, it would be expected that these inhibitors would interact better with *anti* protonators than with *syn* protonators. Indeed, it was found that for a family 10 xylanase (*anti* protonator), the  $K_i$  value of the imidazole analogue of xylobiose is in the nanomolar range, while for a family 11 xylanase (*syn* protonator), the  $K_i$  value is in the millimolar range (41). Structural studies on family 5 and 10 enzymes have also confirmed this key interaction (42, 43). However, this result on its own does not prove the hypothesis since these two enzyme families are thought to operate via transition states of different conformation. Differences in affinity could also reflect the difference in these transition state conformations.

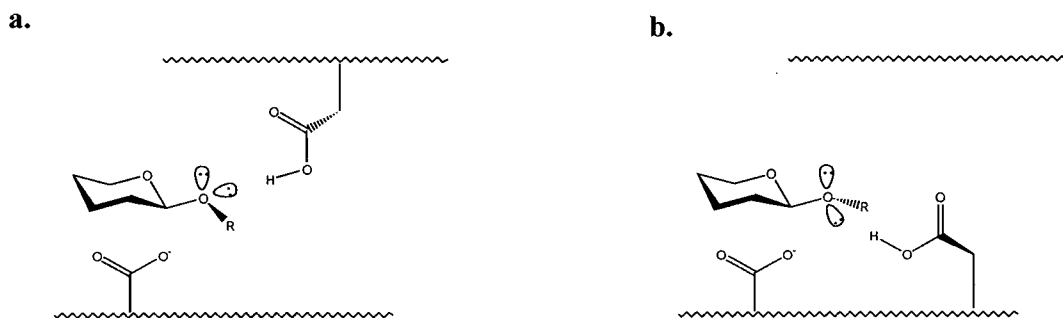


Figure 1.10 Positioning of the acid/base catalyst residue according to the lateral protonation mechanism. (a) Syn protonator and (b) anti protonator.

As with the nucleophile mutants, the catalytic activity of an inactive acid/base mutant enzyme can also be rescued on the addition of an external nucleophile such as azide, which attacks in place of water (Figure 1.11). With these mutant enzymes, a substrate with a good leaving group will undergo the glycosylation step without acid catalysis. However, deglycosylation, where the water requires deprotonation, will be much slower in the absence of this residue. If a good nucleophile not requiring general base catalysis is added, the catalytic activity is restored. In the case of the acid/base mutant of Abg, a 300-fold increase in  $k_{cat}$  was seen upon the addition of 200 mM azide (44). The product formed in this reaction will have the same configuration at the anomeric carbon as the substrate. This is in contrast to the case with the catalytic nucleophile mutant enzymes where inversion of configuration was seen when the rescue experiment was carried out. Therefore, the azide rescue studies, combined with product stereochemistry analysis, may be used to distinguish between mutation of the catalytic nucleophile and acid/base catalyst (18).

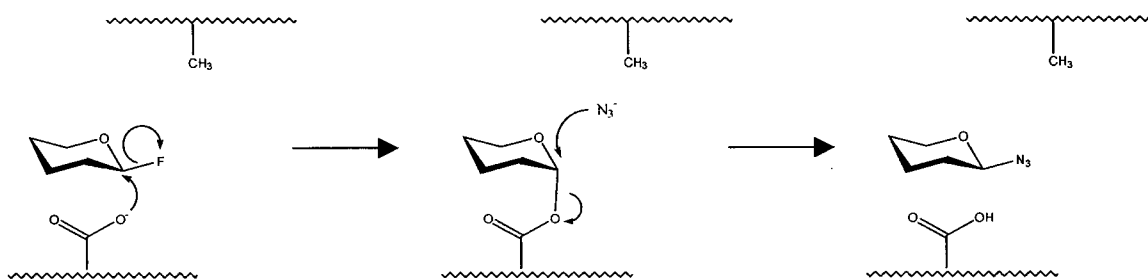


Figure 1.11 Mechanism for the chemical rescue by azide of the activity of an acid/base mutant glycosidase.

One of the key features of the acid/base catalyst is that the residue acts as both a general acid and a general base catalyst. The  $pK_a$  of the residue must therefore shift from a high  $pK_a$  in the glycosylation step to a lower  $pK_a$  in the deglycosylation step. Indeed, elegant NMR studies by McIntosh *et al.* showed that for the  $\beta$ -retaining xylanase from *Bacillus circulans* (Bcx), the  $pK_a$  of the catalytic base was modulated roughly 2.5  $pK_a$  units in going from the free enzyme to the glycosyl-enzyme intermediate (45). This “ $pK_a$  cycling” is most likely the result of different charge states of the nucleophilic carboxylic acid. In the free enzyme, this residue is negatively charged, thereby increasing the  $pK_a$  of the catalytic acid/base residue. In the intermediate, however, this residue becomes neutral as it forms a covalent bond with the glycosyl moiety. Therefore, it no longer perturbs the  $pK_a$  of the acid/base catalyst and as a result, the  $pK_a$  of this residue decreases by about 2.5  $pK_a$  units.

#### 1.5.4 The covalent intermediate

The nature of the intermediate in the double displacement mechanism has always been a controversial issue. As is drawn in Figure 1.5, the intermediate of this reaction is a glycosyl-enzyme intermediate with a covalent bond between the sugar and the enzyme nucleophile. This differs from the widely accepted “textbook” mechanism where an ion-

pair intermediate forms, involving an oxocarbenium ion and an active site carboxylate. This ion-pair mechanism has its origins in an early crystal structure of hen egg-white lysozyme (46). In this work, the lysozyme structure was determined complexed with an oligosaccharide bound to the -4 to -2 subsites (lysozyme has a total of 6 subsites corresponding to subsites -4 to +2). When the sugars for the -1 to +2 subsites were modelled in, it was evident that the anomeric carbon of the -1 sugar was too far from the putative catalytic nucleophile for covalent catalysis to take place. A more recent study with a substrate bound at subsites -3 to -1 has also suggested that nucleophilic catalysis is unlikely without major conformational changes within the active site (47). From this original study, lysozyme has become a case study for glycosidase mechanisms.

A method of probing the nature of the intermediate is to use  $\alpha$ -deuterium kinetic isotope effects ( $\alpha$ DKIE). If the intermediate is an oxocarbenium ion and is ion paired to the active site carboxylate, then the anomeric carbon of the intermediate species should be  $sp^2$  hybridized. However, if the intermediate is covalently linked to the enzyme, then the anomeric carbon should be  $sp^3$  hybridized. In both cases, the transition states of both mechanisms are thought to be oxocarbenium ion-like with  $sp^2$  hybridized anomeric centres. As was mentioned earlier, an  $\alpha$ DKIE greater than unity occurs when the anomeric centre at the transition state has more  $sp^2$  character than that of the ground state. Therefore, if a covalent intermediate does form, the  $\alpha$ DKIE for the deglycosylation step should be greater than unity. In contrast, the  $\alpha$ DKIE for the deglycosylation step for an ion-pair intermediate should be less than unity. In all studies to date where the  $\alpha$ DKIE was measured for the deglycosylation,  $k_H/k_D$  was found to be greater than unity (14); consistent with a covalent intermediate.

Unfortunately, in the classic glycosidase, lysozyme, the rate constants for the two steps are such that it is not possible at present to “see” kinetically the deglycosylation step. Therefore, it had not been possible, until recently, to definitively conclude that a covalent intermediate occurs in this enzyme (*vide infra*).

#### ***1.5.5 Trapping of the covalent intermediate***

Direct isolation of the covalent intermediates of glycosidases has been accomplished in several different ways (48, 49). In all cases, these methods involve somehow decreasing the rate of the deglycosylation step compared to that for glycosylation. This results in the accumulation or “trapping” of this intermediate.

One of the key methods for trapping has involved the use of 2- and 5-fluorosugars as mechanism based inactivators (Figure 1.12a) (50). In the double displacement mechanism, both the glycosylation and deglycosylation steps proceed via oxocarbenium ion-like transition states. As was previously discussed, there is significant positive charge development on both the endocyclic oxygen and anomeric carbon. By attaching an electron-withdrawing group such as fluorine on the carbon adjacent to the site of charge development, both these transition states can be destabilized and the rate lowered. However, if a substrate with a good leaving group such as fluoride or dinitrophenolate (DNP) is used, the rate of the glycosylation step may be increased relative to the rate of deglycosylation. If this difference in rates is great enough, then accumulation of the intermediate may occur (Figure 1.12b).

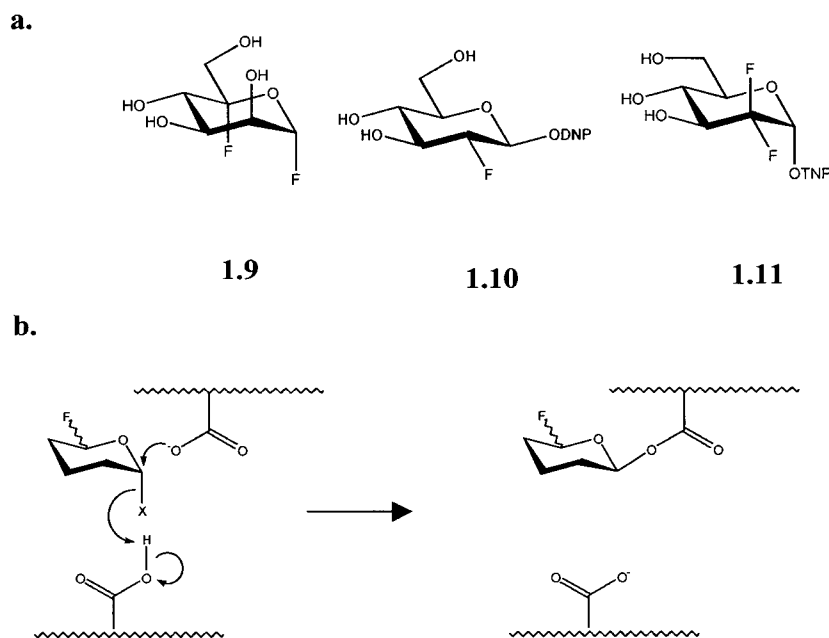


Figure 1.12 (a) Structures of some representative fluoro-inactivators: 5-fluoro- $\alpha$ -D-mannosyl fluoride (**1.9**), 2,4-dinitrophenyl 2-deoxy-2-fluoro- $\beta$ -D-glucoside (**1.10**), and 2,4,6-trinitrophenyl 2-deoxy-2,2-difluoro- $\alpha$ -D-glucoside (**1.11**). (b) Mechanism for the inactivation of a glycosidase by a fluorosugar (X = activated leaving group).

Another approach to trap the intermediate involves the use of mutant enzymes (51, 52). In the double displacement mechanism, both the glycosylation and deglycosylation steps require the acid/base catalyst. If this residue is mutated to a residue not able to perform this task, then the rates of both these steps are decreased. If a substrate with a good leaving group such as fluoride or DNP is used, whereby minimal acid catalysis is required for departure, then the glycosylation step is little affected by the mutation (Figure 1.13). However, deglycosylation, which requires general base catalysis, remains slow, resulting in accumulation of the intermediate.

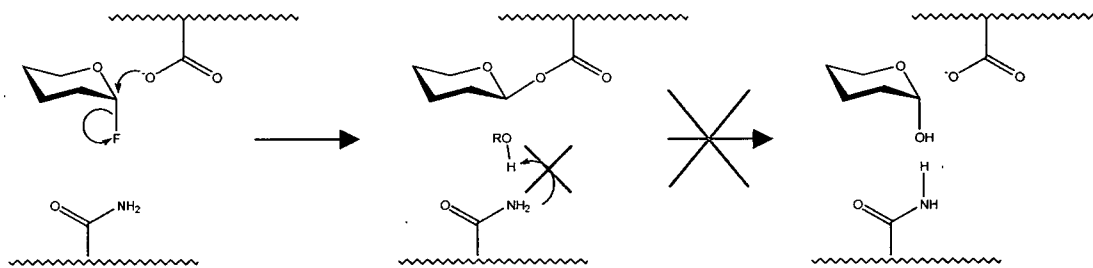


Figure 1.13 Mechanism for the trapping of an intermediate by the using an acid/base catalyst mutant enzyme and a glycosyl fluoride.

The trapped intermediate may be detected by electrospray ionization mass spectrometry (ESI-MS) (53) or by  $^{19}\text{F}$  NMR in the case of fluorosugars (54). These intermediates may be proteolytically digested to identify the residue that acts as the catalytic nucleophile. In fact, a number of nucleophiles have been labelled and identified by means of tandem mass spectrometry experiments (MS-MS; see chapter 2) (55). In recent years, this intermediate has also been visualized by determining the structure of the trapped intermediate using X-ray crystallography. One of the most interesting of these covalent intermediate structures is that of the textbook glycosidase, hen egg-white lysozyme, that was trapped using a combination of the fluorosugar and mutagenesis methods (56).

### 1.5.6 Non-covalent interactions

Linus Pauling suggested in the 1940s that enzymes catalyze reactions by binding to the transition state better than to the ground state (57). Residues in an enzyme active site should therefore be positioned so that new, strong interactions are formed during the transformation of the substrate from the ground state to the transition state. This is evident from studies on Abg where the hydroxyl groups of the substrate were systematically replaced by either a fluorine or hydrogen. The kinetic constants for

enzymatic hydrolysis were determined for each of these modified substrates. The study showed that each hydroxyl group contributes 3-7 kJ/mol towards the binding of the transition state, as was seen by a lowering of the rate constant ( $k_{\text{cat}}$ ) (30). The only exception to this was the 2-hydroxyl group, which contributed significantly more to the stabilization of the transition state (18-22 kJ/mol).

The three-dimensional structure of the covalent intermediate of a  $\beta$ -retaining xylanase from *Cellulomonas fimi* (Cex) has shed some light on the importance and identities of these interactions at the 2-position (52). In the  $\beta$ -retaining glycosidases, the 2-hydroxyl group sits in close proximity to the incoming enzymatic nucleophile. On formation of the covalent intermediate, the non-bonding oxygen of the carboxylic acid forms a short hydrogen bond with the 2-hydroxyl group of the sugar, suggesting that this interaction is also very important in stabilizing the transition state.

Another interaction worth noting is the interaction between an active site tyrosine and the ring oxygen in the structure of a covalent intermediate of Bcx (58). In this structure, the hydroxyl group on the tyrosine forms a bifurcated hydrogen bond with the ring oxygen and glycosidic oxygen of the catalytic nucleophile residue. It is thought that upon bond cleavage, the hydrogen bond develops to the glycosidic oxygen. At the same time, dipolar interactions can take place between the ring oxygen and hydroxyl group oxygen of the tyrosine. This interaction could therefore stabilize charge development on the ring oxygen. Equally, the interaction of the tyrosine with the ring oxygen could destabilize the ground state, which upon going to the transition state gets relieved.

### 1.5.7 Sugar conformations

Sugars exist as a number of different conformers (Figure 1.14). In an enzyme active site, non-covalent interactions and steric hindrance from active site residues can force the sugar to adopt a normally unfavourable conformation. Indeed, this has been seen in several structures of  $\beta$ -retaining glycosidases where a substrate or substrate analogue was bound across its active site (59-61). In these cases, the sugar moiety in the -1 subsite of the glycone adopts a  ${}^1S_3$  skew boat conformation. Structural determination of a  $\beta$ -retaining mannanase (where the sugar adopts a  ${}^1S_5$  structure) has shown that, while substrate distortion seems to be a general trend in  $\beta$ -retaining glycosidases, the conformation is not always the same (62).

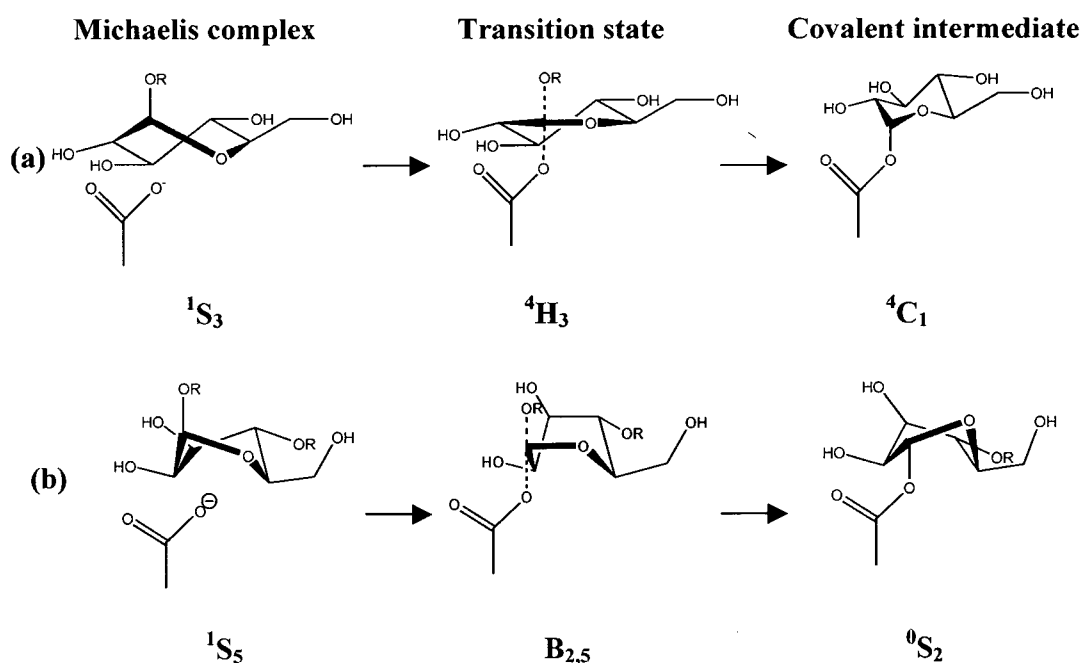


Figure 1.14 Conformations adopted by the substrate along the glycosylation step of a (a)  $\beta$ -glucosidase and (b)  $\beta$ -mannanase (adopted from (62)).

This distortion aids catalysis in several ways. First of all, during nucleophilic attack of the anomeric centre, the enzymatic nucleophile approaches the reaction centre from the opposite face to that of the leaving group. The problem for such attack on a  $\beta$ -

glycoside in a  ${}^4C_1$  chair conformation is that the H-3 and H-5 protons sterically hinder the  $\alpha$ -face. By adopting a skew boat conformation such as the  ${}^1S_3$  skew boat, this hindrance can be minimized. The distortion towards a skew boat form also moves the conformation of the substrate closer to that of the oxocarbenium ion-like transition state. Finally, the pseudo-axial orientation of the leaving group positions the ring oxygen lone pair antiperiplanar to the scissile bond, as required for hydrolysis according to stereoelectronic theories (63).

The structures of the covalent intermediate for several  $\beta$ -retaining glycosidases have shown that the  $\alpha$ -glycosyl-enzyme intermediate does not adopt a constrained conformation but rather, it adopts a  ${}^4C_1$  chair (52, 56, 61, 64). Because in the intermediate, the leaving group is axial, the sugar conformation satisfies both the stereoelectronic and steric requirements for cleavage alluded to above. More recently, several exceptions have been found. In the case of the covalent intermediate for a  $\beta$ -retaining mannanase from *Pseudomonas cellulosa*, the glycosyl moiety found at subsite -1 adopts a  ${}^0S_2$  skew boat (62) and in the case of the  $\beta$ -xylanase, Bcx, the glycosyl moiety adopts a  ${}^{2,5}B$  boat conformation (58). As with the  ${}^4C_1$  chair, both these conformations satisfied both stereoelectronic and steric requirements.

## 1.6 $\alpha$ -Retaining versus $\beta$ -retaining glycosidases

The general chemical mechanism of an  $\alpha$ -retaining glycosidase is thought to be analogous to that of  $\beta$ -retaining glycosidases, with the obvious difference of the inverse stereochemistry at each step. However, there are some subtle differences between the  $\alpha$ - and  $\beta$ -glycosidases.

One of the key differences has been noted in trying to trap the covalent intermediate. 2-Deoxy-2-fluorosugars have been found not to act as mechanism-based inactivators of  $\alpha$ -glycosidases, despite being fairly general and efficient inactivators of  $\beta$ -glycosidases. In fact, with human pancreatic  $\alpha$ -amylase, an  $\alpha$ -retaining glycosidase, the 2-deoxy-2-fluoro  $\alpha$ -maltosyl fluoride acted as a slow substrate with a  $k_{\text{cat}}$  value of  $0.17 \text{ s}^{-1}$  (65). The difference in the ability of 2-deoxy-2-fluorosugars to inactivate these two classes of glycosidases has been attributed to the concept that the transition state for an  $\alpha$ -glycoside going to a  $\beta$ -glycosyl-intermediate ( $\alpha$  to  $\beta$  transformation) might be different from that for the  $\beta$ -glycoside going to an  $\alpha$ -glycosyl enzyme intermediate ( $\beta$  to  $\alpha$  transformation). From the fact that 5-fluorosugars are mechanism-based inactivators of  $\alpha$ -glycosidases while 2-fluoro sugars are not (17), it has been suggested that the charge distribution may be different between the two transition states. In the case of the  $\beta$  to  $\alpha$  transformation, this charge may be located more on the ring oxygen. In the  $\alpha$  to  $\beta$  transformation, this charge may be located on the anomeric carbon.

Such charge distributions in the  $\alpha$ - and  $\beta$ -retaining glycosidase transition states have also been suggested from inhibitor studies. Nitrogen substitution of the sugar ring oxygen is often thought to mimic the positive charge developed at the transition state. Therefore, 1-deoxynojirimycin (1.12), in which the ring oxygen is replaced with nitrogen, and isofagomine (1.13) where the anomeric carbon is substituted by nitrogen, are thought to mimic charge developed on the ring oxygen and anomeric carbon respectively (Figure 1.15). The galactose analogue of these compounds were tested with  $\alpha$ - and  $\beta$ -galactosidases from green coffee bean and *Escherichia coli* respectively. The galactose analogue of 1-deoxynojirimycin (1.15) was a potent inhibitor of  $\alpha$ -galactosidase with a

$K_i$  value in the low nanomolar range while the galactose analogues of **1.13** (**1.16**) had a  $K_i$  value only in the low micromolar range (Table 1.2) (66). In contrast, **1.16** is a considerably better inhibitor of  $\beta$ -galactosidase than was **1.15**. This suggests that, in the case of  $\alpha$ -glycosidases, the charge would be on the ring oxygen while in the  $\beta$ -glycosidases, the charge is located on the anomeric carbon. Indeed the galactose analogue of 1-azafagomine (**1.17**), an inhibitor in which both the ring oxygen and anomeric carbon are replaced with nitrogen, was found to inhibit both  $\alpha$ - and  $\beta$ -galactosidases (67). Recently however, Bols' group has synthesized an isofagomine analogue, noeuromycin (**1.14**), which has a hydroxyl group on the 2-position, next to the ring nitrogen. This compound, with a nitrogen atom at the "anomeric centre", acts as an inhibitor for both  $\alpha$ - and  $\beta$ -glycosidases with  $K_i$  values in the nanomolar range (68), casting some serious doubts on the charge distribution hypothesis. The effectiveness of this inhibitor does provide evidence for the importance of the 2-hydroxyl group in catalysis.

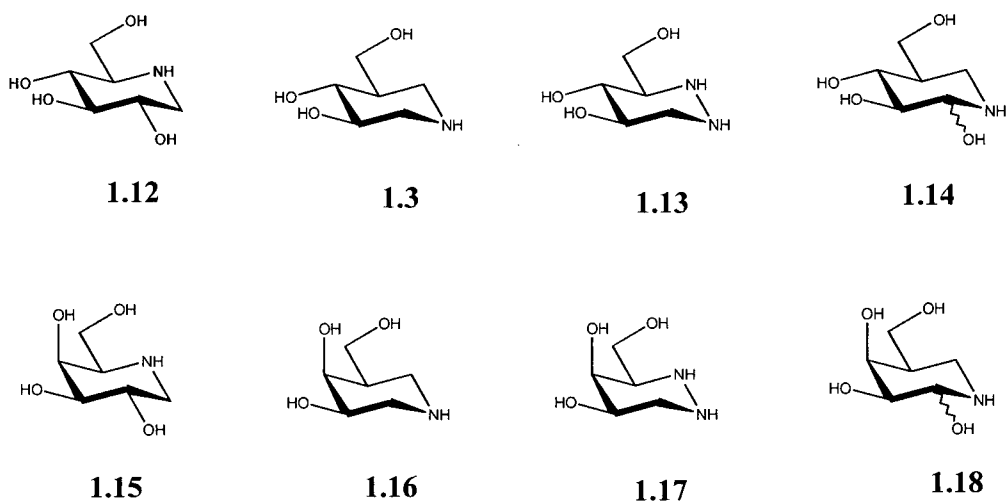


Figure 1.15 Structures of imino-sugars: deoxynojirimycin (**1.12**), isofagomine (**1.3**), 1-azafagomine (**1.13**), noeuromycin (**1.14**), azagalactofagomine (**1.15**), isogalactofagomine (**1.16**), 1-azagalactofagomine (**1.17**), and D-galacto-noeuromycin (**1.18**).

|  | <b>1.12</b>    | <b>1.3</b>   | <b>1.13</b>  | <b>1.14</b>   |
|--|----------------|--------------|--------------|---------------|
| $\beta$ -glucosidase<br>(almond)             | 47 $\mu$ M     | 0.11 $\mu$ M | 0.32 $\mu$ M | 0.069 $\mu$ M |
| $\alpha$ -glucosidase<br>(Yeast)             | 86 $\mu$ M     | 25 $\mu$ M   | 6.9 $\mu$ M  | 0.022 $\mu$ M |
|  | <b>1.15</b>    | <b>1.16</b>  | <b>1.17</b>  | <b>1.18</b>   |
| $\beta$ -galactosidase<br>( <i>E. coli</i> ) | 12.5 $\mu$ M   | 0.2 $\mu$ M  | 0.4 $\mu$ M  | 0.30 $\mu$ M  |
| $\alpha$ -galactosidase<br>(coffee bean)     | 0.0016 $\mu$ M | 50 $\mu$ M   | 0.28 $\mu$ M | 0.74 $\mu$ M  |

Table 1.2 Comparison of the  $K_i$  values for imino-sugars on  $\alpha$ - and  $\beta$ -glucosidase, and  $\alpha$ - and  $\beta$ -galactosidase (66).

The fact that the  $\alpha$ - and  $\beta$ - face are not symmetrical implies that there will be differences in the positioning of the active site residues between the  $\alpha$ - and  $\beta$ -glycosidases. The positioning of the acid/base catalyst in an  $\alpha$ -glycosidase is not on the ring plane but rather, it lies about 1 Å below the plane (39). Therefore, transition state analogues designed to take advantage of the positioning of the acid/base catalyst should include features to accommodate this fact. In addition, the strong hydrogen bonding interaction between the non-bonding oxygen of the catalytic nucleophile and 2-hydroxyl group cannot take place in the case of  $\alpha$ -glucosidases for obvious geometric reasons. Instead, in the case of  $\alpha$ -glycosidases, other residues in the active site interact with this hydroxyl group on going to the transition state (69). The non-bonding oxygen of the catalytic nucleophile is thought to interact with the ring oxygen in the CGTase intermediate structure, possibly in the same way that the tyrosine interacts with this oxygen in the Bcx mechanism (58). Indeed, it has been suggested that this interaction may be the reason why 1-deoxynojirimycin is such an effective inhibitor of  $\alpha$ -glycosidases (17).

As in the case of  $\beta$ -glucosidases, substrate distortion has been seen for  $\alpha$ -glucosidase. However, unlike the  $\beta$ -glucosidases, where there is a significant change in conformation of the sugar on binding, the substrates of the  $\alpha$ -glucosidases are only slightly flattened from a  ${}^4C_1$  conformation, bringing them to a structure closer to that of the flattened transition state. This is also in accordance with stereoelectronic factors where the preferred conformation is a  ${}^4C_1$  chair (63).

Despite these difficulties in trapping the intermediates, the intermediate of several  $\alpha$ -glycosidases have been trapped using 5-fluorosugars or mutagenesis methods (28, 51, 70-72). Of these trapped intermediates, only the structure of the trapped cyclodextrin glucanotransferase (CGTase), a member of the family 13  $\alpha$ -amylases, has been determined (69). In this structure, the covalently bound sugar adopts a normal  ${}^4C_1$  chair conformation. This conformation places the leaving group in an equatorial position, suggesting that stereoelectronic factors are of less importance in the second step of this reaction.

## 1.7 Aim of the thesis

Compared with the  $\beta$ -retaining glycosidases, where the mechanisms of several model enzymes have been extensively characterized, there have been relatively few studies on the mechanisms of  $\alpha$ -retaining glycosidases. Therefore, our understanding of  $\alpha$ -glycosidases comes from inferences of the results of the  $\beta$ -retaining glycosidases.

There are three aims for this thesis:

- 1) Understanding the catalytic mechanism of family 38  $\alpha$ -mannosidases. This will be done through the use of mechanism based inactivators.

- 2) Understanding the mechanism of chloride activation in human pancreatic  $\alpha$ -amylase.
- 3) Synthesis and testing of novel  $\alpha$ -amylase substrates for the rapid screening of inhibitors for human pancreatic  $\alpha$ -amylase.

## **Chapter 2 Family 38 $\alpha$ -mannosidases**

## 2.1 General introduction

### 2.1.1 Asparagine-linked glycosylation

Asparagine-linked (or *N*-linked) glycosylation is a post-translational modification where a complex oligosaccharide is attached to a surface asparagine residue of a protein within the sequence Asn-X-Ser/Thr (where X is any amino acid other than proline) through an *N*-glycosidic bond. In general, the biosynthetic pathway of this modification can be divided into several processes (Figure 2.1). Initially, a lipid-linked oligosaccharide (Glc<sub>3</sub>Man<sub>9</sub>GlcNAc<sub>2</sub>-PP<sub>i</sub>-dolichol) is synthesized at the membrane of the endoplasmic reticulum (ER). An oligosaccharyl transferase then transfers this oligosaccharide from the lipid phosphate to an asparagine within the sequence Asn-X-Ser/Thr of a growing polypeptide chain during translation. Once transferred, an ER  $\alpha$ -glucosidase removes the three terminal glucose moieties and an ER  $\alpha$ -mannosidase trims a single mannose residue to form a Man<sub>8</sub>GlcNAc<sub>2</sub>-Asn intermediate. The glycosylated protein moves from the ER to the Golgi where the glycan is then trimmed down through the action of several glycosidases. Briefly, Golgi  $\alpha$ (1,2)-mannosidase I removes three of the  $\alpha$ (1,2)-linked mannose moieties from the non-reducing end of the deca-saccharide. *N*-Acetylglucosaminetransferase II then transfers a *N*-acetylglucosamine moiety from a nucleotide diphosphate donor specifically to one of the terminal mannoses. Golgi  $\alpha$ -mannosidase II (GMII) then cleaves the terminal  $\alpha$ (1,3)- and  $\alpha$ (1,6)-mannosides to result in a core hexasaccharide structure. Finally, within the Golgi, various glycosyltransferases transfer additional sugars to this core structure to result in the final glycan exhibited on the protein. The initial part of this biosynthetic pathway is highly conserved and has been

well characterized in various organisms (73-75). The latter part is species-, tissue- and cell-dependent and is responsible for the diverse nature of this modification.

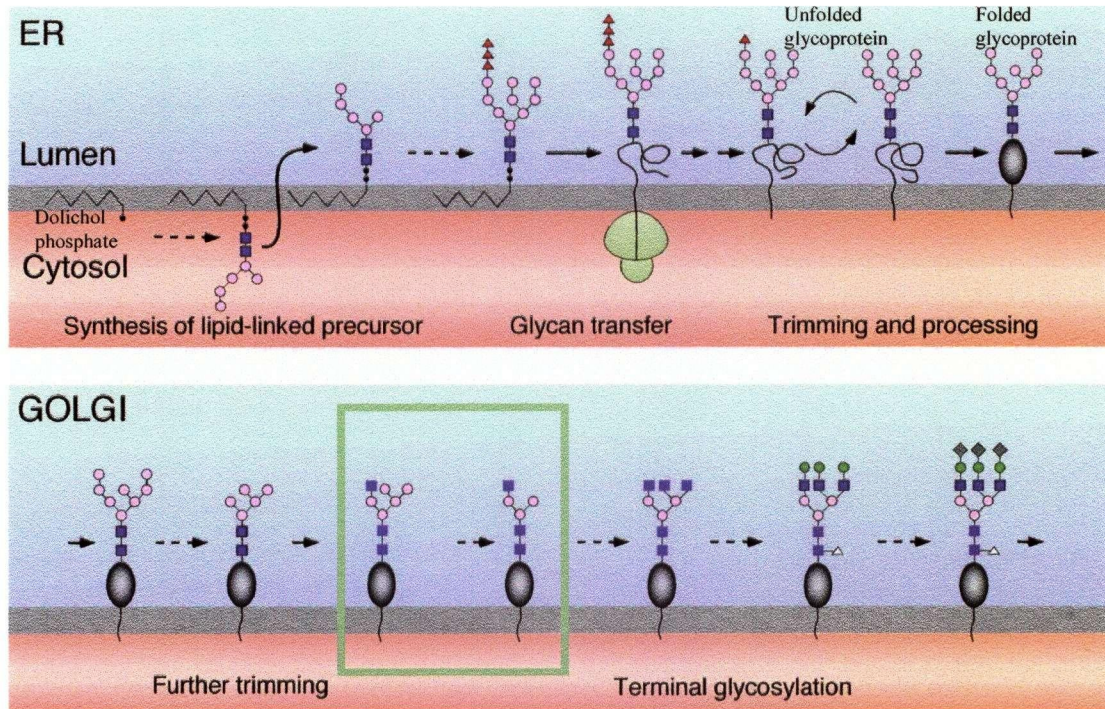


Figure 2.1 Biosynthetic pathway for *N*-linked glycans taken from (2). The symbols represent the following sugars:  $\blacktriangle$  = glucose,  $\bullet$  = mannose,  $\blacksquare$  = *N*-acetylglucosamine,  $\bullet$  = galactose,  $\blacklozenge$  = sialic acid, and  $\blacktriangle$  = fucose. The reaction catalyzed by GMII is boxed in green.

Consistent with the diversity in structures, this post-translational modification seems to play a number of different roles. Because a bulky group is attached to the protein during translation, one of the most intuitively obvious roles that glycosylation plays may be its effect on protein folding. Several studies have shown that the local secondary structures are stabilized when a sugar moiety is attached to the peptide chain (76). Since glycosylation occurs co-translationally, this stabilization may result in a change in the folding pathway. In addition, glycosylation has also been shown to have some stabilizing effects on the overall structure of some proteins (77).

An indirect way in which *N*-linked glycosylation has been implicated in the folding process is its role in the Calnexin/Calreticulin cycle (2). These two chaperones use the *N*-linked glycan, GlcMan<sub>9</sub>GlcNAc<sub>2</sub>, as a recognition element for binding to improperly folded glycoproteins within the ER. Once the glycoprotein is bound to the chaperon, a thioreductase associated with these chaperones helps with the folding process. When the terminal glucose of the *N*-linked glycan is hydrolysed by ER  $\alpha$ -glucosidase II, the glycoprotein is released from the chaperon. If the protein is not folded at this stage, an ER glucosyltransferase re-glucosylates the *N*-linked glycan so that it may bind to the chaperon again. This process is repeated until proper folding of the glycoprotein is achieved, ensuring quality control for proteins going on to the Golgi. Within the Golgi, the *N*-linked glycan is also used as a recognition element for several lectins, which in turn aid in the trafficking and localization of glycoproteins within the cell (3).

The main degradation pathway of *N*-linked glycoproteins takes place in the lysosome of cells. In this pathway, the glycoprotein is degraded from both the glycan and protein sides in a bidirectional fashion (Figure 2.2) (78). While the protein portion is being hydrolysed by various exo- and endo-peptidases, the glycan is digested by exo-glycosidases working from the terminal, non-reducing ends. In general, these exo-glycosidases have fairly broad aglycone specificity and the overall degradation pathway requires relatively few different glycosidases (78). This is in sharp contrast to the biosynthetic pathway of *N*-linked glycans where there is almost one enzyme associated with each sugar linkage formed or broken.

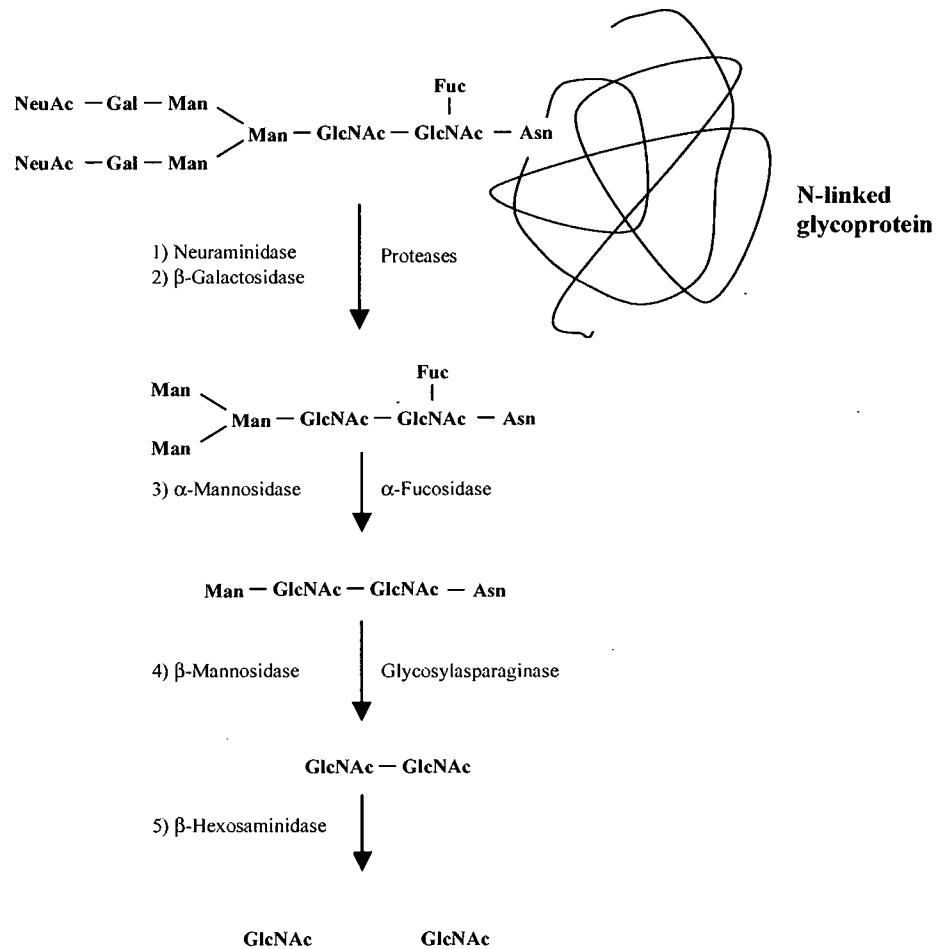


Figure 2.2 Lysosomal degradation pathway for N-linked glycoproteins adapted from (78).

### 2.1.2 Family 38 $\alpha$ -mannosidases

By sequence homology, several  $\alpha$ -mannosidases have been classified into family 38 of Henrissat's glycosidase classification (Figure 2.3) (7-9). This family contains mannosidases from various sources including the GMII, Golgi  $\alpha$ -mannosidase IIX, lysosomal  $\alpha$ -mannosidase and cytosolic/ER  $\alpha$ -mannosidase. By monitoring the hydrolytic reaction by NMR spectroscopy, a representative member of this family was

found to be a retaining glycosidase (79). Therefore, by analogy to other glycosidases, it was deduced that this family of  $\alpha$ -mannosidases employs a double displacement mechanism. Family 38  $\alpha$ -mannosidases are also characterised by their broad natural substrate specificity, their ability to cleave synthetic substrates such as *p*-nitrophenyl  $\alpha$ -D-mannoside, and their susceptibility to the inhibitor swainsonine (80, 81). The other class of  $\alpha$ -mannosidases, family 47  $\alpha$ -mannosidases, which includes the ER  $\alpha$ -mannosidase I, are inverting  $\alpha$ -glycosidases. These enzymes have very strict substrate specificity towards  $\alpha$ (1,2)-linkages and do not hydrolyse synthetic substrates. Family 47  $\alpha$ -mannosidase are also not inhibited by the inhibitor swainsonine.

Arguably the most studied  $\alpha$ -mannosidase is the Jack bean  $\alpha$ -mannosidase. Because the primary sequence of this enzyme is not known, it cannot be definitively classified to a particular family. However, comparison of its kinetic properties with that of known  $\alpha$ -mannosidases strongly suggested that this enzyme belongs to the family 38. The mechanism-based inactivator, 5-fluoro- $\beta$ -L-gulosyl fluoride (5FGulF), was used to trap a covalent intermediate for this enzyme, further supporting the proposed mechanism (Chapter 1.5.5). This trapped intermediate was proteolytically digested and the resulting digest was then analysed by liquid chromatography-mass spectrometry (LC-MS) to identify the labelled peptide. From tandem mass-spectrometry (MS-MS) sequencing of this peptide (RAGQIDPFGHSAVQG), the labelled residue was found to be an aspartate. The amino acid sequence surrounding this residue (including the aspartate itself) was found to align well with a conserved region within the family 38  $\alpha$ -mannosidases (Figure 2.3) (72), strongly suggesting that the catalytic nucleophile for family 38  $\alpha$ -mannosidases is this conserved aspartate.

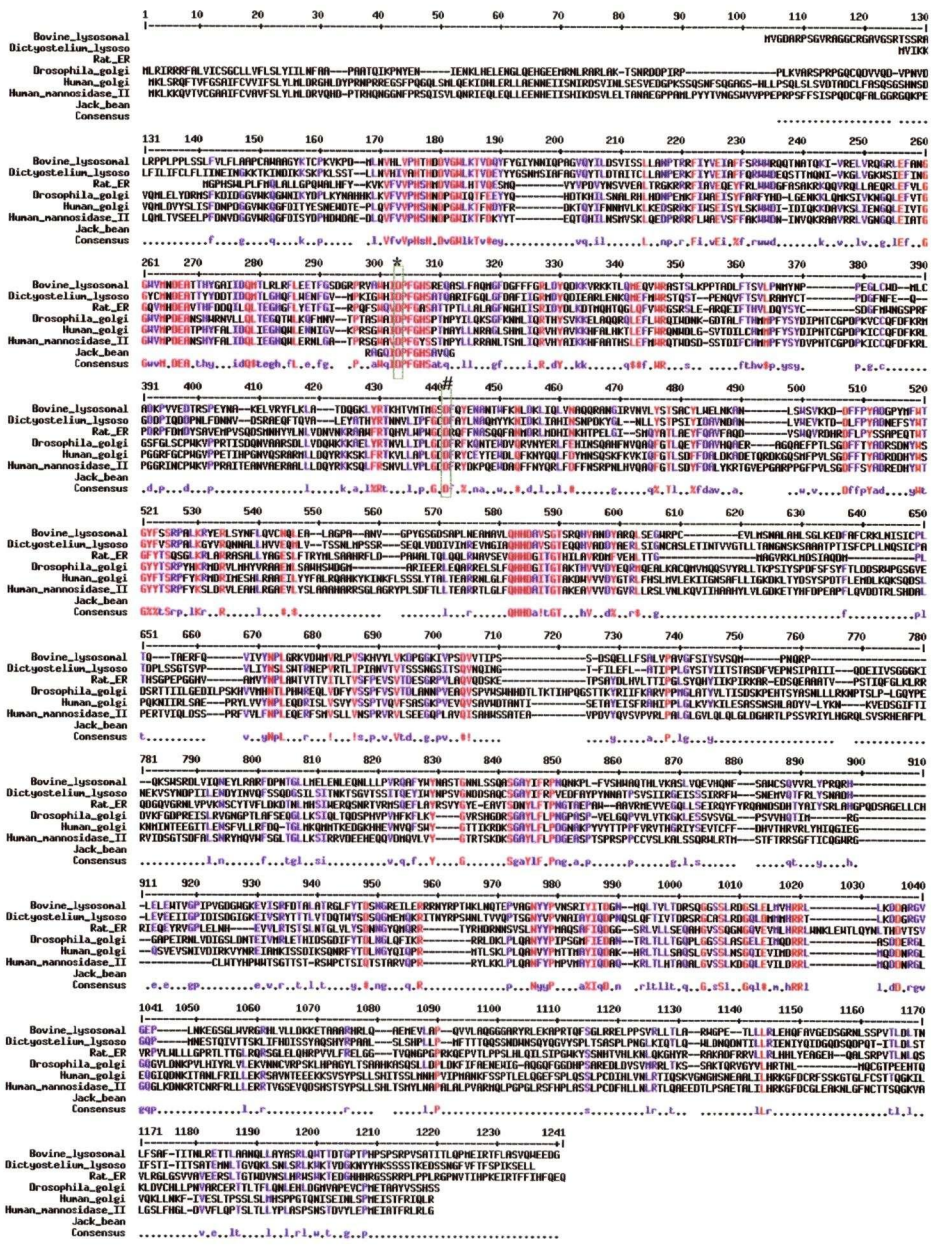


Figure 2.3 Sequence alignment for family 38  $\alpha$ -mannosidases. The highly conserved (70%) regions are highlighted in red while the low conservation regions are highlighted in blue. The putative catalytic nucleophile (\*) and putative acid/base (#) have been labelled. Swiss Prot identifiers are indicated in parentheses. The sequences shown are: bovine lysosomal  $\alpha$ -mannosidase (Q29451), dictyostelium lysosomal  $\alpha$ -mannosidase (P34098), rat ER  $\alpha$ -mannosidase (P21139), *Drosophila* Golgi  $\alpha$ -mannosidase II (Q24451), human Golgi  $\alpha$ -mannosidase II (Q16706), human Golgi  $\alpha$ -mannosidase IIX (P49641), and Jack Bean  $\alpha$ -mannosidase (72).

### **2.1.3 Lysosomal $\alpha$ -mannosidase**

Lysosomal  $\alpha$ -mannosidase (LAMAN; EC 3.2.1.24) is involved in the degradation of *N*-linked glycoproteins (enzyme#3 in Figure 2.2). It is a multimeric complex containing several subunits (the exact number is species-dependent) with an overall size around 125 kDa (82-84). Like most lysosomal glycosidases, it has a broad substrate specificity, hydrolysing  $\alpha(1,2)$ -,  $\alpha(1,3)$ - and  $\alpha(1,6)$ -mannosidic linkages from the non-reducing end. Also, similar to other lysosomal enzymes, this  $\alpha$ -mannosidase is characterized by its low pH optimum (pH 4.5), which is required for activity within the lysosome.

Deficiencies of LAMAN can result in the lysosomal storage disorder,  $\alpha$ -Mannosidosis. Because most enzymes involved in the lysosomal degradation pathway of glycoproteins are exo-glycosidases, operating from the non-reducing end, loss of activity of the LAMAN leads to blockage of the degradation pathway. This, in turn, leads to an accumulation of undigested oligosaccharides in the lysosome.  $\alpha$ -Mannosidosis has been seen in various organisms including humans (85), cattle (86) and cats (87). The symptoms include progressive mental retardation, immunodeficiency and skeletal defects (88). Genetic analysis of subjects with this disease shows that there are a number of possible point or deletion mutations that lead to the loss of enzymatic activity (84, 89, 90). However, the degree of severity of these symptoms does not directly correlate with the enzyme activity, suggesting that some other factor must be involved in determining the severity of the disease.

#### 2.1.4 Golgi $\alpha$ -mannosidase II

GMII (EC 3.2.1.114) is involved in the biosynthesis of *N*-linked glycoproteins (Figure 2.1; the reaction catalyzed has been highlighted with a box). Its role is to trim off two terminal mannose residues from the glycan, GlcNAcMan<sub>5</sub>GlcNAc<sub>2</sub>, which has been transferred to the protein. Although this enzyme has a broad specificity in that it cleaves both  $\alpha(1,3)$ - and  $\alpha(1,6)$ -mannosidic linkages, it is more specific than its lysosomal counterpart in that it does not cleave off the terminal mannose of its product, GlcNAcMan<sub>3</sub>GlcNAc<sub>2</sub>, which is also  $\alpha(1,6)$  linked (91). This has been attributed to the enzyme using the terminal,  $\alpha(1,2)$ -linked *N*-acetylglucosamine moiety to position the substrate within the active site. Also in contrast to LAMAN, GMII is a monomeric, transmembrane protein about 125 kDa in size.

Interestingly, in various tumour cell lines such as those from breast, colon and skin cancer, the distribution of the cell surface *N*-linked glycosylation is altered (92). Because *N*-linked glycosylation is associated with cell-cell interactions, this alteration correlates with the progression of tumour metastasis (93). Indeed, knockout studies in mice have shown that by removing an enzyme within the glycosylation pathway, tumour metastatic progression is drastically decreased (94). Enzymes of this glycosylation pathway are therefore potential targets for drug development in cancer treatment. In fact, GMII has been the target of one such drug candidate, swainsonine. In early clinical trials this well-known GMII inhibitor was found to reduce tumour growth and metastasis when taken orally (95, 96).

### 2.1.5 Structural aspects of Golgi $\alpha$ -mannosidase II

Recently, the three-dimensional structure of the soluble form of GMII from *Drosophila melanogaster* was determined by X-ray crystallography (Figure 2.4a) (97). The protein consists of an *N*-terminal  $\alpha/\beta$  domain and an all- $\beta$  C-terminal domain connected together by a three-helix bundle. The active site of this enzyme was identified from structures of complexes with inhibitors bound (Figure 2.4b for the active site structure with deoxymannojirimycin bound). Within this site are four carboxylic acids, each of which can potentially act as a catalytic residue. As might be expected, among these carboxylic acids is the aspartate (Asp204) that was implicated in the Jack bean  $\alpha$ -mannosidase study as being the catalytic nucleophile (72). This carboxylic acid is positioned  $\sim 4.5$  Å away from the “anomeric carbon” on the “ $\beta$ -face” of the inhibitor, a position which is consistent with the role of a catalytic nucleophile. Although deoxymannojirimycin does not have a glycosidic oxygen, this structure also suggested that another of these aspartate residues (Asp341) is positioned in the to act as the acid/base catalyst (*anti* protonator). An interesting feature of the active site is the presence of a zinc ion, which is coordinated by two histidines (His90, His471), an aspartate (Asp92), and the 2- and 3-hydroxyl groups of the inhibitor. This supports biochemical results that demonstrated the importance of the zinc in catalysis (98-100). The fourth and final aspartate (Asp472) in the active site makes hydrogen bond contact with the 3- and 4-hydroxyl groups of the inhibitor.

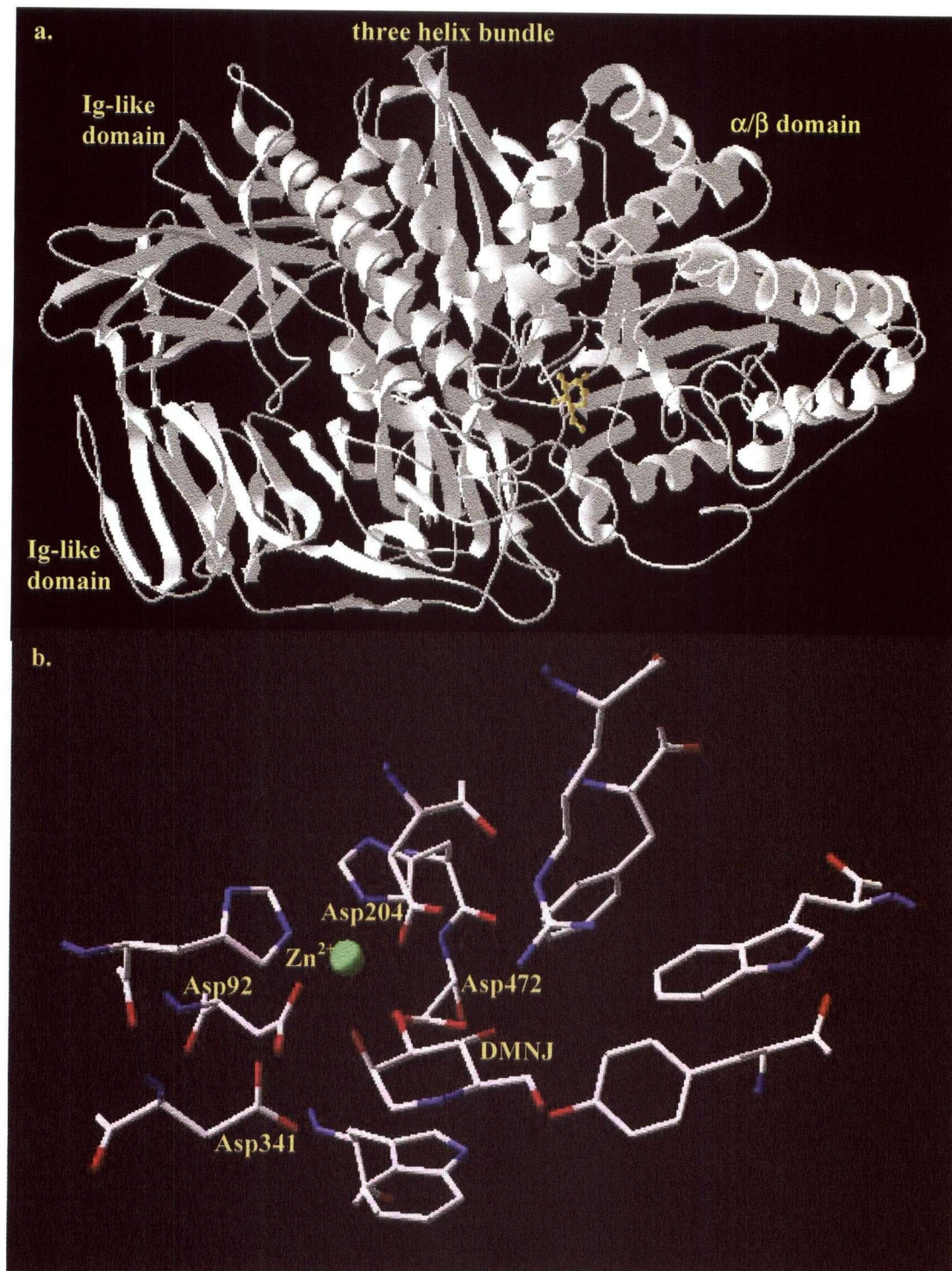


Figure 2.4 (a) Ribbon representation of the *Drosophila* GMII. The inhibitor, deoxymannojirimycin has been shown in yellow. (b) The active site residues of GMII interacting with the inhibitor deoxymannojirimycin.

## 2.2 Specific aims of this study

1) *Identifying the residue involved in nucleophilic catalysis for bovine kidney LAMAN.*

Although Jack bean  $\alpha$ -mannosidase shares a number of properties to that of family 38  $\alpha$ -mannosidases, the complete sequence of this enzyme is not known. Therefore, it is impossible to say with certainty that this enzyme belongs to family 38, and conversely, that the nucleophile identified by sequence alignment of the short segment is indeed the residue involved in nucleophilic catalysis for family 38  $\alpha$ -mannosidases. A similar approach to that used to identify the catalytic nucleophile for Jack bean  $\alpha$ -mannosidase will be used to identify the catalytic nucleophile for a known family 38  $\alpha$ -mannosidase from bovine kidney lysosome.

2) *Determining the structure of the covalent intermediate of GMII from *D. melanogaster*.*

To better understand the mechanism by which an enzyme catalyzes a reaction, it is important to have structural information of some stable complexes on the reaction pathway. One such complex in the hydrolysis of  $\alpha$ -mannosides by family 38  $\alpha$ -mannosidases is the covalent intermediate. Knowing the structure of this complex will not only allow for the determination of the interactions that the intermediate sugar forms with the enzyme but also, it will give insight into the structure of the transition state. To this end, the intermediate of *D. melanogaster* GMII will be trapped using several mechanism based inhibitors. In collaboration with Drs. David Rose and Douglas Kuntz (crystallographers at the Ontario Cancer centre, Toronto), the three-dimensional structure of the trapped intermediate will be determined. Such information should aid in the understanding of the structural aspects of the covalent intermediate.

## 2.3 Results and discussion – the catalytic nucleophile of bovine kidney LAMAN

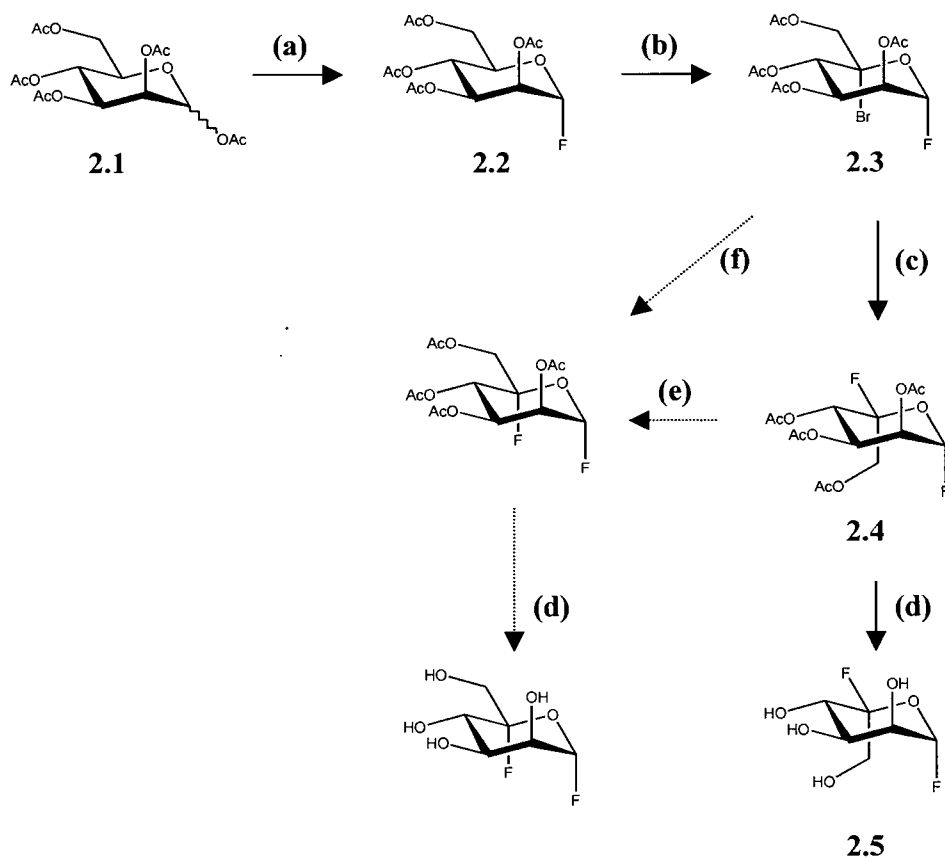
### 2.3.1 Rationale for the selection of the inactivator

5-Fluorosugars have been used to label and identify the catalytic nucleophiles of a number of  $\alpha$ -glycosidases (28, 70-72) including the Jack bean  $\alpha$ -mannosidase. An interesting observation made during these studies was that the 5-fluorosugar corresponding to the C5-epimer of the natural substrate was a better inactivator than was the 5-fluorosugar with the “correct” configuration at C-5. Therefore, it stood to reason that 5-fluoro- $\beta$ -L-gulosyl fluoride (5FGulF), the C5-epimer of 5-fluoro- $\alpha$ -D-mannosyl fluoride (5FManF), should be the first candidate for labelling LAMAN.

### 2.3.2 Synthesis of 5-fluoro- $\beta$ -L-gulosyl fluoride

The synthesis of 5FGulF was adopted from previously published procedures for the same compound (Scheme 2.1) (72). Briefly, the peracetylated mannose (**2.1**) was fluorinated at the anomeric carbon using HF/pyridine to yield the acetylated  $\alpha$ -mannosyl fluoride (**2.2**) in 85% yield after purification (no  $\beta$ -product was formed). The key step of the synthesis involved the selective introduction of the bromine at the 5-position of **2.2** by photo-bromination of peracetylated  $\alpha$ -mannosyl fluoride. Literature report of this reaction was 5 hours, with an overall yield of 53%. Using similar conditions, the reaction had not progressed to a significant level after this time (by TLC) and so the reaction was left refluxing overnight. The prolonged irradiation also resulted in the formation of additional side products, as seen by TLC (most likely polybromination at the acetate protecting groups (101)). Although the pure product, peracetylated 5-bromo- $\alpha$ -D-

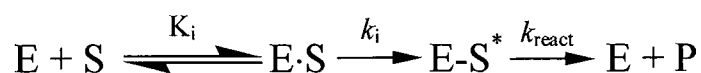
mannosyl fluoride (**2.3**) was obtained, the difficulty in separating the product from these side products resulted in a low overall yield (25%) for this step. Treatment of **2.3** with AgF resulted in the displacement of the bromide by fluoride with an inversion of configuration at C-5 to yield the protected 5FGulF (**2.4**) in 30% yield. Deprotection of the sugar was achieved under basic conditions using ammonia in MeOH to give the final product, 5FGulF (**2.5**), in 30% yield.



Scheme 2.1 An outline of the synthesis of 5FGulF and the proposed synthesis of 5FManF. (a) HF/pyridine, 85% ; (b) NBS, CCl<sub>4</sub>, hv, 25%; (c) AgF, CH<sub>3</sub>CN, 30%; (d) NH<sub>3</sub>, MeOH, (for 2.5) 30%; (e) BF<sub>3</sub>·Et<sub>2</sub>O and (f) AgBF<sub>4</sub>, Et<sub>2</sub>O.

### 2.3.3 Kinetics studies of 5FGulF with bovine kidney LAMAN

The kinetic model for the inactivation of glycosidases is shown in Scheme 2.2. This model is based on the assumption that 5-fluorosugars are extremely bad substrates for glycosidases with the rate of deglycosylation (reactivation;  $k_{\text{react}}$ ) being much lower than the rate of glycosylation (inactivation;  $k_i$ ). If the absolute value of  $k_{\text{react}}$  is significantly small, the hydrolysis of the fluoroglycosyl-enzyme intermediate will not occur within the time-frame of the experiment. The accumulation of this intermediate will be seen as a loss of enzymatic activity over time, or in other words, as time-dependent inactivation. If the rate of reactivation is large though, the intermediate species will be quickly turned over so that no inactivation is seen but rather, the compound will act as a competitive inhibitor or a slow substrate. In this case, because the  $k_{\text{react}} < k_i$ , at steady state there will still be an accumulation of the fluoroglycosyl-enzyme intermediate, the amount depending on the ratio of the two rates. The result of this accumulation is seen in the form of an apparent dissociation constant ( $K_i$  or  $K_m$ ) that is significantly lower than the actual dissociation constant for the compound.



Scheme 2.2 A kinetic model of the reaction of fluorosugars with glycosidases where E is the free enzyme; S is the substrate; E·S is the non-covalent enzyme-substrate complex; E-S\* is the covalent glycosyl-enzyme intermediate; and P is the product.

Incubation of 5FGulF with bovine kidney LAMAN did not result in time-dependent inactivation of this enzyme at 30°C. This is in sharp contrast to the experiment with Jack bean  $\alpha$ -mannosidase where incubation with 5FGulF resulted in complete enzyme inactivation after 200 seconds (72). The 5FGulF was instead found to act as an

apparent tight binding competitive inhibitor of LAMAN with an apparent  $K_i$  value of 67  $\mu\text{M}$  (Figure 2.5). Considering that fact that the substrate, 2,4-dinitrophenyl  $\alpha$ -D-mannoside (DNP-Man), has a  $K_m$  value of 1.2 mM, a  $K_i$  value of 67  $\mu\text{M}$  indicates much tighter binding than would be expected for a simple substrate analogue (note: all graphical data not presented in the text has been included in Appendix 2). The low  $K_i$  is yet more surprising considering the inverted configuration at C-5 and the fact that the aglycone is a fluoride, which is not likely to significantly contribute to binding.

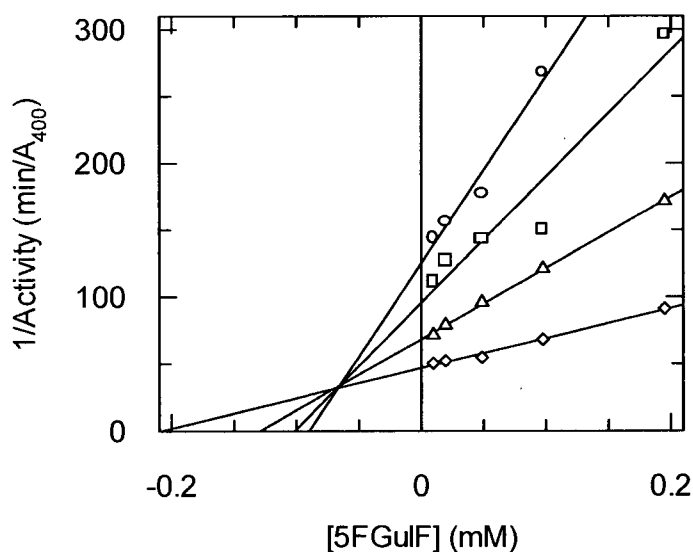


Figure 2.5 Dixon plot of the inhibition of bovine kidney LAMAN by 5FGulF. Enzyme was incubated with the following concentrations of substrate (DNP-Man): 0.25 mM (O), 0.365 mM (□), 0.5 mM (Δ), and 1.0 mM (◇).

These results are fully consistent with a kinetic model where the  $k_{\text{react}}$  is large enough that inactivation is not seen. This sort of behaviour has been previously reported for fluorosugars when 5FManF was tested as an inactivator of Jack bean  $\alpha$ -mannosidase (72). In this case, not only did the 5FManF have a low apparent  $K_i$  but it was also found to be a slow substrate for the Jack bean enzyme. Indeed, when the 5FGulF was tested as a substrate by measuring the rate of fluoride ion release, the 5FGulF was found to be turned

over by LAMAN with a  $k_{\text{cat}} = 0.022 \text{ s}^{-1}$ . It is clear that the fluorine at the 5-position is destabilizing the transition state, resulting in this low rate. By way of comparison, the  $k_{\text{cat}}$  value for hydrolysis of DNP-Man by LAMAN is  $9.9 \text{ s}^{-1}$ . Consistent with the  $K_i$  value of  $67 \mu\text{M}$  determined from inhibition studies, the rate of turnover of 5FGulF was independent of substrate concentrations down to at least  $0.7 \text{ mM}$  (the  $K_m$  could not be determined due to the insensitivity of the instrument being used). Therefore, kinetic results strongly support the accumulation of an intermediate upon incubation of LAMAN with 5FGulF. However, it is clear from the fact that no inactivation is seen that this intermediate is not very stable.

#### **2.3.4 Labelling experiments**

The kinetic data pointed towards a significant steady state population of the intermediate during the hydrolysis of 5FGulF by LAMAN. Therefore, it may be possible to detect this species while the LAMAN is hydrolysing 5FGulF. If this accumulating species involves a covalent bond between the sugar and enzyme, one possible method of detecting this intermediate is through mass spectrometry, where the intermediate species should have a mass corresponding to the mass of the enzyme plus the glycosyl unit. Unfortunately, attempts at determining the mass of bovine kidney LAMAN either in the presence or absence of 5FGulF by electrospray ionisation mass spectrometry (ESI-MS) failed. This is most likely due to the protein in the sample having a distribution of masses (micro-heterogeneity) as a result of differences in the *N*-linked glycans being attached. Therefore, it was not possible to directly detect the accumulated intermediate through this method.

However, during steady state, it should be possible to generate a peptide containing the labelled active site nucleophile by rapid proteolytic digestion of LAMAN during its hydrolysis of 5FGulF. Because *N*-linked glycans are generally attached to the surface residues of proteins, it is unlikely that a peptide containing the catalytic nucleophile, an active site residue, will also contain an *N*-linked glycan. Therefore, unlike in the case of the intact protein, there should be no problems with micro-heterogeneity when determining the mass of this peptide.

LAMAN was therefore incubated with 5FGulF followed by pepsin digestion at pH 2 to generate a mixture of peptides. This mixture was separated by HPLC attached to an ESI-MS detector (Figure 2.6a). The labelled peptide was identified by repeating this process but running the MS-MS in neutral loss mode (55). In this mode, peptides are subjected to mild fragmentation by collision with an inert gas in the second quadrupole. This collision causes a homolytic cleavage of the labile ester bond between the sugar and the peptide, resulting in loss of a neutral sugar. The first and third quadrupoles are scanned in a linked fashion so that only ions whose mass changes by exactly the mass of the label lost in the second quadrupole can pass through the third quadrupole to the detector. In this way it is possible to identify the ion that contained the ester-linked sugar. In the present case, where a 5-fluoro-gulosyl moiety will be lost, this difference is  $m/z$  181 if the peptide is singly charged and  $m/z$  90.5 if the peptide is doubly charged. No peptides of note were observed when scanning for a loss of 181. However, when the analysis was done while scanning for a loss of 90.5, several peptides were identified (Figure 2.6b). Only one of these peptides was absent in the control pepsin digest of LAMAN that had not been incubated with 5FGulF (Figure 2.6c), suggesting that this

fragment is indeed the labelled peptide. The peptide has a  $m/z$  of 688 (Figure 2.6d) and because it is a doubly charged, this corresponds to a mass of 1376.

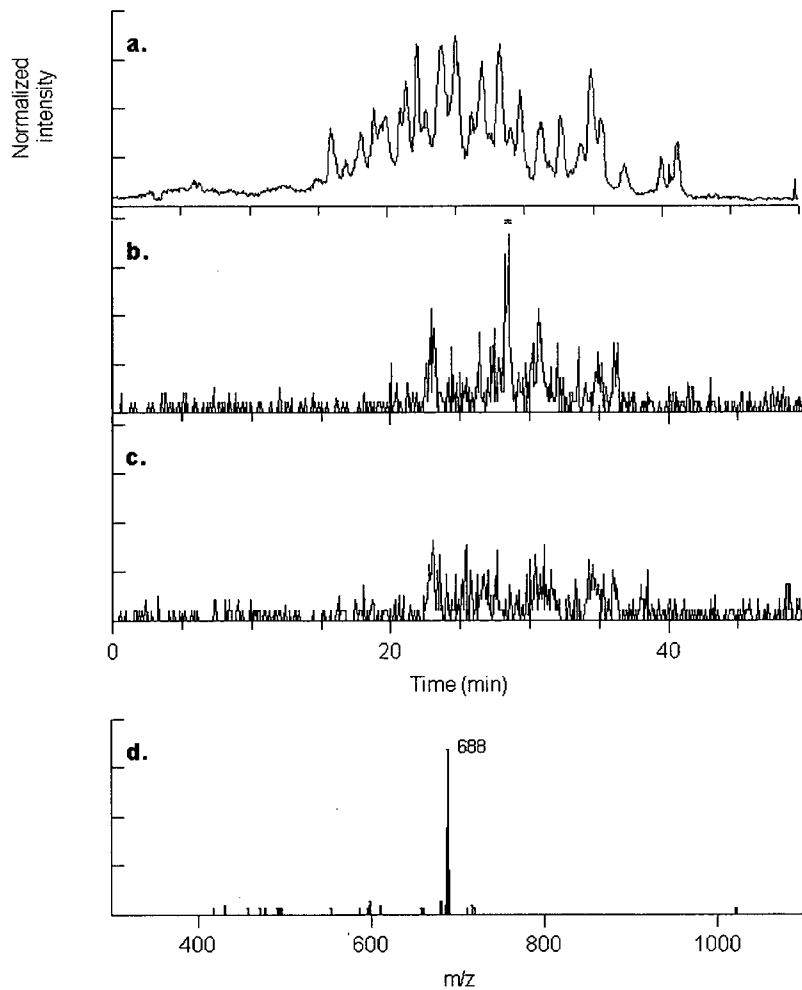


Figure 2.6 ESI-MS experiments on peptic digests of bovine kidney LAMAN. (a) Enzyme incubated with 5FGulF, total ion current in normal MS mode. (b) Enzyme incubated with 5FGulF, total ion current in the neutral loss mode. The labelled peptide of interest is indicated with an asterisk. (c) Unlabelled enzyme, total ion current in neutral loss mode. (d) Mass spectrum of the labelled peptide eluting at 28.37 minutes. The peptide has a  $m/z$  of 688 corresponding to a mass of 1376.

To confirm the neutral loss analysis results, comparative mapping was done on the peptide digests of the enzyme that had either been pre-incubated with 5FGulF with a sample where the enzyme had been incubated with water (control). As was expected, the identified peptide was not present in the control digest. Instead, the corresponding unlabelled peptide ( $m/z = 598$ ) was found to come off the HPLC at around the same retention time. This unlabelled peptide was also found at much lower intensity in the labelled digest. This is most likely due to incomplete labelling, a result consistent with the kinetic analysis that suggested that the intermediate of 5FGulF hydrolysis is quickly turned over.

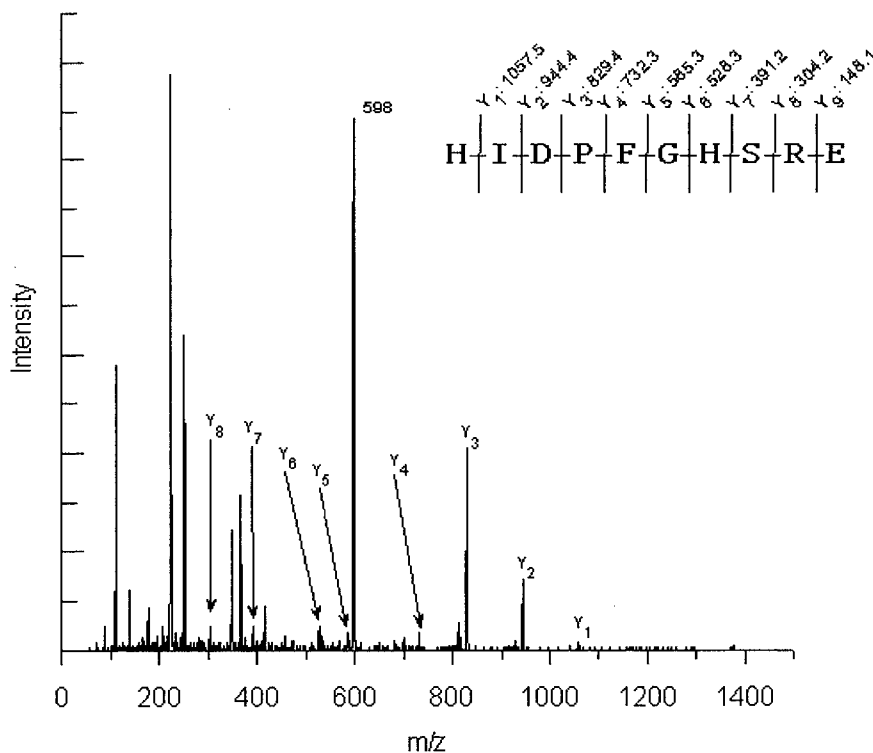


Figure 2.7 ESI-MS-MS spectrum of the 5-fluoro-gulosyl peptide ( $m/z$  688, in doubly charged state). Observed Y series fragments are shown above the peptide sequence.

Both the labelled and corresponding unlabelled peptides were isolated from the protein digest by HPLC and subsequently sequenced using ESI-MS-MS. The two

samples gave very similar mass spectra. Analysis of this fragmentation pattern as shown in Figure 2.7 yields the sequence HIDPFGHSRE which corresponds to a sequence of His195 to Glu204 in the full sequence. Unfortunately, it was not possible, from this spectrum, to identify the specific amino acid residue labelled since no fragments still bearing the label were seen in the MS-MS spectrum. However, this sequence contains only two carboxylic acids, an aspartate and a glutamate. To date, such residues have been shown to act as the enzymatic nucleophile in all retaining glycosidases functioning via the double displacement mechanism. Sequence alignment of this fragment with other members of the family 38  $\alpha$ -mannosidase (Figure 2.3) shows that only the aspartate (Asp197), and not the glutamate, is conserved throughout this family. Furthermore, the aspartate residue is also the residue that was identified through the labelling studies on the Jack bean  $\alpha$ -mannosidase. These two results combined strongly suggest that the catalytic nucleophile in bovine kidney LAMAN is Asp197.

### **2.3.5 Conclusions**

The general assumption made during the initial phases of this study was that, as with previously studied glycosidases, this enzyme catalysed hydrolysis via a double displacement mechanism involving a covalent intermediate. Isolation of a labelled peptide from a digestion mix of enzyme pre-incubated with 5FGulF confirmed this assumption. The residue acting as the nucleophile was determined to be an amino acid found between residues 195 and 204. Unfortunately, because of the labile nature of this ester linkage, it was not possible to unequivocally identify the labelled residue. However, the study strongly suggests that the catalytic nucleophile is Asp197, corresponding to the same residue as that identified in Jack bean  $\alpha$ -mannosidase.

## 2.4 Results and discussion – structural characterization of the covalent intermediate

### 2.4.1 Rationale for the experiments

The studies with the bovine kidney LAMAN demonstrated that covalent catalysis was involved in the hydrolysis mechanism for family 38  $\alpha$ -mannosidases. Furthermore, it pointed to an aspartate side chain playing this role. These results are consistent with a double displacement mechanism. Because this intermediate is a key feature of this mechanism, knowledge of its structure would be invaluable in understanding the finer details of the catalytic mechanism. Although the three-dimensional structure of the bovine kidney LAMAN had not been determined at the time of this study, the tertiary structure of the *D. melanogaster* GMII, another family 38  $\alpha$ -mannosidase, was being solved by van den Elsen *et al.* (97). In addition, the *D. melanogaster* GMII had also been cloned and the recombinant enzyme over-expressed so that mutational studies could be done with the enzyme.

The *D. melanogaster* GMII was therefore a good candidate for structural analysis of the covalent intermediate in family 38  $\alpha$ -mannosidases, and based upon the results with both the Jack bean  $\alpha$ -mannosidase and bovine kidney LAMAN, 5FGulF was used as the initial mechanism-based inactivator to trap this intermediate. In the initial studies, to increase the chance of completely trapping the intermediate, a mutant form of the enzyme was used whereby the putative acid/base catalyst (Asp341; GMII number will be used for the rest of the chapter unless otherwise specified) had been mutated to an asparagine (see section 1.5.5 for details).

#### ***2.4.2 Kinetic analysis of the inactivation of the Asp341Asn mutant GMII by 5FGulF***

The kinetic parameters for the Asp341Asn mutant GMII hydrolysis of the substrate DNP-Man were determined and as might be expected, its  $k_{\text{cat}}$  value was significantly lower than the  $k_{\text{cat}}$  value determined for wild-type GMII with the same substrate ( $0.048 \text{ s}^{-1}$  and  $8.6 \text{ s}^{-1}$ , respectively). Interestingly, the  $K_{\text{m}}$  values for the wild-type and Asp341Asn mutant GMII were 5.5 mM and 0.05 mM respectively. This relatively low  $K_{\text{m}}$  value for the mutant enzyme is suggestive of substantial accumulation of an intermediate during the hydrolysis of DNP-Man. This is promising for the planned structural analysis. However, in order to obtain structural information, the intermediate is required to have a sufficient lifetime that it stays intact while the X-ray diffraction patterns are being collected (a low  $k_{\text{react}}$  value). As such, the 5FGulF was used with the acid/base mutant in order to achieve this trapping.

As with bovine kidney LAMAN, when the Asp341Asn mutant GMII was incubated at  $37^{\circ}\text{C}$  with 5FGulF, no time-dependent inactivation was seen. Instead, 5FGulF acted as an apparent reversible inhibitor with a  $K_{\text{i}}$  value of approximately 0.6 mM. This  $K_{\text{i}}$  value is once again quite low compared to the  $K_{\text{m}}$  value for the substrate DNP-Man with the wild-type enzyme (5.5 mM). This relatively low  $K_{\text{i}}$  value for the mutant GMII is suggestive of substantial accumulation of intermediate during the hydrolysis of 5FGulF. The lack of inactivation may therefore be due to rapid turnover of the fluoroglycosyl-enzyme intermediate so direct detection is not possible under the conditions employed.

In order to increase the chance of observing the inactivation process, the assay to measure residual GMII activity of the inactivation reaction was carried out at a lower

temperature (16°C) to decrease the reactivation rate. Under these conditions, time-dependent inactivation of the Asp341Asn mutant GMII was indeed observed. When the first part of the experiment (inactivation) was carried out at 37°C, the reaction was too fast to allow rates of inactivation to be determined. Therefore, the entire experiment was performed at 16°C and the pseudo-first order rate constants so determined were plotted versus inactivator concentration as shown in Figure 2.8b. Unfortunately, even at this low temperature, inactivation occurred too quickly to determine the pseudo-first order rate constants for inactivation at higher inactivator concentrations where saturation behaviour might be observed. Therefore, it was not possible to determine the parameters,  $k_i$  and  $K_i$ , independently but only a value for the pseudo-second order rate constant,  $k_i/K_i$  of  $33 \text{ s}^{-1} \text{ M}^{-1}$ , could be determined.

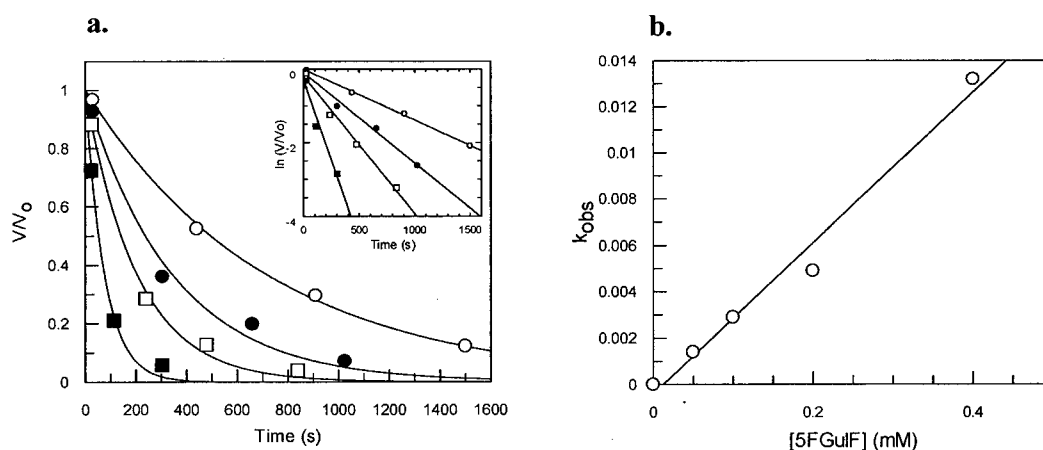


Figure 2.8 (a) Inactivation of Asp341Asn mutant *Drosophila* GMII at 16°C by 5FGulF at the following concentrations: 0.05 mM (○), 0.1 mM (●), 0.2 mM (□), and 0.4 mM (■). (b) Replot of the rate constants from above.

If the 5FGulF is a slow substrate of the mutant GMII, the 5-fluoro-gulosyl-enzyme intermediate should slowly be turned over to product the free enzyme and a hydrolysed product. The reactivation of this intermediate was measured as a function of

time (Figure 2.9). Although the activity of the enzyme did not return to the original rate prior to inactivation, there was evidence of reactivation taking place. This indicates that the 5FGulF is a slow substrate for the mutant GMII. When the 5FGulF was tested as a substrate for Asp341Asn mutant GMII by measuring fluoride ion release, there was no measurable activity at enzyme concentrations of 1.6  $\mu\text{M}$ . This is consistent with the fact that the rate of hydrolysis is normally significantly reduced upon the introduction of fluorine at the C-5 position (28) and the fact that removal of the acid/base catalyst usually reduces the rate by 2-3 orders of magnitude (31, 32).

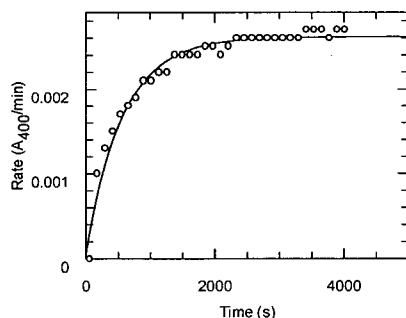


Figure 2.9 Reactivation of the 5-fluoro-gulosyl GMII at 16°C.

#### 2.4.3 Mass spectrometric analysis of the intermediate formed with 5FGulF

In order to verify the covalent nature of the intermediate formed, the mass of the inactivated enzyme was determined by LC-MS analysis. Compared to that of the free enzyme, the mass of the inactivated enzyme was greater by 172 Da (Figure 2.10). This value corresponds within the experimental error ( $\pm 20$  Da) to the expected increase of 181 Da for the addition of a 5-fluoro-gulosyl moiety to an enzyme of molecular weight 120.5 kDa. Since the enzyme is under purified under acidic conditions prior to ESI-MS analysis, there is little chance that this increase reflects a non-covalent complex. Therefore, the inactivation seen by incubating 5FGulF with the Asp341Asn mutant GMII

is likely due to the formation of a covalent glycosyl-enzyme intermediate formed during the hydrolysis reaction. The extra peaks found in the control spectra are most likely due to different glycoforms of the protein.

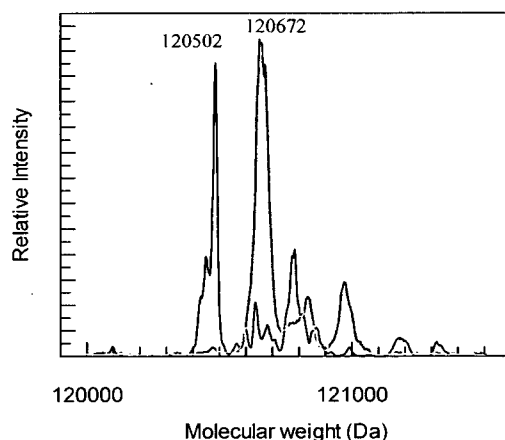


Figure 2.10 Reconstructed electrospray mass spectra of Asp341Asn mutant *Drosophila* GMII in the absence (black) and in the presence (fuchsia) of 5FGulF.

#### 2.4.4 Structural analysis of the covalent intermediate

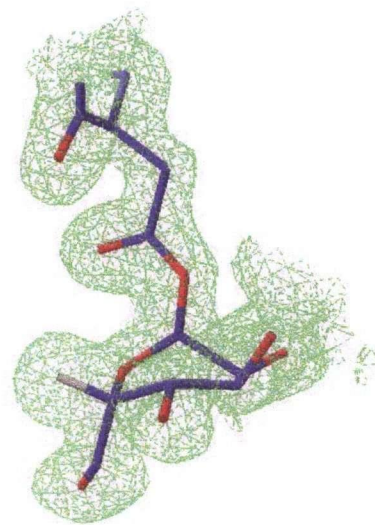
The structures of all complexes in this chapter were determined by Dr. Douglas Kuntz in the laboratory of Professor Rose at the Ontario Cancer Institute in Toronto. In order to minimise hydrolysis of the intermediate and to improve the data quality, the crystals were frozen after being soaked with 5FGulF for 30 minutes. The structure of the Asp341Asn mutant GMII soaked with 5FGulF was determined to 2.03 Å resolution.

The backbone structure of the Asp341Asn mutant GMII soaked with 5FGulF differed very little compared to the structure of wild-type GMII with nothing bound, the main difference being the presence of a sugar bound to the active site of the mutant GMII (Figure 2.11). A closer inspection of this sugar revealed it to correspond to a 5-fluorogulosyl moiety in a  ${}^1S_5$  skew boat conformation. The anomeric carbon of this sugar is 1.50 Å away from the  $\delta_1$ -oxygen of Asp204, a distance that is consistent with a covalent

bond between the two atoms. Further support for the covalent “ $\beta$ ”-linkage (note: This is formally an  $\alpha$ -linkage with an L-sugar, but for the purpose of this discussion,  $\alpha$  and  $\beta$  will be used as applied to the natural substrates, D-mannosides) between the carboxylic acid and sugar comes from the electron density map, which clearly reveals electron density between the two atoms (Figure 2.11a). The aspartate that forms a covalent bond with the sugar is the residue that was predicted to act as the catalytic nucleophile from previous studies on the Jack bean  $\alpha$ -mannosidase (72) and the bovine kidney LAMAN. More importantly, the crystallographic data, taken together with the kinetic and mass spectrometric data, demonstrate that a covalent glycosyl-enzyme intermediate is formed during the hydrolysis of 5FGulF by the Asp341Asn mutant enzyme.

One of the striking, and unexpected, features of the covalently bound sugar is the  $^1S_5$  skew boat conformation adopted by the covalently linked gulosyl moiety. This conformation positions the leaving group, which has a “ $\beta$ ”-configuration, in an axial position and anti-periplanar to the lone pair of the ring oxygen. This is consistent with stereoelectronic expectations. Furthermore, this conformation places the 2-hydroxyl group of the guloside in a favourable pseudo-equatorial position, which would otherwise be axial. Comparison of this structure with that of deoxymannojirimycin bound to wild-type enzyme, where the sugar adopts a  $^4C_1$  chair conformation, shows that there is little change in the positions of the 3- and 4-hydroxyl groups of the sugar. In both cases, the 3-hydroxyl group is held in place by hydrogen bonding to Asp92 and Asp472, as well as by coordinating to the active site zinc ion. The 4-hydroxyl in both sugars is kept in position by hydrogen bonding to Asp472 and Tyr727. In contrast, as would be expected in going from a chair to skew boat conformation, there is a considerable shift of the position of the

a.



b.

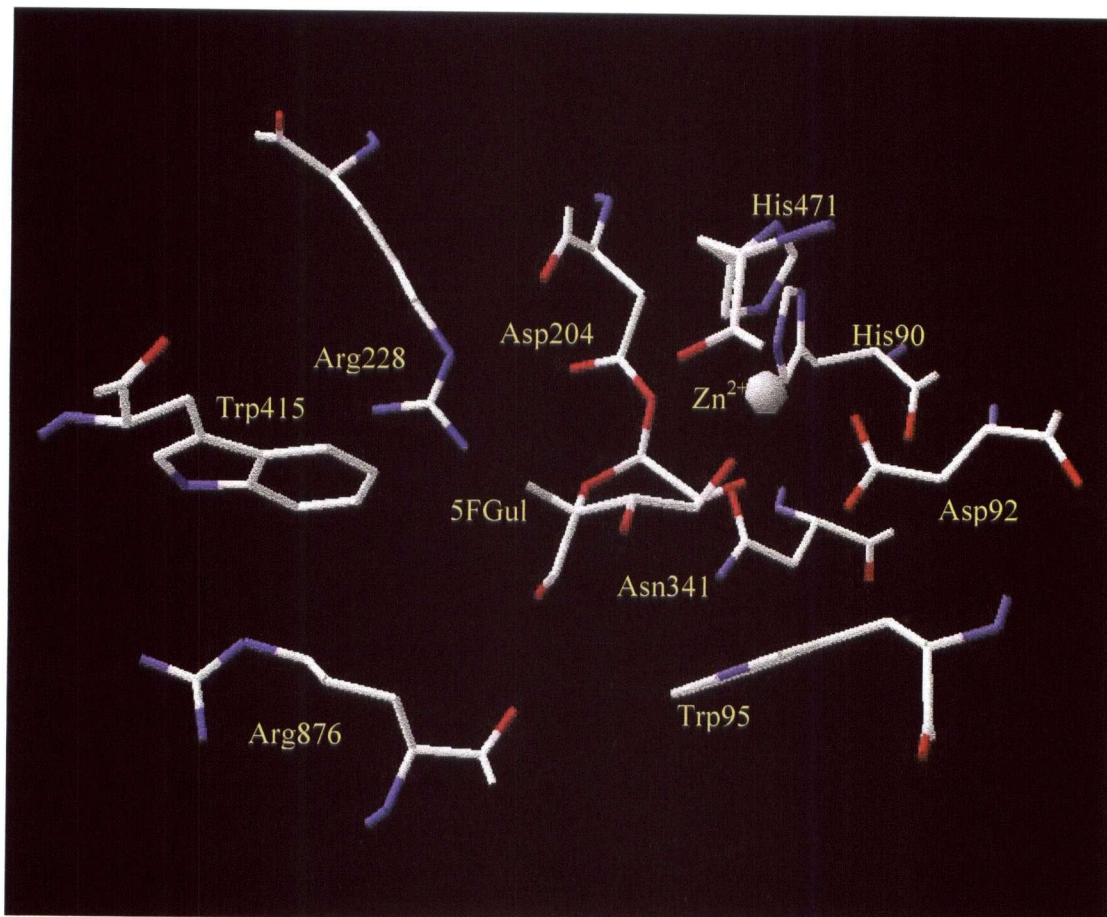


Figure 2.11 (a) Electron density map around the region of Asp204 and the covalently bound sugar. (b) Structure of the covalent intermediate formed during the hydrolysis of 5FGulF by the Asp341Asn mutant *Drosophila* GMII.

2-hydroxyl group and the anomeric carbon. This change, in addition to the newly formed covalent bond, results in the shortening of the distances between the 2-hydroxyl group, and both the zinc ion and Asp92. Interestingly though, there is very little movement in the position of Asp204, the catalytic nucleophile, with respect to the rest of the enzyme. This suggests that the skew boat conformation is adopted because the 3- and 4-hydroxyl groups are tightly held in place by several interactions, and that such a conformation is required to accommodate the newly formed covalent bond.

Another point of interest is the spatial position of the non-bonding oxygen of the catalytic nucleophile. This oxygen is positioned 2.4 Å away from the ring oxygen. A similar interaction was also seen in the structure of the covalent intermediate formed on a family 13 enzyme, cyclodextrin glucanotransferase (CGTase) (69). This oxygen-oxygen interaction is thought to possibly stabilize the positive charge that develops on the ring oxygen during the transition states. This may partially explain why the  $\alpha$ -retaining glycosidases seem to have more charge build-up on the ring oxygen while the  $\beta$ -retaining glycosidases, where this interaction is not possible, seem to have charge build-up on the anomeric carbon during the transition state (17).

However, the skew boat conformation may be an artefact of the experimental design involved in trapping the intermediate and thus, may not be relevant to the hydrolysis of the natural substrate by GMII. Two modifications of the substrate/enzyme system were made in order to trap the covalent intermediate. The first modification was the use of an acid/base mutant GMII. This residue does not make any direct contacts with the covalently bound sugar. However, since this residue is in the active site, its mutation, and consequently the absence of the negatively charged carboxylic acid, may result in a

perturbation in the conformation of the covalently linked sugar. The second modification was the use of a sugar with an inverted configuration at C-5 (5FGulF) relative to mannose. It is possible that this change will favour a skew boat conformation over another form such as a  ${}^4C_1$  chair conformation. For example, by adopting a skew boat conformation the sugar would avoid 1,3-diaxial interactions of the bulky hydroxymethylene with H-1 and H-3. In fact, in the protected form, the 5FGulF adopts a boat-like conformation while the 5FManF adopts a chair conformation (72), indicating that 5-fluoro gulo-type compounds are more prone to adopting this conformation.

#### ***2.4.5 Kinetic analysis of the inactivation of the wild-type GMII by 5FGulF***

In order to determine whether the mutation is affecting the conformation of the covalently bound sugar, it is necessary to determine the structure of the covalent intermediate formed on the wild-type enzyme. To this end, attempts were made at trapping the intermediate formed during 5FGulF hydrolysis by wild-type GMII. As expected, no time-dependent inactivation was seen when the assay for residual activity was done at 37°C. However, when the assay for residual activity was conducted at 8°C, time-dependent inactivation was seen (Figure 2.12). As is apparent, complete inactivation was not observed at an inactivator concentration of 0.4 mM. Rather, a steady state level was attained, presumably due to relatively rapid reactivation. The 5FGulF was tested as a substrate for GMII at 37°C by measuring fluoride ion release, yielding a  $k_{\text{cat}}$  value of  $5.1 \times 10^{-3} \text{ s}^{-1}$  and a  $K_m$  value of 0.2 mM. At higher concentrations (>1 mM), there was kinetic evidence for transglycosylation of the 5FGulF in a self-condensing reaction. This further suggests that the deglycosylation step is rate limiting and that an accumulation of intermediate is taking place.

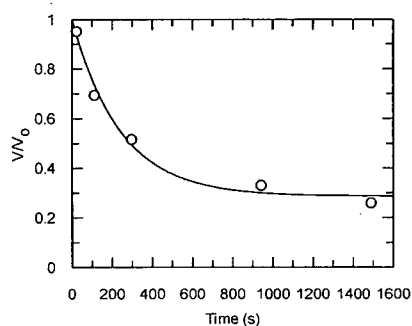


Figure 2.12 Inactivation of wild-type *Drosophila* GMII by 0.4 mM 5FGulF.

The mass of the labelled protein was determined by ESI-MS and was shown to be greater than that of the unlabelled protein by 180 Da (Figure 2.13). This corresponds, within error, to the addition of a single 5-fluoro-gulosyl moiety (theoretical increase: 181 Da), thereby confirming the covalent nature of the intermediate formed during 5FGulF hydrolysis by wild-type GMII. These results suggest that structural analysis of this intermediate should be possible if carried out at low temperatures. A point of interest is the difference in size of the wild-type enzyme compared with the Asp341Asn mutant GMII. This is most likely due to a difference in truncation during the expression of the protein.

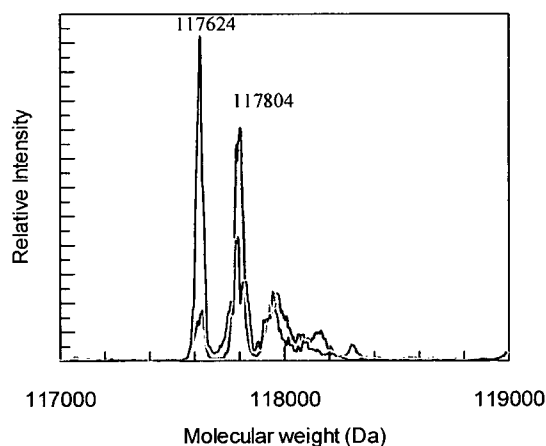


Figure 2.13 Reconstructed electrospray mass spectra of wild-type *Drosophila* GMII in the absence (black) and in the presence (fuchsia) of 5FGulF.

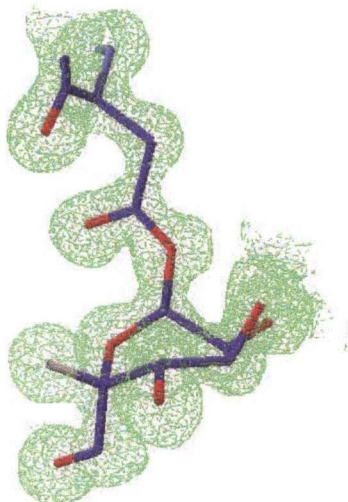
#### ***2.4.6 Structural analysis of the intermediate formed during 5FGulF hydrolysis by wild-type GMII***

Analysis of the structure of the wild-type enzyme, soaked with 5FGulF, determined to 1.20 Å resolution, revealed a sugar bound in the active site. Contiguous electron density was observed from the anomeric carbon to a  $\delta_1$ -oxygen, consistent with a covalent bond between the sugar and the enzyme. The distance between the anomeric carbon and the  $\delta_1$ -oxygen of Asp204 was found to be 1.43 Å, which is also consistent with a covalent bond formed between these two atoms. By overlaying this structure with that of the intermediate formed on the Asp341Asn mutant GMII, it was evident that there are few structural changes in the side chain conformation as a consequence of the mutation of Asp341 (Figure 2.14). More importantly, the covalently bound sugar, as in the Asp341Asn mutant GMII structure, adopts a  ${}^1S_5$  skew boat conformation, suggesting that this conformation is not an artefact of the mutation to the enzyme.

#### ***2.4.7 Synthesis of an alternative inactivator***

A more probable explanation for why a skew boat conformation might be seen in these cases is that the modified “substrate” favours this unusual conformation. As mentioned above, a skew boat conformation would place a bulky hydroxymethyl substituent at C-5 in a more favoured equatorial position. In order to test for this possibility, it is necessary to use inactivators that do not have a bulky substituent in the gulo configuration at C-5. The two inactivators considered were 5-fluoro- $\alpha$ -D-mannosyl fluoride (5FManF) and 2-deoxy-2-fluoro- $\alpha$ -D-mannosyl fluoride (2FManF).

a.



b.

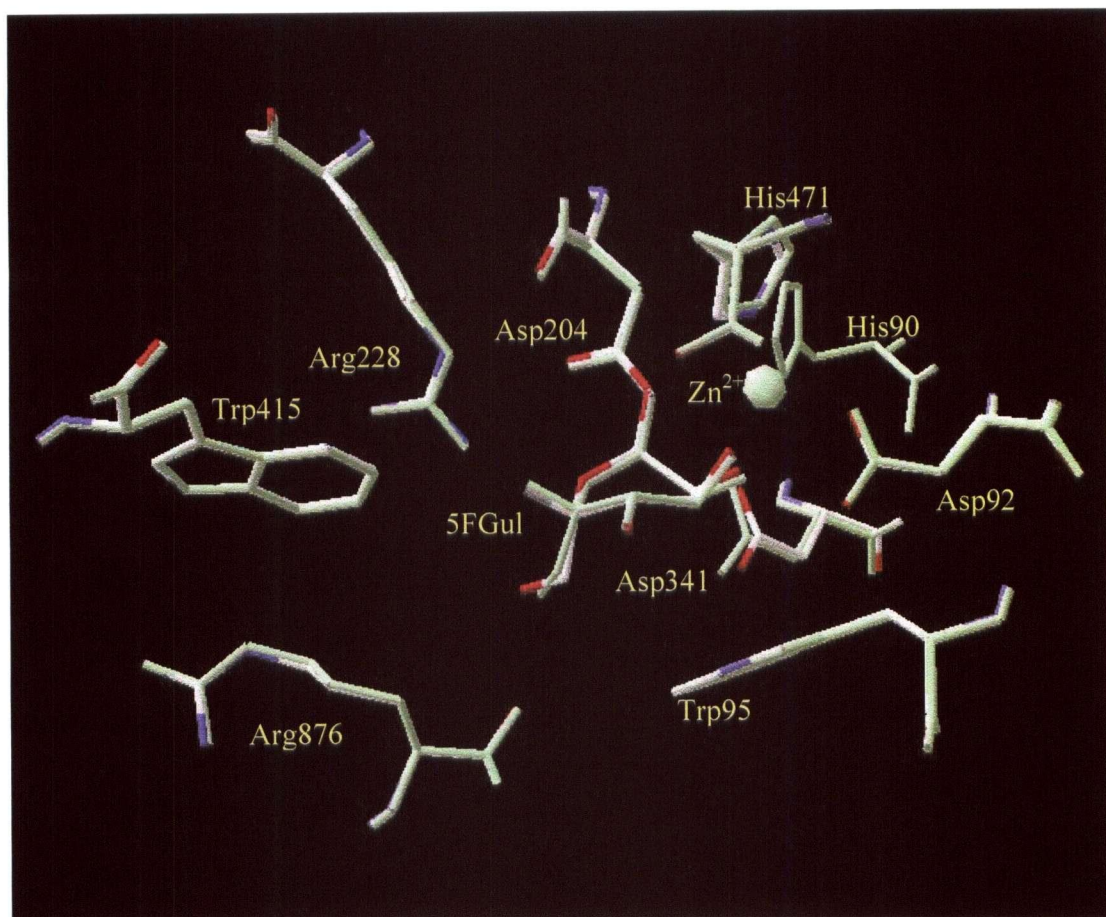
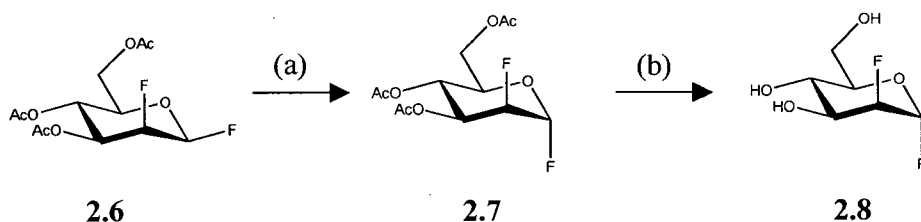


Figure 2.14 (a) Electron density map around the region of Asp204 and the covalently bound sugar. (b) Structure of the covalent intermediate formed during the hydrolysis of 5FGulF by wild-type *Drosophila* GMII. The structure of the covalent intermediate formed during the hydrolysis of 5FGulF by the Asp341Asn mutant *Drosophila* GMII is overlaid (light green).

According to literature precedent, the protected form of 5FManF can be synthesized from **2.4** by treatment with  $\text{BF}_3$  (Scheme 2.1) (72). Unfortunately, several attempts at this transformation resulted in the degradation of starting material to baseline products and possibly an elimination product. An alternate route to this compound involves treatment of **2.3** with  $\text{AgBF}_4$ . However, although some 5FGulF was made in this reaction, no 5FManF was isolated. This approach was therefore abandoned.

Synthesis of 2FManF was started from peracetylated 2-deoxy-2-fluoro- $\beta$ -D-mannosyl fluoride (**2.6**) (synthesized by Dr. David L. Zechel according to (102)) as shown in Scheme 2.3. Treatment of this compound with HF/pyridine resulted in the anomerization of the anomeric fluorine to the desired  $\alpha$ -configuration (**2.7**) (102). The product was then deprotected using  $\text{NH}_3$  in MeOH to yield **2.8** in 20% yield.



Scheme 2.3 An outline of the synthesis of 2FManF. a) HF/pyridine, and (b)  $\text{NH}_3$ , MeOH.

#### 2.4.8 Kinetic analysis of the interaction of 2FManF with GMII

Previous studies of the cleavage of 2-deoxy-2-fluoroglycosides by  $\alpha$ -glycosidases had shown that these compounds were very slow substrates for the enzyme with the rate limiting step being deglycosylation. However, these compounds did not inactivate the enzyme (65). Therefore, 2FManF was tested as a substrate for the wild-type GMII by monitoring fluoride release using a fluoride-selective electrode. Consistent with previous

findings, the 2FManF was found to be a very slow substrate for wild-type GMII with a  $k_{\text{cat}}/K_{\text{m}}$  value of  $8.5 \times 10^{-5} \text{ s}^{-1}\text{M}^{-1}$ . Unfortunately, due to the high  $K_{\text{m}}$  value ( $>25 \text{ mM}$ ) it was not possible to determine the  $k_{\text{cat}}$  and  $K_{\text{m}}$  values independently of each other. The high  $K_{\text{m}}$  value is not surprising as this substrate is missing a 2-hydroxyl group, which could otherwise participate in hydrogen bonding with active site residues. As this  $k_{\text{cat}}/K_{\text{m}}$  value was lower than the value seen for the hydrolysis of 5FGulF by wild-type GMII, the 2FManF was not tested as a substrate for the Asp341Asn mutant GMII since the rates expected are much lower and likely immeasurable. When 2FManF was tested as a reversible inhibitor of the Asp341Asn mutant GMII, a  $K_{\text{i}}$  value of approximately 7.5 mM was determined. This value is lower than the  $K_{\text{m}}$  value for the hydrolysis of 2FManF by wild-type GMII (where the  $K_{\text{m}} > 25 \text{ mM}$ ) and suggests the accumulation of an intermediate.

#### ***2.4.9 Mass spectrometric analysis of the intermediate formed during 2FManF hydrolysis by Asp341Asn mutant***

ESI-MS analysis of a sample of the Asp341Asn mutant GMII revealed several peaks (Figure 2.15). The main peak at 120468 Da corresponds to the mass of the mutant GMII, while the peaks corresponding to higher mass species with lower intensity are most likely different glycoforms. Incubation of the enzyme with 2FManF prior to the ESI-MS analysis results in the shift of the profile by 166 Da, indicating that each of these species is being covalently labelled by the inactivator (expected increase of 165 Da). The fact that there is still a peak that corresponds to the mass of unlabelled enzyme in the sample indicates that this accumulation is probably incomplete.

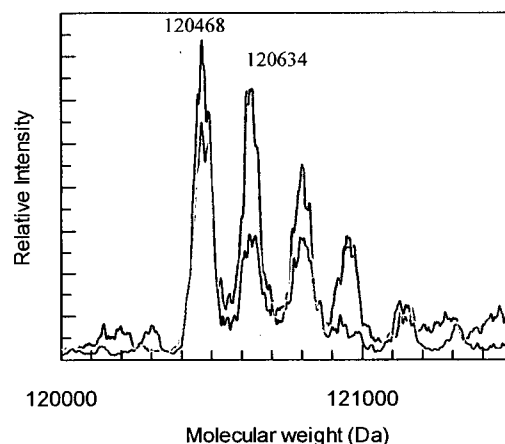


Figure 2.15 Reconstructed electrospray mass spectra of Asp341Asn mutant *Drosophila* GMII in the absence (black) and in the presence (fuchsia) of 2FManF.

#### ***2.4.10 Structural analysis of the intermediate formed during 2FManF hydrolysis by Asp341Asn mutant GMII***

In order to determine the structure of the covalent intermediate formed during 2FManF hydrolysis, crystals of Asp341Asn mutant GMII were soaked with 2FManF for 30 minutes and subsequently frozen. The structure was solved to 1.3 Å resolution. A sugar was seen bound in the active site of the mutant enzyme (Figure 2.16) and again, contiguous electron density was seen between the anomeric carbon and the  $\delta_1$ -oxygen of Asp204. The apparent distance between these two atoms was greater at 1.79 Å and there was less electron density between the two atoms than in the other two structures. This distance is not consistent with any one type of bond or interaction and most likely represents an average structure between the covalent intermediate and another bound species such as the product. In fact, the density seems to fit well to a model where 50% of the bound species is the covalent intermediate. Indeed, this would be consistent with the MS results that suggested that there is less than 100% accumulation of the intermediate at the steady state.

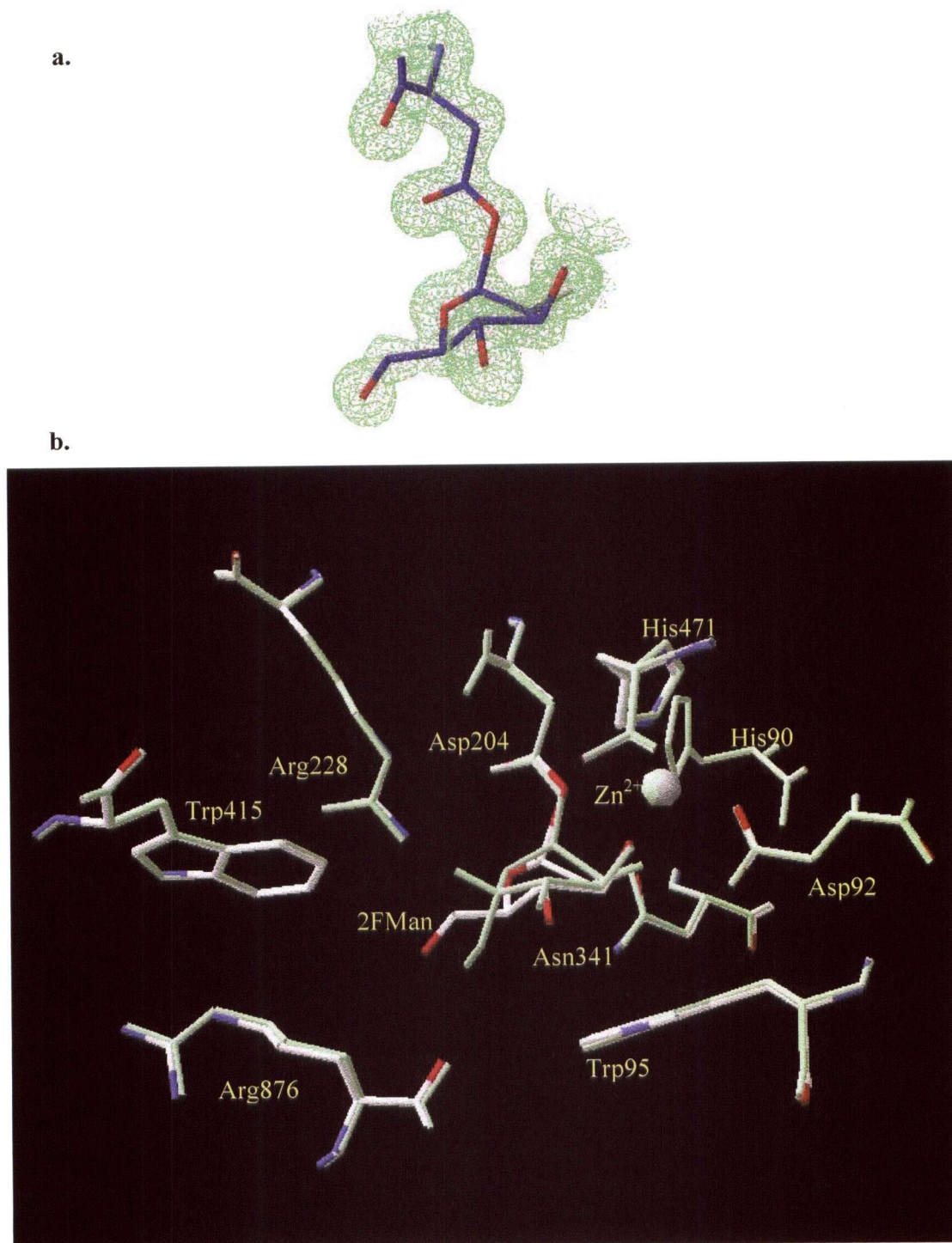


Figure 2.16 (a) Electron density map around the region of Asp204 and the covalently bound sugar. (b) Structure of the covalent intermediate formed during the hydrolysis of 2FManF by Asp341Asn mutant *Drosophila* GMII. The structure of the covalent intermediate formed during the hydrolysis of 5FGulF by wild-type *Drosophila* GMII is overlaid (light green).

Interestingly, the sugar moiety once again adopts a  ${}^1S_5$  skew boat conformation in this trapped intermediate, despite the bulky substituent at C-5 being in an inverted configuration from the 5FGulF compound. Furthermore, overlay of the structure for the intermediate formed during 5FGulF hydrolysis with that of 2FManF hydrolysis showed that the ring carbons of the sugar overlay very well with one another (Figure 2.17a). Consequently, the hydroxymethylene group is equatorial in the intermediate for 2FManF hydrolysis while it is pseudo-axial in the intermediate of 5FGulF hydrolysis. This results in the 6-hydroxyl group being positioned spatially in a similar location within the active site (Figure 2.17b). One of the possible reasons for this similar position of the 6-hydroxyl group is a hydrogen bond to the backbone carbonyl of Arg876. In addition though, there is a hydrophobic pocket above the face of the sugar ring formed by Phe206, Trp415 and Tyr727. Positioning of the 6-hydroxyl group towards this face would result in a steric clash. This may, in part, be why both the intermediates formed during 5FGulF and 2FManF hydrolysis adopt similar conformations.

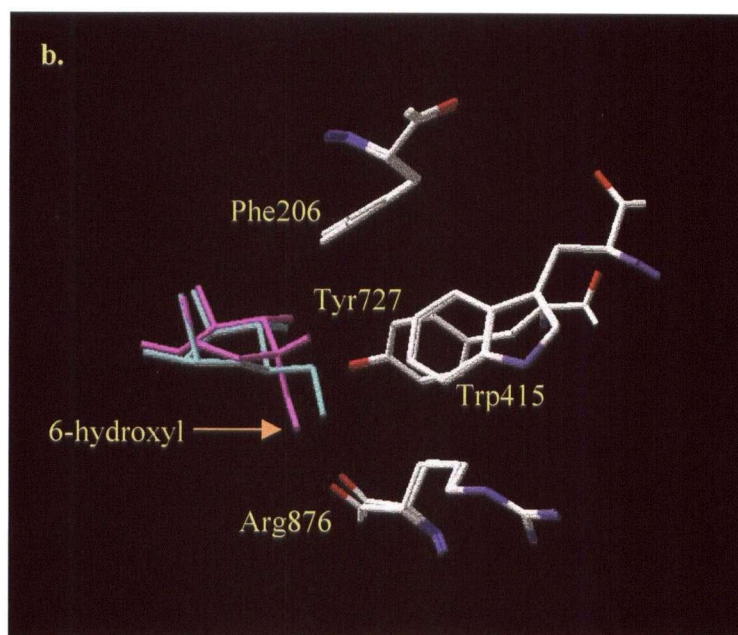
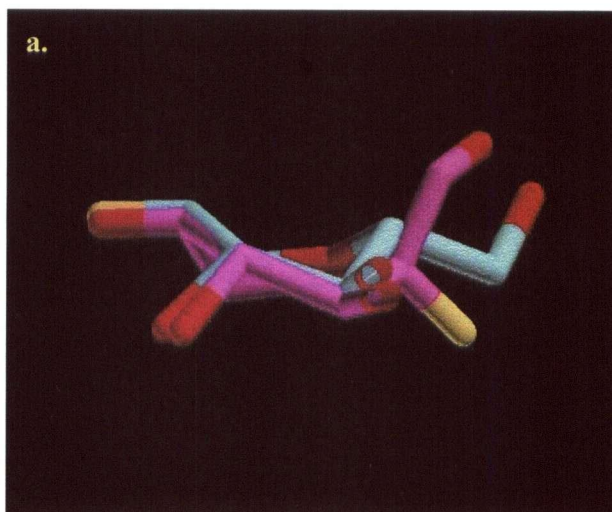


Figure 2.17 (a) Overlays of the structures of the sugar in the covalent intermediate during 2FmanF (cyan) hydrolysis with that of 5FGulF (magenta); courtesy of Dr. Douglas A. Kuntz. (b) The same overlay, this time showing the sugar in respect to select active site residues.

From this, it seems that the configuration at C-5 does not seem to significantly affect the conformation of the sugar in the intermediate formed on GMII during hydrolysis. Because the mutation of the acid/base catalyst was determined not to affect the conformation of the intermediate sugar for 5FGulF hydrolysis, it is likely that this is also the case for 2FManF hydrolysis. The intermediate formed during hydrolysis of 2FManF by the wild-type enzyme is likely to also adopt a  ${}^1S_5$  skew boat conformation. These three structural studies clearly point to a  ${}^1S_5$  skew boat conformation also being adopted in the covalent intermediate formed during hydrolysis of the natural substrate by GMII.

#### ***2.4.11 Implications of the skew boat conformation***

From a catalytic standpoint there are several possible reasons why the glycosyl moiety in the glycosyl-enzyme intermediate might adopt a  ${}^1S_5$  skew boat conformation. In the deglycosylation step, a nucleophilic water molecule attacks the anomeric carbon, displacing Asp204. By adopting this conformation, the hydroxyl groups and hydrogens will not hinder the water from making this attack (Figure 2.18). Kinetic isotope effect analyses conducted on other glycosidases have also suggested that the sugar goes through a transition state where C-2, C-1, O-5 and C-5 are in a plane (14). The energy barrier between the  ${}^1S_5$  skew boat and the  $B_{2,5}$  boat structure, in which these four atoms are in a plane, is fairly low so that minimal energy is required for conformational changes (for example, this barrier is 0.9 kcal/mol for cyclohexane) (103). This conformation therefore brings the intermediate structure closer to the proposed transition state structure. Furthermore, the skew boat conformation also brings the 2-hydroxyl group to a pseudo-equatorial position, further decreasing the energy barrier to the transition state species.

Interestingly, this conformation also places the leaving group anti-periplanar to the lone pair of the ring oxygen. According to the controversial anti-periplanar lone-pair hypothesis, proposed by Deslongchamps', this conformation is required before the departure of the leaving group can take place (63).

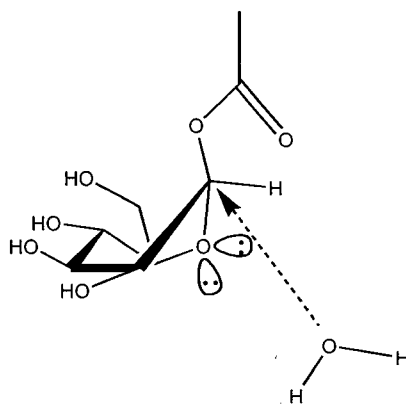


Figure 2.18 Several benefits during catalysis for adopting the skew boat conformation. (1) Water molecule hindered from making a nucleophilic attack of the anomeric carbon. (2) 2-Hydroxyl group is in a pseudo-equatorial configuration. (3) Ring oxygen lone-pair is antiperiplanar to the leaving group.

Recently, the three-dimensional structure of a  $\beta$ -mannanase from *Pseudomonas cellulosa* (endo- $\beta$ -retaining mannosidase) was determined at various points along its reaction coordinate (62). Interestingly, an overlay of the sugar from the substrate bound complex (Michaelis complex) in the  $\beta$ -mannanase structure with that of the covalent intermediate formed on GMII shows that the conformations adopted by these two structures are essentially identical (Figure 2.19a). In this “ $\beta$ -mannosidase” structure, the substrate bound is 2,4-dinitrophenyl 2-deoxy-2-fluoro- $\beta$ -mannotrioxide. The 2,4-dinitrophenyl group seems to bind to the +1 subsite of the enzyme. In this enzyme, the binding to the +1 subsite seems to provide the axial directionality for the scissile bond. Binding of a mannoside to the -2 subsite also locks the position of C-4 on the -1 subsite sugar. The skew boat conformation adopted in the -1 subsite, therefore, seems to be a

consequence of the positions of the sugars bound at the -2 and +1 subsite with respect to the -1 subsite. In addition, several residues form hydrogen bonds with the 2- and 3-hydroxyl groups, further favouring a skew boat conformation (Figure 2.19b).

a.

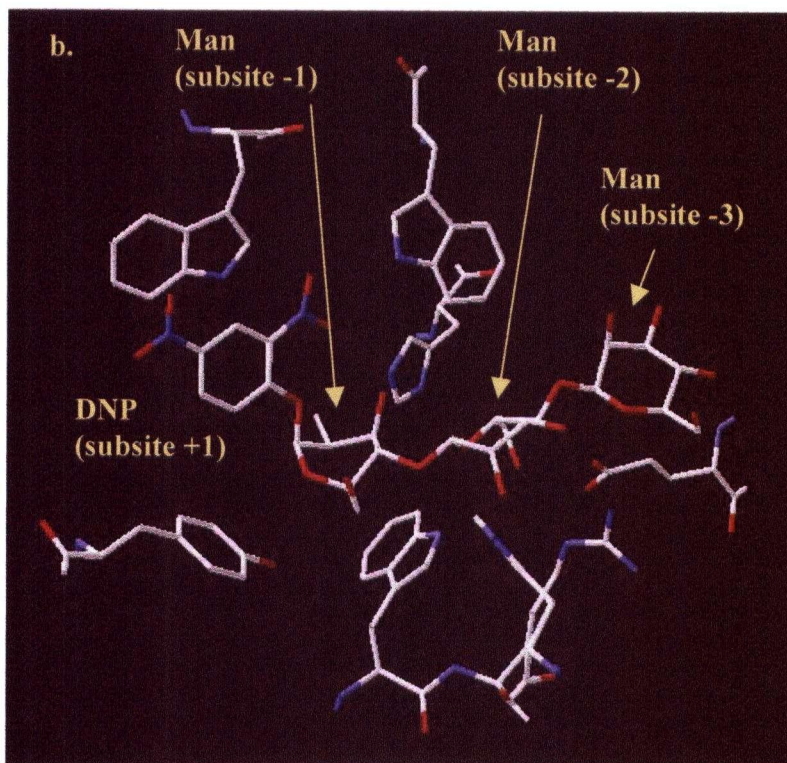


Figure 2.19 (a) Overlays of the structures of the covalent intermediates formed during 2FManF hydrolysis with that of the -1 subsite sugar in the Michaelis complex of  $\beta$ -mannanase (fuchsia). (b) Structure of the Michaelis complex of the  $\beta$ -mannanase (62).

Interestingly, the analogous situation seems to take place in the active site of GMII. As was mentioned earlier, in GMII, the directionality of the scissile bond is determined by the position of the catalytic nucleophile, Asp204, a residue whose position does not shift significantly on going from the free enzyme to the covalent intermediate. An extensive hydrogen-bonding network to the 3- and 4-hydroxyl groups determines the position of C-4. The two different glycosidases, therefore, seemed to have achieved the same conformation through similar, yet different methods.

This commonality in the conformation of the bound sugar may not be completely unexpected. The  $\beta$ -mannanase is a  $\beta$ -retaining mannosidase and as such, during the glycosylation step, a  $\beta$ -mannoside is transformed into an  $\alpha$ -mannoside (Figure 2.20). In the deglycosylation step of the  $\alpha$ -retaining mannosidase, GMII a  $\beta$ -mannoside is transformed into an  $\alpha$ -mannose. It is therefore possible that these two steps go through a similar transition state. Consequently, the ground state conformations adopted would also be expected to be similar. Unfortunately, at this point in time, there are no structural data for a product complex of GMII. Therefore, it is impossible to say with certainty that the two steps have a common transition state. This, though, is the first structural evidence showing that the deglycosylation step of an  $\alpha$ -glycosidase may be similar to the glycosylation step of a  $\beta$ -glycosidase.

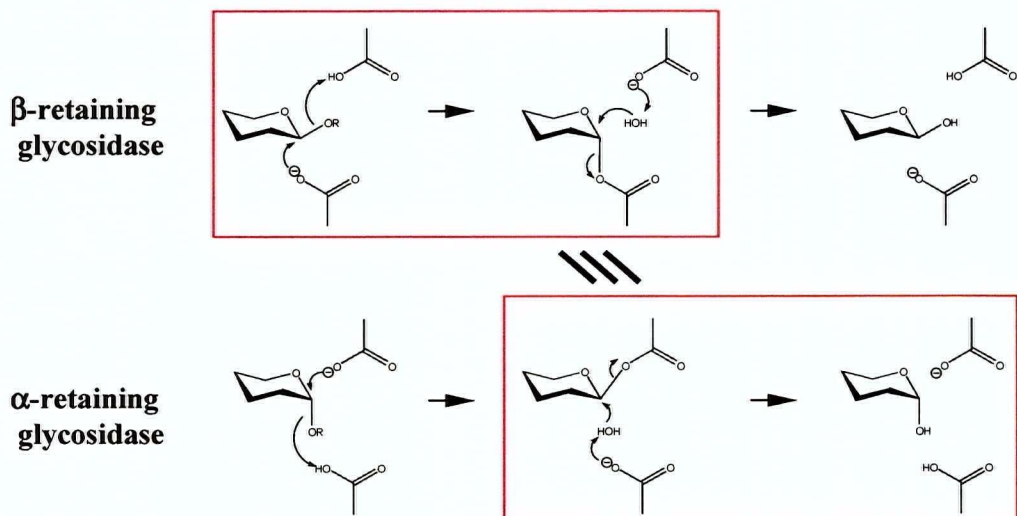


Figure 2.20 Comparison of the double displacement mechanism of an  $\alpha$ -retaining glycosidase versus a  $\beta$ -retaining glycosidase. The deglycosylation step and glycosylation step of the respective enzymes have been highlighted.

Because most  $\alpha$ - and  $\beta$ -retaining glycosidases go through a double displacement mechanism, according to the above hypothesis, the phenomenon of the covalent intermediate of an  $\alpha$ -retaining glycosidase resembling the Michaelis complex of a  $\beta$ -retaining mannosidase and *vice versa* should be general to all  $\alpha$ - and  $\beta$ -retaining glycosidases with “similar” substrates. The structures of a number of Michaelis complexes of “ $\beta$ -glucosidase” have been determined (52, 56, 61, 64). In all cases to date, substantial substrate distortion has been seen with each of these sugars adopting  ${}^1,4B$  boat conformations.

At present, the only structure determined of a covalent intermediate formed on an  $\alpha$ -retaining glycosidase is that of cyclodextrin glucoamyltransferase (CGTase) (69). In this structure, the sugar in the  $-1$  subsite adopts a  ${}^4C_1$  chair conformation. The CGTase is a member of glycosidase family 13, a family that also includes  $\alpha$ -amylases and  $\alpha$ -

glucosidases. As no known Michaelis complex of a  $\beta$ -glucosidase adopts a  ${}^4C_1$  chair conformation, it would seem that the commonality between the  $\alpha$ - and  $\beta$ -glycosidase as seen in the two mannosidases is not a general phenomenon. However, CGTase is not a true glycosidase in that it favours the transglycosylation reaction over the hydrolysis reaction. It is possible that CGTase has some mechanism for avoiding nucleophilic attack of the glycosyl-enzyme intermediate by an incoming water molecule. One such mechanism may involve the requirement for a conformational change of the glucose moiety in the  $-1$  subsite before reaction can take place. Binding of the acceptor sugar to the enzyme could potentially induce this conformational change. If this is the case, then it is possible that the active conformation of the  $-1$  subsite sugar in the covalent intermediate of CGTase is a skew boat conformation. This will require further structural studies.

#### ***2.4.12 Conclusions and future studies***

The structures of the covalent intermediates formed during the hydrolysis of 5FGulF and 2FManF were determined by X-ray crystallography. Both the kinetic and structural analysis of these reactions suggested that GMII hydrolyses  $\alpha$ -mannosides through a double displacement mechanism involving a covalent glycosyl-enzyme intermediate. This is consistent with the huge amount of kinetic and structural evidence for such an intermediate forming on  $\beta$ -glycosidases. The present study also demonstrates that the sugar in the glycosyl-enzyme intermediate adopts a  ${}^1S_5$  skew boat conformation, a conformation also adopted by the Michaelis complex of family 26  $\beta$ -mannanases. This suggests that the glycosylation step of  $\beta$ -glycosidases goes through a similar transition state to that of the deglycosylation step of  $\alpha$ -glycosidases.

In order to establish this commonality in the  $\alpha$ - and  $\beta$ -“mannosidases”, it is necessary to show that the conformation of the product of the  $\alpha$ -mannosidase reaction resembles the covalent intermediate of the  $\beta$ -mannanase. One of the difficulties in determining this lies in the fact that the product of the  $\alpha$ -mannosidase reaction is mannose, which binds poorly to GMII.

Another structure that would be of great interest is the structure of the Michaelis complex of GMII. The structure of this complex, along with the structure of the covalent intermediate determined in this study, would define the conformational pathway that the  $\alpha$ -mannoside takes during the glycosylation step of hydrolysis by the  $\alpha$ -mannosidase. This structure may also show differences between the transition states of the glycosylation step in  $\alpha$ -glycosidases versus that of the glycosylation step in  $\beta$ -glycosidases.

## **Chapter 3 The chloride ion-binding site in $\alpha$ -amylases**

## 3.1 General introduction

### 3.1.1 Family of $\alpha$ -Amylases

$\alpha$ -Amylase ( $\alpha$ -1,4 glucan-4-glucanohydrolase, EC 3.2.1.1) is an endoglycosidase that catalyzes the hydrolysis of  $\alpha$ -(1,4) glycosidic bonds of glucose polymers with net retention of anomeric configuration. Because such polymers are widely used as an energy source in nature, it is not surprising that  $\alpha$ -amylases are produced by various organisms ranging from microorganisms to mammals (104, 105). From sequence analysis, many of these glycosidases has been assigned to family 13 of Henrissat's glycosidase classification (7-9). Enzymes of this family, which also includes  $\alpha$ -glucosidases, cyclodextrin glucanotransferases (CGTase), pullulanases and glycogen debranching enzyme, have significant sequence similarity in only four short regions, each consisting of about 20 amino acids (Figure 3.1).

Being a retaining glycosidase, the  $\alpha$ -amylases, and more generally family 13 glycosidases, are thought to go through a double displacement mechanism (13, 14, 17). Evidence for this mechanism has come from various different studies. The mechanism-based inactivator, 5-fluoro-glucosyl fluoride, has been used to trap the covalent intermediate of a family 13 yeast  $\alpha$ -glucosidase and identify the catalytic nucleophile (106). Low temperature studies using  $^{13}\text{C}$ -NMR also have suggested the presence of a covalent intermediate using natural substrates (107). In addition, the three-dimensional structure of the covalent intermediate of another family 13 enzyme, the cyclodextrin glucanotransferase (CGTase), has been determined by X-ray crystallography (69), further supporting a double displacement mechanism for family 13 enzymes. Mutagenesis (108)

and structural studies (109, 110) of several  $\alpha$ -amylases have probed the role of the conserved carboxylic acid residues within the active site in this mechanism, demonstrating that they play key roles in catalysis.

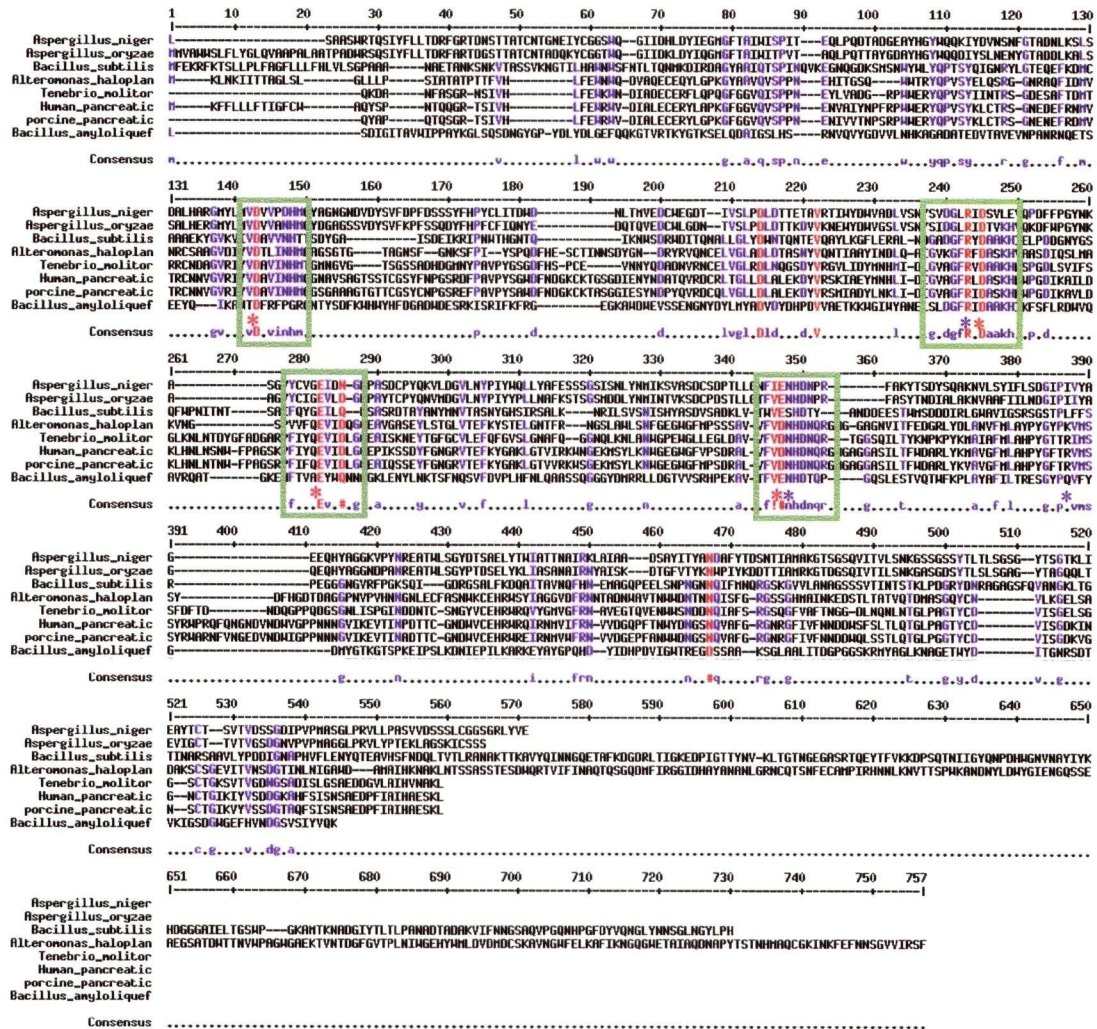


Figure 3.1 Sequence alignment of representative members of family 13  $\alpha$ -amylases. The four conserved regions are boxed in green. The four active site carboxylic acids are labelled (\*), as are the three chloride-ion binding residues (\*). The sequences shown are:  $\alpha$ -Amylase from *Aspergillus niger* (P56271), *Aspergillus oryzae* (P10529), *Bacillus subtilis* (O82953), *Alteromonas haloplanctis* (P29957), *Tenebrio molitor* (P56634), human pancreas (P04746), porcine pancreas (P00690), and *Bacillus amyloliquefaciens* (P00692).

Recently, the three-dimensional structures of a number of  $\alpha$ -amylases have been determined and published, including those from *Alteromonas halioplanctis* (111),

*Aspergillus oryzae* (110), *Aspergillus niger* (112), *Bacillus licheniformis* (113), barley (114), porcine pancreas (115), human saliva (116) and human pancreas (117). Despite relatively weak similarities in the primary structures, the tertiary structures are fairly well conserved within this group of enzymes. In general,  $\alpha$ -amylases are monomeric proteins of about 50 kDa with three structural domains (Figure 3.2). Domain A is an  $\alpha/\beta$  barrel that contains the active site. Domain B consists of a loop that protrudes from Domain A and forms the conserved calcium ion binding site. These two domains closely interact via the bound calcium ion. Domain C is an eight-stranded  $\beta$ -barrel type structure located at the C-terminus. This latter domain is only loosely associated with the other two domains and its function is still not understood.

### ***3.1.2 Chloride-dependent and independent $\alpha$ -amylases***

A comparison of  $\alpha$ -amylases from different sources reveals that these enzymes may be classified into two sub-families. One group of  $\alpha$ -amylases requires the presence of chloride in order to exhibit full catalytic activity (118). The second group of  $\alpha$ -amylases does not have this requirement and the activity of the enzyme is independent of the chloride concentration. These chloride-independent  $\alpha$ -amylases are often produced by lower order organisms such as bacteria and fungi. The chloride-dependent  $\alpha$ -amylases were originally found primarily in higher organisms such as mammals and insects. Recently though, a chloride-dependent  $\alpha$ -amylase produced by the bacterium, *Alteromonas halioplanctis* has been found (119), showing that this property is not unique to  $\alpha$ -amylases produced by higher order organisms.

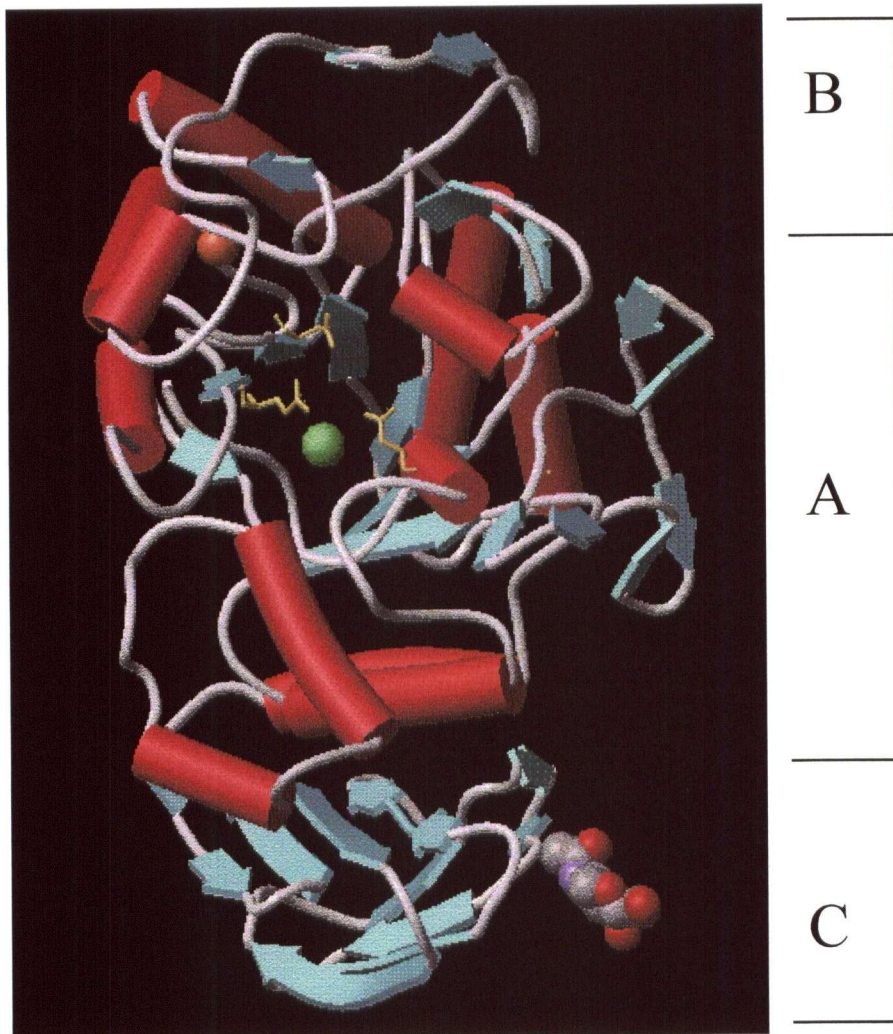


Figure 3.2 Ribbon representation of the human pancreatic  $\alpha$ -amylase. Three of the active site carboxylic acids are shown in yellow. The conserved calcium and chloride are represented in orange and green respectively.

Several studies have been carried out to characterize the activation of  $\alpha$ -amylase by chloride. Early studies on porcine pancreatic  $\alpha$ -amylase (PPA) showed that removal of the chloride not only resulted in the loss of activity, but also, a shift in the pH optimum of this enzyme (120, 121). Titration experiments demonstrated that the chloride ion was activating the  $\alpha$ -amylase with a 1:1 stoichiometry. In addition, circular dichroism (CD)

experiments suggested that addition of chloride did not affect the secondary structure of the protein. These results were found to be more general when Feller *et al.* showed that chloride concentration had similar effects on the  $\alpha$ -amylase from *A. halioplanctis* (119)

### **3.1.3 Structure of the chloride ion-binding site**

The recent determinations of three-dimensional structures of chloride-dependent  $\alpha$ -amylases have shown that members of this group of  $\alpha$ -amylases have a chloride ion-binding site located in Domain A (117). This binding pocket comprises three residues – Arg195, Asn298 and Arg337 (human pancreatic  $\alpha$ -amylase numbering is used throughout the chapter) – that coordinate the chloride ion and position it  $\sim 5$  Å from the active site residues (Figure 3.3). Of these three residues in the binding pocket, Arg195 and Asn298 are conserved in both the chloride-dependent and -independent  $\alpha$ -amylases. This does not come as a surprise as three-dimensional structures have shown that both are involved in additional roles besides that of coordinating the chloride ion. Arg195 is involved in a hydrogen-bonding network with several catalytic residues while Asn298 most likely is involved in the structural stabilization of an active site loop. In contrast, Arg337 is only conserved within chloride-dependent  $\alpha$ -amylases (Figure 3.1). In these  $\alpha$ -amylases a basic residue (Arg or Lys) is consistently found at this position, providing another coordination site for the chloride ion. In the chloride-independent  $\alpha$ -amylases, the identity of this residue seems to be highly variable.

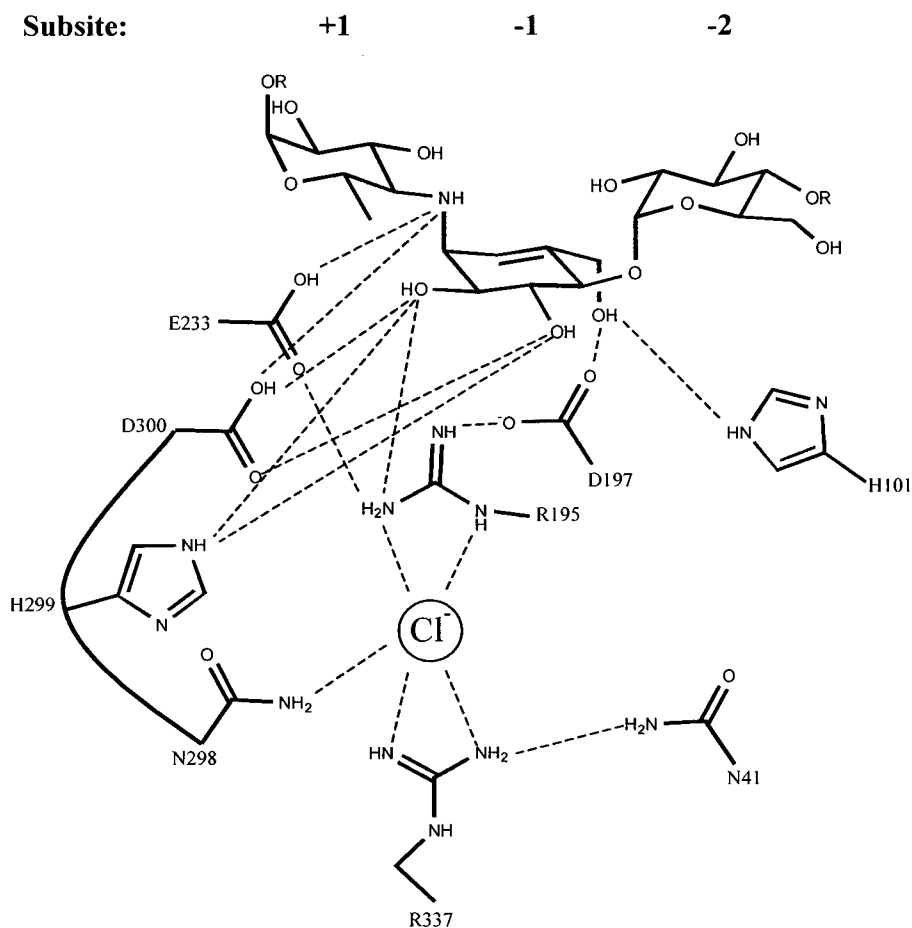


Figure 3.3 Diagram of some representative interactions between the chloride ion-binding site residues, the active site residues and the inhibitor, acarbose in human pancreatic  $\alpha$ -amylase. Dashed lines represent distances shorter than 3.5Å.

### 3.2 Specific aim of this study

*Determination of the mechanism of chloride activation.* Although the effects of chloride on chloride-dependent  $\alpha$ -amylases have been well characterized, no study to elucidate the mechanism of this unique activation has been conducted. Systematic mutations of the residues of the chloride ion-binding site will be made in the chloride-dependent  $\alpha$ -amylase, human pancreatic  $\alpha$ -amylase (HPA). Characterization of these mutant enzymes

should help clarify the role of each of the residues in chloride binding and help in determining the mechanism of chloride activation.

### 3.3 Results and discussion

#### 3.3.1 *Rationale for the mutations to HPA*

In any mutational study, the difficulty lies in dissecting out the relevant information from the results obtained. Of the residues involved in chloride ion binding, Arg195 and Asn298 are involved in other roles aside from chloride binding, thereby complicating analysis. In general, the standard mutation for any mutagenesis study is a mutation to alanine. However, often times, the complete removal of a side chain is considered too drastic to determine the exact role that the side chain plays. Therefore, in addition to the alanine mutations, often, a “conservative” mutation is made where the mutation removes the interaction of interest while trying to keep interactions with other residues.

The interactions that the chloride makes with Arg195 are with the  $\epsilon$ - and  $\gamma_1$ -nitrogen (Figure 3.3). However, it is very likely that the positive charge of the arginine is essential for interaction with the negatively charged chloride ion. The most conservative substitution for arginine that removes a positive charge is that of glutamine. A mutation to this residue would keep the  $\epsilon$ -nitrogen so that it can still make other interactions with the active site residues while removing the basicity and charge of the side chain. Therefore, the Arg195Gln mutation was used to determine the role of this residue in chloride activation.

Asn298 interacts with the chloride through an amide nitrogen. The three-dimensional structures reveal that the amide oxygen of this side chain also seems to stabilize an active site loop by hydrogen bonding to a backbone amide. Sequence alignment of this region (Figure 3.1) showed that in the case of a single  $\alpha$ -amylase from

*Bacillus subtilis*, this residue was a serine. Furthermore, in the three-dimensional structure of this  $\alpha$ -amylase (122), the hydroxyl oxygen of the serine substituted for the amide oxygen as a hydrogen bond acceptor in stabilizing the active site loop. As such, the Asn298Ser mutation was used in order to study the role of this residue in chloride activation.

In contrast to the other two residues, Arg337 does not seem to interact with other active site residues. However, as with Arg195, it is very likely that the chloride interacts with this residue through ionic interactions. Indeed, in chloride-independent  $\alpha$ -amylases, the only qualification at this position seems to be that the side chain carries no positive charge (118). It is possible, however, that the arginine side chain may interact with other residues in solution or that a void left by completely removing the side chain would result in the collapse of other residues to fill the space. As such, the Arg337Gln mutation was made for determination of the role of this residue in chloride activation.

### **3.3.2 Structural analysis of the mutant enzymes**

Crystallization and structural determinations of the Arg195Gln, Arg195Ala, Arg337Gln and Arg337Ala mutant forms of HPA were done by Mrs. Yili Wang, Dr. Robert Maurus and Mr. Gary Sidhu in the laboratory of Professor Brayer at the University of British Columbia. Crystallization conditions were similar to those previously reported for recombinant wild-type HPA from *Pichia pastoris* (123). The data were refined to between 2.0 and 2.1 Å resolution for each of the proteins.

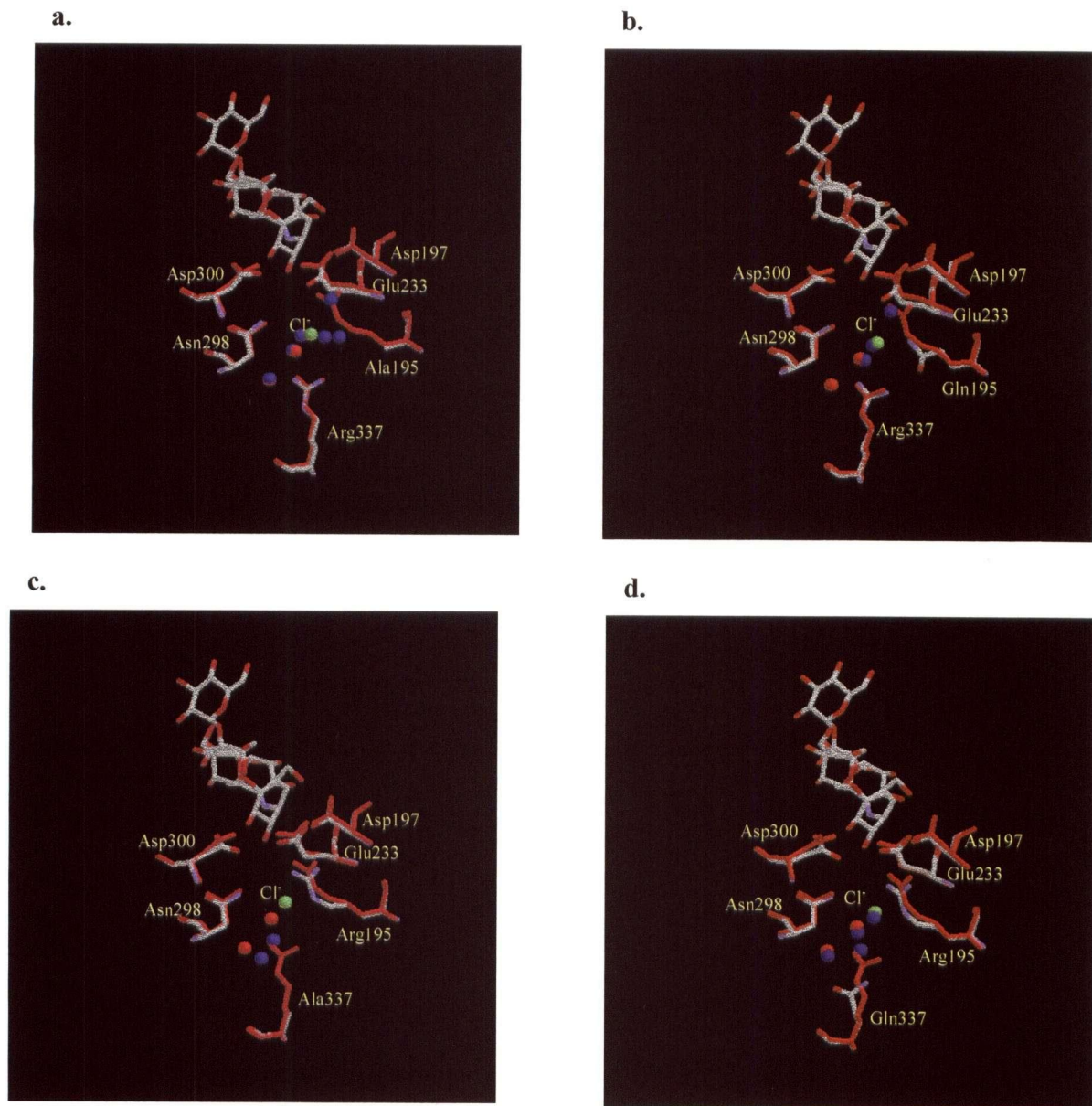


Figure 3.4 Overlay of the chloride binding region and active site of the wild-type HPA (red, except for acarbose) with (a) Arg195Ala mutant HPA, (b) Arg195Asn mutant HPA, (c) Arg337Ala mutant HPA, and (d) Arg337Asn mutant HPA. The chloride ion from the wild-type HPA is represented as a green ball and the water molecules are represented as red (wild-type) or blue (mutant HPA) balls.

Most evident in each of these structures was the absence of the chloride ion from the chloride ion-binding site (Figure 3.4). Instead, in all cases except for that of Arg337Ala mutant HPA, a water molecule was found at this site. The concentration of

chloride ion in the crystallization buffer was estimated at around 5-10 mM. This also suggests that the chloride ion will not bind to these mutant enzymes in solution at this concentration. In contrast, structures of the wild-type HPA crystals grown under similar buffer conditions consistently have a chloride ion bound at this site, consistent with the fact that the main difference between the chloride-dependent and independent  $\alpha$ -amylases seems to be a single arginine in the chloride ion-binding site. This is also consistent with the studies of *A. halioplanctis*  $\alpha$ -amylase (AHA) where removal of a lysine in this binding pocket resulted in a chloride-independent  $\alpha$ -amylase (119).

In the case of HPA, each of the arginines contributed two points of coordination. Furthermore, under normal conditions, arginine, with a  $pK_a$  of 12.5, formally should be positively charged so that one of these coordination points should be an ionic interaction. Therefore, mutation of either of these residues should result in a significant loss in binding affinity of HPA for a chloride ion. In the case of Arg195Gln, the amide nitrogen could still potentially form a hydrogen bond with a bound chloride ion. However, no chloride ion is seen, suggesting that the charge-charge interaction is essential in the formation of this chloride ion-binding pocket.

One of the original hypotheses presented during the original studies of chloride activation was that the chloride ion binding might affect the local structure of the enzyme near the region of the active site. HPA where the Arg337 has been mutated provides a model to test this hypothesis, as it does not bind a chloride ion. Since Arg337 only interacts with the chloride ion and not with the active site residues, modification of the Arg337 side chain should have a minimal effect on the active site structure. These mutant HPA should therefore provide an approximate structure of a chloride ion free  $\alpha$ -amylase.

Comparing the three-dimensional structures of the Arg337Gln and Arg337Ala mutant forms of HPA to that of the wild-type enzyme showed that there are no significant differences in the global folds of the mutant proteins. Closer inspection of the mutated region indicated that a water molecule had filled the void left by the removal of the arginine side chain. More importantly, the side chains of the active site and chloride ion-binding site residues (apart from Arg337) also did not change position to any significant extent (Figure 3.4a,b), in spite of the fact that no chloride ion was bound in the pocket. As a mutation to either an alanine or glutamine results in loss of chloride ion binding but little structural change, it seems that chloride ion is not important in either the global fold or in side chain positioning of the active site residues.

From this comparison, therefore, it would follow that chloride activation does not involve a conformational change but rather, electrostatic interactions. However, it is possible that the positive charge of the arginine affects the local structure of the HPA active site in the absence of the chloride ion. If this is the case, then the structures of HPA mutated at Arg337 do not represent the structure of wild-type HPA in the absence of chloride ion. To answer this question, the ideal solution would be to obtain the structure of the wild-type HPA without a chloride ion bound. Unfortunately, all attempts at completely removing the chloride from the crystallization buffer failed and in all cases, wild-type HPA structures showed a chloride ion bound in the binding pocket. At this point in time, therefore, it is not possible to rule out the possibility that the positive charge of arginine affects local structures.

The combination of a mutation of Arg195 (to either an alanine or glutamine) and the consequent loss of the chloride ion resulted in no significant change in the backbone

structure of HPA. However, careful comparison of these structures to that of the wild-type enzyme showed that there some changes in local structures had occurred around the region of the active site (Figure 3.4c,d). As with the HPA mutated at Arg337, a water molecule occupies the space created by the reduction in size from an arginine to glutamine. Interestingly however, a water molecule was not seen in the Arg195Ala mutation, where a larger space was created. In both the mutant HPA structures, Glu233 (catalytic acid/base), which normally hydrogen bonds to the  $\gamma_2$ -nitrogen of Arg195, also shifted slightly to this newly open space. Notably however, the side chain of Asp197 (catalytic nucleophile), which normally hydrogen bonds to Arg195, did not significantly shift positions. The shift of Glu233 in these mutant enzymes suggests that one of the roles of Arg195 involves the correct positioning of the catalytic acid/base.

From these four structures it is evident that point mutations at the active site of HPA are tolerated, at least structurally. In fact, mutation of a bulky and positively charged arginine to an alanine resulted in very few structural changes, even when the residue was normally involved in numerous interactions with the other active site residues. This, taken together with the fact that in all four structures the chloride was absent, suggests that the chloride ion does not play a role in shaping the local structure of the HPA active site.

### ***3.3.3 Kinetic analysis of HPA - Dependence on chloride of wild-type and mutant enzyme activity***

As with PPA and AHA, the activity of HPA on starch was dependent on the chloride concentration of the reaction solution. The HPA activity increased 12-fold on increasing the chloride concentration from 0 to 10 mM (Figure 3.5a) at pH 6.9. Assuming

that the active form of the enzyme is the form in which the chloride ion is bound, it is possible to determine the  $K_d$  value for the chloride ion by plotting the HPA activity vs. chloride concentration. This assumption was previously validated for PPA by comparing the values obtained by this method to those obtained by equilibrium dialysis (121). Using this method, the  $K_d$  value of the chloride ion with wild-type HPA was determined to be  $0.53 \pm 0.06$  mM (Figure 3.5a), which is comparable to the  $K_d$  value of 0.36 mM seen for the porcine counterpart. Furthermore, when a shorter substrate (reduced maltohexaose) was used to measure the activity, the  $K_d$  value did not change, suggesting that the effect of chloride is independent of substrate size.

In sharp contrast to the wild-type enzyme, the activities of the Arg195 and Arg337 mutant HPAs were independent of chloride concentration up to a concentration of 400 mM (Figure 3.5b,d) at pH 6.9. Taken together with the results of the structural studies, it is likely that all of these enzymes have lost their ability to bind a chloride ion. Interestingly, at concentrations higher than 400 mM, the activity of HPA starts to decrease in a concentration dependent manner (data not shown). This phenomenon though is also seen in the wild-type enzyme and therefore, is most likely due to salt (ionic strength) effects at higher concentrations. However, because of this inhibition by high salt concentrations, it is not possible to determine whether the chloride binds to the “chloride ion-binding site” of the mutant enzymes at higher chloride concentrations.

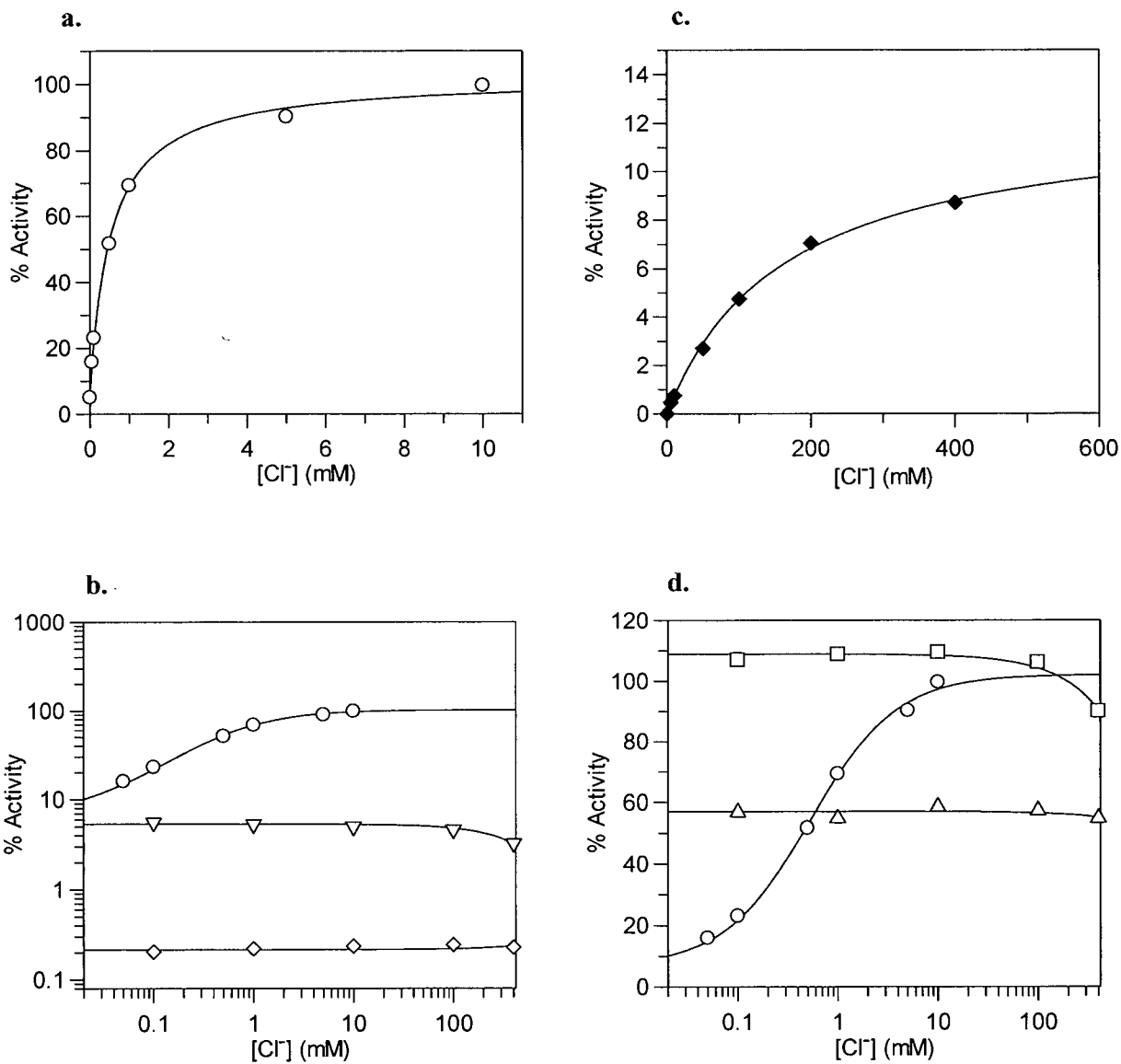


Figure 3.5 The dependence of (a) wild-type (b) R195 mutants (c) N298S mutant (d) R337 mutant enzymatic activities on chloride concentration. Wild-type (○), R195A (◇), R195Q (▽), N298S (◆), R337A (△) and R337Q (□). Activities have been changed to % activity for comparative purposes with wild-type HPA having 100% activity.

### 3.3.4 Kinetic analysis of wild-type HPA

In order to determine the pH dependence of HPA activity, starch was used as a substrate. Because of the unknown molecular weight of this substrate, it was not possible to determine a value for  $k_{\text{cat}}$  or  $K_{\text{m}}$  at each of the pH values. However, when the concentration of starch was increased from 0.25% to 2.0% (w/v), a maximal activity was reached above starch concentrations of ~1%. Furthermore, the concentration of starch required for maximal activity did not change over the range of pH used in the study. Therefore, the activity vs. pH profile is equivalent to that of a  $k_{\text{cat}}$  vs. pH profile where the  $\text{pK}_{\text{a}}$  values reflect the ionizations in the ES complex.

The activity of the wild-type HPA was measured as a function of pH over a range of chloride ion concentrations. In each of the cases, a bell-shaped dependence (two ionization states) was observed (Figure 3.6). According to the double displacement mechanism, the catalytic nucleophile (Asp197) is required to be deprotonated in the glycosylation step. The low  $\text{pK}_{\text{a}}$ , as determined by the acidic limb of the pH profile, most likely reflects the protonation state of this residue. Using the same argument, the basic limb of the pH profile should reflect the protonation state of the acid/base catalyst (Glu233). Indeed, this has been unequivocally demonstrated for another glycosidase, the *B. circulans*  $\beta$ -xylanase, using  $^{13}\text{C}$ -NMR (45).

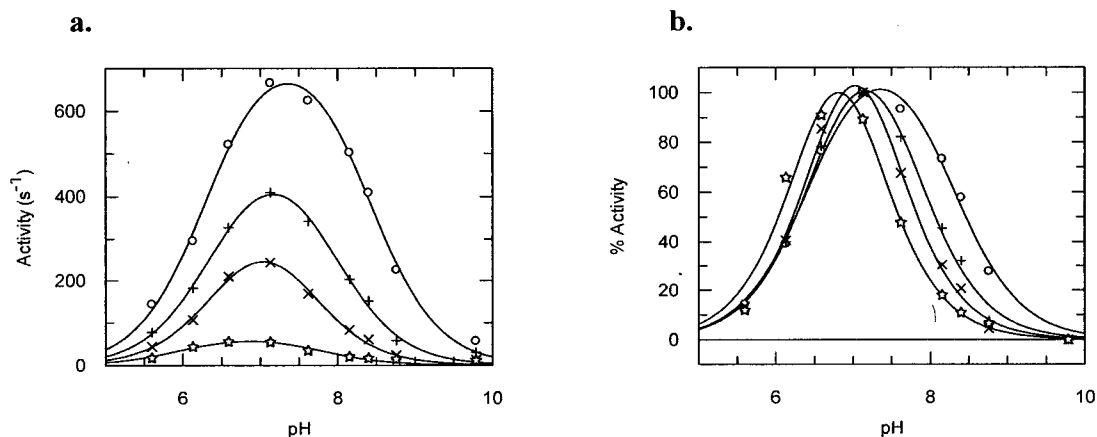


Figure 3.6 (a) The pH profiles for the wild-type HPA activity at 0 mM (★), 0.25 mM (×), 1 mM (+) and 100 mM (○) chloride concentration using starch as a substrate. (b) Normalized curves from the pH profiles of (a). The  $pK_{a1}$  (acidic limb) for the wild-type HPA at 100 mM NaCl was 6.4 compared to 6.4 for 0 mM NaCl. The  $pK_{a2}$  (basic limb) for the wild-type HPA at 100 mM NaCl was 8.3 compared to 7.2 for 0 mM NaCl.

As the chloride concentration increased, the pH optimum of the HPA activity also went to a higher pH value. This change was also associated with an increase in the maximal activity of HPA at the pH optimum, once again consistent with pH studies done for the PPA and AHA. Careful inspection of the pH profile showed that the  $pK_a$  of the basic limb shifted from 7.2 to 8.3 upon increasing chloride concentration from 0 to 100 mM while the  $pK_a$  of the acidic limb stayed constant at around 6.4.

### 3.3.5 Kinetic analysis of Arg195 mutant HPA

Although their enzyme activities were independent of chloride concentration, the absolute activities of the Arg195Ala and Arg195Asn mutant HPA were 450- and 20-fold lower, respectively, than that of the wild-type enzyme in the presence of chloride.

Although this decrease might be attributed to the missing chloride ion or to the slight misalignment of the residues, the equally likely reason is the loss of the other interactions with the arginine side chain of this residue. As was mentioned earlier, in the wild-type

enzyme, Arg195 is involved in a number of hydrogen bonding interactions, both to active site residues and the substrate. In particular, Arg195 makes an interaction with the 2-hydroxy group of the substrate. From kinetic studies with  $\beta$ -glycosidases (30) and inhibition studies of several  $\alpha$ -glycosidases (68), interactions with this 2-hydroxy group are extremely important for stabilization of the transition state, and removal of any such interaction compromises catalysis. The same may well be true of  $\alpha$ -amylases. However, it is not possible at this stage to dissect the causes for the lower activity of these mutant enzymes.

While the pH profiles for the Arg195 mutant HPA were not affected by the chloride concentration, they were both markedly different from that of the wild-type HPA in the presence or absence of chloride (Figure 3.7). The  $pK_a$  of the basic limb of the pH profile was shifted to a higher pH compared to that of the wild-type enzyme in the presence of chloride (from 8.3 to 9.2 and 8.8 in the case of Arg195Ala and Arg195Gln, respectively). The removal of a positively charged residue adjacent to the catalytic residues (Asp197 and Glu233) might indeed be expected to raise their  $pK_a$  values, making them less prone to protonation. However, the removal also results in the loss of the negatively charged chloride ion. Therefore, the resulting shift in  $pK_a$  for the acid/base catalyst is relatively modest compared to what might otherwise have been expected for removal of the arginine alone. This might also explain why there is very little change in the  $pK_a$  of the acidic limb, which presumably corresponds to the catalytic nucleophile (from 6.4 to 6.7 and 6.6 in the case of Arg195Ala and Arg195Gln, respectively).

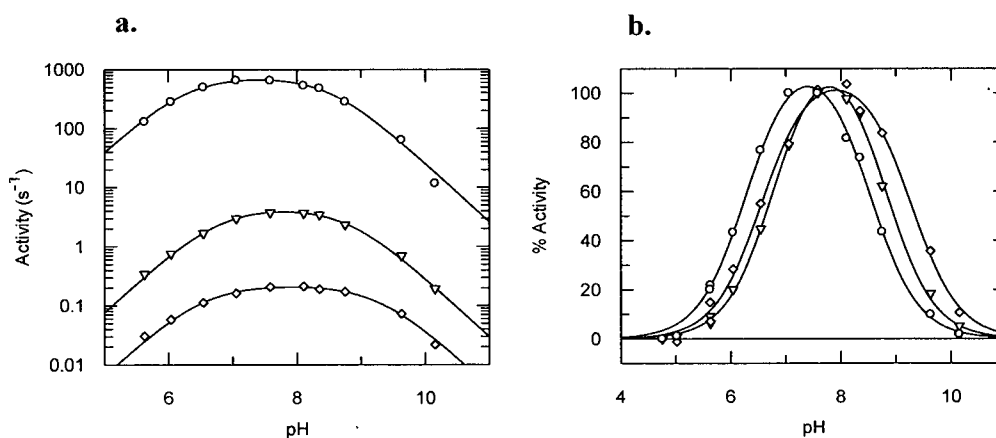


Figure 3.7 (a) The pH profiles for the activities of the R195 mutant HPA, R195A (◇) and R195Q (▽) in the absence of chloride. The pH profile of wild-type HPA in the presence of 100 mM chloride (○) is also plotted for comparative purposes. (b) Normalized curves from the pH profiles of (a). The  $pK_{a1}$  for the R195A and R195Q HPA were 6.6 and 6.7 respectively. The  $pK_{a2}$  for R195A and R195Q HPA were 9.2 and 8.8 respectively.

### 3.3.6 Kinetic analysis of Arg337 mutant HPA

In contrast to what was seen with the Arg195 mutant HPA, the activities of the Arg337Ala and Arg337Asn mutant HPA were comparable to that of the wild-type HPA in the presence of chloride. In fact, in the absence or presence of chloride, the activity of the Arg337Asn mutant HPA was identical within error to that of wild-type HPA. Therefore, somehow, the effect of the removal of the chloride ion is being counteracted by the effect of the mutation to Arg337. Furthermore, comparison of the pH profiles of the wild-type HPA in the presence of chloride, to those of the Arg337 mutant HPA revealed that no significant shift had occurred either in the basic or acidic  $pK_a$  values (Figure 3.8). This profile is the same in the presence or absence of chloride. This is in stark contrast to the case with wild-type enzyme where increasing chloride concentration increases the activity while shifting the pH profile to a higher pH value.

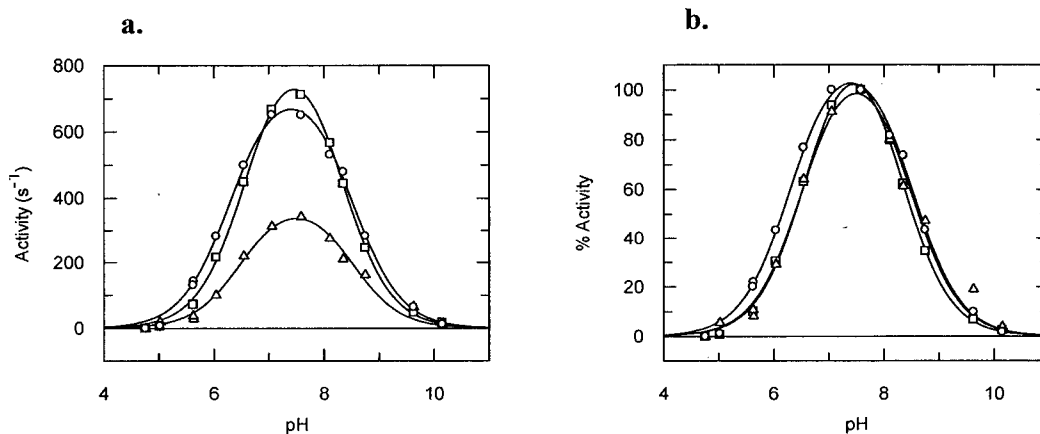


Figure 3.8 (a) The pH profiles for the activities of the R337 mutant HPA, R337A ( $\Delta$ ) and R337Q ( $\square$ ) in the absence of chloride. The pH profile of wild-type HPA in the presence of 100 mM chloride ( $\circ$ ) is also plotted for comparative purposes. (b) Normalized curves from the pH profiles of (a). The  $pK_{a1}$  for the R337A and R337Q HPA were 6.6 and 6.5 respectively. The  $pK_{a2}$  for R337A and R337Q HPA were 8.5 and 8.3 respectively.

This surprising result can be explained if the mechanism of chloride activation involves neutralization of the positive charge from the side chain of Arg337 that would otherwise affect the  $pK_a$  of Glu233 (catalytic acid/base). In wild-type HPA, the side chain of Arg337 is located  $\sim 8$  Å away from the carbonyl group of Glu233 and, aside from the chloride ion, no residue spatially intervenes between these two residues. Thus when no chloride ion is present the positive charge on Arg337 might be expected to shift the  $pK_a$  of Glu233 to a lower value through electrostatic interactions as indeed is seen for wild-type HPA. Inclusion of the chloride ion raises the  $pK_a$  of Glu233 from 7.2 to 8.3 via charge screening.

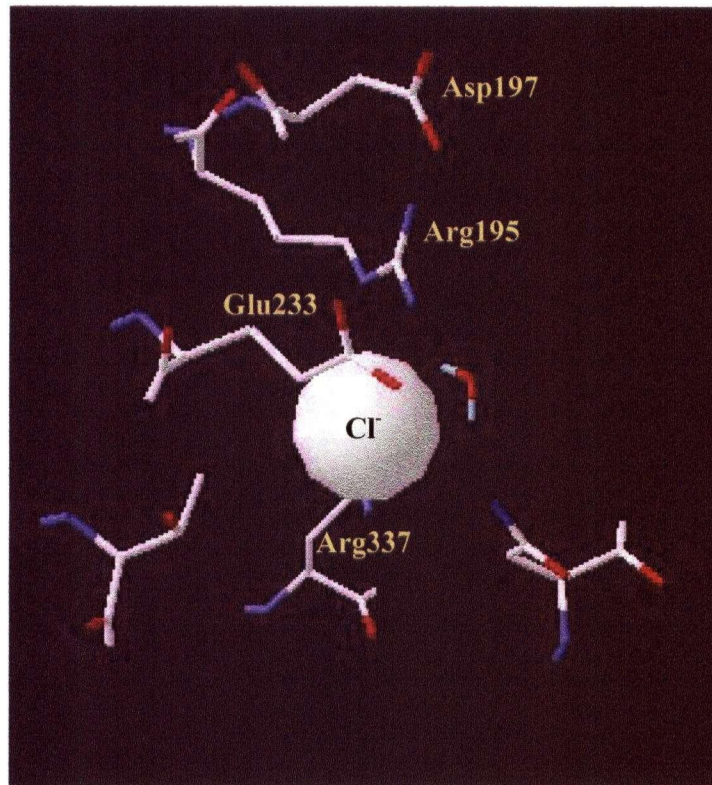


Figure 3.9 Positioning of the catalytic acid/base and catalytic nucleophile with respect to Arg337 (shown here with the chloride ion).

The pH profile for the wild-type HPA suggests that the effect of the chloride on the  $pK_a$  of Glu233 is more significant than its effect on the  $pK_a$  of Asp197. Indeed, the structural data show that Asp197 is “shielded” from the direct effects of Arg337 by Arg195 (Figure 3.9). In this case, as the chloride concentration is reduced, the  $pK_a$  of the basic limb of the pH profile will be lowered while the  $pK_a$  of the acidic limb will stay around the same. As these two  $pK_a$ s get closer in value, the pH profiles for each of the two residues start overlapping with a resultant overall reduction in enzymatic activity (Figure 3.10). In other words, the Arg337 is acting as an “internal inhibitor” of  $\alpha$ -amylase activity and the chloride is acting to relieve the  $\alpha$ -amylase of this inhibition. In the case of the Arg337 mutant HPA, the Arg337 side chain is removed and the positive charge is

no longer present. Therefore, even though the chloride ion does not bind, the Arg337 mutant HPA has similar kinetic properties to those of the wild-type enzyme in the presence of chloride.

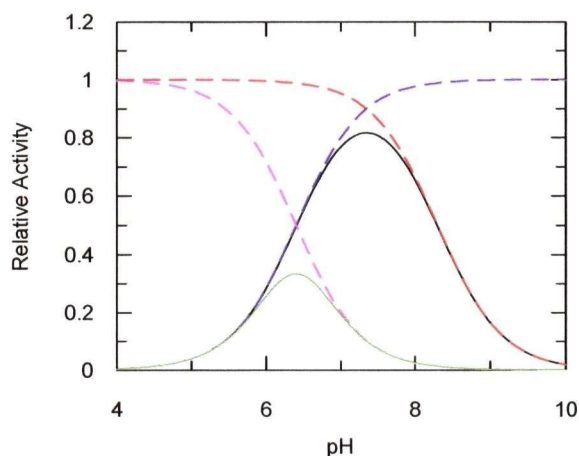


Figure 3.10 Reduction of rates by overlapping  $pK_a$  values: Hypothetical curve for single ionisable group with  $pK_a$  value of 8.3 (activity decreases at basic pH; -), 6.4 (activity decreases at basic pH; --), 6.4 (activity increases at basic pH; -). Hypothetical double ionization curve with  $pK_a$  values of 6.4 and 8.3 (-), and 6.4 and 6.4 (·).

### 3.3.7 Kinetic analysis of *Asn298 mutant HPA*

Because Asn298 has a neutral side chain with only a single point of coordination to the chloride ion, it was not expected that there would be a complete loss of chloride ion binding when this residue was mutated. True to expectations, the activity of the Asn298Ser mutant HPA was still dependent on chloride concentration. The  $K_d$ , as determined by plotting HPA activity vs. chloride concentration (Figure 3.5d), was  $160 \pm 10$  mM, indicating that the hydrogen bond to the chloride does still contribute a significant amount to binding. The maximal activity of this mutant enzyme is lower than that of wild-type enzyme by 8-fold. This is consistent with the fact that this residue is conserved through many members of the  $\alpha$ -amylase family and suggests that serine cannot completely replace the ability of asparagine to hydrogen bond and stabilize the active site loop in HPA. However, more importantly, in this mutant HPA the mechanism

for chloride activation is still intact. This is consistent with the charge shielding hypothesis where the Arg337 is the key residue in chloride activation. Indeed,  $pK_a$  shifts similar to those of wild-type HPA were observed when the pH dependence of the Asn298Ser mutant HPA was determined at varying chloride concentrations (Figure 3.11).

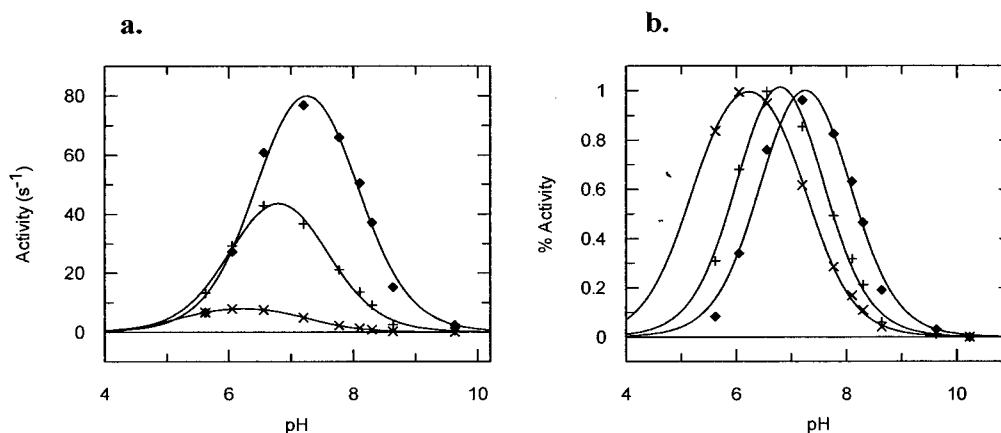


Figure 3.11 (a) The pH profiles for the activity of the N298S mutant at 10 mM (X), 100 mM (+) and 400 mM (◆) chloride concentration using starch as a substrate. (b) Normalized curves from the pH profiles of (a). The  $pK_{a1}$  N298S HPA at 10 mM NaCl was 5.1 compared to 6.5 for 400 mM NaCl. The  $pK_{a2}$  for N298S HPA at 10 mM NaCl was 7.2 compared to 8.0 for 400 mM NaCl.

### 3.3.8 Attempts at chemical rescue of inhibition

If the arginine side chain is truly acting as an internal inhibitor for HPA activity, then reintroducing the positive charge into the Arg337Ala mutant HPA might “recover” this inhibitory activity. One of the classic ways in which this type of recovery has been done in other systems is through the use of small molecules in a chemical rescue experiment. In the Arg337Ala mutant HPA, there is a pocket that has been created because of the difference in size of the two side chains (arginine vs. alanine). This pocket should ideally fit the removed residue; in this case a guanidinium ion.

When the activity of the Arg337 mutant HPA was determined over a range of guanidine concentrations in the absence of chloride from the buffer, inhibition was

indeed observed, according to an  $IC_{50}$  value of the guanidine of 120 mM (Figure 3.12).

When the experiment was done the presence of chloride, a similar  $IC_{50}$  was obtained. The binding of both the guanidine and chloride ion to the pocket is very unlikely and thus, the negative result for the double rescue experiment was not surprising. However, when a similar experiment was done with wild-type HPA in the presence of chloride, the HPA activity was lost at a similar concentration.

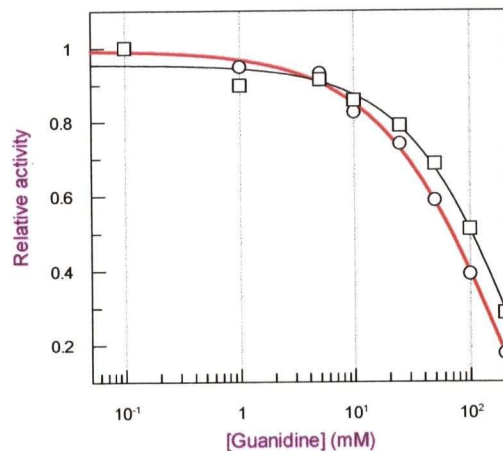


Figure 3.12 Inhibition of Arg337Ala mutant (-O-) and wild-type HPA (-□-) by guanidine in the presence of chloride.

There are two possible sources for this inhibition. The first is that the guanidine is acting as a denaturing agent; that is to say, unfolding the protein so that it is not longer active. The second possibility is that the guanidine is binding to the active site and acting as a competitive inhibitor. In order to test if the protein is being denatured at these guanidine concentrations, the CD spectra of HPA at a range of guanidine concentrations were obtained. These spectra suggested that even at concentrations as low as 50 mM, there was some change in the secondary structure of the protein. Therefore, the inhibition of the HPA seems to come from a partial unfolding of the protein rather than from specific binding of the guanidine.

### 3.3.9 Evolutionary implications

Although the analysis of the mutant HPA does suggest the mechanism by which the chloride ion activates chloride-dependent  $\alpha$ -amylases, it does not suggest an evolutionary reason for the chloride ion-binding site. The most obvious purpose for the chloride ion-binding site is as a switch for  $\alpha$ -amylase activity. However, the  $K_d$  value of the chloride ion was determined to be 0.5 mM *in vitro*. Once the HPA has been secreted from the pancreas, the concentration of chloride is greater than 100 mM (124). Furthermore, within the cell, the chloride concentration is 4 mM, suggesting that the HPA is never inactive. Therefore, if the chloride “switch” hypothesis were true, then the chloride ion-binding site would need to have evolved earlier in time and remained intact. A recent review by D'Amico *et al.* listed a number of sources for chloride-dependent  $\alpha$ -amylases (118). Although this list mainly contains mammalian enzymes, it also includes those from insects and several species of bacteria. It is therefore possible that during one of these stages during evolution, the chloride switch was an important trait for the survival of the organism.

Another possibility is that chloride bound to the chloride ion-binding site increases the stability of the chloride dependent  $\alpha$ -amylases. To test this hypothesis, CD melt experiments were done on the Arg337Asn mutant HPA as well as on the wild-type HPA in the presence and absence of chloride. Unfortunately, the HPA precipitates upon thermal or guanidine (at higher concentration) denaturation rendering quantitative analysis difficult. However, there was no difference in the temperature at which this occurred implying similar thermostability of these forms of HPA. Therefore, it is unlikely that the chloride ion-binding site plays a role in stability. However, because CD studies

only reveal the change in secondary structure, it is still possible that the chloride ion stabilizes the local structure of the active site.

There is a significantly higher level of sequence similarity within these chloride-dependent  $\alpha$ -amylases than between all  $\alpha$ -amylases (118). This is also seen in the tertiary structures of the  $\alpha$ -amylases. Therefore, another possibility for the existence of the chloride ion-binding site is that early on in evolution, the arginine was introduced in a particular source of  $\alpha$ -amylase. Because of the ubiquitous nature of chloride, there was no selective pressure to modify this residue and this change remained. However, this is purely speculation and the author has no further evidence for this hypothesis.

#### ***3.3.10 Possible future directions***

The structural studies presented here focused on the two arginines in the chloride ion-binding site. From these studies, it was determined that the removal of either arginine resulted in the loss of chloride. However, the loss of the chloride ion, together with the mutation, resulted in very little local structural change. From this, it was concluded that the presence of the chloride ion did not induce a local structural change and thus, the mechanism of chloride activation did not involve a change in structure.

Although the structural evidence is very suggestive of this conclusion, it could be argued that the mutation has counteracted the loss of the chloride ion. This was indeed seen in the kinetic results for the Arg337Asn mutant HPA for which the kinetic parameters resembled those of the wild-type HPA in the presence of chloride. The ideal structural study would be to determine the structure of the wild-type enzyme in the presence and absence of chloride ion. However, as mentioned earlier, several attempts at crystallization of the HPA in the absence of chloride failed. In all cases, the structure

determined showed a chloride ion bound in the chloride ion-binding site. This is most likely due to the ubiquitous nature of chloride and the low  $K_d$  of the chloride ion (0.5 mM).

One option in solving this problem is to use the Asn298Ser mutant HPA as a model. Although this mutant HPA has a lower activity than does wild-type HPA, it is activated in much the same way by chloride concentration. Therefore, the chloride activation mechanism is still intact in this mutant enzyme. In addition, the  $K_d$  of the chloride ion is 120 mM so that crystallization in “chloride free” buffer should result in HPA with chloride free structures. Indeed, preliminary structural analysis of Asn298Ser mutant enzymes crystallized under these conditions has indicated that no chloride ion is bound in this mutant HPA. As with other small ligands, the chloride ion may be soaked into the Asn298Ser mutant HPA crystals, thereby providing the chloride-bound version of this enzyme. Comparison of these structures should reveal any structural changes resulting from chloride ion binding and provide direct evidence for any structural roles of the chloride ion in the activation mechanism.

Removal of the side chain of Arg337 resulted in the complete loss of binding ability of the chloride ion. In addition, kinetic and structural results also suggested that this mutant enzyme was a chloride-independent  $\alpha$ -amylase with kinetic properties similar to those of wild-type HPA in the presence of chloride. From these results, we proposed that the Arg337 was acting as an internal inhibitor and that the chloride ion was acting to relieve this inhibition. This implies that the activities of the chloride independent  $\alpha$ -amylases are independent of chloride concentration because they are missing this arginine. In fact, comparing the equivalent region of the chloride ion-binding site in all  $\alpha$ -

amylases shows that the backbone structure (including that of the equivalent of Arg337) is conserved, even in chloride-independent  $\alpha$ -amylases. Therefore, by mutating the residue at this position in a chloride-independent  $\alpha$ -amylase to an arginine, there is a possibility that the region would become a chloride ion-binding site. Furthermore, if the hypothesis that the arginine is acting as an internal inhibitor is correct, then this  $\alpha$ -amylase will require an anion for full catalytic activity.

In order to conduct this experiment, a recombinant chloride-independent  $\alpha$ -amylase is required so that it may be mutated site-specifically. In addition, in order to avoid possible complications, the  $\alpha$ -amylase should be one where additional side chains do not protrude into the putative chloride ion-binding site. By searching the literature and comparing the three-dimensional structures of various  $\alpha$ -amylases, the best candidate for this experiment would be the  $\alpha$ -amylase from *A. oryzae*. At present, we are involved in a collaborative effort with Dr. Carsten Andersen at Novozymes, Denmark, to make these mutations in this  $\alpha$ -amylase. These mutant  $\alpha$ -amylases will be tested to see if they require chloride for catalytic activity and if so, how the chloride affects their pH optima.

## **Chapter 4 Substrates and inhibitors of $\alpha$ -amylase**

## 4.1 General introduction

### 4.1.1 *Human pancreatic $\alpha$ -amylase*

Human pancreatic  $\alpha$ -amylase (HPA) is an enzyme that is involved in the hydrolysis of starch within the digestive system. Initially, when starch is ingested, an enzyme in the saliva, salivary  $\alpha$ -amylase, randomly hydrolyses  $\alpha(1,4)$ -linkages within the starch. By the time that the “starch” reaches the stomach, the size of the polymer has been reduced to  $\sim 8$  glucose units. In order for  $\alpha$ -glucosidases to quickly cleave off glucose units from the digested oligosaccharides for absorption by the intestine, these sugars must be further hydrolysed to maltose, maltotriose and dextrans. HPA is involved in the hydrolysis of larger oligosaccharides to these smaller oligosaccharides within the intestine.

Like all  $\alpha$ -amylases, HPA is an endo-glucosidase that cleaves its substrate at “random” locations within a glucose polymer. In order to orient the scissile bond of the substrate within the active site, HPA binds to several glucose moieties that flank the bond being cleaved. Each glucose moiety of the substrate can be thought of as binding to a pocket, or “subsite”, within the enzyme active site. The subsites would each contribute to substrate binding and thus, the more subsites that a particular substrate occupies, the stronger the binding of the substrate to the enzyme. Furthermore, the number of subsites and the location of the cleavage site with respect to these subsites will dictate the cleavage pattern of the substrates. In fact, by studying the cleavage patterns of various oligosaccharides, the subsites for a number of  $\alpha$ -amylases from different sources have been “mapped” (125). From these studies, it has been shown that the number of subsites

on both sides of the cleavage site differs for  $\alpha$ -amylases from different sources. In the case of HPA, there are thought to be three subsites to the non-reducing end side and two subsites towards the reducing end side of the scissile bond (Figure 4.1) (108).

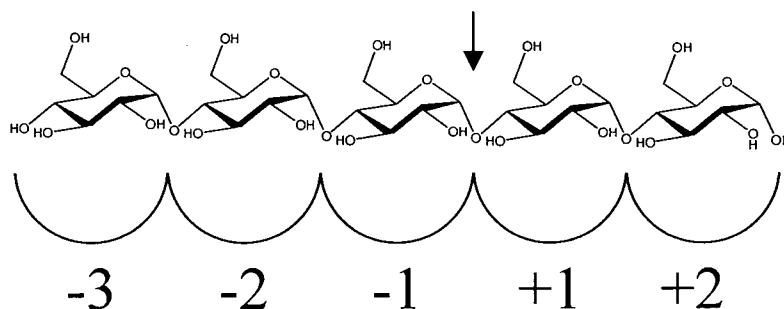


Figure 4.1 Cartoon representation of the subsites in HPA with substrate bound. The scissile bond is indicated with an arrow.

According to transition state theory, enzyme catalysis is thought to take place because the enzyme makes more favorable interactions with the transition state than it does with the ground state structure. In an endo-glycosidase, the greatest transformation of the substrate on going from the ground state to the transition state takes place on the sugar occupying the  $-1$  subsite. Therefore, it stands to reason that the  $-1$  subsite should be particularly optimised to interact with the transition state, and may bind less tightly to the ground state. In fact, this subsite often has a negative contribution towards substrate binding, and removal of enzyme-substrate interactions within this site results in decrease of catalytic activity rather than binding. The other subsites, on the other hand, are thought to contribute more towards the overall binding of the substrate.

#### 4.1.2 Transglycosylation

As was mentioned in chapter 3,  $\alpha$ -amylase catalyzes hydrolysis of glucosidic linkages via a double displacement mechanism (69, 106, 108, 110). A direct consequence of this mechanism is the side reaction, transglycosylation. This reaction occurs when the

nucleophile (acceptor molecule) in the deglycosylation step is not a water molecule, but rather a hydroxyl group on a sugar (Figure 4.2). In this case, the end result is not hydrolysis, but rather, the transfer of a donor sugar from one acceptor sugar to another. Due to the concentration of water in aqueous solutions (~55 M), this reaction is not usually favoured, as indicated by the fact that glycosidases generally hydrolyse glycosidic linkages. Often, the “+” subsites of the enzyme can act as an aglycone binding site and it is possible to favour transglycosylation by increasing the concentration of acceptor. In fact, at high concentrations, the substrate for the enzyme is often able to transglycosylate onto itself in a self-condensation reaction. Indeed, transglycosylation has been demonstrated to be favoured for the porcine pancreatic  $\alpha$ -amylase (PPA)-catalyzed reaction of  $\alpha$ -maltosyl fluoride (G2F) (126).

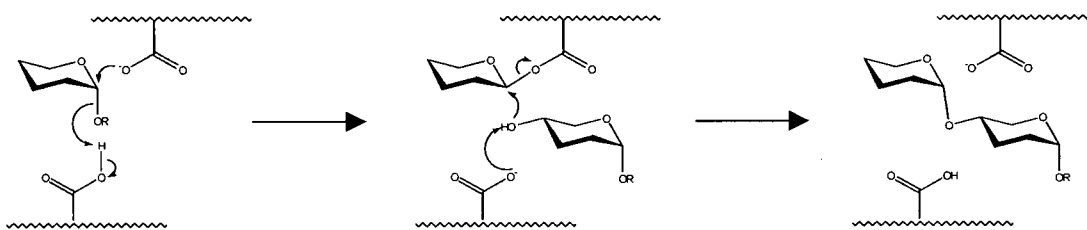
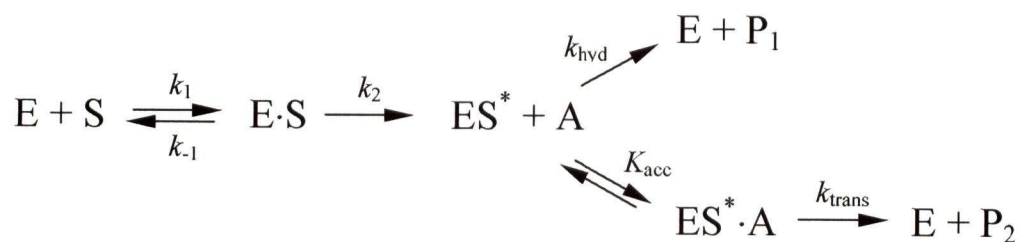


Figure 4.2 Mechanism for the transglycosylation reaction catalysed by a retaining  $\alpha$ -glycosidase.

The most conclusive evidence for whether or not a particular glycosidase catalyzes transglycosylation involves analysis of the reaction products. If a product corresponding to an elongated substrate is found, or if an unexpected cleavage pattern is seen, then it is likely that transglycosylation has taken place. If the deglycosylation step of the reaction is rate limiting, evidence for transglycosylation may also come from kinetic analysis. The kinetic model for transglycosylation (Scheme 4.1) is such that the acceptor competes with water for the species  $E-S^*$ . If transglycosylation occurs, the

overall rate of reaction should increase with increasing acceptor concentrations. If this acceptor is also the donor, then the plot of rate versus substrate concentration will appear as the combination of two Michaelis-Menten profiles (Figure 4.3). In this case, the  $K_m$  value ( $K_{acc}$  value from the model) for transglycosylation represents the apparent binding constant for substrate binding to the aglycone binding site.



Scheme 4.1 Kinetic model for transglycosylation and hydrolysis.

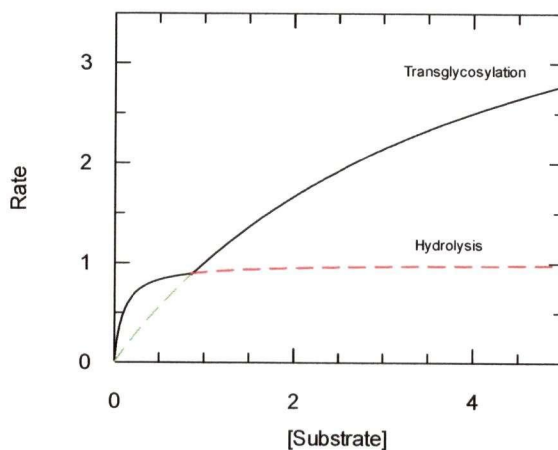


Figure 4.3 First approximation for a hypothetical Michaelis-Menten type plot for a transglycosylating enzyme (solid line). The hypothetical Michaelis-Menten plot for transglycosylation (---) and hydrolysis (---) have also been included.

#### 4.1.3 Inhibitors of $\alpha$ -amylase

The blood glucose levels directly correlate to the absorption of glucose by the intestine. In order for starch to be efficiently taken up as glucose, it needs to be hydrolysed into small oligosaccharides by HPA. Therefore, if it were possible to control the HPA activity, it would also be possible to control the absorption of glucose by the

intestine. This, in turn, would provide a means of controlling blood glucose levels. In fact, the commercially available drug, acarbose, utilizes such a mechanism for the control of post-prandial blood glucose levels in diabetic patients (127-129). As such, inhibitors of HPA are potential drug candidates for conditions such as diabetes and obesity, and are sought after by pharmaceutical industries (130).

There are two classes of  $\alpha$ -amylase inhibitors. The first class of inhibitors is that of the proteinaceous inhibitors that bind selectively to the enzyme through protein-protein interactions. The other class is that of the carbohydrate-based inhibitors that either mimic the substrate, product or transition state of the enzyme. Both kinds of inhibitors are often found as natural products.

#### *4.1.3.1 Proteinaceous inhibitors of $\alpha$ -amylase*

There are a number of different organisms, mainly bacteria and plants, which produce proteinaceous inhibitors of  $\alpha$ -amylase (131, 132). These proteins, ranging in size from just 32 amino acids to over 250 residues, are often extremely tight binders of  $\alpha$ -amylase with some having  $K_d$  values as low as  $10^{-12}$  M (133). In addition, each of these proteinaceous inhibitors is very specific for a particular  $\alpha$ -amylase and, in some cases, the protein will only inhibit an  $\alpha$ -amylase from one specific species. The three-dimensional structures of a number of these inhibitors have been determined (132, 134). As with other types of proteins, these inhibitors may be classified into different families according to their primary and tertiary structures (132, 135). At present, there are 7 known families of proteinaceous inhibitors. At least five of these families have representative three-dimensional structures whereby the inhibitor is complexed with  $\alpha$ -

amylase (for an example see Figure 4.4) (136-140). Each of these structures reveals extensive networks of interactions between the enzyme and inhibitor. There is, however, no apparent common element in the binding of these inhibitors to their respective enzyme. This explains the specificity of the inhibitor towards particular  $\alpha$ -amylases. In all cases, the end result is the positioning of the inhibitor over the enzyme active site, making it inaccessible to substrates.

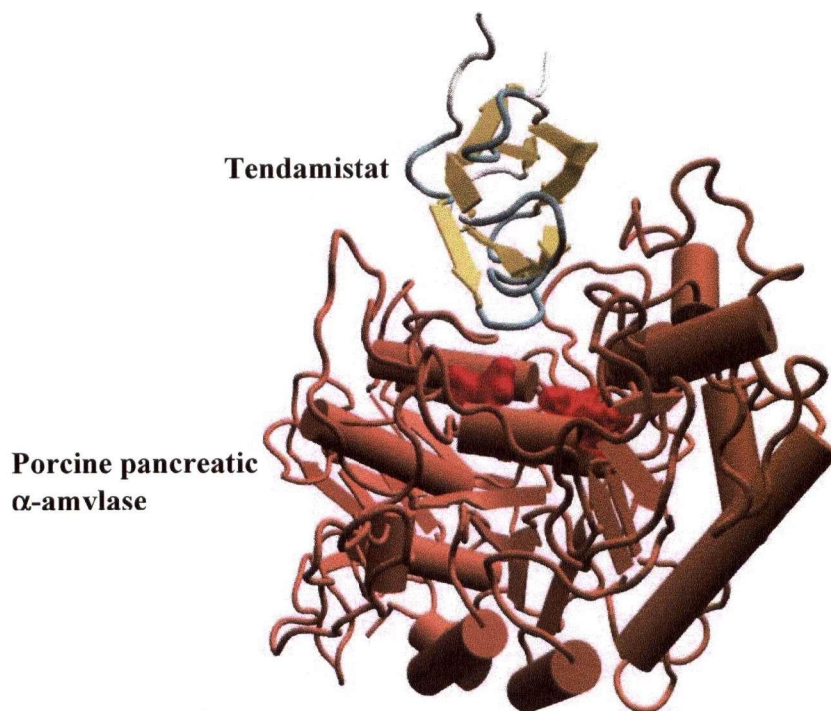


Figure 4.4 Structure of the proteinaceous inhibitor, tendamistat (green), bound to PPA (brown). The active site residues are coloured in red (136).

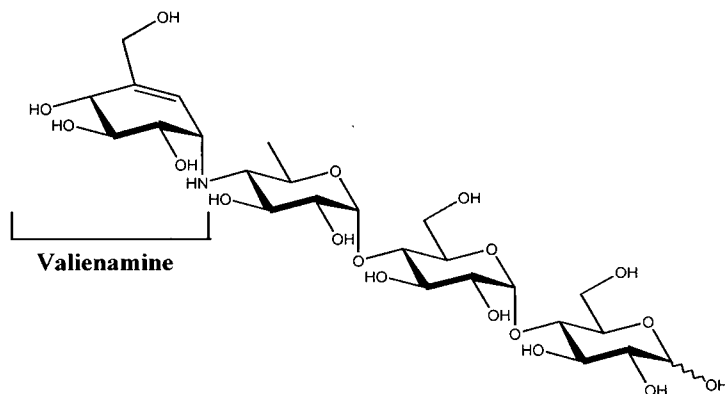
One family of inhibitors includes the protein tendamistat, produced from the microbe *Streptomyces tendae* (141). Tendamistat, a 74 amino acid protein having a  $K_d$  value of  $10^{-10}$  M against PPA, became famous for the fact that it was the first protein to have its structure determined by both X-ray crystallography and NMR spectroscopy (134). A key feature of this family of inhibitors is the conserved Trp-Arg-Tyr (WRY) sequence among family members. From the three-dimensional structures of tendamistat,

both in the free form and bound to enzyme, it has been shown that this sequence is a part of a loop that fits into the  $\alpha$ -amylase active site (136). These three residues make interactions with the active site residues, which are essential for tight binding.

Consequently, the WRY sequence has been used as a lead for various peptide mimics of tendamistat (142-144). Unfortunately, these studies have met with limited success, with the best peptide inhibitor (11-residues) developed having a  $K_i$  value of  $10^{-7}$  M (144) towards PPA. This limited success is not completely surprising as there are numerous other interactions involved in the binding of tendamistat aside from those of the WRY sequence.

#### 4.1.3.2 Carbohydrate-based inhibitors of $\alpha$ -amylase

The classic example of a carbohydrate-based  $\alpha$ -amylase inhibitor is the natural product, acarbose (Figure 4.5), isolated from *Actinoplanes*. This pseudo-tetrasaccharide is a non-competitive inhibitor of HPA with a  $K_i$  value of 20 nM (145). Acarbose consists of a valienamine (unsaturated cyclitol) linked “ $\alpha(1,4)$ ” by an amine linkage to a 6”-deoxy-maltotriose. The flattened conformation of the valienamine is thought to mimic the shape of the oxocarbenium ion-like transition state of starch hydrolysis. Furthermore, if protonated, the exocyclic amine would place a positive charge in a similar position to that of the glycosidic bond oxygen, which, at the transition state, is thought to be protonated. In fact, acarbose has been shown to act, at least in part, as a transition state analogue of another family 13 enzyme, cyclodextrin glucanotransferase (CGTase) (146).



#### 4.1

Figure 4.5 Structure of acarbose (4.1).

One of the interesting properties of acarbose comes from structural analysis of inhibitor-bound complexes with various  $\alpha$ -amylases (108-110, 147). In all cases, the structure of the bound acarbose was not that of the expected pseudo-tetrasaccharide. Although the exact structure of the bound species was different in each case, the species was of a modified form of acarbose where seemingly, several sugar (or sugar analogue) moieties had been attached  $\alpha(1,4)$  to the non-reducing end of the valienamine ring. Although the mechanism by which this modification occurs is not clearly understood, in each case, the bound inhibitor seems to be modified to occupy all of the available subsites (for an example with HPA, see Figure 4.6). Furthermore, the modified acarbose is bound so that the valienamine moiety is positioned in the  $-1$  subsite, a result consistent with the valienamine moiety acting as a transition state analogue. The addition of these glucose moieties at the non-reducing end would be expected to contribute significantly to the binding of the inhibitor by occupying the subsites that would otherwise have been unoccupied. These two features suggest that  $\alpha$ -amylase is modifying the acarbose in such a manner as to result in the tightest binding inhibitor.

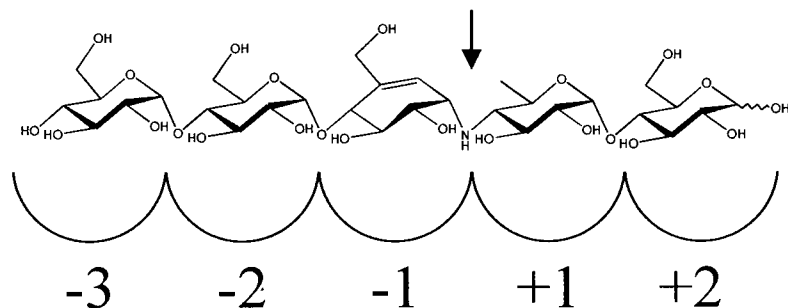


Figure 4.6 Structure of the modified “acarbose” when bound to HPA. HPA subsites are shown to indicate the binding mode of this inhibitor.

Given the amount of work that has been done on  $\alpha$ -amylases, there are relatively few known carbohydrate-based inhibitors for this enzyme. This may, in part, be due to the synthetic difficulties involved in making malto-oligosaccharide based inhibitors. Because all  $\alpha$ -amylases have several subsites, it comes as no surprise that monosaccharide analogues such as deoxynojirimycin, which strongly inhibit  $\alpha$ -glucosidases, are not very good inhibitors of  $\alpha$ -amylases. However, because  $\alpha$ -amylases belong to the same family of glycosidases as  $\alpha$ -glucosidases, namely family 13, their transition states should be similar and the  $-1$  subsite of  $\alpha$ -amylase, which accommodates this transformation, should have a similar active site architecture to that of family 13  $\alpha$ -glucosidases. From this, inhibitors of family 13  $\alpha$ -glucosidases would be expected to bind well to the  $-1$  subsite. A possible reason for the low affinity of  $\alpha$ -glucosidase inhibitors to  $\alpha$ -amylases may therefore be because the monosaccharide analogue is bound too loosely within the  $-1$  subsite of an endo-glycosidase. Binding to the  $-2$  subsite as a

minimum may also be required to constrain the inhibitor to make all of the potential interactions.

If this is the case, then by converting a monosaccharide analogue inhibitor to a di- or trisaccharide by linking a malto-oligosaccharide  $\alpha(1,4)$  to the non-reducing end of the inhibitor, it may be possible to provide this constraint. Indeed, this was seen in the case of acarbose, where, by “extending” the inhibitor by several glucose moieties, the inhibitory portion of the compound was directed into the  $-1$  subsite. Once positioned in the  $-1$  subsite by the other sugar moieties, the inhibitory portion of the compound may exhibit its full inhibitory potential.

In one study, the  $\alpha$ -glucosidase inhibitor, gluconolactone, was extended by a varying number of glucose moieties (Figure 4.7a) (148, 149). The monosaccharide is a 2 mM inhibitor of Limpet  $\alpha$ -glucosidase (150) but does not seem to inhibit  $\alpha$ -amylases to any significant extent. When the “inhibitor” was extended by a single glucose moiety, the  $IC_{50}$  was determined to be 140  $\mu$ M against PPA. More impressive was when the inhibitor was extended at the non-reducing end by a maltose moiety. The  $IC_{50}$  for this extended inhibitor was 0.9  $\mu$ M for PPA and 17  $\mu$ M for HPA (Table 4.1). In contrast, maltose has a  $K_i$  value of 28 mM (151). In a similar study, several iminocyclitols (Figure 4.7b,c) were extended on the non-reducing end by one to four glucose moieties (152). As in the gluconolactone study, the inhibitor extended by a maltose moiety had an  $IC_{50}$  in the range of 20-40  $\mu$ M.

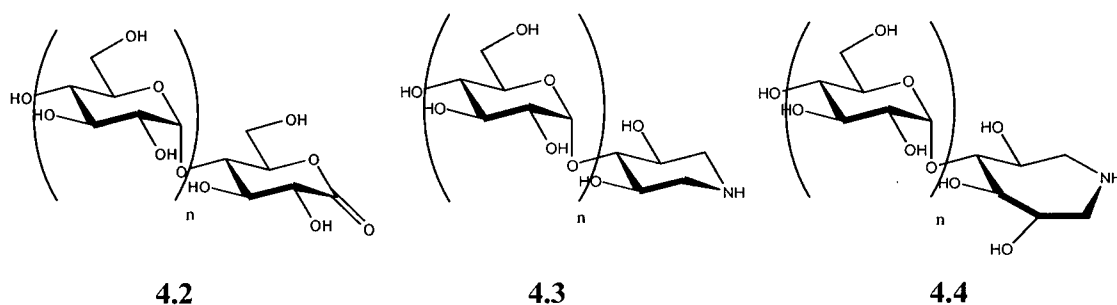


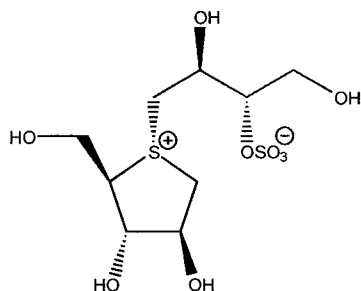
Figure 4.7 Structures of the extended inhibitors: gluconolactone extended by  $n$  glucose moieties (4.2), hexahydro-3,4,5,6-tetrahydroxy-1*H*-azepine extended by  $n$  glucose moieties (4.3), and 3,4,5-trihydropiperidine extended by  $n$  glucose moieties (4.4).

| $n =$ | 0          | 1          | 2        | 3         |
|-------|------------|------------|----------|-----------|
| 4.2   | > 5.0 mM   | 2.5 mM     | 0.043 mM | 0.030 mM  |
| 4.3   | > 5.0 mM   | 3.0 mM     | 0.034 mM | 0.025 mM  |
| 4.4   | Not tested | Not tested | 0.017 mM | 0.0095 mM |

Table 4.1  $IC_{50}$  values for the extended inhibitors from Figure 4.7 (148, 149, 152).

Interestingly, the natural product salacinol was found to be an inhibitor of  $\alpha$ -amylase with  $K_i$  values of 10 and 15  $\mu$ M for PPA and barley  $\alpha$ -amylase, respectively (153). This compound has a five membered ring and contains a zwitterionic sulfonium-sulfate structure (Figure 4.8). The positive charge on the ring sulfur could mimic the positive charge developed in the oxocarbenium ion-like transition state. Furthermore, the five membered ring structure is thought to mimic the planar conformation adopted by C-5, O-5, C-1 and C-2 of the pyranose ring during the transition state. This result suggests that

it is possible for monosaccharide analogues to inhibit  $\alpha$ -amylases at low micromolar concentrations.



4.5

Figure 4.8 Structure of salacinol (4.5).

#### 4.1.4 Substrates and assays for $\alpha$ -amylases

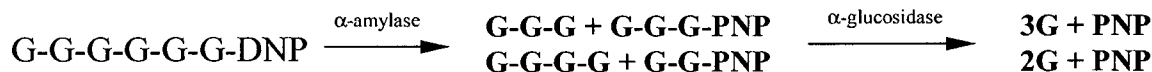
In order to study the mechanisms of enzymes, or develop inhibitors against them, it is essential to have a suitable assay to measure enzymatic activity. In order to accomplish this, the conversion of substrate to product must be accompanied by a change in properties that is quantifiable. The turnover of the natural substrate, however, does not often result in an easily detectable change. Therefore, synthetic substrates are often used in assays as more convenient ways of measuring enzymatic activity.

The natural substrates of  $\alpha$ -amylase are glucose polymers, usually in the form of starch or malto-oligosaccharides. Although it is possible to directly assay for  $\alpha$ -amylase activity by using starch as a substrate (for example, using the 3,5-dinitrosalicylic acid assay (154)), it is very difficult to quantify starch due to its large molecular weight. Furthermore, it is virtually impossible to obtain a homogeneous sample of starch. Therefore, it is difficult to use these assays to obtain meaningful and reproducible kinetic parameters. Malto-oligosaccharides have defined molecular weights, and their hydrolysis may be monitored using HPLC analysis. However, assays involving HPLC separation do

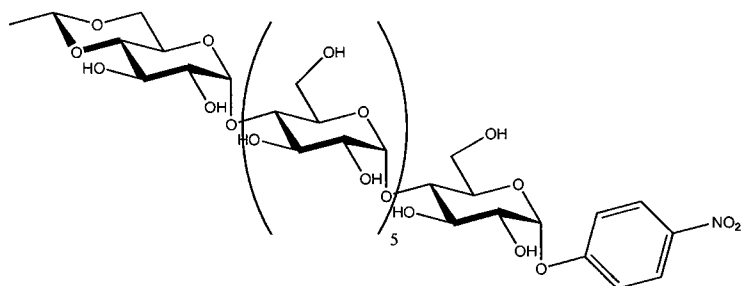
not allow for continuous monitoring of the hydrolysis. In other words, the reaction must be stopped at various time points in order to define a reaction progress profile.

Furthermore, such assays are often time consuming and as such, are not suitable for rapid screening. To solve this problem, a number of small molecules have been synthesized as substrates for  $\alpha$ -amylase. These substrates can be broadly classified into two categories – those requiring coupling enzymes, and those that can be used to directly measure  $\alpha$ -amylase activity.

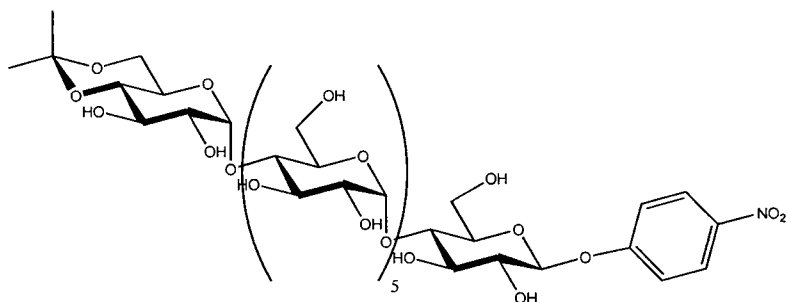
A type of synthetic substrate that is often used for enzyme assays is one that releases a phenol such as *p*-nitrophenol (PNP) upon reaction. The release of such a group can be measured by monitoring the increase in absorbance at a fixed wavelength (which depends on the particular phenolate being used). Unfortunately, when a phenyl group is attached to a malto-oligosaccharide, such as in the case of *p*-nitrophenyl  $\alpha$ -maltotetraoside ( $\alpha$ PNP-G4) or *p*-nitrophenyl  $\alpha$ -maltopentaoside ( $\alpha$ PNP-G5), the  $\alpha$ -amylase does not specifically cleave the glycosidic linkage between the sugar and the phenyl group. Rather it favours hydrolysis between two of the glucose moieties within the substrate and the products of the reaction are shorter *p*-nitrophenyl oligosaccharide such as *p*-nitrophenyl  $\alpha$ -maltoside ( $\alpha$ PNP-G2) and *p*-nitrophenyl  $\alpha$ -maltotrioside ( $\alpha$ PNP-G3). However, since these are good substrates for  $\alpha$ -glucosidases, addition of a coupling enzyme,  $\alpha$ -glucosidase, will lead to the release of PNP, which can be monitored continuously by measuring the increase in absorbance at 400 nm (Scheme 4.2) (155, 156).



Scheme 4.2 Several possible reactions for monitoring  $\alpha$ -amylase activity using PNP-G6 and a coupling enzyme  $\alpha$ -glucosidase. The released PNP can be monitored as an increase in absorbance at 400 nm.



4.6



4.7

Figure 4.9 Structures of two blocked substrates used in coupled assays for determining  $\alpha$ -amylase activity (4.6-4.7).

One problem with this approach is that the coupling enzyme can slowly hydrolyse the parent malto-oligosaccharides. In order to avoid this, substrates with a protecting group attached to the non-reducing end of the *p*-nitrophenyl oligosaccharide have been synthesised (Figure 4.9) (157-159). Because  $\alpha$ -glucosidases are specific for the non-

reducing end sugar, these modified substrates will block  $\alpha$ -glucosidase hydrolysis. If the malto-oligosaccharide portion of this molecule is long enough, the presence of the protecting group does not affect the ability of the  $\alpha$ -amylase to cleave the oligosaccharide. Therefore, these blocked substrates will not undergo background hydrolysis.

One of the main problems with these PNP releasing assays is their requirement for a coupled enzyme. Although these assays are fairly sensitive, making them very useful for clinical detection of  $\alpha$ -amylase activity, the use of a coupled enzyme may result in artefacts during kinetic or inhibition studies.

Several substrates that do not require coupled enzymes have also been developed for the continuous monitoring of  $\alpha$ -amylase activity. One such substrate (Figure 4.10) is a malto-oligosaccharide containing two fluorescence groups, one attached at the reducing end and the other attached at the non-reducing end of the polymer (160). The two groups were chosen so that the fluorescence of one of group would be quenched by the other group through fluorescence resonance energy transfer (FRET). Upon cleavage of the oligosaccharide, FRET cannot occur due to the increase in the average distance between the groups. The cleavage of the substrate is therefore seen as an increase in fluorescence. However, this substrate is not very soluble in aqueous solutions due to the hydrophobic nature of these fluorescence groups and therefore cannot be used at high concentrations.

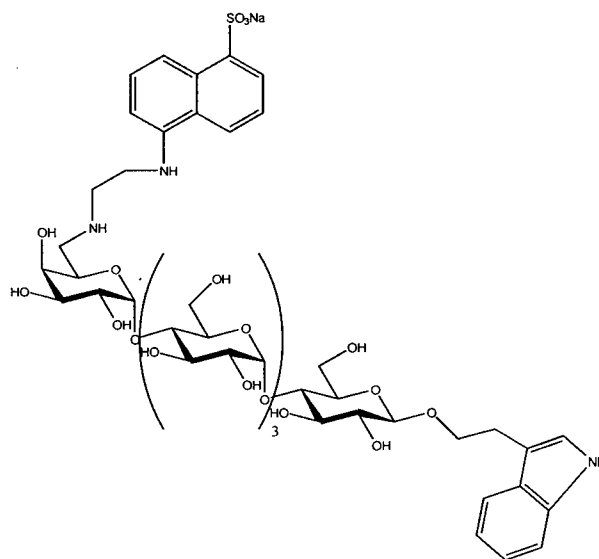


Figure 4.10 Structure of a fluorescence quenched substrate of  $\alpha$ -amylases (4.8).

Maltosides and maltotriosides with leaving groups such as PNP or fluoride have also been used for directly measuring  $\alpha$ -amylase activities. Unlike PNP-G4 or PNP-G5, PNP-G2 is exclusively cleaved by  $\alpha$ -amylase at the glycosidic linkage between the sugar and PNP. Therefore, PNP release can be used as an indicator of substrate turnover. However, PNP-G2 has a very low  $k_{\text{cat}}$  value and thus, is not a very good substrate of this enzyme. In comparison, sugars with a fluoride leaving group, such as maltotriosyl fluoride (G3F), are very good substrates with  $k_{\text{cat}}$  values that are several orders of magnitude higher than that for PNP-maltoside (Table 4.2) (161). When hydrolysed, G3F releases a fluoride ion, which can be detected using a fluoride sensitive electrode. The use of this electrode makes this assay fairly cumbersome and thus, it is not inherently useful for quick screens or for complex experiments.

|                                    | $k_{cat}$                         | $K_m$  | $k_{cat}/K_m$ | Reference   |
|------------------------------------|-----------------------------------|--------|---------------|-------------|
| <b>G2F</b>                         | $1.5 \times 10^2 \text{ s}^{-1}$  | 2.1 mM | 71            | (161)       |
| <b>G3F</b>                         | $2.8 \times 10^2 \text{ s}^{-1}$  | 0.3 mM | 930           | (161)       |
| <b>PNP-G2</b>                      | $4 \times 10^{-2} \text{ s}^{-1}$ | 4      | 0.01          | (162)       |
| <b><math>\alpha</math>DNP-G2</b>   | $0.4 \text{ s}^{-1}$              | 3.6 mM | 0.11          | This thesis |
| <b><math>\alpha</math>DNP-G3</b>   | $2.95 \text{ s}^{-1}$             | 1.5 mM | 2.0           | This thesis |
| <b>Me<math>\alpha</math>DNP-G2</b> | $2.7 \text{ s}^{-1}$              | 5.5 mM | 0.49          | This thesis |
| <b><math>\alpha</math>CNP-G3</b>   | $1.9 \text{ s}^{-1}$              | 3.6 mM | 0.52          | This thesis |

Table 4.2 Kinetic parameters for cleavage of maltoside and maltotrioxide substrates by HPA.

## 4.2 Specific aims of this study

1) *Synthesis and characterization of novel substrates for human pancreatic  $\alpha$ -amylase.*

Although there are various assays that have been developed for  $\alpha$ -amylases, each assay has some problem for specific uses. Ideally, a substrate used in an assay would have a readily detectable change upon reaction that could continuously be measured, a high rate of hydrolysis, a relatively low dissociation constant, and no side reactions to complicate the kinetics. Therefore, a substrate with a high  $k_{cat}$  value like that of G3F but can be monitored by measuring change in absorbance, as in the case of PNP-G2, would be a good candidate for the “ideal substrate”. In order to develop such a substrate, several chromogenic substrates will be synthesized.

*2) Screening and characterisation of novel inhibitors of human pancreatic  $\alpha$ -amylase.*

The substrate developed in the first part of the study will be used to develop a screening method for identifying potential inhibitors of HPA. This screen will be used to rapidly identify potential inhibitors of HPA from a library of monosaccharide analogues. A more detailed analysis of one of the more promising “hits” from this screen will be characterized further to validate this screen.

## 4.3 Results and discussion-part I: Development of a convenient assay

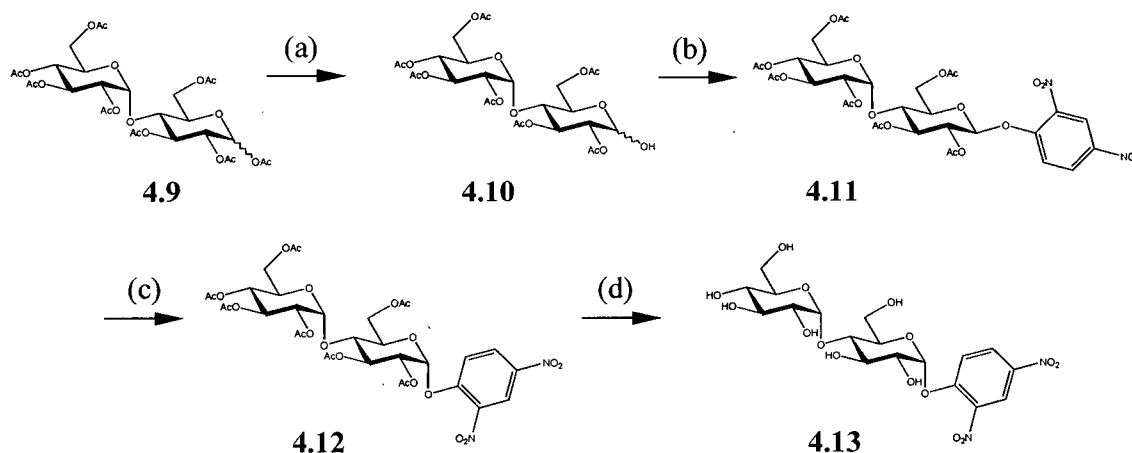
### 4.3.1 Rationale for the design of the novel substrates

The main reason for the large difference in the  $k_{\text{cat}}$  values of PNP-G2 and the glycosyl fluorides, such as G2F and G3F, is likely the greater leaving group ability of fluoride versus *p*-nitrophenolate. This is reflected in the different  $\text{pK}_{\text{a}}$  values of the conjugate acid of the leaving groups; 7.0 for *p*-nitrophenol and 3.2 for fluoride (the lower the  $\text{pK}_{\text{a}}$  value, the better the leaving group ability). Therefore, in order to create a phenyl glycoside that has a high  $k_{\text{cat}}$  value, the conjugate acid of the leaving group must have a low  $\text{pK}_{\text{a}}$ . 2,4-Dinitrophenol has a  $\text{pK}_{\text{a}}$  value of 3.9, a value comparable to that of HF. Therefore, a substrate with a 2,4-dinitrophenolate (DNP) leaving group should have a fairly high  $k_{\text{cat}}$  value. In addition, the extinction coefficient of DNP is about twice as high as that of PNP at pH 7.0, making an assay using this substrate more sensitive to HPA activity. Furthermore, because of the low  $\text{pK}_{\text{a}}$ , the extinction coefficient of DNP is essentially independent of pH down to 6.0, making it usable over a wider pH range. This makes the 2,4-dinitrophenyl  $\alpha$ -maltoside ( $\alpha$ DNP-G2) and the 2,4-dinitrophenyl  $\alpha$ -maltotrioside ( $\alpha$ DNP-G3) potentially good candidates for the ideal HPA substrate.

### 4.3.2 Synthesis of $\alpha$ DNP-G2

The synthesis of the peracetylated  $\alpha$ DNP-G2 (Scheme 4.2) was adopted from a literature synthesis of peracetylated 2,4-dinitrophenyl  $\alpha$ -glucoside ( $\alpha$ DNP-Glc) (163). Initially, the acetate group at the anomeric center was selectively removed from peracetylated maltose (4.9) using 1.1 eq of hydrazine-acetate in DMF. After a quick

workup, the product (**4.10**) was coupled to DNP by stirring overnight with 2,4-dinitrofluorobenzene (DNFB) and diazabicyclo[2.2.2]octane (DABCO) in DMF. This nucleophilic aromatic substitution resulted in primarily the peracetylated 2,4-dinitrophenyl  $\beta$ -maltoside (**4.11**) (roughly 9:1  $\beta/\alpha$  mixture) with a yield of 83% over 2 steps. The peracetylated  $\alpha$ DNP-G2 was obtained by the base-catalyzed anomerization of **4.11**. By treating **4.11** with  $K_2CO_3$  in DMF (*163*) over 2 days, the equilibrium mixture of the  $\alpha$ - and  $\beta$ -anomers was obtained in a ratio of 75:25. As might be expected, this ratio is similar to that previously obtained for the anomerization of peracetylated DNP-Glc (*164*). After workup, the  $\alpha$ -anomer crystallized out from a solution of EtOAc/PetEt to give the peracetylated  $\alpha$ DNP-G2 (**4.12**) in a 37% yield.



Scheme 4.3 Outline for the synthesis of  $\alpha$ DNP-G2. (a)  $NH_2NH_2$ ·acetate, DMF; (b) DNFB, DABCO, DMF, 83% over two steps; (c)  $K_2CO_3$ , DMF, 37%; and (d) 5% AcCl (v/v), MeOH, 20 %.

A number of unsuccessful attempts have been made to synthesize  $\alpha$ -DNP-Glc.

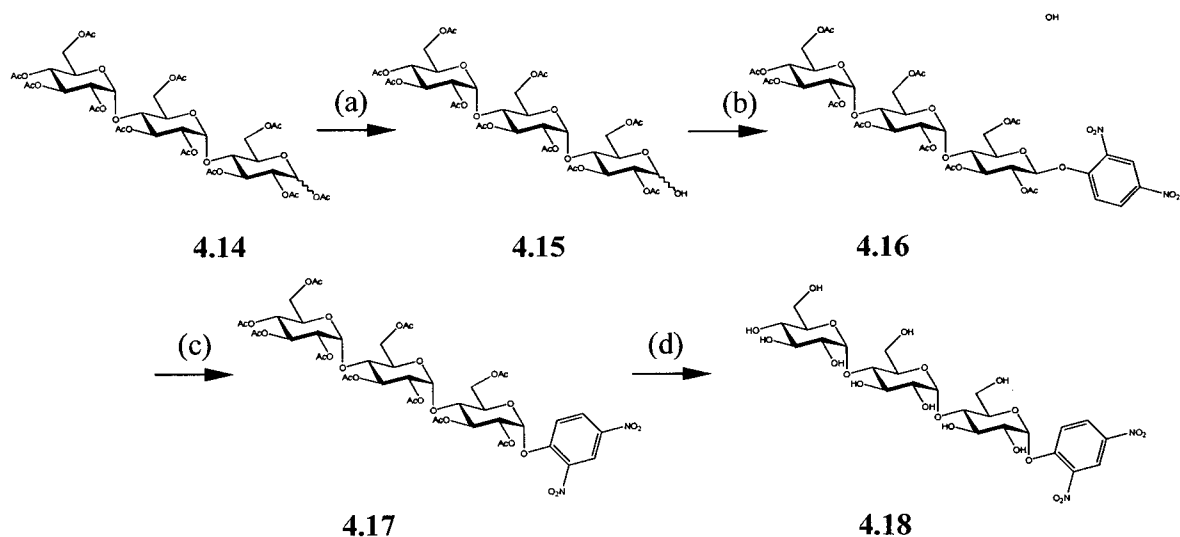
The problem in all cases has been during the deprotection step. Firstly, this deprotected product is inherently hydrolytically labile. In addition, the DNP migrates relatively easily to the *syn* 2-hydroxyl group of the sugar. Recently, it was shown that the peracetylated

$\alpha$ DNP-Glc could be deprotected using 5% HCl in MeOH at 4°C in 5 hours (165). Because the additional glucose moiety adds rigidity to the reducing end glucoside, the deprotected  $\alpha$ DNP-G2 should be more hydrolytically stable than the  $\alpha$ DNP-Glc. The method used for deprotection of  $\alpha$ DNP-Glc should therefore be utilizable for the deprotection of  $\alpha$ DNP-G2. When the reaction was attempted, it was found that deprotection of  $\alpha$ DNP-G2 took a considerably longer time than did the deprotection of  $\alpha$ DNP-Glc. In fact, even after 24 hours, the reaction had not gone to completion. Furthermore, even before all the  $\alpha$ DNP-G2 had been deprotected, TLC analysis suggested that hydrolysis of the DNP group was taking place, resulting in the formation of maltose. Therefore, the reaction was stopped before 100% of the product was deprotected (about 20% mono-acetylated DNP-G2 still remained, by TLC analysis). The purification of the reaction mixture was achieved by flash chromatography using 27:2:1 EtOAc/MeOH/AcOH as the eluant. The AcOH in the eluant was used in order to protonate the DNP, which would otherwise not separate from the desired product. In order to remove the AcOH from the product, the maltoside was precipitated from a MeOH solution by adding Et<sub>2</sub>O. The  $\alpha$ DNP-G2 (4.13) was obtained in a final yield of 20%.

#### 4.3.3 *Synthesis of $\alpha$ DNP-G3*

The synthesis of the  $\alpha$ DNP-G3 was similar to that of  $\alpha$ DNP-G2 (Scheme 4.4). Briefly, the 1-hydroxyl group of the peracetylated maltotriose (4.14) was selectively deprotected using hydrazine-acetate in DMF. This product (4.15) was coupled to DNP by treatment with DNFB and DABCO in DMF to yield the 2,4-dinitrophenyl  $\beta$ -maltotrioside (4.16) in 87% yield over two steps. The peracetylated  $\alpha$ DNP-G3 (4.17) was obtained by

the base-catalyzed anomerization ( $K_2CO_3$  in DMF) of **4.16**. This yielded the equilibrium mixture of the  $\alpha$ - and  $\beta$ -anomers in a ratio of 75:25. Unlike the protected  $\alpha$ DNP-G2 (**4.12**), **4.17** did not crystallize under several conditions attempted. The purification of the  $\alpha$ -anomer was therefore achieved using flash chromatography to give pure **4.17** in a 54% yield. This compound was deprotected under acidic conditions using 5% AcCl/MeOH. As was the case with the deprotection of  $\alpha$ DNP-G2, not all of the  $\alpha$ DNP-G3 was deprotected before hydrolysis of the DNP group became evident. Therefore, the reaction was stopped before completion. The fully deprotected  $\alpha$ DNP-G3 was purified by flash chromatography using 7:2:1 EtOAc/MeOH/AcOH as the eluant. The final product was precipitated from a MeOH solution by addition of  $Et_2O$  to yield the pure  $\alpha$ DNP-G3 (**4.18**) in 27% yield.



Scheme 4.4 Outline for the synthesis of  $\alpha$ DNP-G3. (a)  $NH_2NH_2 \cdot$  acetate, DMF; (b) DNFB, DABCO, DMF, 88% over two steps; (c)  $K_2CO_3$ , DMF, 54%; and (d) 5% AcCl (v/v), MeOH, 27%.

#### **4.3.4 Kinetic analysis of $\alpha$ DNP-G2 as a substrate for HPA**

Testing of  $\alpha$ DNP-G2 as a substrate for HPA was accomplished by monitoring the change in absorbance at 400 nm of the reaction mixture. As would be expected from DNP release through cleavage of the glycosidic bond, there was a time dependent increase in absorbance when the compound was incubated with enzyme. In comparison, the background rate of hydrolysis for  $\alpha$ DNP-G2 in the absence of enzyme was negligible over the timeframe of the assay (20 minutes). Enzyme catalyzed hydrolysis rates were constant over the first several minutes and the initial rates, with respect to substrate concentration, fit well to the Michaelis-Menten equation. From this, the kinetic parameters for this substrate were determined (Table 4.2).

Comparison of the  $K_m$  value for  $\alpha$ DNP-G2 with that of PNP-G2 or G2F revealed that there is no significant difference in the apparent binding of these substrates. This is expected as each of the substrates is thought to occupy the -2 and -1 subsites during hydrolysis. The main difference between these substrates was seen in their  $k_{cat}$  values. As might be expected from the  $pK_a$  values of the conjugate acids of these three leaving groups, the  $k_{cat}$  value of the G2F was greater than that for  $\alpha$ DNP-G2, which was greater than that for PNP-G2. Somewhat unexpected, and disappointing, was the fact that the  $k_{cat}$  value for  $\alpha$ DNP-G2 was only one order of magnitude higher than that for PNP-G2, and three orders of magnitude lower than the  $k_{cat}$  value for G2F.

#### **4.3.5 Analysis of the products of HPA catalysed cleavage of $\alpha$ DNP-G2**

To determine the mode by which HPA was catalyzing the release of DNP, the products formed from the HPA catalyzed reaction of  $\alpha$ DNP-G2 were determined by using an HPLC attached in series to both a UV detector and evaporative light scattering

detector (ELSD). After 20 minutes, the predominant products formed were maltose, DNP, DNP-Glc and DNP-G4 (Figure 4.11). The formation of the DNP-glycosides was only observed in the UV detector and not with the ELSD suggesting that these products are only produced in a small quantity. However, the ELSD has different response factors for different molecules and therefore, it may be possible that the DNP-glycosides are formed in significant amounts but not detected (from standards, the DNP-glycosides seemed to give roughly half of the response of their respective malto-oligosaccharide).

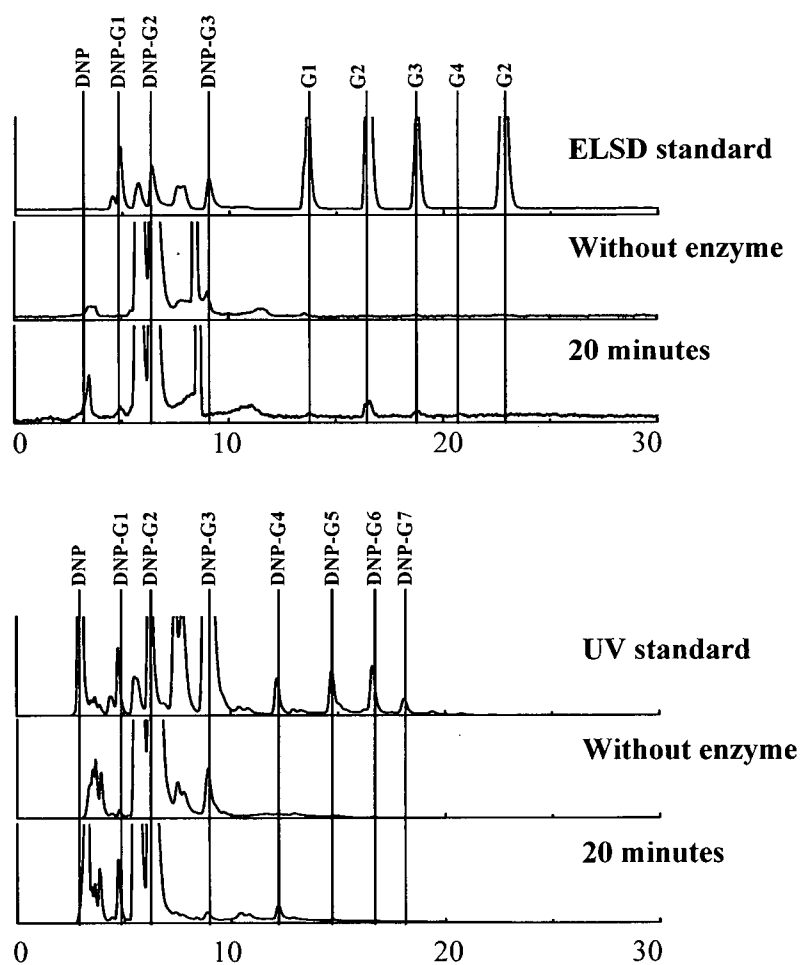


Figure 4.11 HPLC analysis of the reaction products of the HPA catalyzed reaction of  $\alpha$ DNP-G2 after 20 minutes. Compound was detected using (a) UV detector, and (b) ELSD detector. Conditions: Tosoh Amide-80 column, 0.7 mL/min ( $\text{CH}_3\text{CN}/\text{H}_2\text{O}$  75:25  $\rightarrow$  55:45 in 10 minutes followed by hold at this concentration).

The DNP-G4, which seems to be formed in small quantity, is a possible intermediate species for the formation of all other products. This species is the product of a transglycosylation of  $\alpha$ DNP-G2 onto another molecule of  $\alpha$ DNP-G2 with the release of DNP. The product can be hydrolysed in three different ways – by formation of maltotetraose and DNP; by formation of maltotriose and  $\alpha$ DNP-Glc; and finally, by formation of  $\alpha$ DNP-G2 and maltose. Alternatively, formation of maltose could be explained by direct hydrolysis of the DNP group from  $\alpha$ DNP-G2. From these data, either route is plausible and more detailed studies are required in order to determine the mode of DNP release.

#### **4.3.6 Kinetic analysis of $\alpha$ DNP-G3 as a substrate for HPA**

Not surprisingly,  $\alpha$ DNP-G3 was also a substrate for HPA. The kinetic parameters for hydrolysis of this compound were once again determined by fitting initial rates at varying substrate concentrations to the Michaelis-Menten equation (Table 4.2). In the case of the glycosyl fluorides, the  $K_m$  value of G3F was 10 fold lower than that for G2F. It was therefore expected that the same trend would be seen for the  $K_m$  values of  $\alpha$ DNP-G3 and  $\alpha$ DNP-G2. The  $K_m$  value of  $\alpha$ DNP-G3 was indeed lower than the  $K_m$  value for  $\alpha$ DNP-G2 but only by a factor of two. However, the  $k_{cat}$  value for  $\alpha$ DNP-G3 was 10 fold higher than that of  $\alpha$ DNP-G2. This is in sharp contrast to the glycosyl fluorides, where G3F and G2F had similar  $k_{cat}$  values.

Recently, we were able to obtain a sample of 2-chloro-4-nitrophenyl  $\alpha$ -maltotrioside ( $\alpha$ CNP-G3; Figure 4.12, Genzyme, Massachusetts) (166). Although this compound had been reported as a substrate for HPA, its kinetic parameters had only been reported at pH 6.0. This made comparison of these parameters with respect to other

substrates difficult. Therefore, the kinetic parameters of  $\alpha$ CNP-G3 (Table 4.2) were determined under standard conditions (50 mM NaP<sub>i</sub> buffer, pH 7.0, 100 mM NaCl). Under these conditions, the  $K_m$  value for this substrate is two fold higher than for  $\alpha$ DNP-G3. This is consistent with the fact that these two substrates are similar in structure. More intriguing was the fact that the  $k_{cat}$  value for this compound was  $1.9 \text{ s}^{-1}$ , a value only slightly lower than the  $k_{cat}$  value for  $\alpha$ DNP-G3. Because the  $pK_a$  value of 2-chloro-4-nitrophenol is 5.1, an entire pH unit higher than DNP, the  $k_{cat}$  value might be expected to reflect this difference. These results seem to indicate that decreasing the  $pK_a$  of the leaving group does not result in a significant increase in the  $k_{cat}$  value of the substrate.

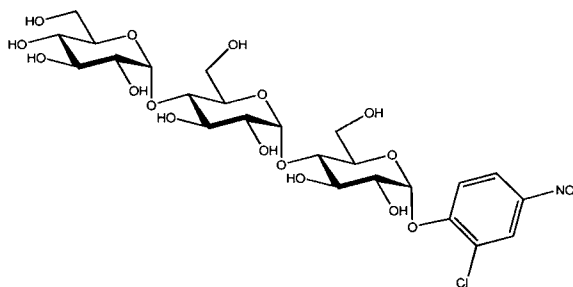


Figure 4.12 Structure of  $\alpha$ CNP-G3.

#### 4.3.7 Analysis of the products of HPA catalysed cleavage of $\alpha$ DNP-G3

Product analysis was performed on the HPA catalyzed cleavage of  $\alpha$ DNP-G3 in order to determine the mode of DNP release (Figure 4.13). After 20 minutes of reactions, several products including DNP, maltotriose, DNP-G6 and DNP-G4 were formed. Unfortunately, due to a trace contamination of glucose and maltose in the starting material, it was not possible to determine whether small amounts of these compounds were formed during the reaction. As was the case with  $\alpha$ DNP-G2, the transglycosylation

product,  $\alpha$ DNP-G6, was formed to a significant level. In fact, this product was formed to the extent that it was observable with the ELSD. The DNP release and the formation of maltotriose could be due to either the direct hydrolysis of the glycosidic bond between the DNP and maltotriose moiety, or to transglycosylation followed by hydrolysis. Once again, without a more detailed kinetic study on the hydrolysis of longer DNP-malto-oligosaccharides, it is not possible to say with certainty the mode of DNP release.

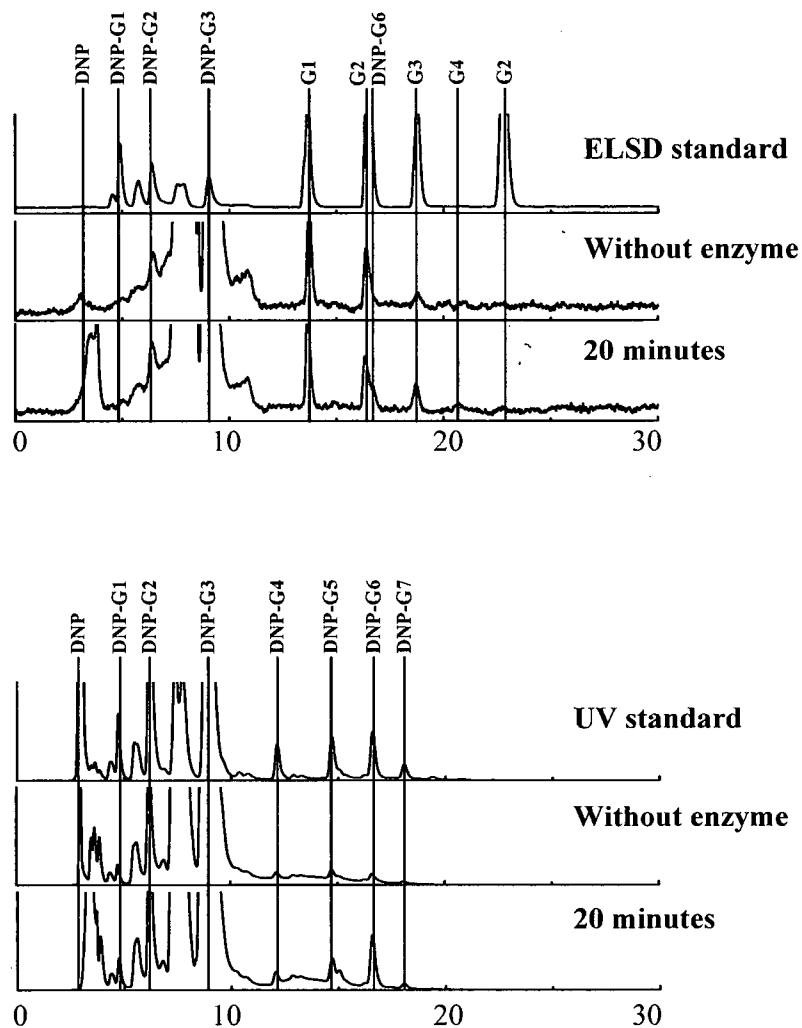


Figure 4.13 HPLC analysis of the reaction products of the HPA catalyzed reaction of  $\alpha$ DNP-G3 after 20 minutes. Compound was detected using (a) UV detector, and (b) ELSD detector. Conditions: Tosoh Amide-80 column, 0.7 mL/min ( $\text{CH}_3\text{CN}/\text{H}_2\text{O}$  75:25  $\rightarrow$  55:45 in 10 minutes followed by hold at this concentration).

#### 4.3.8 Kinetic analysis of DNP-Glc as a substrate for HPA

By way of comparison,  $\alpha$ DNP-Glc was also tested as a substrate for HPA. The data do not fit to the Michaelis-Menten equation, but rather, the rate seemed to increase exponentially with concentration (Figure 4.14) in much the same way as was seen for the HPA catalyzed reaction of glucosyl fluoride (GlcF) (151). Product analysis in this case showed that the main product was maltose (Figure 4.15), resulting from transglycosylation of GlcF onto another molecule of itself. It is very likely that the

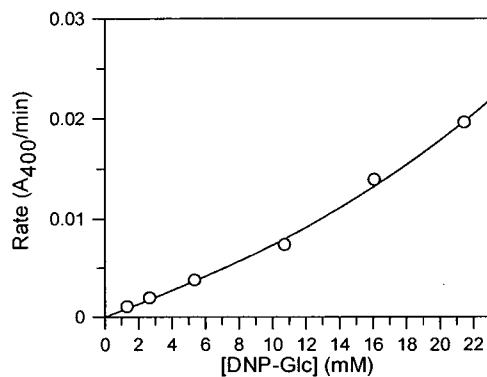


Figure 4.14 The Michaelis-Menten plot for the reaction of  $\alpha$ DNP-Glc catalyzed by HPA.

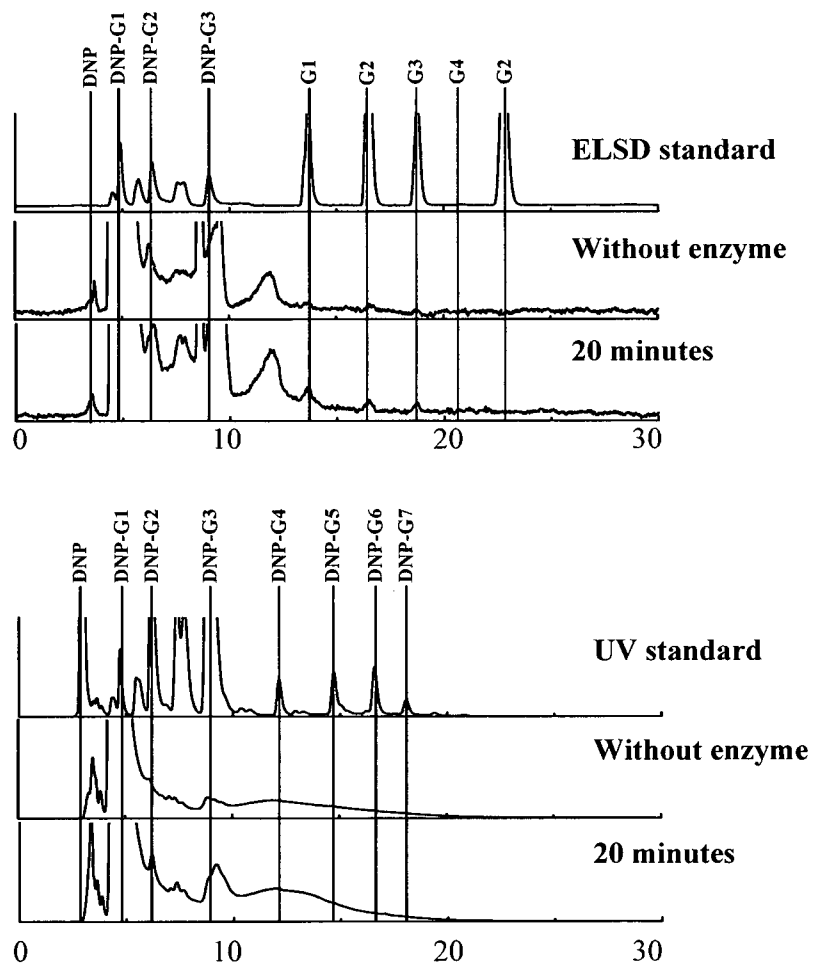


Figure 4.15 HPLC analysis of the reaction products of the HPA catalyzed reaction of  $\alpha$ DNP-Glc after 20 minutes. Compound was detected using (a) UV detector, and (b) ELSD detector. Conditions: Tosoh Amide-80 column, 0.7 mL/min ( $\text{CH}_3\text{CN}/\text{H}_2\text{O}$  75:25  $\rightarrow$  55:45 in 10 minutes followed by hold at this concentration).

$\alpha$ DNP-Glc is also acting in the same manner as this substrate. As would be expected from transglycosylation, the product analysis showed the formation of glucose, maltose, and maltotriose as well as their respective DNP-glycosides.

#### ***4.3.9 Conclusions and future directions***

Two compounds,  $\alpha$ DNP-G2 and  $\alpha$ DNP-G3, were synthesized and tested as substrates for HPA. The initial rates were linear with respect to time and gave good fits to the Michaelis-Menten equation. Both these substrates seemed to react, at least in part, via transglycosylation mechanisms. Because each of these reactions and their reaction products add another level of complication to the overall kinetics of the reaction, a better substrate may be one in which the substrate is blocked at the non-reducing end so that transglycosylation may not occur. This may be accomplished, for example, by methylating the non-reducing end 4-hydroxyl group or by removing this functional group completely. Of these substrates, the  $\alpha$ DNP-G3 had the highest  $k_{cat}$ , as well as the highest  $k_{cat}/K_m$ , making it the most favourable substrate for use for kinetic studies.

## **4.4 Results and discussion: Rapid screening of monosaccharide inhibitors**

### ***4.4.1 Rationale for searching for monosaccharide inhibitors***

As was demonstrated in previous studies with gluconolactone, and iminocyclitol analogues (148, 149, 152), linking a malto-oligosaccharide to the non-reducing end of a potential monosaccharide “inhibitor” can transform a seemingly poor inhibitor of  $\alpha$ -amylase into an inhibitor with a  $K_i$  value in the low micromolar range, decreasing the  $K_i$  value at least 3 orders of magnitude. Therefore, if the initial monosaccharide already has significant inhibitory activity towards  $\alpha$ -amylase, then the extended inhibitor may have a  $K_i$  value comparable to that of acarbose.

Presently, in the literature, there are very few examples of monosaccharide inhibitors of  $\alpha$ -amylases, an apparent notable exception being salacinol (Figure 4.8). A reason for this relative scarcity may be that these enzymes are not routinely included in inhibition studies when a novel compound is isolated or synthesized. It is, however, still possible that a number of known  $\alpha$ -glucosidase inhibitors may also inhibit  $\alpha$ -amylases. In order to determine whether any of these compounds have inhibitory activity towards  $\alpha$ -amylases, a convenient screen is required to rapidly identify potential candidates.

### ***4.4.2 Rapid screen for identifying potential HPA inhibitors***

Previous studies showed that in certain cases, the  $K_i$  value decreased by over 3 orders of magnitude when monosaccharide analogues were extended by two glucose moieties (148, 149, 152). Therefore, if a monosaccharide significantly inhibits HPA activity at 1 mM concentration, then it could be considered a potential candidate for

future extension studies. If a DNP-glycoside is used as a substrate, these assays could be done spectrophotometrically and as such, large libraries of compounds could be quickly screened for potential inhibitors. Because  $\alpha$ DNP-G3 has a higher  $k_{\text{cat}}$  value and lower  $K_m$  value than does  $\alpha$ DNP-G2, it was used as the substrate of these assays.

The  $IC_{50}$  measured for an inhibitor is dependent on the concentration of substrate that is used in the assay – thus it is of limited inherent value. In the case of a competitive inhibitor, if the substrate is at saturating concentrations ( $[\text{Substrate}] \gg K_m$ ), the  $IC_{50}$  will be considerably higher than the  $K_i$  value. Conversely, at substrate concentrations much lower than the  $K_m$  value, the  $IC_{50}$  will be lower than the  $K_i$  value. Therefore, a substrate concentration around the  $K_m$  value (1.5 mM in the case of  $\alpha$ DNP-G3) was chosen for the assay so as to give meaning to the  $IC_{50}$  values measured.

#### ***4.4.3 Positive control for the new screen***

To show that an assay using  $\alpha$ DNP-G3 would identify HPA inhibitors, the  $K_i$  value for a well characterized  $\alpha$ -amylase inhibitor, acarbose, was determined using this substrate. Previously, when G3F was used as a substrate, acarbose was found to be a non-competitive inhibitor of HPA with a  $K_i$  value of 20 nM (145). Using  $\alpha$ DNP-G3 as a substrate, the approximate  $K_i$  value for acarbose with HPA was determined to be 20  $\mu$ M, a value 3 orders of magnitude higher than the value that was previously determined for this compound.

At first glance, this would seem to indicate that changing the substrate changes the  $K_i$  value of this inhibitor. However, several results, both from this study and from the literature, seemed to suggest that another factor could underlie this variable  $K_i$  value. Firstly, the initial rates measured for  $\alpha$ DNP-G3 hydrolysis performed at an acarbose

concentration of  $1.8 \times 10^{-6}$  M showed that the rate steadily decreased over several minutes (Figure 4.16), with the rate after 20 minutes being  $\sim 30\%$  of the initial rate. This is a significantly larger decrease in rate than would be expected for substrate depletion, and in fact, in the control assay where no acarbose was present, such a decrease was not observed. Secondly, it had been shown previously that G3F, at least in part, transglycosylates onto itself (161). Because acarbose is a pseudo-tetrasaccharide, it is possible that HPA adds a maltotriosyl unit onto the non-reducing end of acarbose by transglycosylation to create an elongated acarbose molecule *in situ*. If the extended acarbose is a better inhibitor than is the unmodified form, its formation would result in a progressively decreasing rate. Indeed, as was mentioned in earlier, structural studies of acarbose bound to HPA have consistently shown that the bound form of acarbose has been modified.

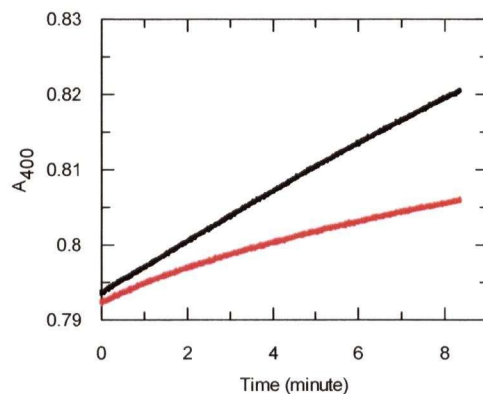


Figure 4.16 Hydrolysis of  $\alpha$ DNP-G3 in the presence (-) and absence (-) of  $1.8 \times 10^{-6}$  M acarbose.

Therefore, it is possible that the  $K_i$  value determined for acarbose, using G3F as a substrate, was that of a modified form of acarbose. Because the  $k_{cat}$  value for  $\alpha$ DNP-G3 hydrolysis is 100 times lower than the  $k_{cat}$  value for G3F hydrolysis, the formation of  $ES^*$  (Scheme 4.1) will occur at least 100 times more slowly. This, in turn, means that the transformation of acarbose to a more potent inhibitory form will also be 100 times slower

when using  $\alpha$ DNP-G3 versus G3F (assuming similar reaction conditions). The first 15-30 seconds after enzyme addition during G3F hydrolysis cannot be observed due to the nature of the fluoride electrode assay. By this time, the reaction leading to acarbose modification may have already been completed. The time that is required for acarbose modification would be considerably longer if  $\alpha$ DNP-G3 were used as the substrate. This would explain the decreasing rate seen when monitoring  $\alpha$ DNP-G3 hydrolysis in the presence of acarbose. Therefore, the  $K_i$  value determined by using the initial rates of  $\alpha$ DNP-G3 hydrolysis (in the presence of acarbose) most likely represents the  $K_i$  value of the unmodified acarbose.

If the above hypothesis is correct and the true inhibiting species in the previous inhibition study is the elongated version of acarbose, the extended acarbose should have the same  $K_i$  regardless of whether the substrate is G3F or  $\alpha$ DNP-G3. Chemical synthesis of such a compound is extremely challenging (although recently, an enzymatic synthesis of this compound was published (167)) and as such, it was not possible to test the hypothesis directly. However, the extended acarbose should form *in situ* within the first 15-30 seconds if G3F and acarbose are incubated with HPA. If such an extended acarbose is created, then the HPA activity should be inhibited at nanomolar acarbose concentrations, even if  $\alpha$ DNP-G3 is used as a substrate. Indeed, when HPA activity was measured using  $\alpha$ DNP-G3 (1 mM) in the presence of both G3F (0.2 mM) and acarbose (180 nM), the initial rate was found to be 67% of that in the control reaction where acarbose was not present (Figure 4.17). In contrast, when the HPA activity was measured using  $\alpha$ DNP-G3 in the presence of only acarbose (180 nM), the initial rate was similar to that in the control reaction where acarbose was not present.

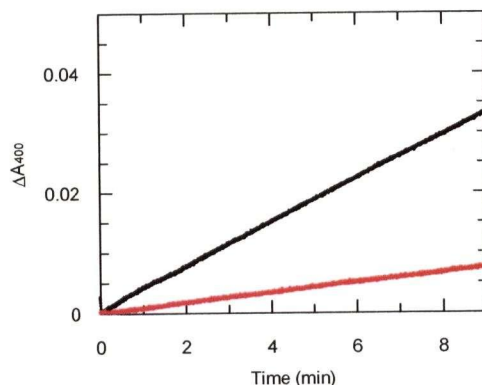


Figure 4.17 Hydrolysis of  $\alpha$ DNP-G3 in the presence of  $1.8 \times 10^{-7}$  M acarbose that had been pre-incubated with G3F and HPA (-). Control where G3F was pre-incubated with HPA (-) prior to assaying with  $\alpha$ DNP-G3.

When acarbose was pre-incubated for 1 hour with G3F and HPA prior to assaying for enzymatic activity with  $\alpha$ DNP-G3, the inhibitory activity was significantly lower than for the control where HPA was pre-incubated with only G3F. This pre-incubation was done at varying concentrations of acarbose to determine a rough  $K_i$  value for the G3F-extended acarbose. First approximation showed that the  $K_i$  value for the extended acarbose was 140 nM. Although this value is one order of magnitude higher than the  $K_i$  value determined for acarbose using G3F, it is also considerably lower than the 20  $\mu$ M  $K_i$  value determined for acarbose by using  $\alpha$ DNP-G3 as a substrate. Due to the low concentrations of acarbose being used, no product analysis for the HPA-catalyzed reaction of acarbose and G3F was performed. Therefore, there is no conclusive evidence to say that the potent inhibitor in the reaction mix is an acarbose extended at the non-reducing end by a maltotriosyl moiety. However, these results clearly demonstrate that G3F is playing a role in reducing the apparent  $K_i$  value of acarbose.

These results demonstrate that the  $K_i$  value obtained for acarbose using G3F is likely not the  $K_i$  value of acarbose but rather that of a modified acarbose. In fact, it is

likely that  $K_i$  values determined for acarbose by using substrates with similar  $k_{cat}$  values to that of G3F (including malto-oligosaccharides) are also plagued with this problem. Because of the lower  $k_{cat}$  value for  $\alpha$ DNP-G3, the  $K_i$  value determined using this substrate is probably a more accurate measure of the true  $K_i$  value of acarbose. As such,  $\alpha$ DNP-G3 is a better substrate for determining true  $K_i$  values than are the other substrates.

#### ***4.4.4 Design of a rapid screen for identifying potential elongated HPA inhibitors***

In light of these results, a secondary assay may be envisioned to quickly determine whether an extended version of a monosaccharide analogue would be a good HPA inhibitor. In this assay, the HPA would first be pre-incubated with G3F and the monosaccharide analogue. During this time, the compound may be elongated by several glucose moieties via transglycosylation, in much the same way as in the case of acarbose. The activity of the HPA would then be determined using  $\alpha$ DNP-G3. If the extended compound inhibits HPA activity, then this will be seen as a lower rate of  $\alpha$ DNP-G3 hydrolysis than in the control where the HPA is pre-incubated with only G3F. The ratio of these two rates can be compared to the ratio for the rate of HPA catalyzed hydrolysis for  $\alpha$ DNP-G3 in the presence and absence of the monosaccharide analogue (no pre-incubation or G3F). A significant difference in these two ratios will indicate whether the extended compound is a better inhibitor than is the unmodified compound.

A negative result from this assay, however, does not immediately imply that the extended version of the compound is not a good HPA inhibitor. It is equally possible that under the conditions of the assay, the inhibitor is not extended; that is to say that the inhibitor does not act as a good acceptor. This will depend on the  $K_{acc}$  and  $k_{trans}$  of the

compound (Scheme 4.1). A positive result, though, would strongly suggest that the addition of several glucose moieties to the non-reducing end of this compound would result in a good inhibitor of HPA.

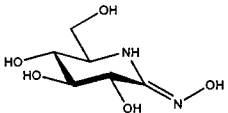
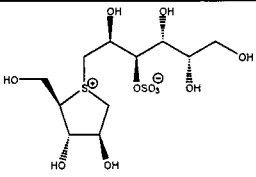
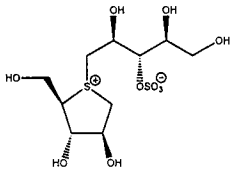
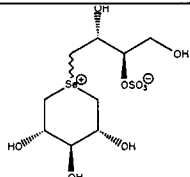
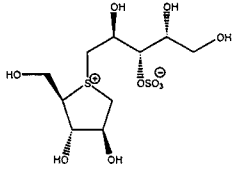
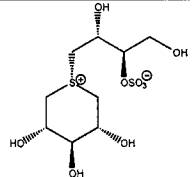
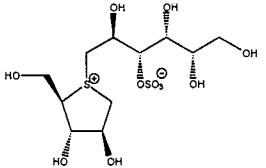
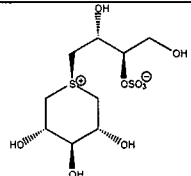
The screen for HPA inhibitors would therefore consist of two parts. In the first (Assay#1),  $\alpha$ DNP-G3 would be used to assay for inhibition of HPA activity at a single concentration of inhibitor (1 mM). In the second part, the inhibitor would be pre-incubated with G3F and HPA for 15 minutes. After this time, the HPA activity would be measured using  $\alpha$ DNP-G3 (Assay#2). These two experiments would show (a) if the monosaccharide is able to inhibit HPA activity, and (b) if the inhibitor, when extended by several glucose moieties, is better able to inhibit HPA activity.

#### ***4.4.5 Results of the rapid $\alpha$ -amylase screen for potential inhibitors***

The monosaccharide inhibitors that were screened in this study included a “library” of seven salacinol-like compounds provided to us by Professor Pinto at Simon Fraser University and the potent  $\alpha$ -glucosidase inhibitor, D-gluconohydroximino-1,5-lactam (GHIL) (168), synthesized by Dr. Tanja Wrodnigg (Table 4.3).

The results of the Assay#1 and Assay#2 are summarized in Table 4.3. To our disappointment, although not totally unexpected, neither the seven salacinol-like compounds, nor the GHIL inhibited HPA activity significantly at a concentration of ~1 mM. The best inhibitor among these compounds was the GHIL, which reduced the HPA activity to 88 % of the control rate. As all of the compounds tested were monosaccharide analogues, it may have been optimistic to set the threshold of the inhibitor concentration at 1 mM.

Table 4.3 Results of the screen using Assay#1 and Assay#2. The numbers in each of the columns refers to the percentage of HPA activity still left when tested with the assay.

| Compound  | Assay#1 | Assay#2 | Compound  | Assay#1 | Assay#2 |
|---|---------|---------|---|---------|---------|
| <br>(GHIL) | 82%     | 25%     |    | 93%     | 100%    |
|            | 85%     | 100%    |    | 89%     | 100%    |
|           | 85%     | 89%     |   | 95%     | 100%    |
|          | 89%     | 89%     |  | 100%    | 100%    |

When the compounds were tested with Assay#2, once again, there was no significant inhibition of HPA activity by any of the seven salacinol-like compounds. As was mentioned earlier, these negative results may have several explanations. The first is that the elongated forms of these compounds do not inhibit  $\alpha$ -amylase to any significant level. The other possibility is that HPA is not able to transglycosylate the maltotriose unit onto the salacinol-like compound due to the high  $K_{acc}$  or low  $k_{trans}$  values for the salacinol-like compounds. If the latter is the case, it may be possible to favour transglycosylation onto the inhibitor by increasing its concentration in the assay mix. However, because these compounds showed little inhibition in either of these assays, they were not studied any further. In sharp contrast, GHIL was found to substantially inhibit HPA activity when pre-incubated with HPA and G3F. In fact, the rate of  $\alpha$ DNP-G3 hydrolysis was 25% of the rate of the control where no inhibitor was present. This compound was therefore chosen for further studies.

#### ***4.4.6 Analysis of GHIL as an inhibitor of HPA***

Using  $\alpha$ DNP-G3 as a substrate, an approximate  $K_i$  value of 11 mM was determined for GHIL with HPA. This value is 4 orders of magnitude higher than that with yeast  $\alpha$ -glucosidase. This difference in  $K_i$  values may be due to the fact that HPA is an endo-glycosidase. As alluded to in Section 4.3.1.2, endo-glycosidases may also require binding at the  $-2$  subsite in order to orient the sugar in the  $-1$  subsite to make appropriate interactions with active site residues. Indeed, when various malto-oligosaccharides were tested as substrates for HPA, it was found from  $k_{cat}/K_m$  values that the both the  $-1$  and  $-2$  subsites are important for catalysis (108).

Results of a three-dimensional structural analysis for HPA, where GHIL had been soaked in, showed that this inhibitor bound in an unexpected fashion (169). The GHIL was bound in the +1 subsite with the “reducing end” pointing towards the -1 subsite (Figure 4.18). Furthermore, there was no electron density for a sugar bound in the -1 subsite. If GHIL were acting as a transition state analogue, or it were binding in the same manner as it does for  $\alpha$ -glucosidase, then the inhibitor should bind to the -1 subsite. Although this reverse binding mode may be an artefact of crystallization, the structural study strongly suggests that binding to the -1 subsite is not the most favoured binding mode for this monosaccharide inhibitor.

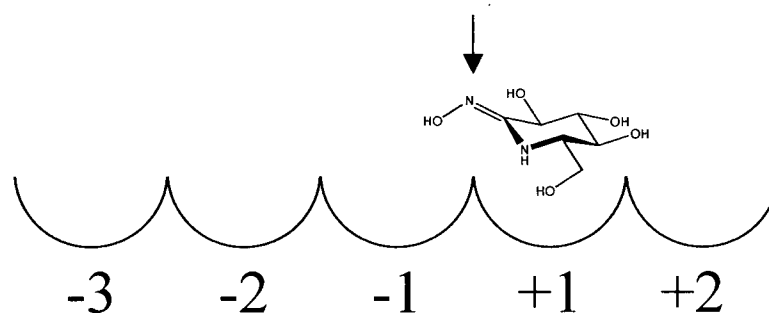


Figure 4.18 Schematic of the binding mode of D-gluconhydroximolactam in HPA (169).

Interestingly, when GHIL was pre-incubated with G3F and HPA, it seemed to better inhibit HPA activity than it did in the absence of G3F. This suggests that, as in the case of acarbose, the GHIL is being extended *in situ*, presumably through transglycosylation, to result in a potent inhibitor of HPA. When HPA activity was monitored using  $\alpha$ DNP-G3 in the presence of GHIL (1 mM) but without G3F, there was a time dependent change in the rate of DNP hydrolysis. This is consistent with the formation of a modified inhibitor as was seen in the case of acarbose. The formation of the modified inhibitor could be monitored by incubating GHIL (1 mM) with G3F (0.4

mM) and HPA for varying time periods. The residual HPA activity could then be measured with  $\alpha$ DNP-G3. From this, it was evident that the modification reaction was complete after 30 minutes under these conditions.

To quantitate the change in inhibitory activity, an approximate  $K_i$  value was determined for the inhibitory species in the reaction mix. As was done in the acarbose study, the extended inhibitor was created *in situ* by pre-incubating varying concentrations of GHIL with a fixed concentration of G3F (0.4 mM) and HPA. After 1 hour of incubation at 30°C, the HPA activity was measured using  $\alpha$ DNP-G3 (0.9 mM). Assuming complete conversion of the GHIL to the inhibitory form, the data was plotted in the form of a Dixon plot. From this, the approximate  $K_i$  value was determined to be 265  $\mu$ M. As the  $K_i$  value of GHIL is 11 mM, this is an improvement in the  $K_i$  value by 3 orders of magnitude.

If this approximate  $K_i$  value for the G3F-extended GHIL is close to the actual  $K_i$  value, then the strategy for extending an  $\alpha$ -glucosidase inhibitor may not be as promising as originally hypothesized. Although extension of the monosaccharide analogue did significantly decrease the  $K_i$  value, the final  $K_i$  value is not close to the 20 nM seen for acarbose. Furthermore, even the extended gluconolactone (4.2, Figure 4.7) had a  $K_i$  value of 30  $\mu$ M (148), implying that a lower  $K_i$  value of the  $\alpha$ -glucosidase inhibitor does not necessarily equate to a lower  $K_i$  value of the extended compounds for HPA.

However, in order to determine this approximate  $K_i$  value for the extended GHIL, it was necessary to make several assumptions. As stated before, the key assumption made was that the GHIL was completely converted into the inhibitory form. Such an assumption was required to plot a Dixon plot. However, even from the point of the

experimental design, it was clear that this assumption is not true. In this experiment, for most of the data points, the limiting reagent was G3F (0.3 mM) as opposed to the GHIL. This concentration was chosen in order to avoid inhibition by G3F, which could be considered a competing substrate ( $K_m$  value of 0.5 mM). Therefore, the maximal concentration of extended GHIL would be 0.3 mM. The fact that the Dixon plot gave a straight line, though, does suggest that there is a linear correlation between the concentrations of inhibitor added and the modified inhibitor formed.

The maximal concentration of modified inhibitor formed in this experiment is probably even lower than 0.3 mM as this value assumes that transglycosylation is the predominant reaction. As seen from analysis of the products of HPA catalyzed reaction with G3F, hydrolysis, rather than transglycosylation of G3F onto another molecule of G3F is the preferred mode of action (161). Since G3F is a trisaccharide, it is more likely to be a better acceptor than is GHIL. Therefore, it is likely that the extended D-gluconhydroximolactam makes up a very small percentage of the reaction product. In fact, MALDI-TOF analysis of this reaction mixture showed little sign of an extended GHIL.

When crystals of HPA were soaked with both GHIL and G3F, the results seemingly contradicted the kinetic analysis (169). The structure determined in this case showed that a bound maltotriose (occupying -3 to -1 subsites) and the GHIL (similar binding mode to the previous structure) were both bound. However, these two compounds seemed to be bound as independent molecules and not as an extended GHIL. This might suggest that the increased inhibitory potency of the GHIL is not due to its

modification *in situ*. However, it may be also be possible that under the conditions used for obtaining this data, the modification was not favourable.

Because structural analysis did not show any modified inhibitors bound in the active site, it was necessary to show that extension of GHIL, in the presence of HPA and G3F, was a feasible hypothesis. To demonstrate this, 10 mM of G3F and 9 mM of GHIL were incubated for 1 hour in the presence of HPA (1.2 mg·ml<sup>-1</sup>). Under these conditions, the transglycosylation of a maltotriose unit onto GHIL would be more favoured than in the previous experiment due to the high acceptor concentrations. Furthermore, unlike in the previous case, the high concentrations of both starting materials made it possible for a significant level of extended product to be formed so that they could be detected by MALDI-TOF (Figure 4.19).

Indeed, the spectra from the MALDI-TOF analysis showed that in this reaction mix, there were compounds with masses of 539 and 702, which corresponding to GHIL extended by 2 or 3 sugars. These data demonstrate that HPA is able to extend GHIL by several glucose units, most likely *via* transglycosylation. The fact that, even under these conditions, the predominant product is maltotriose and maltotetraose ( $2 \times \text{G3F} \rightarrow \text{G6F} \rightarrow \text{G2F} + \text{G4}$ ) confirms the previously suggested notion that under the conditions of the previous kinetic experiments, the extended GHIL make up a very small percentage of the product. In turn, this implies that the actual  $K_i$  value of the inhibitory species is significantly lower than than the  $K_i$  value determined from this study (possibly by several orders of magnitude).

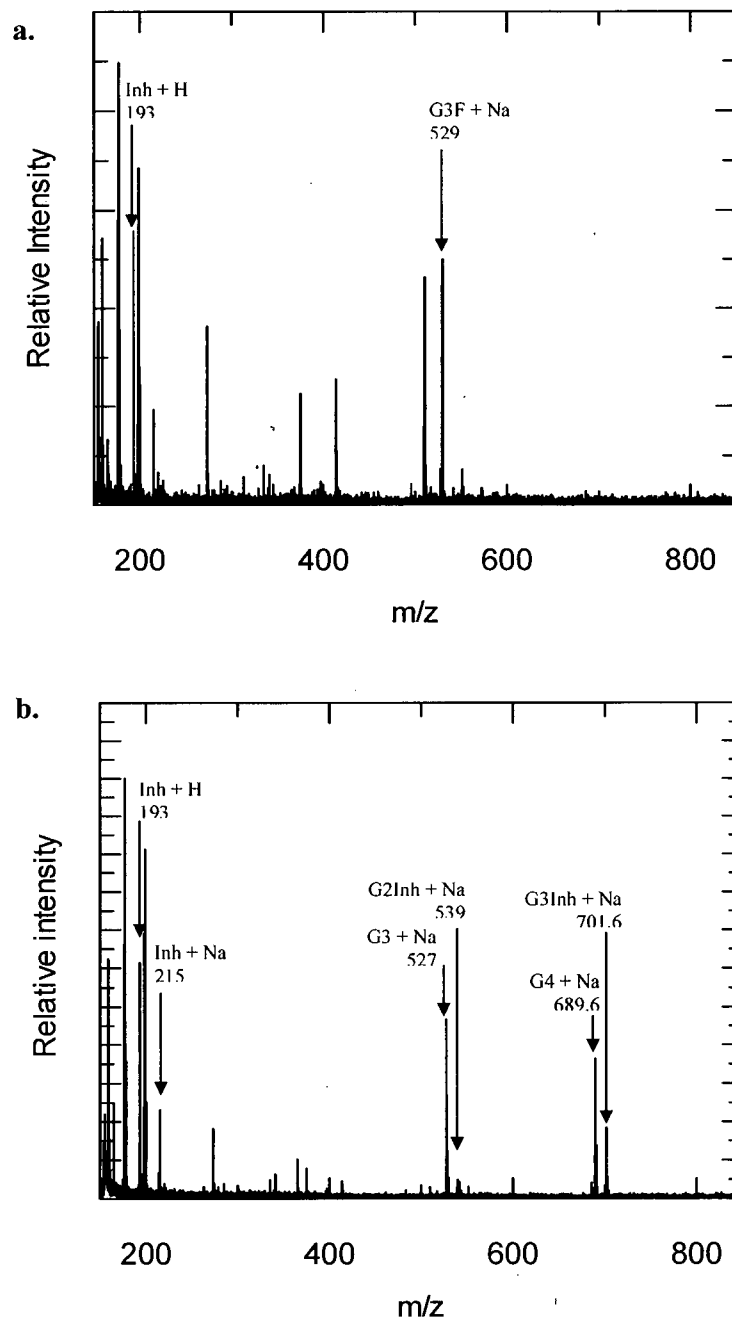


Figure 4.19 MALDI-TOF spectra for the reaction of G3F and GHIL (a) prior to addition of enzyme, and (b) after 1 hour of incubating with the enzyme. Inh = GHIL; InhGX = GHIL extended by X glucose moieties; GX = glucose polymer of X monomeric units; Na = sodium ion; and H = proton.

#### 4.4.7 Conclusions and future directions

This study has demonstrated that rapid screening using  $\alpha$ DNP-G3 can identify potential HPA inhibitors. By pre-incubating the inhibitor with G3F and HPA, a secondary screen can also be set up in parallel to determine the possibility that an inhibitor can be extended *in situ* to create a better inhibitor of HPA. The two assays were validated using acarbose as the model inhibitor of  $\alpha$ -amylase. When these screens were used to test a small library of monosaccharide inhibitors, the GHIL was found to be of potential interest.

Further analysis of GHIL showed that, although this compound only has a  $K_i$  value of 11 mM, by pre-incubating it with G3F and HPA, it becomes a significantly more potent inhibitor of HPA with a  $K_i \ll 260 \mu\text{M}$ . The modification that occurs is most likely the extension of the inhibitor at the non-reducing end by several glucose moieties. This is consistent with kinetic and structural analysis of acarbose, another inhibitor that is thought to be modified *in situ*. However, the evidence provided in this thesis is still circumstantial, as we have not demonstrated that the extended form of the GHIL is an actual inhibitor of HPA.

To conclusively demonstrate this, it is necessary to determine the true  $K_i$  value for the extended GHIL. To achieve this, firstly such a species must be made and isolated. There are two approaches that could be taken to accomplish this goal. As was shown in the present study, HPA will create detectable amounts of various extended forms of GHIL through transglycosylation. These species could be isolated by standard analytical methods such as HPLC, and then used for kinetic characterization to determine their  $K_i$  values. However, enzymatic synthesis of the enzyme's own inhibitor may be problematic

since the formation of the inhibitor would shut down the catalytic activity of the enzyme. Furthermore, from the analysis of the products using MALDI-TOF, the overall yield of this reaction would not be very high. The second approach, which is much more labour-intensive, is to chemically synthesize extended GHIL by coupling various malto-oligosaccharides to the GHIL (or a precursor). Although synthesis of each species would not be trivial, this approach would most likely have a higher overall yield and provide access to useful quantities of inhibitor.

## **Chapter 5 Experimental**

## 5.1 Synthesis

### 5.1.1 Synthesis of 5-fluoro- $\beta$ -L-gulosyl fluoride

The synthesis of 5FGulF was adopted from (72). All spectra for the compounds made during the synthesis of 5FGulF were compared with the assignments from this reference. However, each NMR spectra was also independently assigned.

**1,2,3,4,6-Penta-O-acetyl-D-mannopyranose (2.1).** Mannose (10 g, 55.5 mmol) was dissolved in pyridine (100 mL) and acetic anhydride (100 mL) was added in excess. The reaction mixture was left stirring overnight. The solvent was then evaporated off *in vacuo* and the remaining syrup was redissolved in EtOAc. This solution was washed with aqueous 1 M HCl, sat. NaHCO<sub>3</sub>, and brine, and then dried over MgSO<sub>4</sub>. The solvent was evaporated off *in vacuo* yield in **2.1** (18 g, 84%) as a brown syrup.

**2,3,4,6-Tetra-O-acetyl- $\alpha$ -D-mannosyl fluoride (2.2).** Compound **2.1** (13 g, 33.3 mmol) was transferred to a plastic vial and 25 mL of HF/pyridine was added at 0°C. The reaction mixture was left stirring overnight at 4°C and for a further 2 to 3 h at room temperature, then quenched by addition of sat. NaHCO<sub>3</sub> solution (excess). The product was extracted with EtOAc and the organic layer was washed with 1 M HCl, sat.

NaHCO<sub>3</sub>, and brine. After drying over MgSO<sub>4</sub>, the solvent was evaporated *in vacuo*.

Purification of the product was achieved by column chromatography (EtOAc/PetEt 1:1) to yield **2.2** (9.9 g, 85%) as a white solid. **<sup>1</sup>H NMR data** (CDCl<sub>3</sub>, 300 MHz):  $\delta$  5.55 (dd, 1 H,  $J_{1,2} = 1.8$  Hz,  $J_{1,F} = 48.5$ , H-1), 5.30-5.40 (m, 3 H, H-2, H-3, H-4), 4.28 (dd, 1 H,  $J_{5,6} = 5.4$ ,  $J_{6a,6b} = 12.8$ , H-6a), 4.10-4.20 (m, 2 H, H-5, H-6b), 2.15, 2.09, 2.04, 1.99 (4  $\times$  s, 4  $\times$  3 H, -OAc). **<sup>19</sup>F NMR data** (proton-decoupled, referenced to TFA):  $\delta$  -61.72.

**2,3,4,6-Tetra-O-acetyl-5-bromo- $\alpha$ -D-mannosyl fluoride (2.3).** Compound **2.2** (6.5 g, 18.6 mmol) was dissolved in 125 mL of dry  $\text{CCl}_4$  and *N*-bromosuccinimide (13 g, 73 mmol) added. The reaction mixture irradiated two 250 W tungsten lamps and left refluxing overnight. The  $\text{CCl}_4$  was evaporated under reduced pressure and the resulting solid was redissolved in  $\text{CH}_2\text{Cl}_2$ . This solution was washed with sat.  $\text{NaHCO}_3$ , 1 M HCl, water, and brine. The organic layer was then dried with  $\text{MgSO}_4$  and the solvent evaporated under reduced pressure. The product was purified by column chromatography (2%  $\text{CH}_3\text{CN}$  in  $\text{CH}_2\text{Cl}_2$ ) to yield **2.3** (2 g, 25% yield) as a clear oil.  **$^1\text{H}$  NMR data** ( $\text{CDCl}_3$ , 300 MHz):  $\delta$  5.68 (dd, 1 H,  $J_{2,3} = 2.3$  Hz,  $J_{3,4} = 10.7$ , H-3), 5.66 (dd, 1 H,  $J_{1,2} = 1.5$ ,  $J_{1,F} = 48.4$ , H-1), 5.47 – 5.56 (m, 2 H, H-2, H-4), 4.40 (s, 2 H, H-6a, H-6b), 2.16 (s, 3 H, -OAc), 2.09 (s, 6 H,  $2 \times$  -OAc), 2.00 (s, 3 H, -OAc).  **$^{19}\text{F}$  NMR data** (referenced to TFA):  $\delta$  -58.73 (d,  $J_{1,F} = 48.3$  Hz). **MS data** (ES): Calculated for  $\text{C}_{14}\text{H}_{18}\text{BrFO}_9$  451 ( $\text{M} + \text{Na}^+$ ), found 451.1.

**2,3,4,6-Tetra-O-acetyl-5-fluoro- $\beta$ -L-gulosyl fluoride (2.4).** Compound **2.3** (1.5 g, 3.49 mmol) was dissolved in 20 mL of dry  $\text{CH}_3\text{CN}$ . To this solution, AgF (0.9 g, 7.1 mmol) was added and the suspension was stirred in the dark for 24 h. The mixture was filtered through a celite/silica column and the filtrate was dried under reduced pressure. The solid was redissolved in EtOAc and this was washed with 1 M HCl and brine. The organic phase was dried using  $\text{MgSO}_4$  and the solvent evaporated under reduced pressure. Column chromatography (1:2 EtOAc/Pet Et) yielded **2.4** (0.5 g, 30%) as a clear oil.  **$^1\text{H}$  NMR data** ( $\text{CDCl}_3$ , 400 MHz):  $\delta$  5.83 (dd, 1 H,  $J_{1,2} = 7.3$  Hz,  $J_{1,F1} = 53.3$ , H-1), 5.36 (dd, 1 H,  $J_{3,4} = 7.6$ ,  $J_{2,3} = 3.7$ , H-3), 5.30 (m, 1 H, H-4), 5.20 (ddd, 1 H,  $J_{2,F1} = 10.7$ , H-2), 4.47 (dd, 1 H,  $J_{6a,6b} = 12.5$ ,  $J_{6a,F5} = 23.8$ , H6a), 4.13 (dd, 1 H,  $J_{6b,F5} = 13.7$ , H-6b), 2.12, 2.11,

2.08, 2.06 (s  $\times$  4, 3 H  $\times$  4, -OAc).  **$^{19}\text{F}$  NMR data** (proton decoupled, referenced to TFA):  $\delta$  -42.08 (F-5), -75.22 (F-1). **MS data** (ES): Calculated for  $\text{C}_{14}\text{H}_{18}\text{F}_2\text{O}_9$  391.1 (M +  $\text{Na}^+$ ), found 391.3.

**5-Fluoro- $\beta$ -L-gulosyl fluoride (2.5).** Compound **2.4** (93 mg, 0.25 mmol) was dissolved in 2 mL dry MeOH under  $\text{N}_2$  and  $\text{NH}_3$  gas was bubbled into the solution for 10 minutes at  $0^\circ\text{C}$ . The solution was warmed to room temperature and then reaction was left stirring for 2 h. The solvent was removed under reduced pressure and the product purified by column chromatography (EtOAc/MeOH/ $\text{H}_2\text{O}$  27:2:1) to yield **2.5** (15 mg, 30%) as a clear oil.  **$^1\text{H}$  NMR data** ( $\text{CDCl}_3$ , 300 MHz):  $\delta$  5.61 (dd, 1 H,  $J_{1,2} = 6.7$  Hz,  $J_{1,\text{F}1} = 54.8$ , H-1), 3.95-4.03 (m, 2 H, H-3, H-4), 3.75-3.93 (m, 2 H, H-2, H-6), 3.59 (dd, 1 H,  $J_{6,6b} = 12.3$ ,  $J_{6b,\text{F}5} = 17.8$ , H-6b).  **$^{19}\text{F}$  NMR data** (referenced to TFA):  $\delta$  -45.99 (m, F-5), -74.84 (dd,  $J_{\text{F}1,\text{F}2} = 8.5$ , F-1). **MS data** (ES): Calculated for  $\text{C}_6\text{H}_{10}\text{F}_2\text{O}_5$  200.1 (M +  $\text{Na}^+$ ), found .

### 5.1.2 Synthesis of 2-deoxy-2-fluoro- $\alpha$ -D-mannosyl fluoride

The synthesis of 2FManF was adopted from (102). All spectra for the compounds made during the synthesis of 2FManF were compared with the assignments from this reference. However, each NMR spectra was also independently assigned.

**3,4,6-Tri-O-acetyl-2-deoxy-2-fluoro- $\alpha$ -D-mannosyl fluoride (2.7).** Tri-O-acetyl-2-deoxy-2-fluoro- $\beta$ -D-mannosyl fluoride (**2.6**) was synthesized by Dr. David L. Zechel. This compound (315 mg, 1 mmol) was dissolved in 4 mL HF/pyridine at  $-78^\circ\text{C}$  and brought to room temperature. The reaction was stirring overnight. The reaction was quenched with sat.  $\text{NaHCO}_3$ , and extracted with  $\text{CH}_2\text{Cl}_2$ . The organic layer was washed with  $\text{H}_2\text{O}$ , 1 M HCl and brine. The solvent was removed under reduced pressure and the product was purified by column chromatography (4:1 PetEt/EtOAc) to yield **2.6** (100 mg,

33%) as a white solid. **<sup>1</sup>H NMR data** (CDCl<sub>3</sub>, 300 MHz): δ 5.72 (dddd, 1 H, J<sub>1,2</sub> = 2.3 Hz, J<sub>1,F1</sub> = 48.3, J<sub>1,F2</sub> = 2.3, H-1), 5.40 (dd, 1 H, H-4), 5.24 (dddd, 1 H, J<sub>2,3</sub> = 2.3, J<sub>3,4</sub> = 10.3, J<sub>3,F1</sub> = 2.3, J<sub>3,F2</sub> = 27.6, H-3), 4.88 (ddd, 1 H, J<sub>2,F2</sub> = 48.8, H-2), 4.27 (dd, 1 H, J<sub>5,6a</sub> = 4.7, J<sub>6a,6b</sub> = 12.7, H-6a), 4.07-4.21 (m, 2 H, H-6b, H-5), 2.10, 2.09, 2.04 (s × 3, 3 H × 3, -OAc). **<sup>19</sup>F NMR data** (referenced to TFA): δ -66.95 (dd, F-1), -130.73 (ddd, F-2). **MS data** (ES): Calculated for C<sub>12</sub>H<sub>16</sub>F<sub>2</sub>O<sub>7</sub> 333.1 (M + Na<sup>+</sup>), found 332.9.

**2-Deoxy-2-fluoro-α-D-mannosyl fluoride (2.7).** Compound **2.6** (50 mg, 0.16 mmol) was dissolved in 5 mL dry MeOH under N<sub>2</sub> and NH<sub>3</sub> gas was bubbled into the solution for 10 minutes at 0°C. The temperature was brought back up to room temperature and the reaction was left stirring for overnight. The solvent was removed *in vacuo* and the product purified by column chromatography (EtOAc/MeOH/H<sub>2</sub>O 27:2:1) to yield **2.7** (22.9 mg, 77%) as a white solid. **<sup>1</sup>H NMR data** (CDCl<sub>3</sub>, 300 MHz): δ 5.67 (ddd, 1 H, H-1), 4.68 (ddd, 1 H, H-2), 3.58-3.83 (m, 5 H, H-3, H-4, H-5, H-6a, H-6b). **<sup>19</sup>F NMR data** (referenced to TFA): δ -67.34 (dd, F-1), -133.03 (ddd, F-2). **MS data** (ES): Calculated for C<sub>6</sub>H<sub>10</sub>F<sub>2</sub>O<sub>4</sub> 207.0 (M + Na<sup>+</sup>), found 207.3.

### 5.1.3 Synthesis of 2,4-dinitrophenyl α-D-mannoside

**2,4-Dinitrophenyl 2,3,4,6-tetra-O-acetyl-α-D-mannoside (2.8).** Compound **2.1** (5 g, 13 mmol) was dissolved in 25 mL of dry CH<sub>2</sub>Cl<sub>2</sub> and 25 mL of HBr/AcOH was added at 0°C. The mixture was warmed to room temperature and left standing for 2 h. The solution was quenched by adding the reaction mixture to an excess of saturated solution of NaHCO<sub>3</sub>. The product was extracted from the aqueous layer with CH<sub>2</sub>Cl<sub>2</sub> and the organic layer was washed repeatedly with sat. NaHCO<sub>3</sub> followed by brine. The organic layer was dried over MgSO<sub>4</sub> and the solvent removed *in vacuo*. The product was

dissolved in dry  $\text{CH}_2\text{Cl}_2$  (50 mL) and dried over 4 Å molecular sieves for 1 h. Separately,  $\text{Ag}_2\text{CO}_3$  (5 g, 18 mmol), 2,4-dinitrophenol (5 g, 27 mmol), and  $\text{I}_2$  (several crystals) were suspended in dry  $\text{CH}_2\text{Cl}_2$  (50 mL) and dried with 4 Å molecular sieves. The dried solution of **2.8** was added to the reaction mixture and left stirring overnight. The reaction was filtered through a short celite/silica column and the filtrate was washed with 1 M NaOH, sat.  $\text{NaHCO}_3$  and brine. The solvent was removed under reduced pressure to yield a yellow foam. After work-up, the protected product was recrystallized from EtOH to yield white needles (2 g, 30%).  **$^1\text{H}$  NMR data** ( $\text{CDCl}_3$ , 300 MHz):  $\delta$  8.80 (d, 1 H, -Ar), 8.42 (dd, 1 H, -Ar), 7.48 (dd, 1 H, -Ar), 5.79 (d, 1 H,  $J_{1,2} = 1.9$  Hz, H-1), 5.51 (dd, 1 H,  $J_{2,3} = 3.4$ ,  $J_{3,4} = 9.9$ , H-3), 5.47 (dd, 1 H, H-2), 5.40 (dd, 1 H,  $J_{4,5} = 9.8$ , H-4), 4.20-4.30 (m, 1 H, H-6a), 4.02-4.11 (m, 2 H, H-5, H-6b), 2.20, 2.05 (s  $\times$  2, 3 H  $\times$  2, -OAc  $\times$  2), 2.02 (s, 3 H  $\times$  2, -OAc  $\times$  2). **MS data** (ES): Calculated for  $\text{C}_{12}\text{H}_{14}\text{N}_2\text{O}_{10}$  537.1 (M +  $\text{Na}^+$ ), found 537.3.

**2,4-Dinitrophenyl  $\alpha$ -D-mannoside (2.10).** Compound **2.9** (0.85 g, 1.6 mmol) was dissolved in dry MeOH (10 mL) and cooled to 0°C. While stirring, AcCl was added slowly to a final concentration of 5% (v/v). The reaction was left overnight at 0°C. After completion, the solvent was removed under *in vacuo* and the HCl azeotroped off with  $\text{Et}_2\text{O}$ . The product was purified using column chromatography (EtOAc/MeOH/AcOH 27:2:1) to yield **2.9** (250 mg, 45%) as a yellow powder.  **$^1\text{H}$  NMR data** ( $\text{CDCl}_3$ , 300 MHz):  $\delta$  8.78 (d, 1 H, -Ar), 8.49 (dd, 1 H, -Ar), 7.78 (dd, 1 H, -Ar), 5.87 (d, 1 H,  $J_{1,2} = 1.6$  Hz, H-1), 4.08 (dd, 1 H,  $J_{2,3} = 3.3$ , H-2), 3.92 (dd, 1 H,  $J_{3,4} = 9.5$ , H-3), 3.66-3.85 (m, 3 H, H-4, H-6a, H-6b), 3.56 (m, 1 H, H-5). **MS data** (ES): Calculated for  $\text{C}_{12}\text{H}_{14}\text{N}_2\text{O}_{10}$  369.1 (M +  $\text{Na}^+$ ), found 369.1.

#### 5.1.4 Synthesis of 2,4-dinitrophenyl $\alpha$ -maltoside

Conditions for the synthesis of peracetylated  $\alpha$ DNP-G2 was adopted from (163).

**1,2,2',3,3',4',6,6'-Octa-O-acetyl- $\beta$ -maltose (4.9).** Maltose (20.1 g, 58.7 mmol) was dissolve in pyridine (75 mL), and acetic anhydride (75 mL) was added. The solution was stirred overnight. The solvent was removed *in vacuo* and the product redissolved in EtOAc and then extensively washed with sat. NaHCO<sub>3</sub>, 1 M HCl solution and brine. The solvent was evaporated under reduced pressure to yield a white foam. The  $\beta$ -anomer was recrystallized from hot EtOH to yield **4.9** as white needles (32.11 g, 81%). **<sup>1</sup>H NMR data** (CDCl<sub>3</sub>, 300 MHz):  $\delta$  5.71 (d, 1 H,  $J_{1,2} = 8.1$  Hz, H-1), 5.37 (d, 1 H,  $J_{1',2'} = 4.2$ , H-1'), 5.32 (dd, 1 H, H-3'), 5.26 (dd, 1 H, H-3), 5.02 (dd, 1 H, H-4), 4.94 (dd, 1 H,  $J_{2,3} = 9.1$ , H-2), 4.82 (dd, 1 H,  $J_{2',3'} = 10.5$ , H-2'), 4.42 (dd, 1 H,  $J_{5,6a} = 2.3$ ,  $J_{6a,6b} = 12.3$ , H-6a), 4.15-4.24 (m, 2 H, H-6b, H-6a'), 3.95-4.05 (m, 2 H, H-6b', H-4), 3.90 (ddd, 1 H,  $J_{4',5'} = 10.0$ ,  $J_{5',6a'} = 2.3$ ,  $J_{5',6b'} = 3.6$ , H-5'), 3.80 (ddd, 1 H,  $J_{4,5} = 9.6$ ,  $J_{5,6b} = 4.2$ , H-5), 2.01 (s, 3 H, -OAc), 2.06 (s  $\times$  2, 6 H, -OAc  $\times$  2), 2.01, 1.99, 1.98, 1.97 (s  $\times$  4, 3H  $\times$  4, -OAc  $\times$  4). **MS data** (ES): Calculated for C<sub>28</sub>H<sub>38</sub>O<sub>19</sub> 701.2 (M + Na<sup>+</sup>), found 701.3.

**2,2',3,3',4',6,6'-Hepta-O-acetyl-maltose (4.10).** Compound **4.9** (5 g, 7.4 mmol) was dissolved in 40 mL of DMF and treated with hydrazine acetate (1 g, 1.5 eq) at 50°C. The reaction mixture was warmed to room temperature and left stirring for 2 h. The DMF was then removed *in vacuo* and the remaining syrup redissolved in CHCl<sub>3</sub>. The solution was washed twice with sat. NaHCO<sub>3</sub> and once with brine, and then dried over MgSO<sub>4</sub>. The solvent was removed *in vacuo* to yield **4.10** as a white foam. This product was used without further purification. **MS data** (ES): Calculated for C<sub>26</sub>H<sub>36</sub>O<sub>18</sub> 659.2 (M + Na<sup>+</sup>), found 659.3.

**2,4-Dinitrophenyl 2,2',3,3',4',6,6'-hepta-O-acetyl- $\beta$ -maltoside (4.11).** Compound **4.10** was dissolved in 50 mL of dry DMF. To this solution, 2,4-dinitrofluorobenzene (DNFB; 1.37 g, 7.4 mmol) and diazabicyclo[2.2.2]octane (DABCO; 0.83 g, 7.4 mmol) was added and the reaction was left stirring in the dark for overnight. The DMF was then removed *in vacuo* and the remaining syrup was dissolved in CHCl<sub>3</sub>. The solution was washed with sat. NaHCO<sub>3</sub> and brine, and then dried over MgSO<sub>4</sub>. The solvent was removed *in vacuo* and the crude product was purified by column chromatography (PetEt/EtOAc 2:1) to yield **4.11** (4.9 g, 83% over 2 steps) as a yellowish foam. **<sup>1</sup>H NMR data** (CDCl<sub>3</sub>, 300 MHz):  $\delta$  8.69 (d, 1H, -Ar), 8.44 (dd, 1H, -Ar), 7.41 (dd, 1 H, -Ar), 5.43 (d, 1 H, J<sub>1',2'</sub> = 4.2 Hz, H-1'), 5.36 (dd, 1 H, J<sub>2',3'</sub> = 10.4, J<sub>3',4'</sub> = 9.6, H-3'), 5.36 (d, 1 H, J<sub>1,2</sub> = 6.6, H-1), 5.27 (dd, 1 H, H-3), 5.13 (dd, 1 H, J<sub>2,3</sub> = 7.7, H-2), 5.05 (dd, 1 H, H-4'), 4.85 (dd, 1 H, J<sub>2',3'</sub> = 10.4, H-2'), 4.55 (dd, 1 H, J<sub>5',6a'</sub> = 3.1, J<sub>6a',6b'</sub> = 12.7, H-6a'), 4.16-4.28 (m, H-6b', H-6a), 4.01-4.16 (m, H-4, H-5), 3.91-4.05 (m, H-6b, H-5'), 1.98, 2.00, 2.01, 2.03, 2.05, 2.06, 2.08, 2.10 (s  $\times$  7, 3H  $\times$  7, -OAc  $\times$  7). **MS data** (ES): Calculated for C<sub>26</sub>H<sub>38</sub>N<sub>2</sub>O<sub>22</sub> 825.5 (M + Na<sup>+</sup>), found 825.3.

**2,4-Dinitrophenyl 2,2',3,3',4',6,6'-hepta-O-acetyl- $\alpha$ -maltoside (4.12).** Compound **4.11** (4.9 g, 6.1 mmol) was dissolved in 15 mL of DMF, treated with K<sub>2</sub>CO<sub>3</sub> (2.3 g, 16.6 mmol) and left stirring overnight in the dark. The DMF was then removed *in vacuo* and the resulting syrup was redissolved in CHCl<sub>3</sub>. The solution was washed with sat. NaHCO<sub>3</sub> and brine, and then dried over MgSO<sub>4</sub>. The solvent was removed *in vacuo* to yield a yellow foam. The solid was recrystallized from EtOAc/PetEt to yield **4.12** (1.8 g, 37%) as the pure  $\alpha$ -anomer. **<sup>1</sup>H NMR data** (CDCl<sub>3</sub>, 300 MHz):  $\delta$  8.75 (d, 1 H, -Ar), 8.42 (dd, 1 H, -Ar), 7.48 (dd, 1 H, -Ar), 5.86 (d, 1 H, J<sub>1,2</sub> = 3.9 Hz, H-1), 5.69 (dd, 1 H, J<sub>2,3</sub> =

10.0,  $J_{3,4} = 8.5$ , H-3), 5.44 (d, 1 H,  $J_{1,2'} = 4.2$ , H-1'), 5.33 (dd, 1 H,  $J_{2',3'} = 10.4$ ,  $J_{3',4'} = 9.6$ , H-3'), 5.04 (dd, 1 H, H-4'), 4.92 (dd, 1 H, H-2), 4.85 (dd, 1 H, H-2'), 4.45 (dd, 1 H,  $J_{5,6a} = 1.5$ ,  $J_{6a,6b} = 2.7$ , H-6a), 4.16-4.28 (m, 2 H, H-6b, H-6a'), 4.00-4.15 (m, 3 H, H-5, H-6b', H-4), 3.93 (ddd, 1 H,  $J_{4',5'} = 10.4$ ,  $J_{5',6a'} = 3.5$ ,  $J_{5',6b'} = 2.3$ , H-5'), 2.10, 2.09 (s  $\times$  2, 3 H  $\times$  2, -OAc  $\times$  2), 2.08 (s, 6 H, -OAc  $\times$  2), 2.05, 2.04, 2.00, 1.98 (s  $\times$  4, 3H  $\times$  4, -OAc  $\times$  4).

**MS data** (ES): Calculated for  $C_{26}H_{38}N_2O_{22}$  825.5 (M + Na<sup>+</sup>), found 825.3.

**2,4-Dinitrophenyl  $\alpha$ -maltoside (4.13).** Compound **4.12** (0.84 g, 1.0 mmol) was dissolved in 10 mL of MeOH, cooled to 0°C. AcCl (0.5 mL, 5% v/v) was slowly added and the reaction was left stirring for 2 days at 4°C. The solvent was removed under reduced pressure and the solid was purified by column chromatography (EtOAc/MeOH/AcOH 17:2:1). Most of the AcOH was removed by azeotroping with hexane. The remaining solid was precipitated from MeOH/Et<sub>2</sub>O to yield **4.13** (100 mg, 20%) as a yellow powder. **Selected <sup>1</sup>H NMR data** (MeOH, 300 MHz):  $\delta$  8.75 (d, 1 H, -Ar), 8.46 (dd, 1 H, -Ar), 7.68 (dd, 1 H, -Ar), 5.92 (d, 1 H,  $J_{1,2} = 3.5$  Hz, H-1), 5.17 (d, 1 H,  $J_{1',2'} = 3.7$ , H-1'). **MS data** (ES): Calculated for  $C_{18}H_{24}N_2O_{15}$  531.4 (M + Na<sup>+</sup>), found 531.3.

### 5.1.5 Synthesis of 2,4-dinitrophenyl $\alpha$ -maltotrioside

Conditions for the synthesis of peracetylated  $\alpha$ DNP-G3 was adopted from (163).

**1,2,2',2'',3,3',3'',4'',6,6',6''-Undeca-O-acetyl-maltotriose (4.14).** Maltotriose (8 g, 15.9 mmol) was dissolved in 75 mL of pyridine and acetic anhydride (75 mL) and the solution was stirred overnight. The solvent was removed *in vacuo*, the product redissolved in EtOAc, and the solution washed extensively with sat. NaHCO<sub>3</sub>, 1 M HCl solution, and

brine. The solvent was removed under reduced pressure to yield a **4.14** (15.3 g, 99.8%) as white foam. **MS data (ES)**: Calculated for  $C_{40}H_{54}O_{27}$  989.3 ( $M + Na^+$ ), found 989.5.

**2,2',2'',3,3',3'',4'',6,6',6''-Deca-O-acetyl-maltotriose (4.15)**. Compound **4.14** (6 g, 6.2 mmol) was dissolved in 50 mL of dry DMF and treated with hydrazine acetate (0.64 g, 1.1 eq) at 50°C. The reaction mixture was warmed to room temperature and left stirring for 2 h. The DMF was then removed *in vacuo* and the remaining syrup redissolved in  $CHCl_3$ . The solution was washed twice with sat.  $NaHCO_3$  and once with brine and dried over  $MgSO_4$ . The crude product was purified by column chromatography (Pet Et/EtOAc 3:1) to yield **4.15** as a white foam. **MS data (ES)**: Calculated for  $C_{38}H_{52}O_{26}$  947.8 ( $M + Na^+$ ), found 947.5.

**2,4-Dinitrophenyl 2,2',2'',3,3',3'',4'',6,6',6''-deca-O-acetyl- $\beta$ -maltotrioside (4.16)**.

Compound **4.15** (3.0 g, 3.2 mmol) was dissolved in 40 mL of dry DMF and to this solution, DNFB (0.67 g, 1.1 eq) and DABCO (0.37 g, 1 eq) were added, followed by stirring overnight in the dark. The DMF was then removed *in vacuo* and the remaining syrup was dissolved in  $CHCl_3$ . The solution was washed with sat.  $NaHCO_3$  and brine, and then dried over  $MgSO_4$ . The solvent was removed under reduced pressure and the crude product was purified by column chromatography (PetEt/EtOAc 2:1) to yield **4.16** (3.1 g, 88% over two steps) as a yellowish foam.  **$^1H$  NMR data** ( $CDCl_3$ , 400 MHz):  $\delta$  8.67 (d, 1 H, -Ar), 8.42 (dd, 1 H, -Ar), 7.46 (dd, 1 H, -Ar), 5.24-5.40 (m, 6 H, H-1, H-1', H-1'', H-3, H-3', H-3''), 5.10 (dd, 1 H,  $J_{1,2} = 6.5$  Hz,  $J_{2,3} = 7.7$ , H-2), 5.04 (dd, 1 H,  $J_{3'',4''} = 9.9$ ,  $J_{4'',5''} = 9.9$ , H-4''), 4.82 (dd, 1 H,  $J_{1'',2''} = 4.1$ ,  $J_{2'',3''} = 10.5$ , H-2''), 4.71 (dd, 1 H,  $J_{1',2'} = 4.0$ ,  $J_{2',3'} = 10.3$ , H-2'), 4.53 (dd, 1 H,  $J_{5,6} = 3.0$ ,  $J_{6a,6b} = 12.2$ , H-6a), 4.43 (dd, 1 H,  $J_{5,6b} = 4.5$ , H-6b), 4.21 (dd, 1 H,  $J_{5'',6a''} = 3.6$ ,  $J_{6a'',6b''} = 12.5$ , H-6a''), 4.17 (dd, 1 H,  $J_{5',6'} = 3.3$ ,

$J_{6a',6b'} = 12.4$ , H-6b'), 4.10 (dd, 1 H, H-4), 3.88-4.05 (m, 5 H, H-4', H-5, H-5', H-5'', H-6b''), 2.12, 2.08, 2.06, 2.05, 2.03, 2.02 (s  $\times$  6, 3H  $\times$  6, -OAc  $\times$  6), 1.99 (s, 6H, -OAc  $\times$  2), 1.97 (s, 6  $\times$  2, -OAc  $\times$  2). **MS data** (ES): Calculated for  $C_{44}H_{54}N_2O_{30}$  1113.9 (M + Na<sup>+</sup>), found 1113.4.

**2,4-Dinitrophenyl 2,2',2'',3,3',3'',4'',6,6',6''-deca-O-acetyl- $\alpha$ -maltotrioside (4.17).**

Compound **4.16** (2.2 g, 2.0 mmol) was dissolved in 7 mL of dry DMF, treated with  $K_2CO_3$  (0.7 g, 5.1 mmol) and the reaction mixture left stirring overnight. The DMF was then removed *in vacuo* and the resulting syrup was dissolved in  $CHCl_3$ . The solution was washed with sat.  $NaHCO_3$  and brine, and then dried over  $MgSO_4$ . The solvent was removed *in vacuo* to yield a yellow foam. The solid was purified by column chromatography (EtOAc/PetEt 1:3) to yield **4.17** (1.2 g, 54%). **<sup>1</sup>H NMR data** ( $CDCl_3$ , 400 MHz):  $\delta$  8.75 (d, 1 H, -Ar), 8.43 (dd, 1 H, -Ar), 7.53 (dd, 1 H, -Ar), 5.84 (d, 1 H,  $J_{1,2} = 3.7$  Hz, H-1), 5.66 (dd, 1 H,  $J_{2,3} = 9.8$ ,  $J_{3,4} = 8.6$ , H-3), 5.27-5.39 (m, 4 H, H-1', H-1'', H-3', H-3''), 5.04 (dd, 1 H, H-4''), 4.92 (dd, 1 H, H-2), 4.83 (dd, 1 H,  $J_{1'',2''} = 4.0$ ,  $J_{2'',3''} = 10.5$ , H-2''), 4.74 (dd, 1 H,  $J_{1',2'} = 4.1$ ,  $J_{2',3'} = 9.9$ , H-2'), 4.41-4.51 (m, 2 H, H-6a, H-6a'), 4.29 (dd, 1 H,  $J_{5,6} = 4.0$ ,  $J_{6a,6b} = 12.5$ , H-6b), 4.22 (dd, 1 H,  $J_{5',6'} = 3.5$ ,  $J_{6a',6b'} = 12.5$ , H-6b'), 4.10-4.19 (m, 2 H, H-6a'', H-5'), 4.00-4.08 (m, 2 H, H-4, H-6''), 3.87-3.98 (m, 3 H, H-4', H-5, H-5''), 2.14 (s, 6H, -OAc  $\times$  2), 2.08 (s, 3 H, -OAc), 2.05 (s  $\times$  2, 3 H  $\times$  2, -OAc  $\times$  2), 2.03, 2.02, 2.00, 1.99, 1.97 (s  $\times$  5, 3 H  $\times$  5, -OAc  $\times$  2). **MS data** (ES): Calculated for  $C_{44}H_{54}N_2O_{30}$  1113.9 (M + Na<sup>+</sup>), found 1113.4.

**2,4-Dinitrophenyl  $\alpha$ -maltotrioside (4.18).** Compound **4.17** (120 mg, 0.11 mmol) was dissolved in 10 mL of dry MeOH. This solution was cooled to 0°C and AcCl (0.5 mL, 5% v/v) was added slowly while stirring and the reaction mixture left stirring for 2 days

at 4°C. The solvent was evaporated under reduced pressure and the solid was purified by column chromatography (EtOAc/MeOH/AcOH 7:2:1). Most of the AcOH was removed by azeotrope with hexane. The product was precipitated from MeOH/Et<sub>2</sub>O to yield **4.18** (20 mg, 27%) as a yellow powder. **Selected <sup>1</sup>H NMR data** (MeOH, 300 MHz): δ 8.77 (d, 1 H, -Ar), 8.48 (dd, 1 H, -Ar), 7.71 (dd, 1 H, -Ar), 5.95 (d, 1 H, J<sub>1,2</sub> = 3.5 Hz, H-1), 5.19, 5.16 (d × 2, 1 H × 2, H-1', H-1''). **MS data** (ES): Calculated for C<sub>24</sub>H<sub>34</sub>N<sub>2</sub>O<sub>20</sub> 693.5 (M + Na<sup>+</sup>), found 693.3.

## 5.2 Protein Chemistry

### 5.2.1 Site directed mutagenesis

Specific mutations were created in the human pancreatic  $\alpha$ -amylase (HPA) gene in the plasmid pPIC9-AMY (123) by using the QuikChange site-directed mutagenesis kit (Stratagene). In this method, a complementary pair of oligodeoxyribonucleotides containing the desired mutation (see table) was used as primers in a primer extension of the entire plasmid. All primers were chemically synthesized at the Nucleic Acid and Protein Services (NAPS) Unit at the University of British Columbia (Vancouver, Canada). The extension reaction mixture contained the pair of primers (125 ng), the vector (10 ng), each of the four deoxynucleotides (100  $\mu$ mol), and *Pfu* polymerase (2.5 units) in the supplied polymerase buffer (Stratagene). The reaction was repeated 13 times by cycling the temperature of the reaction mixture using a GeneAmp PCR system 2400 (Perkin-Elmer). In all of the PCR reactions performed, the temperature cycle was 95°C (10 seconds) – 55°C (5 seconds) – 67°C (15 minutes). The wild-type DNA was digested after the final extension reaction by addition of the restriction enzyme *DpnI* (New England Biolab).

After 1 hour of digestion, 5  $\mu$ L of reaction mixture was used to transform *Escherichia coli* (DH5 $\alpha$ ) (170). The transformed cells were plated on LB-plates containing ampicillin. Generally, each transformation resulted in 2-6 colonies. Each of the colonies was grown up in liquid LB culture and the plasmid was isolated. The isolated plasmids were then screened for the desired mutations by sequencing the region of interest, carried out by the NAPS Unit. Usually, 2-3 clones were sequenced per mutation reaction and in all cases,

the plasmid contained the desired mutation. The entire HPA gene was then sequenced for each of the mutated plasmids to confirm the fidelity of the extension reaction.

| Primer name | Primer sequence                                     | Mutant generated |
|-------------|---|------------------|
| R195A-S     | CATTGGTGTTCAGGGTTC <u>GCA</u> CTTGATGCTTCCAAGCAC    | R195A            |
| R195A-A     | GTGCTTGGAAGCATCAAGT <u>GCG</u> AACCCTGCAACACCAATG   |                  |
| R195Q-S     | CATTGGTGTTCAGGGTTC <u>CAA</u> CTTGATGCTTCCAAGCAC    | R195Q            |
| R195Q-A     | GTGCTTGGAAGCATCAAGT <u>TGG</u> AACCCTGCAACACCAATG   |                  |
| N298S-S     | CTCGTTGATTGTCATGG <u>CT</u> ATCCACAAAGACAA          | N298S            |
| N298S-A     | CTTGCTTTTGTGGAT <u>AGCC</u> ATGACAATCAAGGA          |                  |
| R337A-S     | CATCCTTACGGATTTACAG <u>CAG</u> TAATGTCAAGCTACCGTTGG | R337A            |
| R337A-A     | CCAACGGTAGCTTGACATT <u>ACTGCT</u> GTAATCCGTAAGGATC  |                  |
| R337Q-S     | CATCCTTACGGATTTACAC <u>AGG</u> TAATGTCAAGCTACCGTTGG | R337Q            |
| R337Q-A     | CCAACGGTAGCTTGACATT <u>ACTG</u> TGTAATCCGTAAGGATG   |                  |

Table 5.1 Oligonucleotides used for mutating the chloride ion-binding site in recombinant HPA.

The pPIC-AMY plasmid containing the mutation (linearized with the restriction enzyme *SacI*) was transformed into the *P. pastoris* strain GS115 by electroporation using the Invitrogen protocol (Invitrogen, 1995). The transformed cells were then plated on Yeast extract Peptone digest (YPD, 1% yeast extract (w/v), 2% peptone (w/v), 2% glucose (w/v)) plates and grown for two days. Colonies were streaked onto minimal dextrose (1.34% yeast nitrogen base (w/v),  $4 \times 10^{-5}$  % biotin (w/v), 2% dextrose (w/v)) plates and grown for another two days. Those cells were finally transferred again to YPD plates to be used in expression.

### **5.2.2 Growth and expression of recombinant HPA from Pichia Pastoris**

The conditions for growing *P. pastoris* and expressing recombinant HPA were those described in the *Pichia* Expression Kit (Invitrogen). Briefly, a colony was picked from a YPD plate and grown in a 5 mL culture overnight at 30°C in buffered glycerol-complex medium (BMGY, 1% peptone (w/v), 2% yeast extract (w/v), 100 mM potassium phosphate, pH 6.0, 1.34% yeast nitrogen base (w/v),  $4 \times 10^{-5}$  % biotin (w/v), 1 % glycerol (v/v)). This culture was used to inoculate 500 ml of BMGY, which was then grown at 30°C for a day in a baffled flask. The cells were harvested by centrifugation (5000 rpm, 10 minutes) and were resuspended in 100 ml of buffered methanol-complex medium (BMMY, 1% peptone (w/v), 2% yeast extract (w/v), 100 mM potassium phosphate, pH 6.0, 1.34% yeast nitrogen base (w/v),  $4 \times 10^{-5}$  % biotin (w/v), 0.5 % MeOH (v/v)). The culture was left to induce for 2 days at 30°C with the addition of 1 mL 50% MeOH every 12 hours. After 2 days, the cells were removed from the supernatant by centrifugation (7000 rpm, 10 minutes). The expression of HPA was checked by the appearance of a band at ~55 kDa on SDS-PAGE.

### **5.2.3 Purification of recombinant deglycosylated HPA**

The cells were removed from the supernatant by centrifugation at 8000 rpm for 20 minutes followed by filtration using a Gelman 0.45 µm filter. 5 M NaCl was added to this filtered supernatant to a final concentration of 0.4 M. The filtrate was then loaded on a phenyl-sepharose column (50 × 200 mm) that had been equilibrated with 100 mM sodium phosphate buffer, pH 7.4, containing 0.4 M NaCl. The column was washed with the same buffer followed by elution with water. The fractions were then pooled and concentrated by ultrafiltration using an Amicon centricon.

To the concentrated protein solution, endoglycosidase F-cellulose binding domain fusion protein was added and left at room temperature for 2 days. The endoglycosidase F-cellulose binding domain fusion protein was then removed by the addition of cellulose, which was then removed by centrifugation. The solution was then passed through a Q-sepharose column (10 × 20 mm) that had been equilibrated with water. The flow-through, which contains the HPA, was concentrated by ultrafiltration using an Amicon centricon.

The protein was checked for purity using SDS-PAGE and the activity was checked using the 3,5-dinitrosalicylic acid-assay (DNS-assay, (154)). The protein concentration was determined by taking an  $A_{280}$  using  $\epsilon = 2.6 \text{ mgcm}^{-1}\text{ml}^{-1}$ . The molecular weight was determined by ESI-MS.

#### **5.2.4 Circular dichroism spectroscopy**

All measurements of UV circular dichroism (CD) were carried out using a Jasco Model J-720 spectropolarimeter interfaced with a circulating water bath. Protein samples were buffer exchanged with 20 mM sodium phosphate buffer, pH 6.9 in the presence of 0 or 5 mM NaCl. Samples were then placed in a water-jacketed, cylindrical quartz cuvette (pathlength 0.1 cm). All spectra (190-250 nm) were collected using a scan rate of 20 nm/min, a spectral slit of 1 nm and a 16 second time constant. The background signal from the appropriate buffer was then subtracted from the spectra. Initial spectra were averages of 10 spectral scans and were collected at 25°C. For thermostability studies, the temperature was increased from 25 - 55°C at a rate of 50°C/hour. The CD spectrum of the protein (0.45 mgml<sup>-1</sup>) was measured at 25, 35, 40, 43, 45, 47, 49, 51, 53 and 55°C. In this case, a single scan was measured per temperature point and the background spectrum subtracted from each spectrum.

## 5.3 Enzymology

### 5.3.1 General methods for kinetic analysis

#### 5.3.1.1 UV-spectroscopy

Determination of the rate of hydrolysis of chromogenic substrates by an enzyme was performed by following the increase in the absorbance at 400 nm upon the addition of enzyme in the appropriate buffer. These measurements were made in 1 cm pathlength quartz cuvettes with a UNICAM UV4 UV/Vis spectrophotometer attached to a circulating water bath or a Varian CARY 4000 spectrophotometer attached to a temperature control unit. The rates were calculated by using the extinction coefficient of  $\Delta\epsilon = 8440 \text{ M}^{-1} \text{ cm}^{-1}$  (pH 4.5),  $\Delta\epsilon = 10600 \text{ M}^{-1} \text{ cm}^{-1}$  (pH 5.6), and  $\Delta\epsilon = 10900 \text{ M}^{-1} \text{ cm}^{-1}$  (pH 6.9).

#### 5.3.1.2 Fluoride electrode

Determination of the rate of hydrolysis of glycosyl fluorides was performed by following the increase in fluoride ion concentration upon the addition of enzyme in the appropriate buffer. These measurements were made using an ORION 96-04 combination fluoride electrode interfaced to a personal computer running the program LoggerPro (Vernier Software, Oregon).

#### 5.3.1.3 DNS-assay

Determination of the rate of hydrolysis of starch by an enzyme was performed by quantifying the increase in reducing ends after incubation of starch with a substrate (154). Briefly, enzyme was added to a solution of 1% starch (w/v) and incubated for an

appropriate length of time, depending on the activity of the enzyme. The enzyme reaction was stopped by addition of an equal volume of stop solution (4.4 mM 3,5-dinitrosalicylic acid, 1 M sodium potassium tartrate, 0.4 M NaOH). The increase in reducing sugar was determined by boiling this reaction mix for 6 minutes and measuring the absorption at 546 nm using a UNICAM UV/Vis spectrophotometer. Each point was done in duplicate and the average of the two values was reported.

### **5.3.2 Kinetic analysis of bovine kidney LAMAN**

#### **5.3.2.1 Steady state kinetics**

All studies on the bovine kidney LAMAN were carried out at 30°C in 100 mM sodium acetate buffer, pH 4.5 containing 0.1% BSA. Initial rates were measured using the UV-spectroscopy method (typically 3 nM final concentration of enzyme) at varying concentrations of DNP-Man (typically 6-8 points). The kinetic parameters were estimated by direct fit of the data to the Michaelis-Menten equation using the program GraFit 4.0.14 (171). A  $K_i$  value for 5FGulF was determined by measuring rates of hydrolysis of a range of DNP-Man concentrations (0.25 mM to 1.0 mM) at each of a series of 5FGulF concentrations (10  $\mu$ M to 200  $\mu$ M). The data were plotted in the form of a Dixon plot (1/rate vs. [inhibitor]). Linear regression of each line was done using the program GraFit. The  $K_i$  was determined from the intersection of these lines ( $K_i = -$ intersection).

### **5.3.3 Kinetic analysis of *Drosophila melanogaster* Golgi $\alpha$ -mannosidase II**

#### **5.3.3.1 Steady state kinetics**

All studies of the *Drosophila melanogaster* Golgi  $\alpha$ -mannosidase II (GMII) were carried out at 37°C in 50 mM MES buffer, pH 5.6, containing 0.1 mM ZnSO<sub>4</sub> and 0.1%

BSA unless otherwise specified. Determination of kinetic parameters for the hydrolysis of DNP-Man by wild-type and Asp341Asn mutant GMII was performed by using the UV-spectroscopy method (typically 3 nM and 30 nM final concentration of enzyme respectively) at varying substrate concentrations (typically 10-12 points). The kinetic parameters were estimated by direct fit of the data to the Michaelis-Menten equation using the program GraFit 4.0.14 (171). Approximate  $K_i$  values for both 5FGulF and 2FManF with the mutant enzyme were determined by measuring rates of hydrolysis of DNP-Man (0.1 mM) at varying inhibitor concentrations (4 points). The data were plotted in the form of a Dixon plot (1/rate vs. [inhibitor]) and then fit to a line using the program GraFit 4.0.14 (171). Assuming competitive inhibition, an approximate  $K_i$  value is the negative value (x-axis) of the intersection of this line with the line for  $y = 1/V_{max}$ .

Kinetic parameters for the hydrolysis of 5FGulF and 2FManF by wild-type GMII were determined by using the fluoride electrode assay (typically 10 nM and 20 nM enzyme final enzyme concentrations respectively) at varying “substrate” concentrations (typically 6-8 points). In the case of 5FGulF, because transglycosylation seemed to be taking place, only rates at lower concentrations (6 points) were fit to the Michaelis-Menten equation. In the case of 2FGulF, saturation was not seen and as such, the data were fit to a line using linear regression to determine the  $k_{cat}/K_m$ .

#### 5.3.3.2 *Inactivation studies*

The inactivation of Asp341Asn mutant GMII by 5FGulF was monitored by incubating the enzyme (1.2 mgml<sup>-1</sup>) under the above conditions in the presence of various concentrations of 5FGulF at 16°C. Residual activities were determined at various time intervals by taking 10 µL aliquots of the inactivation mixture and adding them to a

solution of DNP-Man (1.5 mM, 110  $\mu$ L) in the above buffer and measuring DNP release for 30 s at 16°C. Pseudo-first-order inactivation rate constants were determined by fitting the data for the residual activity versus time to a first-order rate equation using the program GraFit 4.0.14 (171). The  $k_i/K_I$  was determined by measuring the slope of the plot of  $k_{obs}$  against 5FGuIF concentrations. The inactivation of the wild-type GMII by 5FGuIF was observed in the same manner except the enzyme concentration was lower (0.22  $\text{mgml}^{-1}$ ) and the temperature of the experiment was reduced to 8°C.

#### **5.3.4 Kinetic analysis of the chloride binding site mutant HPA**

All kinetic analyses of HPA activities for the wild-type and mutant HPA during the chloride ion binding site study were carried out in 50 mM sodium phosphate buffer, pH 6.9 at 30°C. All buffers salts used contained less than 0.005% chloride. Chloride dependence of HPA activity was determined by measuring the HPA activity using the DNS-assay at varying chloride concentrations (0-100 mM). The data (chloride concentration vs. activity) were fit to a ligand-binding equation by non-linear regression using the program GraFit 4.0.14 (171).

The dependence of HPA activity on pH was determined by measuring the activities of the wild-type and mutant enzymes using the DNS-assay under the same conditions as above with the exception of the buffer. At a pH of 5.6, 6.0, 6.5, 7.1, 7.6, 8.1 and 8.4, sodium phosphate buffer was used while at pH 8.7, 9.6 and 10.2, sodium carbonate buffer was used. The plot of pH versus activity was fit to a double-ionization pH curve by non-linear regression using the program GraFit 4.0.14 (171). The  $K_m$  values for starch were determined at various pH values using the above method at a series of

starch concentrations (0.1%-1.58% (w/v)). The data were fit to the Michaelis-Menten equation by non-linear regression using the program GraFit 4.0.14 (171).

### ***5.3.5 Kinetic analysis of HPA using the novel substrates***

All studies were carried out at 30°C in 50 mM sodium phosphate buffer, pH 6.9 containing 100 mM NaCl. Determinations of kinetic parameters for the various substrates were performed by UV-spectroscopy (1.4  $\mu$ M, 0.5  $\mu$ M, 50 nM final enzyme concentration for DNP-Glc, DNP-G2, and DNP-G3 respectively) to a range of concentrations (10-12 points) of substrate. Typically, the rate was determined on the basis of the first 2 minutes of hydrolysis. The data (rate vs. substrate concentration) were fit to the Michaelis-Menten equation by non-linear regression using the program GraFit 4.0.14 (171). For the substrates used in this study, the background hydrolysis was negligible and was therefore not considered in calculating the rate of reaction.

### ***5.3.6 Kinetic analysis of inhibitors of HPA***

#### ***5.3.6.1 Rapid assay for determining inhibition potential***

All studies were carried out at 30°C in 50 mM sodium phosphate buffer, pH 6.9 containing 100 mM NaCl.

Assay#1 was performed by determining the rate of hydrolysis of  $\alpha$ DNP-G3 by HPA (final enzyme concentration at 10 nM) at a concentration of 0.4 mM in the presence of 1 mM inhibitor using UV-spectroscopy. This rate was compared to the rate of  $\alpha$ DNP-G3 hydrolysis in the absence of inhibitor. The difference of these two rates was reported as a percentage where the control rate has 100%.

Assay#2 was performed by pre-incubating 1 mM of inhibitor with 0.2 mM G3F and 10 nM HPA for 15 minutes at 30°C. To this mixture,  $\alpha$ DNP-G3 was added to a final

concentration of 0.4 mM and the HPA activity was assayed using UV-spectroscopy. This rate was compared to the value for the same assay performed in the absence of inhibitor. The difference was reported as a percentage where the control rate is 100%.

#### 5.3.6.2 Kinetic analysis of the GHIL as an inhibitor of HPA

An approximate  $K_i$  value for the GHIL was determined by measuring the rate of hydrolysis of  $\alpha$ DNP-G3 (1.8 mM) using UV-spectroscopy at varying inhibitor concentrations (4-5 points). The data were plotted in the form of a Dixon plot (1/rate vs. [inhibitor]) and then fit to a line using the program GraFit 4.0.14 (171). Once again, an approximate  $K_i$  value was determined from the intersection of this line with the line for  $y = 1/V_{\max}$  (where  $K_i = -\text{intersection}$ ).

An approximate  $K_i$  value for the extended GHIL was determined by using a similar set up to Assay #2 at various inhibitor concentrations. Briefly, inhibitor (4 points) was pre-incubated with 0.3 mM G3F and 10 nM HPA for 1 hour at 30°C. To this mixture,  $\alpha$ DNP-G3 was added to a final concentration of 0.7 mM and the HPA activity was assayed using UV-spectroscopy. The data were plotted in the form of a Dixon plot (1/rate vs. [inhibitor]) and then fit to a line using the program GraFit 4.0.14 (171). The kinetic parameters for HPA activity under these conditions were also determined by pre-incubating the G3F (0.3 mM) with HPA for 1 hour at 30°C. To this mixture  $\alpha$ DNP-G3 was added to various concentrations (6 points). The data were fit to the Michaelis-Menten equation by non-linear regression using the program GraFit 4.0.14 (171). The upper limit for the  $K_i$  of the extended GHIL was determined from the intersection of the Dixon plot with the line for  $y = 1/V_{\max}$  ( $K_i = -\text{intersection}$ ).

### **5.3.7 HPLC product analysis**

All product analyses were performed on a Waters 600 HPLC system equipped with a Waters 2487 UV detector and a Sedex 75 Evaporative Light Scattering detector. The protein was first removed from the sample using a 10 kDa molecular weight cutoff centrifugal device (Millipore) and the filtrate was diluted to 25% (v/v) with acetonitrile. Approximately 30  $\mu$ L of sample was loaded onto a Tosoh Amide-80 (4.6 mm  $\times$  25 cm) column. The products were then eluted at 0.7 mL/min with an acetonitrile/water (75:25 – 55:45) gradient for 10 minutes followed by acetonitrile/water (55:45) elution.

### **5.3.8 Mass spectrometric analysis**

#### *5.3.8.1 Analysis of the covalent intermediate formed on LAMAN*

Enzyme stock (25  $\mu$ L of 8 mg/ml in 100 mM sodium acetate, pH 4.5) was mixed with 1  $\mu$ L of 5FGulF (40 mM in water) and incubated for 3 minutes at room temperature. The sample was diluted with 60  $\mu$ L of pepsin solution (0.3 mg/mL in 200 mM sodium phosphate buffer, pH 2.0) and incubated for 60 minutes at room temperature. The sample was then frozen until ready for analysis and was used immediately upon thawing.

All MS analyses of proteins and peptide samples were carried out by Dr. Shouming He. Peptides were separated by reverse-phase HPLC onto an Ultra Microprotein Analyzer (Michrom BioResources Inc., Pleasanton CA, U.S.A.) directly interfaced with the mass spectrometer. In each MS experiment, the proteolytic digest was loaded on to a C<sub>18</sub> column (Reliasil; 1 mm  $\times$  150 mm) and then eluted with a gradient of 0-60 % solvent B over 60 min at a flow rate of 50  $\mu$ l/min (solvent A was 0.05% (v/v) TFA/2 % (v/v) CH<sub>3</sub>CN in water; solvent B was 0.045% (v/v) TFA/90% (v/v) CH<sub>3</sub>CN in water). In the single quadrupole mode, the MS conditions were as follows. The mass

analyser was scanned over the range of 300 to 2200 amu with a step size of 0.5 amu, a dwell time of 5.0 ms, an ion source voltage of 5 kV, and an orifice voltage of 50 V. The neutral loss spectra were obtained in the triple quadrupole mode searching for the loss of  $m/z$  of 90.5, which corresponds to the loss of the label on a doubly charged species. A scan range of 400-1800 amu was used with a step size of 0.5 amu and a dwell time of 1.5 ms. Other parameters were as follows: ion source voltage = 4.8 kV; orifice energy = 45 V; IQ2 = -42; Q0 = -10; the collision gas was argon/N<sub>2</sub> (9:1).

The MS-MS spectrum of the isolated, labelled peptide was obtained by selectively introducing the  $m/z$  688 peptide from the first quadrupole (Q1) into the collision cell (Q2) and then observing the daughter ions in the third quadrupole (Q3). The following settings were used: Q1 was locked on  $m/z$  688; Q3 scanned over the range  $m/z$  50-1390; the step size was 0.5 and the dwell time 2.0 ms; the ion source potential was 4.8 kV; the orifice potential was 45 V; the focusing ring voltage was 200 V; the Q0 potential was -10 V; the Q2 potential was -42 V; the collision gas was N<sub>2</sub>.

#### 5.3.8.2 Analysis of the covalent intermediate formed on GMII

The analyses of protein samples were carried out by Dr. Shouming He using a Sciex API-300 mass spectrometer interfaced with an LC-Packings HPLC system. Briefly, the intact protein (10-20  $\mu$ g) was pre-incubated for 5 minutes with either 4 mM 5FGulF (wild-type or Asp341Asn mutant GMII), or 40 mM 2FManF (Asp341Asn mutant GMII). This sample was introduced into the mass spectrometer through a microbore PRLP column (1  $\times$  50 mm) and eluted with a gradient of 20-100% solvent B in solvent A at a flow rate of 50  $\mu$ L/min over 10 minutes (solvent A, 0.06% TFA/2% CH<sub>3</sub>CN in water; solvent B, 0.05% TFA/90% CH<sub>3</sub>CN in water). The MS was scanned over a range of 600

– 2400 Da (4 second/scan) with a step size of 0.5 Da. The ion source voltage was 4.8 kV and the orifice energy was 50 V.

#### 5.3.8.3 *Product analysis of HPA reactions*

Product formation of the HPA catalyzed reaction of G3F with GHIL was determined by MALDI-TOF MS analysis. G3F and GHIL were incubated with HPA (0.06 mgml<sup>-1</sup>) at 30°C in 5 mM sodium phosphate buffer, pH 6.9 containing 10 mM NaCl for 1 hour. A saturated solution of 2,5-dihydroxybenzoic acid in de-ionized water was used as the matrix. Sample and matrix solution were mixed in a 1:20 ratio and 1 µL of this sample was spotted on the target plate and dried under vacuum. The MALDI-TOF spectra were collected using a Voyager-DE-STR (Applied Biosystems) system in reflectron mode with an acceleration voltage of 20 kV.

## Chapter 6 References:

1. McEver, R. P., McIntyre, T. M., Moore, K. L., Prescott, S. M., and Zimmerman, G. A. (1995) *J. Clin. Invest.* 96, 171-82.
2. Helenius, A., and Aebi, M. (2001) *Science* 291, 2364-2369.
3. Hauri, H. P., Appenzeller, C., Kuhn, F., and Nufer, O. (2000) *FEBS Lett.* 476, 32-37.
4. Wells, L., Vosseller, K., and Hart, G. W. (2001) *Science* 291, 2376-2378.
5. Williams, S. J., and Davies, G. J. (2001) *Trends Biotechnol.* 19, 356-62.
6. Davies, G. J., Wilson, K. S., and Henrissat, B. (1997) *Biochem. J.* 321, 557-559.
7. Henrissat, B. (1991) *Biochem. J.* 280, 309-16.
8. Henrissat, B., and Bairoch, A. (1993) *Biochem. J.* 293, 781-8.
9. Henrissat, B. (1998) *Biochem. Soc. Trans.* 26, 153-156.
10. Gebler, J., Gilkes, N. R., Claeysens, M., Wilson, D. B., Beguin, P., Wakarchuk, W. W., Kilburn, D. G., Miller, R. C., Jr., Warren, R. A., and Withers, S. G. (1992) *J. Biol. Chem.* 267, 12559-61.
11. Davies, G. J., and Henrissat, B. (2002) *Biochem. Soc. Trans.* 30, 291-297.
12. Wolfenden, R., Lu, X. D., and Young, G. (1998) *J. Am. Chem. Soc.* 120, 6814-6815.
13. Koshland, D. E. (1953) *Biol. Rev.* 28, 416-436.
14. Sinnott, M. L. (1990) *Chem. Rev.* 90, 1171-1202.
15. Ly, H. D., and Withers, S. G. (1999) *Annu. Rev. Biochem.* 68, 487-522.
16. Rye, C. S., and Withers, S. G. (2000) *Curr. Opin. Chem. Biol.* 4, 573-580.
17. Zechel, D. L., and Withers, S. G. (2000) *Acc. Chem. Res.* 33, 11-18.
18. Zechel, D. L., and Withers, S. G. (2001) *Curr. Opin. Chem. Biol.* 5, 643-649.
19. Capon, B. (1969) *Chem. Rev.* 69, 407-498.
20. Wang, Q., Graham, R. W., Trimbur, D., Warren, R. A. J., and Withers, S. G. (1994) *J. Am. Chem. Soc.* 116, 11594-11595.
21. McCarter, J. D., and Withers, S. G. (1994) *Curr. Opin. Struct. Biol.* 4, 885-892.
22. Withers, S. G., Rupitz, K., Trimbur, D., and Warren, R. A. J. (1992) *Biochemistry* 31, 9979-9985.
23. Sinnott, M. L. (1978) *FEBS Lett.* 94, 1-9.
24. Umezurike, G. M. (1988) *Biochem. J.* 254, 73-6.
25. Li, B. F., Holdup, D., Morton, C. A., and Sinnott, M. L. (1989) *Biochem. J.* 260, 109-14.
26. Kempton, J. B., and Withers, S. G. (1992) *Biochemistry* 31, 9961-9.
27. Tull, D., and Withers, S. G. (1994) *Biochemistry* 33, 6363-6370.
28. McCarter, J. D., and Withers, S. G. (1996) *J. Am. Chem. Soc.* 118, 241-242.
29. Withers, S. G., Rupitz, K., and Street, I. P. (1988) *J. Biol. Chem.* 263, 7929-7932.
30. Namchuk, M. N., and Withers, S. G. (1995) *Biochemistry* 34, 16194-16202.
31. MacLeod, A. M., Lindhorst, T., Withers, S. G., and Warren, R. A. J. (1994) *Biochemistry* 33, 6371-6376.
32. MacLeod, A. M., Tull, D., Rupitz, K., Warren, R. A. J., and Withers, S. G. (1996) *Biochemistry* 35, 13165-13172.
33. Kirby, A. J. (1997) *Acc. Chem. Res.* 30, 290-296.

34. Lawson, S. L., Wakarchuk, W. W., and Withers, S. G. (1997) *Biochemistry* 36, 2257-2265.
35. Lawson, S. L., Wakarchuk, W. W., and Withers, S. G. (1996) *Biochemistry* 35, 10110-10118.
36. Ermert, P., Vasella, A., Weber, M., Rupitz, K., and Withers, S. G. (1993) *Carbohydr. Res.* 250, 113-128.
37. Tatsuta, K., Miura, S., Ohta, S., and Gunji, H. (1995) *J. Antibiot.* 48, 286-288.
38. Heightman, T. D., Locatelli, M., and Vasella, A. (1996) *Helv. Chim. Acta* 79, 2190-2200.
39. Heightman, T. D., and Vasella, A. T. (1999) *Angew. Chem. Int. Ed. Engl.* 38, 750-770.
40. Granier, T., Panday, N., and Vasella, A. (1997) *Helv. Chim. Acta* 80, 979-987.
41. Williams, S. J., Hoos, R., and Withers, S. G. (2000) *J. Am. Chem. Soc.* 122, 2223-2235.
42. Varrot, A., Schulein, M., Pipelier, M., Vasella, A., and Davies, G. J. (1999) *J. Am. Chem. Soc.* 121, 2621-2622.
43. Notenboom, V., Williams, S. J., Hoos, R., Withers, S. G., and Rose, D. R. (2000) *Biochemistry* 39, 11553-11563.
44. Wang, Q., Trimbur, D., Graham, R., Warren, R. A. J., and Withers, S. G. (1995) *Biochemistry* 34, 14554-14562.
45. McIntosh, L. P., Hand, G., Johnson, P. E., Joshi, M. D., Korner, M., Plesniak, L. A., Ziser, L., Wakarchuk, W. W., and Withers, S. G. (1996) *Biochemistry* 35, 9958-9966.
46. Blake, C. C., Johnson, L. N., Mair, G. A., North, A. C., Phillips, D. C., and Sarma, V. R. (1967) *Proc. R. Soc. Lond., B, Biol. Sci.* 167, 378-88.
47. Strynadka, N. C. J., and James, M. N. G. (1991) *J. Mol. Biol.* 220, 401-424.
48. Mosi, R. M., and Withers, S. G. (2002) in *Enzyme Kinetics and Mechanism, Pt F: Detection and Characterization of Enzyme Reaction Intermediates* pp 64-84, Academic Press Inc, San Diego.
49. Wicki, J., Rose, D. R., and Withers, S. G. (2002) in *Enzyme Kinetics and Mechanism, Pt F: Detection and Characterization of Enzyme Reaction Intermediates* pp 84-105, Academic Press Inc, San Diego.
50. Namchuk, M., Braun, C., McCarter, J. D., and Withers, S. G. (1996) in *Biomedical Frontiers of Fluorine Chemistry* pp 279-293, Amer Chemical Soc, Washington.
51. Mosi, R., He, S. M., Uitdehaag, J., Dijkstra, B. W., and Withers, S. G. (1997) *Biochemistry* 36, 9927-9934.
52. Notenboom, V., Birsan, C., Nitz, M., Rose, D. R., Warren, R. A. J., and Withers, S. G. (1998) *Nat. Struct. Biol.* 5, 812-818.
53. Withers, S. G., Warren, R. A. J., Street, I. P., Rupitz, K., Kempton, J. B., and Aebersold, R. (1990) *J. Am. Chem. Soc.* 112, 5887-5889.
54. Withers, S. G., and Street, I. P. (1988) *J. Am. Chem. Soc.* 110, 8551-8553.
55. Withers, S. G., and Aebersold, R. (1995) *Protein Sci.* 4, 361-72.
56. Vocadlo, D. J., Davies, G. J., Laine, R., and Withers, S. G. (2001) *Nature* 412, 835-838.
57. Pauling, L. (1946) *Chem. Eng. News* 24, 1375.

58. Sidhu, G., Withers, S. G., Nguyen, N. T., McIntosh, L. P., Ziser, L., and Brayer, G. D. (1999) *Biochemistry* 38, 5346-5354.
59. Tews, I., Perrakis, A., Oppenheim, A., Dauter, Z., Wilson, K. S., and Vorgias, C. E. (1996) *Nat. Struct. Biol.* 3, 638-648.
60. Sulzenbacher, G., Driguez, H., Henrissat, B., Schulein, M., and Davies, G. J. (1996) *Biochemistry* 35, 15280-15287.
61. Davies, G. J., Mackenzie, L., Varrot, A., Dauter, M., Brzozowski, A. M., Schulein, M., and Withers, S. G. (1998) *Biochemistry* 37, 11707-11713.
62. Ducros, V. M. A., Zechel, D. L., Murshudov, G. N., Gilbert, H. J., Szabo, L., Stoll, D., Withers, S. G., and Davies, G. J. (2002) *Angew. Chem. Int. Ed. Engl.* 41, 2824-2827.
63. Deslongchamps, P. (1983) *Stereoelectronic Effects in Organic Chemistry*, Vol. 1, Pergamon Press, Oxford.
64. Sulzenbacher, G., Mackenzie, L. F., Wilson, K. S., Withers, S. G., Dupont, C., and Davies, G. J. (1999) *Biochemistry* 38, 4826-4833.
65. McCarter, J. D., Adam, M. J., Braun, C., Namchuk, M., Tull, D., and Withers, S. G. (1993) *Carbohydr. Res.* 249, 77-90.
66. Lillelund, V. H., Jensen, H. H., Liang, X. F., and Bols, M. (2002) *Chem. Rev.* 102, 515-553.
67. Jensen, H. H., and Bols, M. (2001) *J. Chem. Soc. Perkin Trans. 1*, 905-909.
68. Liu, H. Z., Liang, X. F., Sohoel, H., Bulow, A., and Bols, M. (2001) *J. Am. Chem. Soc.* 123, 5116-5117.
69. Uitdehaag, J. C., Mosi, R., Kalk, K. H., van der Veen, B. A., Dijkhuizen, L., Withers, S. G., and Dijkstra, B. W. (1999) *Nat. Struct. Biol.* 6, 432-6.
70. Ly, H. D., Howard, S., Shum, K., He, S. M., Zhu, A., and Withers, S. G. (2000) *Carbohydr. Res.* 329, 539-547.
71. Lee, S. S., He, S. M., and Withers, S. G. (2001) *Biochem. J.* 359, 381-386.
72. Howard, S., He, S. M., and Withers, S. G. (1998) *J. Biol. Chem.* 273, 2067-2072.
73. Burda, P., and Aebi, M. (1999) *Biochim. Biophys. Acta* 1426, 239-257.
74. Herscovics, A. (1999) *Biochim. Biophys. Acta* 1473, 96-107.
75. Kornfeld, R., and Kornfeld, S. (1985) *Annu. Rev. Biochem.* 54, 631-64.
76. Imperiali, B. (1997) *Acc. Chem. Res.* 30, 452-459.
77. Wang, C. Q., Eufemi, M., Turano, C., and Giartosio, A. (1996) *Biochemistry* 35, 7299-7307.
78. Aronson, N. N., Jr., and Kuranda, M. J. (1989) *FASEB J.* 3, 2615-22.
79. Howard, S., Braun, C., McCarter, J., Moremen, K. W., Liao, Y. F., and Withers, S. G. (1997) *Biochem. Biophys. Res. Commun.* 238, 896-8.
80. Moremen, K. W., Trimble, R. B., and Herscovics, A. (1994) *Glycobiology* 4, 113-25.
81. Daniel, P. F., Winchester, B., and Warren, C. D. (1994) *Glycobiology* 4, 551-66.
82. Liao, Y. F., Lal, A., and Moremen, K. W. (1996) *J. Biol. Chem.* 271, 28348-58.
83. Merkle, R. K., Zhang, Y., Ruest, P. J., Lal, A., Liao, Y. F., and Moremen, K. W. (1997) *Biochim. Biophys. Acta* 1336, 132-146.
84. Tollersrud, O. K., Berg, T., Healy, P., Evjen, G., Ramachandran, U., and Nilssen, O. (1997) *Eur. J. Biochem.* 246, 410-9.

85. Chester, A. M., Lundblad, A., Ockerman, P.-A., and Autio, S. (1982) in *Genetic errors of glycoprotein metabolism* (Durand, P., and O'Brien, J., Eds.) pp 89-120, Edi-Ermes, Milan.
86. Hocking, J. D., Jolly, R. D., and Batt, R. D. (1972) *Biochem. J.* 128, 69-78.
87. Burditt, L. J., Chotai, K., Hirani, S., Nugent, P. G., Winchester, B. G., and Blakemore, W. F. (1980) *Biochem. J.* 189, 467-73.
88. Michalski, J. C., and Klein, A. (1999) *Biochim. Biophys. Acta* 1455, 69-84.
89. Gotoda, Y., Wakamatsu, N., Kawai, H., Nishida, Y., and Matsumoto, T. (1998) *Am. J. Hum. Genet.* 63, 1015-24.
90. Berg, T., Riise, H. M., Hansen, G. M., Malm, D., Tranebjaerg, L., Tollersrud, O. K., and Nilssen, O. (1999) *Am. J. Hum. Genet.* 64, 77-88.
91. Harpaz, N., and Schachter, H. (1980) *J. Biol. Chem.* 255, 4894-902.
92. Couldrey, C., and Green, J. E. (2000) *Breast Cancer Res.* 2, 321-323.
93. Dennis, J. W., Granovsky, M., and Warren, C. E. (1999) *Biochim. Biophys. Acta* 1473, 21-34.
94. Granovsky, M., Fata, J., Pawling, J., Muller, W. J., Khokha, R., and Dennis, J. W. (2000) *Nat. Med.* 6, 306-312.
95. Goss, P. E., Baker, M. A., Carver, J. P., and Dennis, J. W. (1995) *Clin. Cancer Res.* 1, 935-44.
96. Goss, P. E., Reid, C. L., Bailey, D., and Dennis, J. W. (1997) *Clin. Cancer Res.* 3, 1077-1086.
97. van den Elsen, J. M. H., Kuntz, D. A., and Rose, D. R. (2001) *EMBO J.* 20, 3008-3017.
98. Snaith, S. M., Hay, A. J., and Levvy, G. A. (1971) *J. Endocrinol.* 50, 659-67.
99. Snaith, S. M. (1975) *Biochem. J.* 147, 83-90.
100. Rabouille, C., Kuntz, D. A., Lockyer, A., Watson, R., Signorelli, T., Rose, D. R., van den Heuvel, M., and Roberts, D. B. (1999) *J. Cell Sci.* 112, 3319-3330.
101. Blattner, R., and Ferrier, R. J. (1980) *J. Chem. Soc. Perkin Trans. 1*, 1523-1527.
102. Hall, L. D., Johnson, R. N., Adamson, J., and Foster, A. B. (1971) *Can. J. Chem* 49, 118-123.
103. Stoddart, J. F. (1971) *Stereochemistry of Carbohydrates*, Wiley-Interscience, New York.
104. Thoma, J., Spradlin, J., and Dygert, S. (1971) in *The Enzymes* (Boyer, P., Ed.) pp 115-189, Academic Press, New York.
105. Vihinen, M., and Mantsala, P. (1989) *Crit. Rev. Biochem. Mol. Biol.* 24, 329-418.
106. McCarter, J. D., and Withers, S. G. (1996) *J. Biol. Chem.* 271, 6889-6894.
107. Tao, B. Y., Reilly, P. J., and Robyt, J. F. (1989) *Biochim. Biophys. Acta* 995, 214-220.
108. Brayer, G. D., Sidhu, G., Maurus, R., Rydberg, E. H., Braun, C., Wang, Y. L., Nguyen, N. T., Overall, C. M., and Withers, S. G. (2000) *Biochemistry* 39, 4778-4791.
109. Qian, M. X., Haser, R., Buisson, G., Duee, E., and Payan, F. (1994) *Biochemistry* 33, 6284-6294.
110. Brzozowski, A. M., and Davies, G. J. (1997) *Biochemistry* 36, 10837-10845.
111. Aghajari, N., Feller, G., Gerday, C., and Haser, R. (1998) *Protein Sci.* 7, 564-572.

112. Boel, E., Brady, L., Brzozowski, A. M., Derewenda, Z., Dodson, G. G., Jensen, V. J., Petersen, S. B., Swift, H., Thim, L., and Woldike, H. F. (1990) *Biochemistry* 29, 6244-6249.
113. Machius, M., Wiegand, G., and Huber, R. (1995) *J. Mol. Biol.* 246, 545-559.
114. Kadziola, A., Abe, J., Svensson, B., and Haser, R. (1994) *J. Mol. Biol.* 239, 104-121.
115. Buisson, G., Duee, E., Haser, R., and Payan, F. (1987) *EMBO J.* 6, 3909-3916.
116. Ramasubbu, N., Paloth, V., Luo, Y. G., Brayer, G. D., and Levine, M. J. (1996) *Acta Crystallogr. D* 52, 435-446.
117. Brayer, G. D., Luo, Y., and Withers, S. G. (1995) *Protein Sci.* 4, 1730-1742.
118. D'Amico, S., Gerday, C., and Feller, G. (2000) *Gene* 253, 95-105.
119. Feller, G., Bussy, O., Houssier, C., and Gerday, C. (1996) *J. Biol. Chem.* 271, 23836-23841.
120. Wakim, J., Robinson, M., and Thoma, J. A. (1969) *Carbohydr. Res.* 10, 487-503.
121. Levitzki, A., and Steer, M. L. (1974) *Eur. J. Biochem.* 41, 171-180.
122. Fujimoto, Z., Takase, K., Doui, N., Momma, M., Matsumoto, T., and Mizuno, H. (1998) *J. Mol. Biol.* 277, 393-407.
123. Rydberg, E. H., Sidhu, G., Vo, H. C., Hewitt, J., Cote, H. C., Wang, Y., Numao, S., MacGillivray, R. T., Overall, C. M., Brayer, G. D., and Withers, S. G. (1999) *Protein Sci.* 8, 635-643.
124. Guyton, A. C. (1991) *Textbook of Medical Physiology*, 8th ed., W.B. Saunders Company, Philadelphia.
125. (1988) *Handbook of amylases and related enzymes: Their Sources, Isolation Methods, Properties and Applications*, Pergamon Press, Oxford.
126. Okada, G., Genghof, D. S., and Hehre, E. J. (1979) *Carbohydr. Res.* 71, 287-98.
127. Jenkins, D. J., Taylor, R. H., Goff, D. V., Fielden, H., Misiewicz, J. J., Sarson, D. L., Bloom, S. R., and Alberti, K. G. (1981) *Diabetes* 30, 951-4.
128. Taylor, R. H., Jenkins, D. J., Barker, H. M., Fielden, H., Goff, D. V., Misiewicz, J. J., Lee, D. A., Allen, H. B., MacDonald, G., and Wallrabe, H. (1982) *Diabetes Care* 5, 92-6.
129. Meyer, B. H., Muller, F. O., Kruger, J. B., Clur, B. K., and Grigoleit, H. G. (1984) *S. Afr. Med. J.* 66, 222-3.
130. Bailey, C. J. (1998) *Chem. Ind.*, 53-57.
131. Truscheit, E., Frommer, W., Junge, B., Muller, L., Schmidt, D. D., and Wingender, W. (1981) *Angew. Chem. Int. Ed. Engl.* 20, 744-761.
132. Franco, O. L., Rigden, D. J., Melo, F. R., and Grossi-de-Sa, M. F. (2002) *Eur. J. Biochem.* 269, 397-412.
133. Powers, J. R., and Whitaker, J. R. (1977) *J. Food Biochem.* 1, 239-260.
134. Kline, A. D., Braun, W., and Wuthrich, K. (1988) *J. Mol. Biol.* 204, 675-724.
135. Richardson, M. (1991) in *Methods in Plant Biochemistry: Amino Acids, Proteins and Nucleic Acids* (Rogers, L. J., Ed.) pp 295-, Academic Press Inc, San Diego.
136. Wiegand, G., Epp, O., and Huber, R. (1995) *J. Mol. Biol.* 247, 99-110.
137. Strobl, S., Maskos, K., Wiegand, G., Huber, R., Gomis-Ruth, F. X., and Glockshuber, R. (1998) *Struct. Fold. Des.* 6, 911-921.
138. Vallee, F., Kadziola, A., Bourne, Y., Juy, M., Rodenburg, K. W., Svensson, B., and Haser, R. (1998) *Struct. Fold. Des.* 6, 649-659.

139. Pereira, P. J. B., Lozanov, V., Patthy, A., Huber, R., Bode, W., Pongor, S., and Strobl, S. (1999) *Struct. Fold. Des.* 7, 1079-1088.
140. Nahoum, V., Farisei, F., Le-Berre-Anton, V., Egloff, M. P., Rouge, P., Poerio, E., and Payan, F. (1999) *Acta Crystallogr. Sect. D-Biol. Crystallogr.* 55, 360-362.
141. Vertesy, L., Oeding, V., Bender, R., Zepf, K., and Nesemann, G. (1984) *Eur. J. Biochem.* 141, 505-12.
142. Matter, H., and Kessler, H. (1995) *J. Am. Chem. Soc.* 117, 3347-3359.
143. Sefler, A. M., Kozlowski, M. C., Guo, T., and Bartlett, P. A. (1997) *J. Org. Chem.* 62, 93-102.
144. Ono, S., Umezaki, M., Tojo, N., Hashimoto, S., Taniyama, H., Kaneko, T., Fujii, T., Moria, H., Shimasaki, C., Yamazaki, I., Yoshimura, T., and Kato, T. (2001) *J. Biochem.* 129, 783-790.
145. Rydberg, E. H. (2000), PhD Thesis.
146. Mosi, R., Sham, H., Uitdehaag, J. C. M., Ruitkamp, R., Dijkstra, B. W., and Withers, S. G. (1998) *Biochemistry* 37, 17192-17198.
147. Brzozowski, A. M., Lawson, D. M., Turkenburg, J. P., Bisgaard-Frantzen, H., Svendsen, A., Borchert, T. V., Dauter, Z., Wilson, K. S., and Davies, G. J. (2000) *Biochemistry* 39, 9099-9107.
148. Takada, M., Ogawa, K., Saito, S., Murata, T., and Usui, T. (1998) *J. Biochem.* 123, 508-515.
149. Takada, M., Ogawa, K., Murata, T., and Usui, T. (1999) *J. Carbohydr. Chem.* 18, 149-163.
150. Legler, G. (1990) *Adv. Carbohydr. Chem. Biochem.* 48, 319-384.
151. Braun, C. (1995), PhD Thesis.
152. Uchida, R., Nasu, A., Tokutake, S., Kasai, K., Tobe, K., and Yamaji, N. (1999) *Chem. Pharm. Bull.* 47, 187-193.
153. Ghavami, A., Johnston, B. D., Jensen, M. T., Svensson, B., and Pinto, B. M. (2001) *J. Am. Chem. Soc.* 123, 6268-6271.
154. Bernfeld, P. (1955) *Meth. Enzymol.* 1, 149-158.
155. Hagele, E. O., Schaich, E., Rauscher, E., Lehmann, P., Burk, H., Wahlefeld, A. W., and James, G. P. (1982) *Clin. Chem.* 28, 2201-5.
156. Wallenfels, K., Laule, G., and Meltzer, B. (1982) *J. Clin. Chem. Clin. Biochem.* 20, 581-6.
157. Kruse-Jarres, J. D., Kaiser, C., Hafkenschied, J. C., Hohenwallner, W., Stein, W., Bohner, J., Klein, G., Poppe, W., and Rauscher, E. (1989) *J. Clin. Chem. Clin. Biochem.* 27, 103-13.
158. Usui, T., Ogawa, K., Nagai, H., and Matsui, H. (1992) *Anal. Biochem.* 202, 61-7.
159. Tokutake, S., Uchida, R., Kotani, K., Saito, K., and Yamaji, N. (1993) *Carbohydr. Res.* 238, 109-33.
160. Payre, N., Cottaz, S., and Driguez, H. (1995) *Angew. Chem. Int. Ed. Engl.* 34, 1239-1241.
161. Rydberg, E. H., Li, C., Maurus, R., Overall, C. M., Brayer, G. D., and Withers, S. G. (2002) *Biochemistry* 41, 4492-502.
162. Ishikawa, K., Matsui, I., Honda, K., and Nakatani, H. (1992) *Biochem. Biophys. Res. Comm.* 183, 286-91.

163. Koeners, H. J., De Kok, A. J., Romers, C., and Van Boom, J. H. (1980) *Recl. Trav. Chim. Pays-Bas* 99, 355-62.
164. Berven, L. A., Dolphin, D. H., and Withers, S. G. (1988) *J. Am. Chem. Soc.* 110, 4864-4866.
165. Lee, S. S. personal communication.
166. Winn-Deen, E. S., David, H., Sigler, G., and Chavez, R. (1988) *Clin. Chem.* 34, 2005-8.
167. Yoon, S. H., and Robyt, J. F. (2002) *Carbohydr. Res.* 337, 509-16.
168. Hoos, R., Vasella, A., Rupitz, K., and Withers, S. G. (1997) *Carbohydr. Res.* 298, 291-298.
169. Li, C. (2002) personal communication.
170. Sambrook, J., Fritsch, E. F., and Maniatis, T. (1989) *Molecular Cloning: A Laboratory Manual*, Cold Spring Harbor Laboratory, Cold Spring Harbor, N.Y.
171. Leatherbarrow, R. J. (2001), Erithacus Software Limited.
172. Vasella, A., Davies, G.J. and Bohm, M. (2002) *Curr. Opin. Chem. Biol.* 6, 619-629.

# **Appendix 1**

## **Basic Kinetics**

## Fundamental Equations for Enzyme Kinetics

In 1913, Michaelis and Menten proposed a simple model to account for the relationship between the rate of enzyme catalysis and the concentration of substrate. In 1925, Briggs and Haldane extended this model include the concept of steady state. The general scheme for an enzyme-catalyzed reaction is shown below. Free enzyme, E, combines with free substrate, S, to form an enzyme-substrate complex, ES, which is then turned over to yield the product, P.



Under steady state conditions,

$$\frac{d[ES]}{dt} = k_1[E][S] - k_{-1}[ES] - k_2[ES] = 0 \quad [1]$$

The total concentration of enzyme  $[E]_o$  is equal to the concentration of free enzyme  $[E]$ , plus the concentration of the enzyme bound in the ES complex,  $[ES]$ .

$$[E]_o = [E] + [ES] \quad [2]$$

Solving for  $[ES]$  using equations 1 and 2, we get

$$[ES] = \frac{[E]_o[S]}{[S] + \frac{k_{-1} + k_2}{k_1}} \quad [3]$$

Under steady state conditions, the initial velocity of the reaction, is equal to the rate of formation of product:

$$v = \frac{dP}{dt} = k_2[ES] \quad [4]$$

By substituting the expression for [ES] from equation 3 into equation 4, one obtains

$$v = \frac{k_2[E]_o[S]}{\frac{k_{-1} + k_2}{k_1} + [S]} \quad [5]$$

The ratio of the rate constants  $(k_{-1} + k_2)/k_1$  is defined as  $K_m$ , the Michaelis constant, while the rate constant,  $k_2$ , is defined as the catalytic constant, or  $k_{cat}$  (the turnover number).

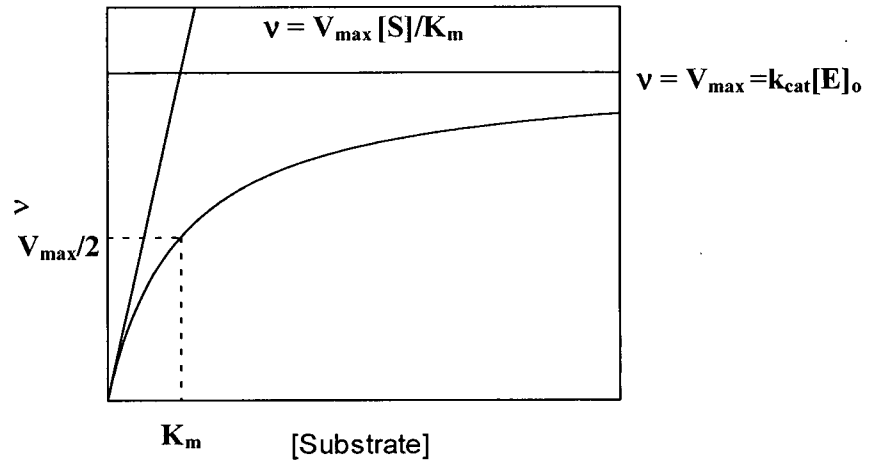
Therefore, equation 5 can be expressed in a more general format, also known as the Michaelis-Menten equation:

$$v = \frac{k_{cat}[E]_o[S]}{K_m + [S]} \quad [6]$$

In this equation, the product of  $k_{cat}$  and  $[E]_o$  is also referred to as  $V_{max}$  and represents the maximal velocity.

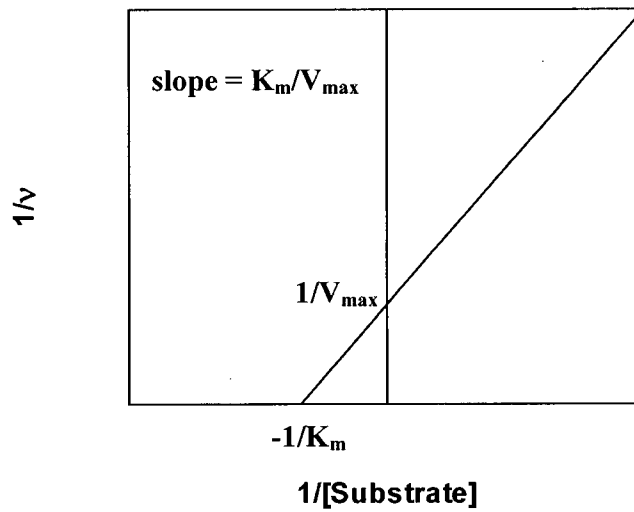
Interestingly, when the substrate concentration is equal  $K_m$ , the initial rate of the reaction is equal to one-half the maximal velocity ( $v=V_{max}/2$ ). In its simplest form, the Michaelis constant is a measure of the binding affinity of an enzyme for a particular substrate. Therefore, a substrate that binds well to the enzyme will have a low  $K_m$  value.

A graphical representation of the Michaelis-Menten equation is shown below.



The Michaelis-Menten equation can also be plotted as a reciprocal plot ( $1/v$  vs.  $1/[S]$ ).

This is known as a Lineweaver-Burke plot.



At high substrate concentrations ( $[S] \gg K_m$ ),  $v$  approaches its maximal value,  $V_{\max}$ , and the rate becomes independent of  $[S]$ . Thus, the Michaelis-Menten equation can be rewritten in the form:

$$v = V_{\max} = k_{\text{cat}} [E]_0 \quad [7]$$

At low concentrations ( $[S] \gg K_m$ ), the initial rate of the reaction is proportional to  $[S]$ :

$$v = \frac{k_{cat}[E]_o[S]}{K_m} \quad [8]$$

The Michaelis-Menten approach can be expanded to a more complex enzyme system where two distinct reaction steps occur. Such is the case for the double displacement mechanism. The reaction scheme for this mechanism is as follows: free enzyme, E, combines with free substrate, S, to form an enzyme-substrate complex, ES, with a rate constant,  $k_1$  (association step). The conversion of ES to EP is termed the glycosylation step ( $k_2$ ) and the turnover of EP to P is the deglycosylation step ( $k_3$ ).



Assuming that steady state concentration of both EP and ES is reached,

$$\frac{d[EP]}{dt} = k_2[ES] - k_3[EP] = 0 \quad [9]$$

$$\frac{d[ES]}{dt} = k_1[E][S] - k_{-1}[ES] - k_2[ES] = 0 \quad [10]$$

The total concentration of enzyme is equal to free enzyme plus all of the enzyme bound species:

$$[E]_o = [E] + [ES] + [EP] \quad [11]$$

By substituting for  $[EP]$  using equation 9, one obtains

$$[E]_o = [E] + [ES] + \frac{k_2}{k_3}[EP] \quad [12]$$

By solving equation 10 for [E] and substituting for [E] into equation 12, followed by a rearrangement:

$$[ES] = \frac{k_1[E]_o[S]}{k_{-1} + k_2 + \frac{k_1(k_2 + k_3)}{k_3}[S]} \quad [13]$$

At steady state, the rate of product formation is equal to

$$\frac{dP}{dt} = k_3[EP] = k_2[ES] \quad [14]$$

Substituting equation 13 into equation 14, yields an expression in the form of the Michaelis-Menten equation:

$$[ES] = \frac{\frac{k_2 k_3}{k_2 + k_3} [E]_o [S]}{\left( \frac{k_3}{k_2 + k_3} \right) \left( \frac{k_{-1} + k_2}{k_1} \right) + [S]} \quad [15]$$

From the form of the Michaelis-Menten equation:

$$k_{cat} = \frac{k_2 k_3}{k_2 + k_3} \quad [16]$$

$$K_m = \left( \frac{k_3}{k_2 + k_3} \right) \left( \frac{k_{-1} + k_2}{k_1} \right) \quad [17]$$

Therefore, it becomes evident that the values obtained experimentally for  $k_{cat}$  and  $K_m$  are composed of the individual rate constants.

### **Enzyme kinetics in the presence of a mechanism-based inactivator**

The inactivation of an enzyme, E, by a mechanism-based inactivator and its eventual reactivation by water is shown in the following scheme:



This is similar to the kinetic model for the double displacement mechanism seen above. If  $k_3 \ll k_2$ , such that  $k_3$  approaches zero, then an extremely stable glycosyl-enzyme intermediate will accumulate and the enzyme will be inactivated. The model then simplifies to:



This model predicts a time dependent inactivation of the enzyme. If  $[I] \gg [E]$ , then  $[I]$  can be assumed to be essentially constant during the reaction and pseudo first-order kinetics with respect to  $[E]$  will be observed. The equation for this expression is analogous to the Michaelis-Menten equation:

$$v = \frac{k_i[E][I]}{K_i + [I]} \quad [18]$$

where  $k_i$  is the rate constant for inactivation ( $k_i = k_2$ ) and  $K_i$  is an apparent dissociation constant for all forms of enzyme-bound inactivator ( $K_i = k_{-1}/k_1$ ). The model then appears as:



Equation 18 can be rewritten as:

$$v = k_{obs}[E] \quad [19]$$

where

$$k_{obs} = \frac{k_i[I]}{K_i + [I]} \quad [20]$$

Equation 19 can then be expressed as a differential equation:

$$\frac{d[E]}{dt} = k_{obs}[E] \quad [21]$$

which can be solved with respect to time to give

$$\ln[E] = -k_{obs} \cdot t \quad [22]$$

If  $K_i \gg [I]$ , then equation 20 simplifies to

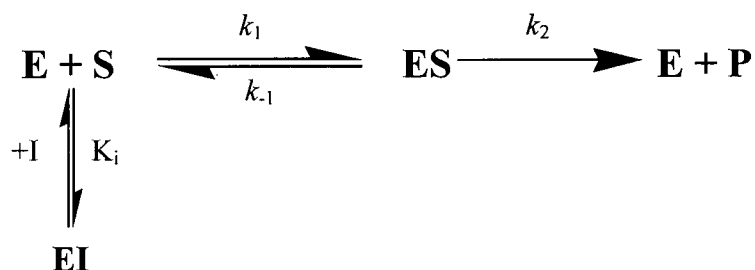
$$k_{obs} = \frac{k_i[I]}{K_i} \quad [23]$$

### Enzyme kinetics in the presence of a reversible inhibitor

There are three main types of reversible inhibition, competitive, non-competitive and uncompetitive.

#### i. Competitive inhibition

A competitive inhibitor competes directly with the substrate for binding to the free enzyme. The kinetic model for this must account for this second equilibrium.



Here,  $K_i$  is the dissociation constant for the enzyme-inhibitor complex:

$$K_i = \frac{[E][I]}{[EI]} \quad [24]$$

and the total enzyme concentration now equals:

$$[E]_o = [E] + [ES] + [EI] \quad [25]$$

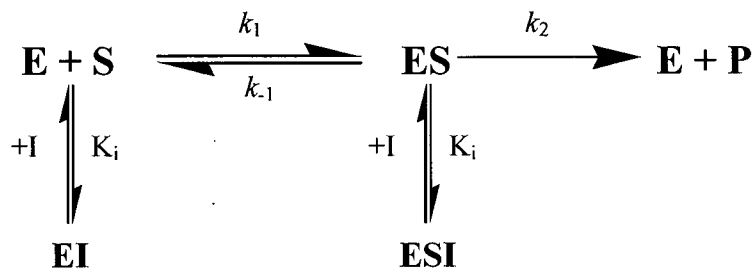
Using the steady state assumption ( $d[ES]/dt = 0$ ), we can get the expression:

$$v = \frac{V_{\max}[S]}{K_m \left(1 + \frac{[I]}{K_i}\right) + [S]} \quad [26]$$

Thus, a competitive inhibitor increases the apparent  $K_m$  by a factor of  $1 + [I]/K_i$ . The value of  $V_{\max}$  remains unchanged since at high  $[S]$  the inhibitor is displaced from the enzyme.

## ii. Non-competitive inhibition

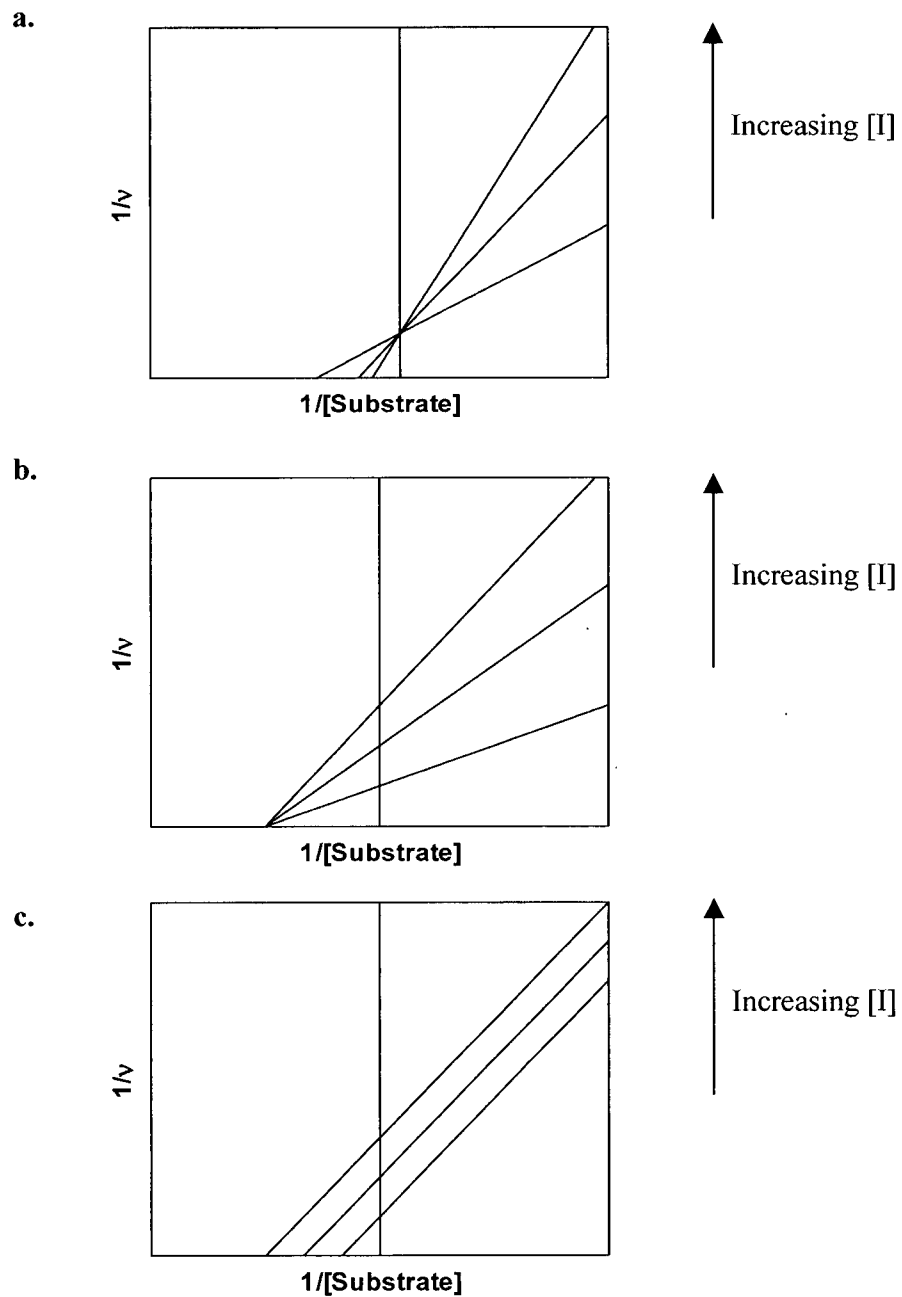
Non-competitive inhibition occurs when the inhibitor and substrate can bind simultaneously to the enzyme instead of competing for the same binding site. The kinetic model therefore becomes:



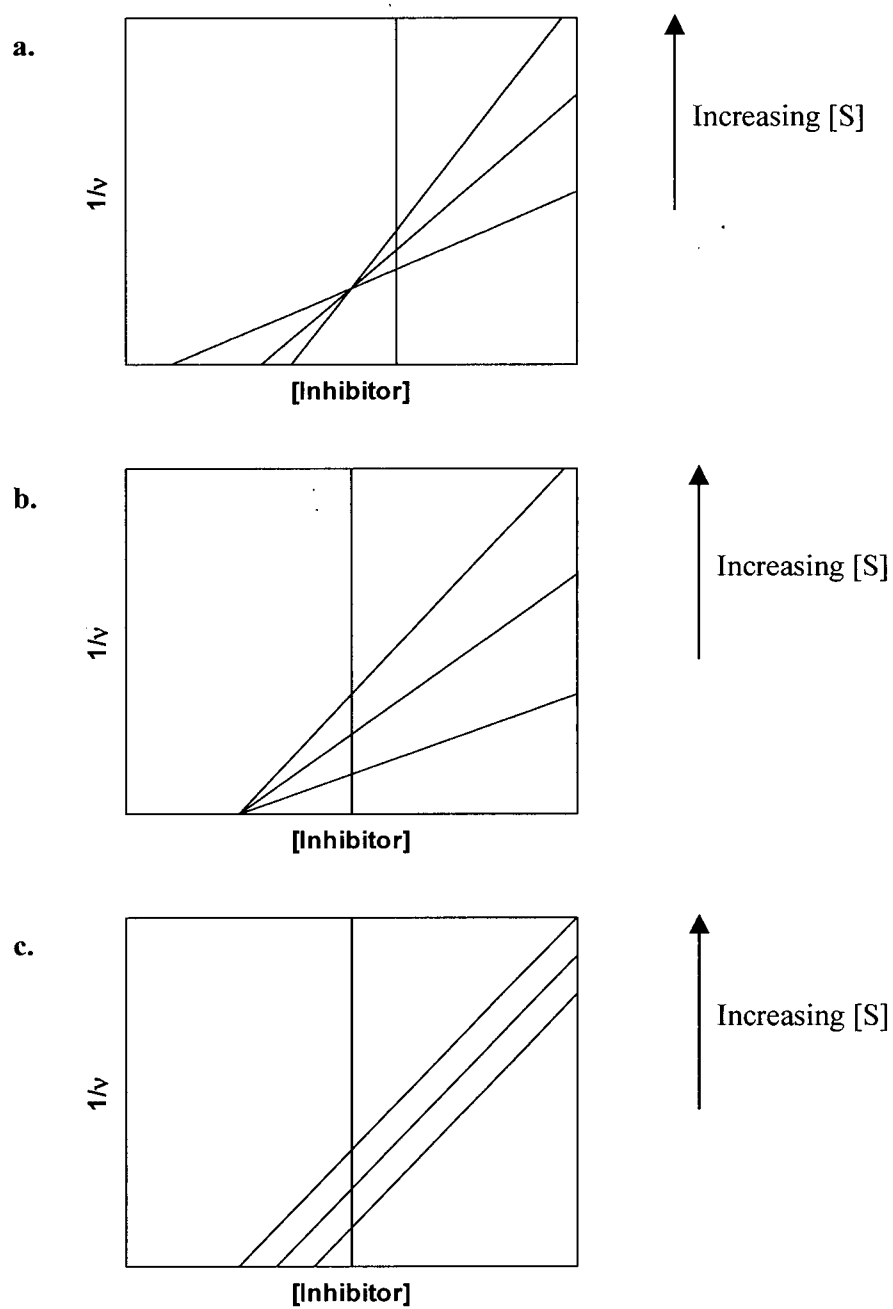
If we assume that the  $K_i$  does not change upon binding of the inhibitor, then using steady state assumption, we can get the expression:

$$v = \frac{V_{\max}[S]}{\left(1 + \frac{[I]}{K_i}\right) K_m + [S]} \quad [27]$$





Graphical representation for the determination of the modes of inhibition with a Lineweaver-Burke plot. (A) Competitive inhibition, (B) Non-competitive inhibition, and (C) Uncompetitive inhibition.



Graphical representation for the determination of the modes of inhibition with a Dixon plot. (A) Competitive inhibition, (B) Non-competitive inhibition, and (C) Uncompetitive inhibition.

## **Appendix 2**

# **Graphical representation**

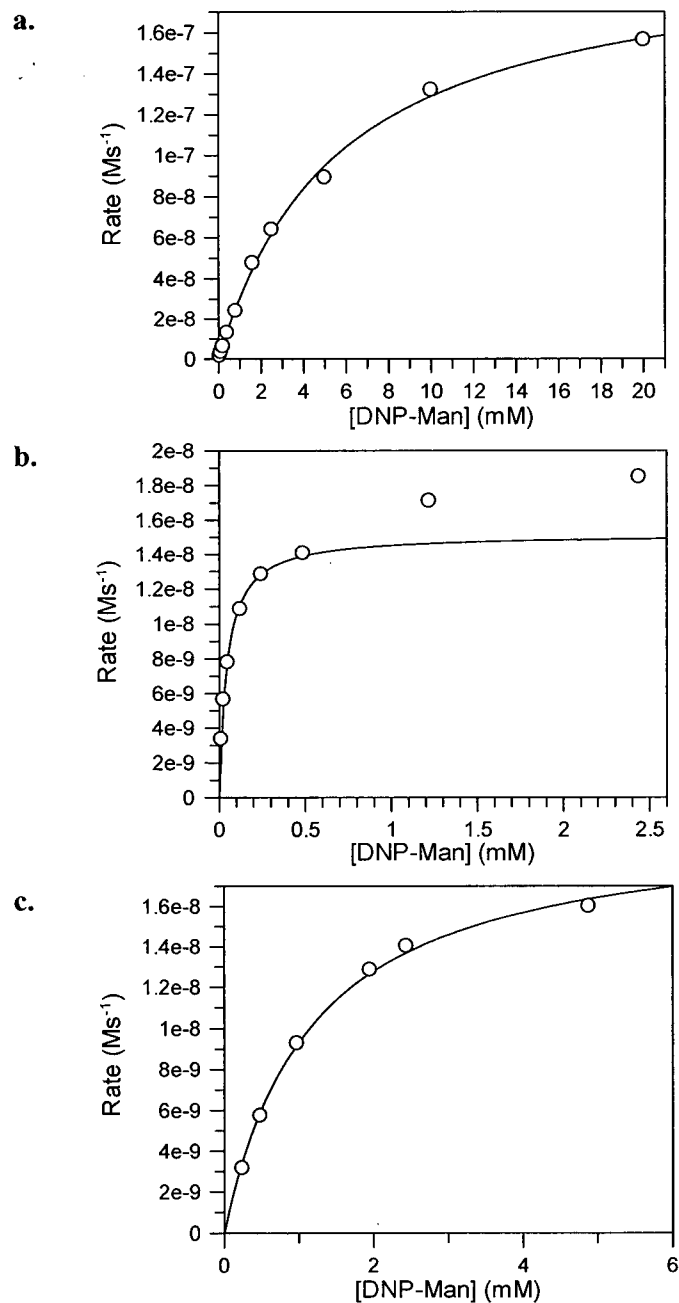


Figure B-1 Michaelis-Menten plots for the hydrolysis of DNP-Man by (a) bovine kidney lysosomal  $\alpha$ -mannosidase, (b) wild-type *Drosophila* Golgi  $\alpha$ -mannosidase II, and (c) Asp341Asn mutant *Drosophila* Golgi  $\alpha$ -mannosidase II. Fits shown are to the Michaelis-Menten equation.

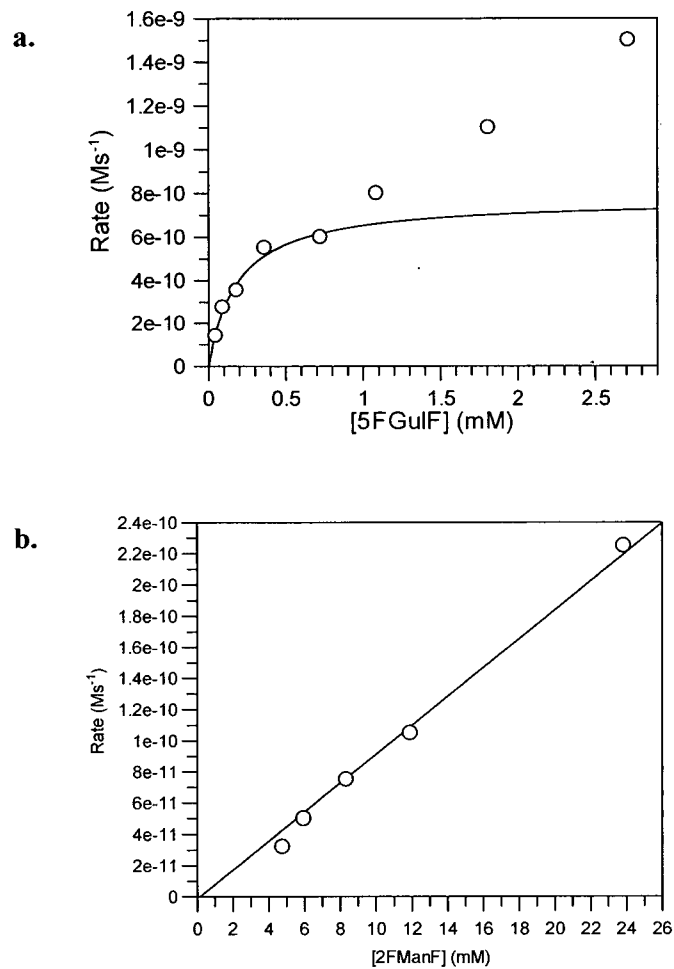


Figure B-2 Michaelis-Menten plot for the hydrolysis of (a) 5FGulF, and (b) 2FManF by wild-type *Drosophila* Golgi  $\alpha$ -mannosidase II. Fits shown are to the Michaelis-Menten equation.

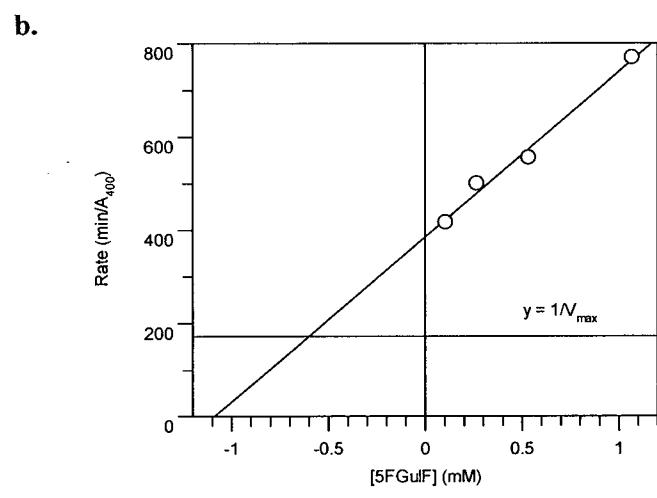
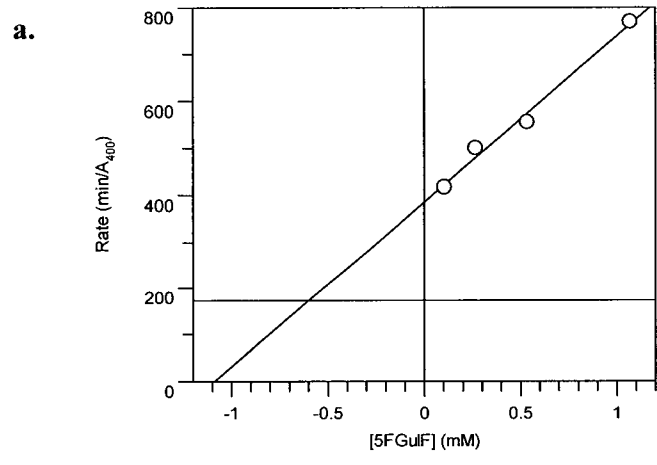


Figure B-3 Dixon plots used to approximate the  $K_i$  value for (a) 5FGulF, and (b) 2FManF with Asp341Asn mutant *Drosophila* Golgi  $\alpha$ -mannosidase II.

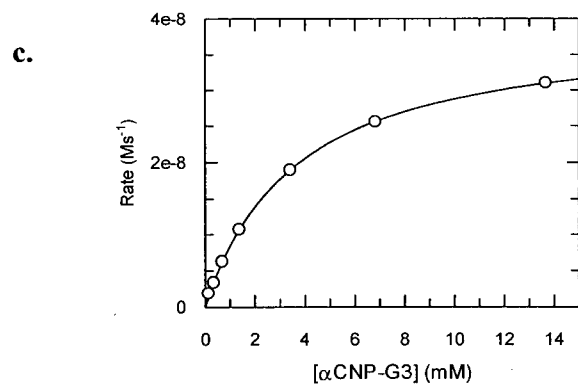
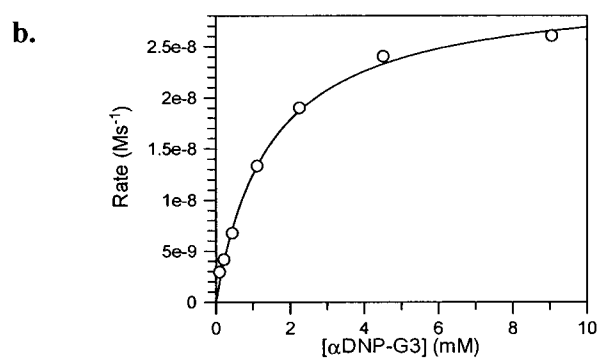
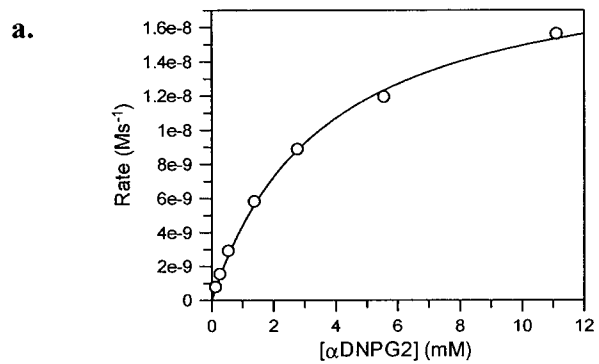


Figure B-4 Michaelis-Menten plots for the HPA catalyzed hydrolysis of (a)  $\alpha$ -DNP-G2, (b)  $\alpha$ -DNP-G3, and (c)  $\alpha$ -CNP-G3. Fits shown are to the Michaelis-Menten equation.

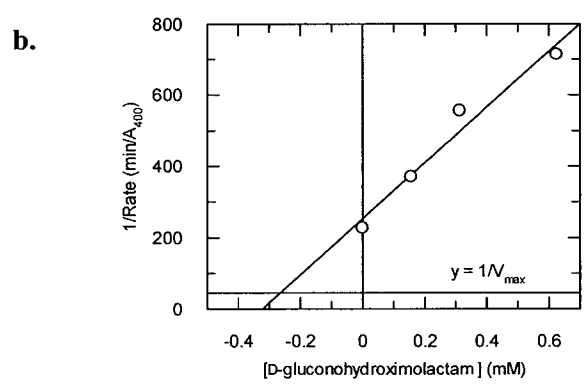
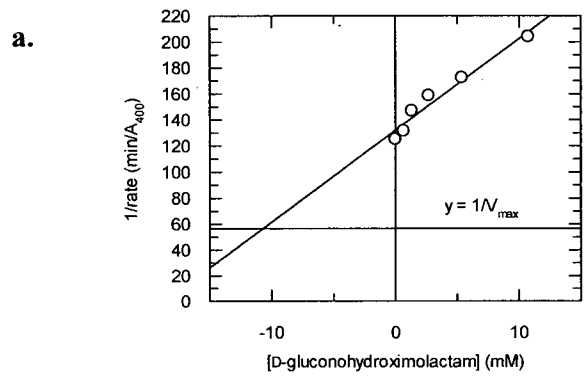


Figure B-5 Dixon plots used to determine the  $K_i$  value of (a) GHIL, and (b) extended GHIL.